FLUID FLOW AND HEAT TRANSFER IN A RECTANGULAR GEOMETRY WITH/WITHOUT SUCTION/INJECTION

A THESIS SUBMITTED TO
NATIONAL INSTITUTE OF TECHNOLOGY WARANGAL, (T.S.)
FOR THE AWARD OF THE DEGREE OF

DOCTOR OF PHILOSOPHY
IN
MATHEMATICS

BY
PAVAN KUMAR REDDY M
(ROLL NO: 716185)

UNDER THE SUPERVISION OF
Prof. J.V. RAMANA MURTHY

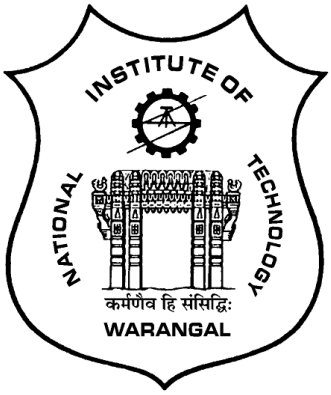

DEPARTMENT OF MATHEMATICS

NATIONAL INSTITUTE OF TECHNOLOGY

WARANGAL - 506 004 INDIA

JULY, 2019

CERTIFICATE

This is to certify that the thesis entitled **" FLUID FLOW AND HEAT TRANSFER IN A RECTANGULAR GEOMETRY WITH/WITHOUT SUCTION/ INJECTION "** *submitted to National Institute of Technology, Warangal for the award of the degree of* ***DOCTOR OF PHILOSOPHY****, is the bonafide research work done by* ***Mr. PAVANKUMAR REDDY M*** *under my supervision. The contents of this thesis have not been submitted elsewhere for the award of any degree.*

J.V. RAMANA MURTHY
(Supervisor)
Professor of Mathematics,
Department of Mathematics,
National Institute of Technology,
Warangal - 506 004,
Telangana State, India.

Date**:**
Place**:** Warangal.

DECLARATION

This is to certify that the work presented in the thesis entitled **" FLUID FLOW AND HEAT TRANSFER IN A RECTANGULAR GEOMETRY WITH/WITHOUT SUCTION/INJECTION "** *is a bonafide work done by me under the supervision of* ***PROF. J.V. RAMANA MURTHY*** *was not submitted elsewhere for the award of any degree.*

I declare that this written submission represents my ideas in my own words. Where-ever others' ideas or words have been included. I have adequately cited and referenced the original sources. I also declare that I have adhered to all principles of academic honesty and integrity and have not misrepresented or fabricated or falsified any idea / data / fact /source in my submission. I understand that any violation of the above will be a cause for disciplinary action by the Institute and can also evoke penal action from the sources which have thus not been properly cited or from whom proper permission has not been taken when needed.

PAVANKUMAR REDDY M

Roll No. 716185

Date: _____

Dedicated to

My Parents, Wife, Children, Guru

&

Lord Ganesha

ACKNOWLEDGEMENTS

I gratefully acknowledge my Supervisor, **Prof. J.V. Ramana Murthy**, Department of Mathematics, National Institute of Technology Warangal–506004, India, for his guidance, time, patience, invaluable discussions, continuous support and constant encouragement throughout the preparation of the thesis. With great patience and his insight, he has mentored me in developing my research abilities, critical thinking, and research writing skills at every stage of my research work. He inspired and motivated me, first for pursuing research and then encouraged me to work on this particular field. Without him, it would not have been possible to achieve this work. I also thank his wife **Smt. J. Prasanna Ramana Murthy** for her hospitality and her patience during our elongated discussions.

I wish to thank **Prof. D. Srinivasacharya**, Head of the Department and member of the Doctoral Scrutiny Committee, Department of Mathematics, for his constant moral support and encouragement at every stage.

I extended my sincere thanks to the members of the Doctoral Scrutiny Committee, **Prof. R.L.N. Sai Prasad,** Department of Physics, **Prof. K.N.S.K. Viswanadham,** Professor, Department of Mathematics for spending their valuable time in providing suggestions, feedback, and support while reviewing the progress of my work.

I take this opportunity to express my thanks from the bottom of my heart to the dynamic personality, (Late) **Prof. T. K. V. Iyengar**, Retired Professor, Department of Mathematics, **Prof. G. Radhakrishnamacharya (Retd.), Prof. Y. N. Reddy, Prof.**

D. Dutta, Dr. P. Muthu, Dr. A. Benarji Babu, Dr. H. P. Rani, Dr. R. S. Selvaraj, Dr. T. Kurmayya, Dr. J. Pranitha, Dr. Ch. Ram Reddy, Dr. D. Bhargavi, Dr. E. Satyanarayana, Dr. Y. Sreenivasa Rao and non teaching staff of the Department for their valuable suggestions, support and timely help.

I thank Prof. **N. V. Ramana Rao**, Director, National Institute of Technology, Warangal.

I also express my thanks to my co-research scholars **Dr. J. Sharath Kumar Reddy, Mr. N.V. Koteswar Rao, Mr. G. Shiva Kumar Reddy,** and other scholars for their suggestions, technical help and encouragement during my research period. Also express my thanks to my best friends **Mr. B. Sharath Babu, Mr. P. Ranjith Kumar, Mr. R. Maheswar, Mr. G. Mahesh** and all other friends for their continuous support, encouragement to do this research work.

I express my sincere thanks to **Dr. G. Srinivas Reddy**, Secretary, Sree Vaageswari Educational Society and **Dr. A. Anjaneyulu**, Former Principal of Vaageswari Engineering College for grateful support and encouragement for pursuing my Ph.D. I gratefully acknowledge the management members of **Sree Vaageswari Educational Society**, Karimnagar, for their extended support and encouragement for carrying out my Ph.D. work.

I thank my well wishers **Dr. K. Phaneendra, Dr. G.B.S.L. Soujanya, Mr. D. Anji Reddy** and **Mr. M. Mukunda Reddy** for their continuous support, encouragement to do this research work.

There are no words to express my sincere gratitude to my parents **Sri. Raji Reddy** and **Smt. Vijaya**, my wife **Smt. Swathi**, loving children **Chi. Srivardhan Reddy** and **Chi. Srimayi Reddy** and all my family members, who supported me a lot

throughout my academic career. Your's love and affection are the most important part of my life, which always encourages me to bravely chase my dream. Finally, I would like to take this opportunity to extend my heartfelt thanks to my father in law **Sri. Raghupathi Reddy**, mother in law **Smt. Padma** for their continuous support, encouragement cooperation to do this research work.

Finally, I bow down before the almighty that has made everything possible.

PAVANKUMAR REDDY M

ABSTRACT

The study of fluid flow and heat transfer is very important in micro reactor channels, filtration units and in membrane reactor ducts. It is important in Nuclear waste management and to determine residence time distributions in the process of drying of solids in fluidized beds and in cooling devices. In chemical engineering, there are major applications on laminar flow in channels. The effect of suction/injection over the walls in the flow field is encountered in filtration units, micro reactor channels, membrane reactor ducts and in fuel cell manifolds.

The objective of the present studies is to investigate the two dimensional flow and the heat transfer due to laminar flow convection in a rectangular channel with suction on neighboring and opposite walls when (i) the fluid is a viscous fluid, (ii) the fluid is Couple stress fluid and (iii) a circular cylinder is inserted in the channel. Geometry considered in this thesis is a rectangular geometry.

Analytical or numerical solutions have been obtained for flow field in the above geometry under the cases: (i) Fluid is Newtonian and viscous, (ii) Fluid is couple stress fluid, (iii) Flow is along the axial direction of the channel, (iv) Flow is due to suction/injection in the plane perpendicular to the channel and (v) A cylinder is inserted in the flow.

The values of the parameters characterizing the different problems are taken as follows. Reynolds number Re=0.5, 1, 5, 10, 20 and 30. Suction parameter: V_0= 0.2, 0.5, 0.8, 2, 5, 10, 50, 100 and 200. Peclet number: Pe = 0.001, 0.005, 0.01 and 0.02.

Prandtl number Pr=0.71, 1 and 10. Brinkman number: Br = 0.4 and 0.8. Hartmann number M=1, 3, 5 and 7. Couple stress parameter S=1, 10, 20, 30 and 50.

The thesis consists of Five parts and nine chapters. Part - I and Chapter one is introductory in nature. Part – II is devoted to viscous fluid flows in a rectangular channel with adjacent wall suction and contains Three chapters (Chapters two to four). Part – III is devoted to Couple stress fluid flows in a rectangular channel with/without suction and contains Two chapters (Chapters five and six). Part – IV is devoted to Stokes flows past a circular cylinder in a square cavity with adjacent and opposite wall suction and contains Two chapters (Chapters seven and eight). Part–V and Chapter nine gives concluding remarks of the thesis and possible directions in which further work can be carried out.

In all these chapters, the expressions for the stream function, temperature, entropy generation number, Bejan number, heat function and pressure for viscous fluids and velocity field and temperature for Stokes flow past cylinder and for Couple-stress fluids are obtained. The Volumetric flow rate and Skin friction is derived analytically and the effect of physical parameters like Reynolds number, Magnetic parameter and Couple stress parameter on the Volumetric flow rate and Skin friction are studied graphically. The effect of Reynolds number and suction parameter on stream lines, isothermal lines, entropy generation number, Bejan number, heat lines and pressure are studied.

NOMENCLATURE

a	length of the rectangular cross section along X–Direction
b	length of the rectangular cross section along Y–Direction
a,b,c,d	Distances in the stencil from (i, j) to the neighbouring points
Be	Bejan Number $\left(= \frac{N_h}{N_h + N_f} \right)$
Br	Brinkman Number $\left(= \frac{\mu V_1^2 T_0}{2k(T_2 - T_1)^2} \right)$
C_f	Skin friction
c_p	Specific heat, J/g °C
c	Cross viscosity parameter or coupling number
D	Differential operator with respect to y
D_1	Differential operator with respect to x
e	Ratio of Couple Stress Viscosities Parameter
$\mathbf{H}$	Magnetic intensity vector
H^*	Dimensional Heat function
H	Non–Dimensional Heat function
H_0	Magnitude of constant magnetic field
h	Length of the interval
$\mathbf{I}$	Identity Matrix (Tensor)
$\mathbf{J}$	Electric current density vector
k	Thermal conductivity, W/(m. K)
$\mathbf{M}$	Couple stress tensor

M	Magnetic parameter $\left(= \sqrt{\frac{\sigma H_0^2 a^2}{c\mu}} \right)$
Nu	Nusselt number
N_s	Non–Dimensional Entropy generation number
N_h	Non–Dimensional Entropy generation number due to heat transfer
N_f	Non–Dimensional Entropy generation number due to fluid friction
P	Dimensional Pressure
p	Non–Dimensional Pressure, kg $m^{-1}s^{-2}$
Pe	Peclet Number $\left(= \frac{\rho c_p V_1 a}{k} \right)$
Pr	Prandtl Number $\left(= \frac{c_p \mu}{k} \right)$
$\mathbf{Q}$	Dimensional Velocity (U, V, W)
q	Geometric ratio
Q_1, Q_2	Dimensional heat flux on the walls
q_1, q_2	Non–Dimensional heat flux on the walls
Re	Reynolds number $\left(= \frac{\rho V_1 a}{\mu} \right)$
S	Couple stress parameter $\left(= \frac{\mu a^2}{\eta} \right)$
$\bar{S}_{gen}$	Dimensional Entropy Generation Number
$\bar{S}_{gen,\, ht}$	Dimensional Entropy Generation Number due to heat transfer
$\bar{S}_{gen,\, ff}$	Dimensional Entropy Generation Number due to fluid friction
$\mathbf{T}^*$, $\mathbf{T}$	Dimensional and Non–Dimensional Stress Tensor
T	Dimensional Temperature

T_1, T_2	Constant wall Temperatures
T_0	Reference Temperature (=0.5(T_1+T_2))
U, u	Dimensional and Non–Dimensional velocities in X–Direction
U_0	Suction velocity for couple stress fluids
V, v	Dimensional and Non–Dimensional velocities in Y–Direction
V	Volumetric flow rate, m^3/s
V_0	Suction Parameter $\left(= \frac{V_2}{V_1} \right)$
V_1	Injection Velocity at the wall
V_2	Suction Velocity at the wall
W, w	Dimensional and Non–Dimensional velocities in Z–Direction
W_0	Average entrance velocity
X, Y,Z	Dimensional coordinates
x, y, z	Non–Dimensional coordinates
y_0	Geometric Parameter $\left(= \frac{b}{a} \right)$

Greek Symbols

∇_0, ∇	Dimensional and Non–Dimensional Gradient Operator
∇_0^2, ∇^2	Dimensional and Non–Dimensional Laplace Operator
ΔT	$T_2 - T_1$
ε	Maximum Limit of the error in calculation of ψ
Ψ, ψ	Dimensional and Non–dimensional Stream Functions
θ	Non–dimensional Temperature
ρ	Fluid Density

μ	Coefficient of viscosity
$\eta,\ \eta'$	Couple stress viscosities
ζ	Vorticity Function
σ	Electrical conductivity

Contents

Part – I

INTRODUCTION

Chapter 1

INTRODUCTION

1.1 Introduction

The history of fluid flow is very old and began its existence in the form of laws of buoyance by Archimedes (200BC). Later, one of the early studies is the work of Leonardo Da Vinci's which gave rapid advancement to the study of fluid mechanics about 500 years ago, but earlier than this time; prehistoric relics of irrigation canals have shown that the study of fluid behaviour were much more available by the time of ancient Egyptian (Nakayama and Boucher, 1999). In 18^{th} century Johann and Jacob Bernoulli brothers began more modern understanding of fluids motion and elasticity and developed Bernoulli's equation. Since then, many researchers have done numerous work on fluid mechanics. Fluid Mechanics can be described as the study of the flow behaviour of the fluid under external body forces or pressure or body motions. It involves application of the fundamental laws encountered in Physics. The laws are Newton's laws of linear momentum principle, conservation of mass, first law of thermo-dynamics. Studying the behaviour of fluids is an essential part in the analysis of fluid flow models, it is needed in order to understand various problems ranging from the study of blood flow in the capillaries to the flow of crude oil across Niger-Delta of Nigeria. Fluid mechanics principles are required to explain why airplanes are made with smooth surfaces for the most efficient flight, while in the other way golf balls are made with rough surfaces to improve their efficiency.

Fluids consist of liquid or gas (or vapour) phases of the physical forms in which matter exists. The distinguishing feature between a fluid and the solid state of matteris seen by comparing fluid and solid behaviour. Under the application of a shear stress, solids deform, but its deformation does not increase with time (Fox, McDonald and Pritchard, 2004) whereas a fluid deforms continuously (Rajput, 2004). Fluid can be defined as a substance that flows with negligible resistance to a change of shape. This implies that a fluid isa material that continuously deforms under the application of shear stress of even for a small magnitude. A shear stress (force acting per unit area) is a tangential force acting on a surface of the material.

1.2 Heat Transfer

The laws that are governing heat transmission are very important to the engineers in the construction, design, testing and operation of heat exchangers. Whenever there exists a temperature difference in a medium or between media, heat transfer occurs. Heat transfer occurs in three modes: conduction, convection and radiation.

In conduction, heat is transferred from one particle to the other particle through the material without the actual motion of the particles. If a steel rod is heated at one end, the molecules near the hot end vibrate (but do not move) with higher amplitude (kinetic energy) and transfer the heat energy to the adjacent molecules and so on. However, mean positions of the molecules in equilibrium does not change. Heat transfer by conduction is most common in the case of solids. The property of transmission of heat has been used in Davy's safety lamp. Materials such as brick walls, granite etc. having less conductivity are utilised in the construction of a cold storage, furnace of a boiler etc. The space between the two walls of a thermos flask is evacuated because vacuum is a poor conductor of heat. The air enclosed in the woollen fabric helps in protecting us from cold, because air is a poor conductor of heat.

In convection heat is transferred from one point to the other by the actual movement of the fluid particles carrying heat. This convection process is most common in the case of gases and liquids. Convection is the main cause for formation of land and sea breezes and trade winds. It plays a vital role in gas filled electric lamps, ventilation, and heating of buildings by hot water circulation.

In Radiation heat is transferred from one point to the other directly without the presence of the carrying medium. From the sun, we heat radiations directly through vacuum without the help of any medium. The properties of heat radiation are similar to light radiations and also form a part of the spectrum in electromagnetic waves.

Heat radiation and mass transfer play a vital role in production industries in the design of nuclear power plants, fins, steel rolling, combustion and furnace design, materials processing, food processing and cryogenic engineering, gas turbines and various propulsion device for aircraft, energy utilization, temperature measurements, remote sensing for astronomy and spaceexploration, in a number of applications related to

health, agricultural and military. If the surrounding fluid temperature is very high, radiation effects play a prominent role and this phenomena does occur in space technology. In such situations, an account of the combined effect of thermal radiation and mass diffusion is to be taken.

Various modes of electromagnetic radiation occur through various mechanisms. For example, in nuclear reactions gamma rays are produced, by the bombardment of metals with high-energy electrons X-rays are produced, microwaves by special types of electron tubes such as klystrons and magnetrons, and radio-waves are produced by the excitation of some crystals or by the flow of alternating current through electric conductors.

The short-wave length rays like gamma rays and X-rays are of importance to nuclear engineers. The long-wave length rays like radio-waves and microwaves are of importance to electrical engineers. The type of electromagnetic radiation that is pertinent to heat transfer is the thermal radiation emitted as a result of energy transitions of molecules, atoms and electrons of a substance. The power or intensity of these activities is realised through the measure of temperature at the microscopic level, and the rate of thermal radiation emission increases with increasing temperature. Thermal radiation is continuously emitted and absorbed by all matter at critical temperatures. This means that every substance around us such as walls, furniture and our friends continuously emits and absorbs radiation. Thermal radiation is contained in the electromagnetic spectrum that extends from about 0.1 to 100μm, since the radiation emitted by surfaces due to their temperature falls in this range of wave lengths. Hence, thermal radiation contains the entire visible and infrared (IR) radiationas well as a portion of the ultraviolet (UV) radiation.

The heat transfer by convective mode occurs in two basic processes: natural convection and forced convection. In natural convection heat transport in the fluid flow is not due to any external source but only due to differences in the density of fluid by temperature gradient. The fluid receives heat from the surrounding heat source and becomes light in density and rises up. The fluid which is cooler is of high density then flows down to replace it. This cooler fluid is then heated and the process continues, forming convection current; In this way the energy in the form of heat is transferred from the bottom of the convection cell to top. In natural convection, the

driving force is the buoyancy which arises due to the differences in fluid density. Because of this, the presence of a proper acceleration arises from resistance to gravity, or an equivalent force (arising from acceleration or centrifugal force), is essential for natural convection. Forced convection occurs when the fluid is forced to flow over the surface by external agency such as fans and pumps. It is created artificially by induced convection current.

Internal and external flow can also classify convection. Internal flow occurs when the fluid is enclosed by a solid boundary such as a flow through a pipe. An external flow occurs when the fluid extends indefinitely without encountering a solid surface. Both these convections, either natural or forced, can be internal or external as they are independent of each other.

To determine the load on air-conditioning plants and refrigerating equipment, the knowledge of the quantity of heat transfer due to natural convection is absolutely necessary. In the design of the insulation thickness of transmitting wires and insulation thickness of stream carrying pipes and furnaces, the free convection plays an equally important role.

1.3 Viscosity

Viscosity can be considered as a measure of the resistance of a fluid that flows due to shear stress or tensile stress. Viscosity is literally "thickness" or "internal friction" of the fluid. Hence, water is referred to as "thin", with a lower viscosity, while honey is considered as "thick", with high viscosity. Putting it in simple way, the lesser the viscosity of the fluid is, the higher its ease to flow (Symon R. Keith, 1971). Viscosity explains the internal resistance of a fluid to flow and may thus be considered as a measure of fluid friction. For illustration, felsic magma having high-viscosity creates a steep and tall stratovolcano, because it takes very long time to cool due to its high viscosity, where as mafic lava due to its low-viscosity forms a shallow-sloped and wide shield volcano. All natural (or real) fluids (excepting super fluids) are having some resistance to the external stress and therefore are treated as *viscous*, but a fluid that offers no resistance to shear stress is considered as an *ideal fluid* or *inviscid fluid*.

1.4 Couple Stress Fluid

In continuum mechanics, fluid particles may have size-effect within the flow and this is neglected. In Newtonian flows negligence of rotational interaction among particles results to symmetrical nature of force-stress tensor. However, in the very important cases like fluid containing suspended particles, this is not true (i.e., stress tensor is not symmetric). Hence, the theory that explains couple stresses is required. The spin field due to micro-rotation of freely suspended particles sets up an anti-symmetric stress, which is called couple-stress, and thus this leads to the foundation of couple-stress fluid theory.

The theory of fluids with Couple stresses was introduced by Stokes (1966), it has special features like the existence of couple stresses, body couples and non-symmetric stress tensor. The important feature of couple stress is the introduction of size-dependent effect. According to Sunil et al. (2002), couple stresses appear in fluids with very large molecules. Examples of such fluids include various types of lubricants with small amount of polymer additives, blood, electro-rheological fluids, synthetic fluids, etc.

Several authors have discussed various aspects of couple stress fluid under different flow configurations. For example Srivastava (1985) investigated the flow of couple-stress fluid through stenotic blood vessels. Zakaria (2002) investigated hydro-magnetic oscillating flow of a couple stress fluid in the porous medium. Rudraiah and Chandrashekara (2010) presented couple stress effects on the growth rate of Rayleigh-Taylor instability in a small thickness region of couple stress fluid at the interface. Devakar and Iyengar (2010) considered the run up flow of a couple stress fluid in between two parallel plates, while Srinivasacharya and Kaladhar (2012) presented the analytical solution of free and forced convection flow of a couple stress fluid in between annular circular cylinders taking into the effects of ion-slip and Hall currents. Furthermore, Rani et al. (2011) took up numerical investigation of couple stress fluid flow in between two vertical cylinders of infinite length. Double diffusive mixed convection in couple stress fluids with variable fluid properties was analysed by Dinesh et al. (2015).

The analysis of couple stress fluid flows is important to study in many industrial processes like the extraction of polymer fluids, solidification of liquid crystals, suspensions fluids in polymers (Lin and Hung, 2007), polymer-thickened oils and physiological fluid mechanics (Shehawey and Mekhemer, 1994). Application of couple stress fluids are equally found in synovial joints (shoulder, hip, knee and ankle) (Walicki and Walicka, 1999), tribology of thrust bearings (Naduvinamani and Patil, 2009) and the lubrication of engine rod bearings (Lahmar and Bou-Sad, 2008), geophysics, chemical engineering and astrophysics. Walicki and Walicka (1999) and Kumar et al. (2015) modelled synovial fluids as couple stress fluids in human joints because of the long chain of lauronic acid molecules found as additives in synovial fluid.

1.5 Magneto-hydrodynamics

The study of fluid flows which are electrically conducting is termed as magneto-hydrodynamics (MHD). Magneto means magnetic field, hydro means fluids and dynamics mean forces and the laws of motion. Magneto-hydrodynamics (MHD) is the mathematical model for the low frequency interaction that exists between electrically conducting fluids and electro-magnetic fields (Schnack, 2009). In other words, magneto-hydrodynamics can be described as the study of the interaction between magnetic fields and moving, conducting fluids (Dawson, 2001). Other terms used to describe MHD include magneto fluid dynamics or hydro-magnetics. Examples are liquid metals (such as mercury, gallium, molten magnesium, molten antimony, liquid sodium etc.), plasmas (ionized gases or electrically conducting gases) such as the solar atmosphere and salt water or electrolyte.

The fundamental concept behind MHD is that the relative movement of a conducting fluid and a magnetic field causes an electromotive force to develop, this will induce electrical currents with density of order $\sigma(u \times B)$, where σ is the electrical conductivity, B is the magnetic field and u is the velocity field. The currents will give rise to another induced magnetic field which is added to the original magnetic field and the fluid appears to flow along with magnetic field lines. The combined magnetic field (i.e., both the imposed and induced) then interacts with the induced current density, J, giving rise to a Lorentz force (per unit volume), $J \times B$. This acts on the conductor and it is directed so as to impede the relative movement of the magnetic

field and the fluid. In the description above, it is observed that fluid can “drag” magnetic field lines while magnetic fields can pull on the conducting fluids, this partial “freezing together” of medium and the magnetic field is referred to as MHD. The interest to explore MHD came as a result of three technological innovations.

(i) Fast-breeder reactors which use liquid sodium as a coolant and this needs to be pumped,

(ii) Controlled thermonuclear fusion requires that the hot plasma be confined away from material surfaces by magnetic forces and

(iii) MHD power generation, in which ionized gas is propelled through magnetic field, was thought to offer improved power station efficiencies.

1.6 Literature Survey

The study of fluid flow and heat transfer is very important in micro reactor channels, filtration units and in membrane reactor ducts. It is important in Nuclear waste management and to determine residence time distributions in the process of drying of solids in fluidized beds and in cooling devices. In chemical engineering, there are major applications on laminar flow in channels. The effect of suction/injection over the walls in the flow field is encountered in filtration units, micro reactor channels, membrane reactor ducts and in fuel cell manifolds. The viscous fluid flow in parallel plate channels generated due to suction/injection at the walls was first studied by Berman (1953). Experimental results of paper preparation were analyzed Mathematically by Taylor (1956). Pan and Acrivoas (1967) and Shankar (1993) presented analytical solutions for the Stokes flow in a two-dimensional cavity of rectangular section. Shankar (1993, 1997, 1998) presented analytical solutions for stream function for Stokes flow in a cavity and analysed eddy structures. He obtained solution for Circular cylindrical cavity flow due to motion of end walls at the top and bottom. Shankar and Deshpande (2000) presented a extensive review of flows in a cavity and discussed in detail about corner eddies, longitudinal vertices, Poincare sections and turbulence. Many researchers (Hwang and Cheng (1993), Song and Sundmacher (2010), Cheng and Hwang (1994), Chabani et al. (2017), Ahmed Bahlaoui et al. (2014)) have attempted the viscous flow in a rectangular tube with suction at the opposite walls. Natural and mixed convection flows in a cavity were

investigated Numerically using FDM second order schemes by Sivasankaran et al. (2010) and Sheremet et al. (2015).

The couple stress fluid theory developed by Stokes (1966) has distinct features, such as the presence of couple stresses, body couples and non-symmetric stress tensor. The couple stress fluids are capable of explaining the behaviour of various types of lubricants, blood, suspension fluids, liquid crystals etc. The theory of couple stresses defines the rotational field in terms of the velocity field itself. In couple stress fluid theory, the only unknown vector field of velocity is governed by a single vector differential equation analogues to the classical Navier Stokes equation, but with an increased order.

Magnetic flow in a rectangular channel is a classical problem that has significant applications in magneto hydrodynamic power generators and pumps *etc*. Nowadays, magnetic field has earned great value due to wide spread applications in industry and bioengineering, such as electrostatic precipitation, power generators, petroleum industry, aerodynamic heating, the purification of molten metals from non-metallic materials, polymer technology and fluid droplet sprays. Hartmann (1937) was the first person to obtain a solution for this type of flows to compare with his experimental results on mercury. Hartmann and Lazarus (1937) studied the impact of a transverse uniform magnetic field on the flow of a viscous incompressible electrically conducting fluid between two infinite parallel stagnant and insulating plates.

Stokes flow generated within rectangular shaped cavities is a feature encountered in several manufacturing processes. Examples include coating systems (Higgins, 1982 and Aidun et al.,1991), polymer melts (Canedo and Denson, 1989) and ceramic tape casting (Hellebrand, 1996). The motion of a fluid past a cylindrical obstruction with its longitudinal axis aligned normal to the approaching flow has practical importance and is of fundamental interest. Bluff body cross–flow configurations arise in several industrial applications and environmental settings, including: the passages in equipments used for heat and mass transfer processes; the cooling of electronic components and equipment; flow-metering devices; moving ground vehicles; the obstructed spaces between co–rotating disks in magnetic disk storage devices; tall buildings and structures such as cooling towers, chimneys, offshore oil rigs and electrical pylons. The hydrodynamic forces and flow characteristics of laminar fluid

flow past a stationary isolated cylinder have been analysed by many researchers like Williamson, (1989); Henderson, (1995, 1997); Norberg (2003); Baranyi and Lewis (2006).

In the past for many years, heat transfer by convection was studied by examining temperature field and first law of thermodynamics. Nowadays emphasis on design of a model is developed as a science. Hence a deeper study of the subject is necessary. The study of flow lines, temperature and heat flow lines together with second law of thermodynamics are important, since by this one can know the regions of available energy or useful energy and regions of dissipation of energy.

1.7 Scope and Objectives

The objective of the present thesis is to study the two dimensional flow of fluids and the heat transfer due to convection occurring in a rectangular channel when suction and injection is applied on a) neighboring walls and b) opposite walls in the cases when

i) the fluid is a viscous fluid

ii) the fluid is Couple stress fluid

iii) a circular cylinder is inserted in the channel.

Geometry considered in this thesis is a rectangular geometry.

1.7.1 Description of the Geometry and Governing equations

The two-dimensional governing equations for steady, incompressible and laminar flows of viscous fluids

Continuity equation: $\nabla.\mathbf{Q} = 0$

Momentum equation: $\rho \frac{d\mathbf{Q}}{dt} = -\nabla P + \mu \nabla^2 \mathbf{Q}$

Energy equation: $\rho c_p \frac{dT}{dt} = k \nabla^2 T$

The two-dimensional governing equations for steady, incompressible and laminar flows of couple stress fluids with body force due to applied magnetic and electrical fields are

Continuity equation: $\nabla.\mathbf{Q} = 0$

Momentum equation: $\rho\mathbf{Q}.\nabla\mathbf{Q} = -\nabla P + \mu\nabla^2\mathbf{Q} - \eta\nabla^4\mathbf{Q} + \mathbf{J}\times\mathbf{H}$

Energy equation: $\rho c_p U_0 \frac{dT}{dX} = k\nabla^2 T$

where **Q**, *P*, **J**, **H** and *T* are usual symbols for velocity, pressure, electric current, magnetic intensity and temperature. The Cartesian coordinate system with origin at the bottom left corner and *X* and *Y* axes along the walls is taken. The tube is of length *a* and height *b*. Injection with velocity V_1 at the wall *Y*=*b* and suction with velocity V_2 at the wall *X*=*a* are imposed. The flow is developed because of the suction and injection. Velocity of fluid satisfies impermeability condition and no slip condition on walls *X*=0, *Y*=0 and suction and no slip condition at the permeable walls *X*=*a* and *Y*=*b*. The temperature field satisfies constant heat flux at the permeable walls *X*=*a* and *Y*=*b* and constant temperature is maintained on the impermeable walls *X*=0, *Y*=0. Due to no slip condition on the all walls the tangential velocities are zero.

Analytical or numerical solutions have been obtained for flow and temperature fields in the above geometry under the following cases:

1. Fluid is Newtonian viscous.
2. Fluid is couple stress fluid.
3. Flow is along the axial direction of the channel
4. Flow is due to suction/injection in the plane perpendicular to the channel.
5. A cylinder is inserted in the flow.

The values of the parameters characterizing the different problems are taken as follows. Reynolds number *Re*=0.5, 1, 5, 10, 20 and 30. Suction parameter: V_0= 0.2, 0.5, 0.8, 2, 5, 10, 50, 100 and 200. Peclet number: *Pe* = 0.001, 0.005, 0.01 and 0.02. Prandtl number *Pr*=0.71, 1 and 10. Brinkman number: *Br* = 0.4 and 0.8. Hartmann number *M*=1, 3, 5 and 7. Couple stress parameter *S*=1, 10, 20, 30 and 50.

1.8 Applications

The study of fluid flow and heat transfer is very important in Nuclear waste management and to determine residence time distributions in the process of drying of solids in fluidized beds and in cooling devices. In chemical engineering, there are major applications on laminar flow in channels. The effect of suction/injection over the walls in the flow field is encountered in

- filtration units
- micro reactor channels
- membrane reactor ducts
- fuel cell manifolds.

The viscous fluid flow in parallel plate channels generated due to suction/injection at the walls was first studied by Berman (1953).

1.9 The boundary conditions on Velocity and Temperature

1.9.1 No-slip condition:

The No-slip boundary condition implies that the fluid particles in contact with a surface will have the same velocity as the velocity of the surface. Often the boundary walls are not moving and hence the fluid velocity is zero. In drag flows, the boundary wall velocity is finite and hence the fluid velocity is equal to the wall velocity.

1.9.2 Uniform wall heat flux/ Uniform wall temperature conditions:

The most usual temperature boundary conditions consist one of the following assumptions:
The heat flux is uniform on the wall. In this case, the boundary condition is written as

$$\left(\frac{\partial T}{\partial n}\right)_{wall} = Q$$

The solid wall is at uniform temperature: $T = T_w$.

1.9.3 Hyper-stick condition:

For couple-stress fluids, Along tangential direction $\bar{t}$ on the wall: $\frac{1}{2}\nabla \times \mathbf{Q}.\,\bar{t} = 0$.

1.10 Planning of the Thesis

The thesis is divided into FIVE parts**.**

PART–I

This part consists of only one chapter.

Chapter 1

Introduction and literature study for the present research study are given. Brief survey on fluid flow and heat transfer in ducts with suction is given. Numerical schemes used in thesis are described.

PART–II

This part consists of three chapters.

Chapter 2

Heat flow in a rectangular plate

Steady-state temperature distribution in a rectangular plane sheet with non-homogeneous boundary conditions is solved using Fourier series. The results are compared with the numerical results. For different values of geometric ratio, the isothermal curves are obtained.

Form this chapter, we observed that finding analytical solution is not easy for this type of problems. So, we considered numerical method for obtaining solution to this kind of problems in subsequent chapters in this part.

Chapter 3

Stokes Flow and Heat Transfer by Heat Function and Entropy Generation in a Rectangular Channel with Suction.

A viscous fluid flow is generated in a rectangular channel of uniform cross section by applying suction/ injection at the adjacent side walls. The other opposite side walls are maintained at constant temperatures and the walls with suction are maintained at constant heat flux. The flow is assumed as Stokes flow and non-linear convective terms are neglected. The stream lines due to the flow and isothermal lines and heat

function contours are drawn. The regions of high friction are found by plotting entropy generation number and Bejan number. The regions of low and high pressures are also drawn. The 13 point formula is used to solve the biharmonic equation (convective term is neglected) for stream function and 5 point formula is used to solve for all other harmonic equations. For derivative boundary conditions, central difference formula with fictitious nodes is used. It is observed that corner points are regions of high energy dissipation points. Least dissipation of energy is near to the wall where non-dimensional temperature is 1.

Chapter 4

Entropy Analysis for Heat Transfer in a Rectangular Channel with Suction

Chapter 4 deals with the heat transfer in a rectangular channel with suction applied at the adjacent two side walls. A two dimensional laminar viscous fluid flow is generated due to the application of suction/injection. The other opposite two sides are kept at constant temperatures and the walls with suction are maintained at constant heat flux. The stream lines thus obtained due to the flow and isothermal lines and heat function are analyzed. The regions of high and low frictions are found by drawing contours of entropy generation number and Bejan number. Expressions for the heat transfer coefficient, Nusselt number is also derived. The 4^{th} order Partial Differential equation for stream function is numerically solved by FDM using 13 point formula and 5 point formula is used to solve for all other harmonic equations for temperature, heat function and pressure. For derivative boundary conditions, central difference formula with fictitious nodes is used. In the analysis, we note that corner points are regions of high energy dissipation. Least dissipation of energy is near to the wall where non–dimensional temperature is 1. This chapter analyses the heat transfer in the rectangular channel through heat function and Entropy generation number.

PART–III

This part consists of two chapters

Chapter 5

Steady Flow of Couple Stress Fluid through a Rectangular Channel Under Transverse Magnetic Field

Chapter 5 deals with the steady and an incompressible conducting couple stress fluid flow in the presence of transverse magnetic field through a rectangular channel with uniform cross–section. The induced magnetic field is neglected. We consider the case that there is no externally applied electric field. Under these conditions, we get 4^{th} order PDE for velocity *w* along the axis of the rectangular tube. The usual no slip and hyper stick boundary conditions are used to obtain the solution for *w*. We obtained the velocity *w* in terms of Fourier series. Skin friction on the walls and volumetric flow rate are obtained in terms of physical parameters like couple stress parameter and Hartmann number. The effects of these parameters on skin friction and volumetric flow rate are studied through graphs.

Chapter 6

Steady Flow of Couple Stress Fluid through a Rectangular Channel Under Transverse Magnetic Field with Suction on opposite walls

Chapter 6 deals with the steady and an incompressible conducting couple stress fluid flow with suction/ injection at the opposite walls in the presence of transverse magnetic field through a rectangular channel with uniform cross–section. The induced magnetic and electric fields are neglected to obtain velocity *w* along the axis of the rectangular tube. The usual no slip and hyper stick boundary conditions are used to obtain the solution for *w*. We obtained the velocity *w* and temperature θ in terms of Fourier series. The volumetric flow rate and skin friction are obtained and the effects of physical parameters like magnetic parameter, Reynolds number and couple stress parameter on this are studied through graphs.

PART–IV

This consists of two chapters.

Chapter 7

Stokes Flow and Heat Transfer Past a Circular Cylinder in a Square Cavity with Suction/Injection on Adjacent Walls.

A laminar viscous fluid flow is generated past a circular cylinder placed in a square cavity of uniform cross section by applying suction/ injection at the adjacent side walls. The other opposite side walls and the boundary of the cylinder are maintained at

constant temperatures and the walls with suction are maintained at constant heat flux. The stream lines due to the flow and isothermal lines are drawn. The flow is assumed to be Stokesian. The biharmonic equation for stream function is solved by writing into two coupled equations and 5 point formula is used to solve the equations. For derivative boundary conditions of stream function, central difference formula with fictitious nodes and for derivative boundary conditions of temperature 3 point backward difference formula are used.

Chapter 8

Stokes Flow and Heat Transfer Past a Circular Cylinder in a Square Cavity with Suction/Injection on Opposite Walls.

A laminar viscous fluid flow is generated past a circular cylinder placed in a square cavity of uniform cross section by applying suction/ injection at the opposite side walls is considered. The other opposite side walls and the boundary of the cylinder are maintained at constant temperatures and the walls with suction are maintained at constant heat flux. The stream lines due to the flow and isothermal lines are drawn. The flow is assumed to be Stokesian. The biharmonic equation for stream function is solved by writing into two coupled equations and 5 point formula is used to solve the equations. For derivative boundary conditions of stream function, central difference formula with fictitious nodes and for derivative boundary conditions of temperature 3 point backward difference formula are used.

PART - V

This consists of a single chapter.

Chapter 9

Finally, chapter ten concentrates on the overall conclusions drawn with references to the problems discussed in the thesis. We also indicate the direction for possible future work.

Part – II

VISCOUS FLUID FLOWS

Chapter 2

Heat Flow in a Rectangular Plate

2.1 Introduction

Steady state temperature distribution in a rectangular plane sheet with non-homogeneous boundary conditions is solved by using Fourier series. The results are compared with the numerical results. For different values of geometric ratio, the isothermal curves are obtained.

The problem of steady state temperature distribution is classical and very old, since the time of Laplace (1787, 1832). Crank (1975) in his treatise on Mathematics of diffusion theory has discussed some typical problems with homogeneous boundary conditions. The related problems involving Laplacian equation in flow through channels of uniform cross-section were discussed by Langolois and Deville (2014). Recently analysis of heat flow in microchannels by theoretical and experimental studies is increasing due to their wide applications (Van Male et al. (2004), Shokouhmand et al. (2007), Khan et al. (2008), Mirmanto et al. (2012)). Lee et al. (2005) presented the experimental study of heat flow in rectangular microchannels. Schmith and kandlikar (2005) have discussed the pressure drop in a microchannel. The problem of solving steady state temperature when non-homogeneous derivative boundary conditions are given, though classical, is not attempted by many analytically. Here our aim is to solve this problem. The results of our problem are matched with the results of steady state diffusion problem of Crank (1975, Pages 65–66) when in the problem $q_2 = 0$, $T_2 = 0$.

2.2 Mathematical Formulation

Consider the case of conduction of heat in a rectangular plate with the two adjacent sides maintained at constant temperatures and with other two adjacent sides maintained at constant heat flux. The plate is insulated on the top and bottom surfaces so that heat will not escape. To find the temperature profiles in the plate, the Cartesian coordinate system is selected with origin at the left bottom corner of the plate with X and Y axes along the sides of the plate. The plate has sides of length a and b along X and Y directions. The temperature profiles in the plate follow heat conduction equation in steady state as given by

$$\nabla^2 T = 0 \tag{2.1}$$

subjected to the boundary conditions:

$$T=T_1 \text{ on } X=0;\ T=T_2 \text{ on } Y=0;\ \ k\frac{\partial T}{\partial X} = -Q_1 \ \text{ on } X=a \text{ and } \ k\frac{\partial T}{\partial Y} = -Q_2 \ \text{ on } Y=b \tag{2.2}$$

where T is the temperature in the plate at a point (x, y), k is the coefficient of thermal conductivity and Q_1, Q_2 are heat fluxes imposed on the sides. The first two conditions in (2.2) are for constant temperatures and the last two conditions of (2.2) are for constant heat flux. We introduce the following non-dimensional scheme with capital on LHS as physical quantities and small letters on RHS as the corresponding non-dimensional quantities:

$$X=ax;\ Y=ay;\ \ Q_1 = \frac{q_1 k\Delta T}{a};\ \ Q_2 = \frac{q_2 k\Delta T}{a} \ \text{ and } T = \Delta T.\theta + T_1 \text{ where } \Delta T = T_2 - T_1 \tag{2.3}$$

Now we have the non-dimensional equation as

$$\nabla^2 \theta = 0 \tag{2.4}$$

subject to

$$\theta = 0 \text{ on } x=0;\ \theta = 1 \text{ on } y=0; \tag{2.5a}$$

$$\frac{\partial \theta}{\partial x} = q_1 \text{ on } x=1 \text{ and } \frac{\partial \theta}{\partial y} = q_2 \text{ on } y=y_0, \text{ where } y_0=b/a \qquad (2.5b)$$

Though it appears simple, it is difficult to solve (2.4) with conditions (2.5a) and (2.5b), since it involves infinite system of equations. Again this method is useful in solving fluid flow and heat transfer with convection problems.

The solution of the problem can be obtained by two methods as given below. The physical representation of the problem is given in Fig. 2.1.

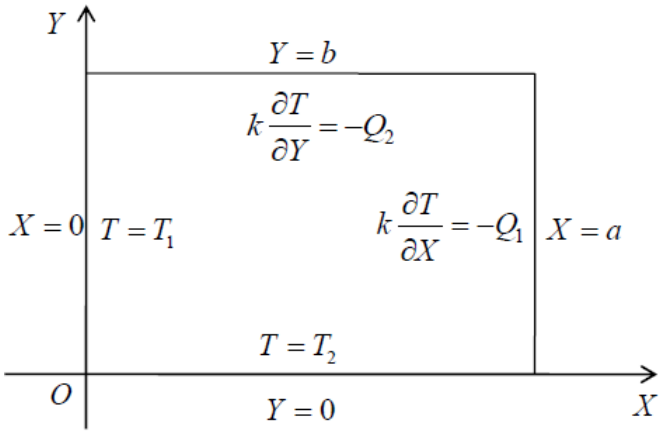

Fig. 2.1: Temperature distribution in a rectangular plate.

2.3 Solution of the Problem

2.3.1 Method 1

We assume the solution in two parts such that the first part satisfies homogeneous conditions on x=0 and x=1 and the second part satisfies homogeneous conditions on y=0 and $y=y_0$. The arbitrary constants in the general solution are adjusted such that the boundary conditions satisfied for the solution. Hence the solution is taken in the form as follows.

$$\theta = \sum_{n=1}^{\infty} \sin(n\pi x)\left[A_n \cosh(n\pi y) + B_n \sinh(n\pi y)\right] + \sin\left(\frac{n\pi y}{y_0}\right)\left[C_n \sinh\left(\frac{n\pi y}{y_0}\right) + D_n \cosh\left(\frac{n\pi y}{y_0}\right)\right] \qquad (2.6)$$

From the condition (2.5a), we get $D_n=0$

and $\sum_{n=1}^{\infty} A_n \sin(n\pi x) = 1$

Expanding $f(x)$ =1 on RHS in half range sine series over $0 \le x \le 1$, we get

$A_n = \frac{4}{n\pi}$ if $n = (2m+1)$ and $A_n = 0$ if $n = 2m$

Again from the condition (2.5b), we have

$$\frac{\partial \theta}{\partial x} = \sum_{n=1}^{\infty} n\pi \left\{ \cos(n\pi x)[A_n \cosh(n\pi y) + B_n \sinh(n\pi y)] + \frac{C_n}{y_0} \sin\left(\frac{n\pi y}{y_0}\right) \cosh\left(\frac{n\pi x}{y_0}\right) \right\} = q_1$$

This implies that

$$\sum_{n=1}^{\infty} n\pi \left\{ (-1)^n [A_n \cosh(n\pi y) + B_n \sinh(n\pi y)] + \frac{C_n}{y_0} \cosh\left(\frac{n\pi}{y_0}\right) \sin\left(\frac{n\pi y}{y_0}\right) \right\} = q_1 \qquad (2.7)$$

Expanding q_1, $\cosh(n\pi y)$ and $\sinh(n\pi y)$ in half range sine series over $0 \le y \le y_0$, we get

$q_1 = \sum_{n=1}^{\infty} A'_n \sin\left(\frac{n\pi y}{y_0}\right)$ which gives that $A'_n = q_1 A_n$ if n is odd and $A'_n = 0$ if n is even.

$$\cos h(n\pi y) = \frac{2}{\pi} \sum_{m=1}^{\infty} \frac{m(1-(-1)^m \cosh(n\pi y_0)}{y_0^2 n^2 + m^2} \sin\left(\frac{m\pi y}{y_0}\right) = \sum_{m=1}^{\infty} c_{n,m} \sin\left(\frac{m\pi y}{y_0}\right)$$

$$\sin h(n\pi y) = \frac{2}{\pi} \sum_{m=1}^{\infty} \frac{m(-1)^{m+1} \sinh(n\pi y_0)}{y_0^2 n^2 + m^2} \sin\left(\frac{m\pi y}{y_0}\right) = \sum_{m=1}^{\infty} s_{n,m} \sin\left(\frac{m\pi y}{y_0}\right)$$

Substituting these above expressions in (2.7) and taking the coefficients of $\sin(n\pi y/y_0)$ we get,

$$\frac{n\pi}{y_0} \cosh\left(\frac{n\pi}{y_0}\right) C_n = q_1 A_n - \sum_{m=1}^{\infty} (-1)^m m\pi (A_m c_{m,n} + B_m s_{m,n}) \qquad (2.8)$$

Similarly the condition (2.5b) gives us,

$$\frac{\partial \theta}{\partial y} = \sum_{n=1}^{\infty} n\pi \left\{ \sin n\pi x [A_n \sinh(n\pi y_0) + B_n \cosh(n\pi y_0)] + (-1)^n \frac{C_n}{y_0} \sinh\left(\frac{n\pi x}{y_0}\right) \right\} = q_2$$

Expanding q_2, $\sinh(n\pi x/y_0)$ in half range sine series, and collecting the coefficients of $\sin(n\pi x)$ on both sides we get,

$$n\pi [A_n \sinh(n\pi y_0) + B_n \cosh(n\pi y_0)] = q_2 A_n - \sum_{m=1}^{\infty} m\pi (-1)^m \frac{C_m}{y_0} s1_{m,n} \tag{2.9}$$

where $\sinh\left(\frac{n\pi x}{y_0}\right) = \sum_{m=1}^{\infty} s1_{n,m} \sin(m\pi x)$.

Equations (2.8) and (2.9) can be simplified by introducing the following notation

$$A_n^* = \sinh(n\pi y_0) A_n,\ B_n^* = B_n \cosh(n\pi y_0),\ C_n^* = C_n \frac{n\pi}{y_0} \cosh\left(\frac{n\pi}{y_0}\right)$$

and $c_{m,n}^* = \frac{c_{m,n}}{\sinh(m\pi y_0)},\ s_{m,n}^* = \frac{s_{m,n}}{\cosh(m\pi y_0)}, s1_{m,n}^* = \frac{s1_{m,n}}{\cosh(m\pi / y_0)}$

Now equations (2.8) and (2.9) become

$$C_n^* = q_1 A_n - \sum_{m=1}^{\infty} (-1)^m m\pi (A_m^* c_{m,n}^* + B_m^* s_{m,n}^*) \tag{2.10}$$

and $q_2 A_n - n\pi (A_n^* + B_n^*) = \sum_{m=1}^{\infty} (-1)^m C_m^* s1_{m,n}^*$ (2.11)

Substituting (2.10) in the equation (2.11), we get

$$\sum_{m=1}^{\infty} (-1)^m s1_{m,n}^* \{ q_1 A_m - \sum_{k=1}^{\infty} (-1)^k k\pi (A_k^* c_{k,m}^* + B_k^* s_{k,m}^*) \} = q_2 A_n - n\pi (A_n^* + B_n^*)$$

Rewriting this we get,

$$\sum_{k=1}^{\infty} \{ \sum_{m=1}^{\infty} (-1)^{k+m} k\pi s_{k,m}^* s1_{m,n}^* \} B_k^* - \mathrm{n}\pi B_n =$$

$$- q_2 A_n + n\pi A_n^* + q_1 \sum_{m=1}^{\infty} (-1)^m s1_{m,n}^* A_m - \sum_{k=1}^{\infty} \sum_{m=1}^{\infty} (-1)^{k+m} k\pi c_{k,m}^* s1_{m,n}^* A_k^* \tag{2.12}$$

The first term on LHS within inner summation can be written as

$$bb_{k,n} = \sum_{m=1}^{\infty} (-1)^{k+m} k\pi s^*_{k,m} s1^*_{m,n} = \frac{4kny_0^2}{\pi} \tanh(k\pi y_0) \sum_{m=1}^{\infty} \frac{(-1)^{k+n} \tanh\left(\frac{m\pi}{y_0}\right)}{\left(k^2 y_0^2 + m^2\right)\left(m^2 + n^2 y_0^2\right)} \quad if \quad k \neq n$$

This equation (2.12) can be solved for B_n^* and then substituting B_n^* in (2.10) we get C_n^*. Now all the constants A_n, B_n and C_n are known. Hence, the temperature can be computed from (2.6). By choosing q_1=2, q_2=4, the temperature profiles are obtained as shown in Fig. 2.2. We can observe that as n increases the solution converges more near to an exact solution. When we take only 5 terms (with each term containing 3 constants A_n, B_n and C_n) in the series, we can find many discrepancies in the corners. As n increases, we get a good approximate solution near to n=20. But again, if n is more than 20, so many fluctuations will develop due to multiplication of very large and very small numbers.

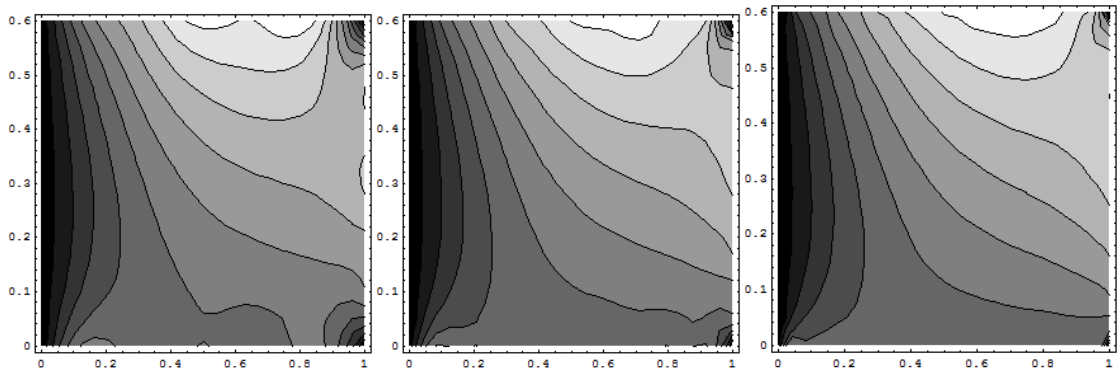

Fig. 2.2: Method 1 with 5, 10 and 20 terms.

2.3.2 Method 2

In this method, the solution is taken in two parts as $\theta = \theta_1 + \theta_2$. The part θ_1 satisfies Laplacian and boundary conditions on y. The conditions on x will be homogeneous. The part θ_2 satisfies the Laplacian and boundary conditions on x. The conditions on y will be

homogeneous. Hence, θ satisfies all the boundary conditions. We assume $\theta=\theta_1+\theta_2$ is the solution for

$$\nabla^2\theta = 0 \tag{2.13}$$

with the conditions

$\theta = 0$ on $x = 0$; $\theta = 1$ on $y = 0$; $\dfrac{\partial\theta}{\partial x} = q_1$ on $x = 1$ and $\dfrac{\partial\theta}{\partial y} = q_2$ on $y = y_0$ are split as:

$$\begin{aligned} &\theta_1 = 0 \text{ on } x = 0 && \theta_2 = 0 \text{ on } x = 0 \\ &\frac{\partial\theta_1}{\partial x} = 0 \text{ on } x = 1 && \frac{\partial\theta_2}{\partial x} = q_1 \text{ on } x = 1 \\ &\theta_1 = 1 \text{ on } y = 0 && \theta_2 = 0 \text{ on } y = 0 \\ &\frac{\partial\theta_1}{\partial y} = q_2 \text{ on } y = y_0 && \frac{\partial\theta_2}{\partial y} = 0 \text{ on } y = y_0 \end{aligned} \tag{2.14}$$

The solution for θ_1, which satisfies homogeneous conditions on x of (2.14) is taken as

$$\theta_1 = \sum_{n=1}^{\infty} \sin\frac{(2n+1)\pi x}{2}\left(A_n \cosh\frac{(2n+1)\pi y}{2} + B_n \sinh\frac{(2n+1)\pi y}{2}\right) \tag{2.15}$$

the constants A_n and B_n are found from the conditions on y of (2.14) for θ_1 as below:

$$\theta_1 = 1 \text{ on } y = 0 \quad \Rightarrow \quad \sum_{n=1}^{\infty} A_n \sin\frac{(2n+1)\pi x}{2} = 1 \text{ for } 0 \le x \le 1 \tag{2.16}$$

since $\sin((2n+1)\pi x/2)$ functions are orthogonal, from (2.16) we get

$$A_n = 2\int_0^1 \sin\frac{(2n+1)\pi x}{2}\,dx = \frac{4}{(2n+1)\pi} \tag{2.17}$$

again $\dfrac{\partial\theta_1}{\partial y} = q_2$ on $y = y_0$ which reduces to the following:

$$q_2 = \sum_{m=1}^{\infty} \frac{(2m+1)\pi}{2} \sin\frac{(2m+1)\pi x}{2}\left(A_m \sinh\frac{(2m+1)\pi y_0}{2} + B_n \cosh\frac{(2m+1)\pi y_0}{2}\right) \tag{2.18}$$

multiplying by $\sin((2n+1)\pi x/2)$ on both sides of (2.18) and then integrating with respect to x from 0 to 1, by orthogonal property of $\sin((2n+1)\pi x/2)$ functions, we get B_n as

$$B_n = \frac{q_2 A_n^2}{2}\operatorname{sech}\frac{(2n+1)\pi y_0}{2} - A_n \tanh\frac{(2n+1)\pi y_0}{2} \tag{2.19}$$

Now the solution for θ_2, which satisfies homogeneous conditions on y of (2.14), is taken as

$$\theta_2 = \sum_{n=1}^{\infty} \sin\frac{(2n+1)\pi y}{2y_0}\left(C_n \sinh\frac{(2n+1)\pi x}{2y_0} + D_n \cosh\frac{(2n+1)\pi x}{2y_0}\right) \tag{2.20}$$

from the conditions on x of (2.14), i.e., $\theta_2 = 0$ on $x = 0$ we get $D_n = 0$ (2.21)

again we have $\frac{\partial\theta_2}{\partial x} = q_1$ on $x = 1$, we get

$$q_1 = \sum_{n=1}^{\infty} C_n \frac{(2n+1)\pi}{2y_0} \sin\frac{(2n+1)\pi y}{2y_0} \cosh\frac{(2n+1)\pi}{2y_0} \tag{2.22}$$

C_n's are obtained from the orthogonal property of $\sin((2n+1)\pi y/2y_0)$, as

$$C_n = \frac{y_0 q_1 A_n^2}{2} \operatorname{sech}\frac{(2n+1)\pi}{2y_0} \tag{2.23}$$

Substituting (2.17), (2.19) in (2.15) and (2.21), (2.23) in (2.20) we get θ_1 and θ_2. Now combining the two solutions θ_1 and θ_2 we get the complete solution. It is computed numerically and presented below with n=20 number of terms in the solution. The solution is more close to the exact solution than the solution obtained in Method 1. This problem is solved by five point iterative formula by numerical method. The solution obtained at 3500 iterations is presented in Fig. 2.3.

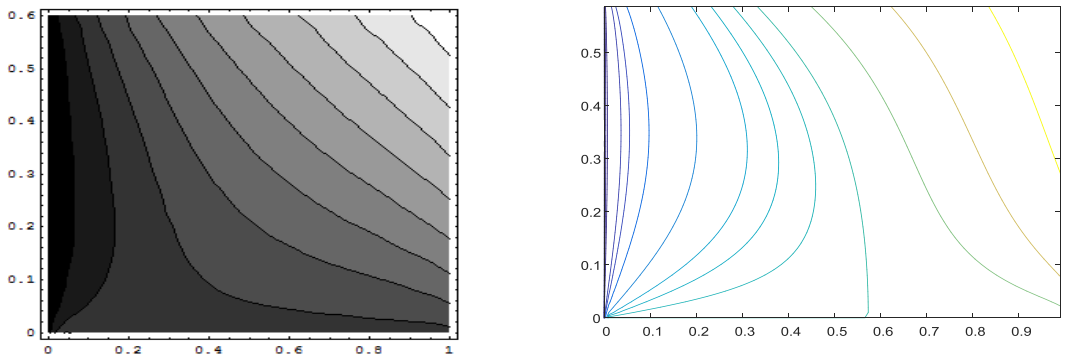

Fig. 2.3: Isothermal lines between Method 2 with 20 terms and by Numerical method at 3500 iterations.

2.4 Results and Discussion

The analytical solution is very fast converging with 20 terms and accurate enough whereas the numerical solution take hundreds of iterations even with Gauss-seidal iterations and is not as accurate as analytical solution. The effect of heat flux at the edges is shown below. When the ratio $q=q_1/q_2$ is very high as 200 (Fig. 2.4 (a)), the isothermal lines are vertical. When q = 0.1 (Fig. 2.4 (b)), the isothermal lines are inclined with much variations near to down left corner and when q= 0.001 (Fig. 2.5), the isothermal lines are nearly parallel to the walls. In all the cases, there exists a small region of no heat flow zone at which the pattern changes its nature in direction of thermal flow.

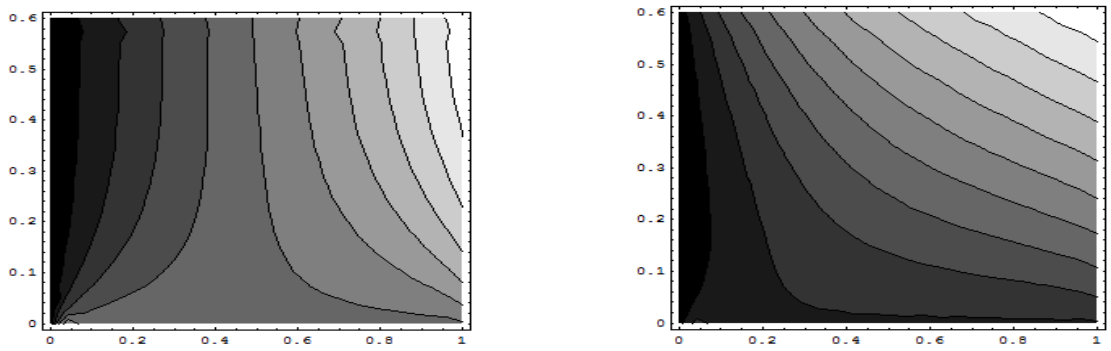

(a) (b)

Fig. 2.4: Isothermal lines for (a) q= 200 and (b) q=0.1.

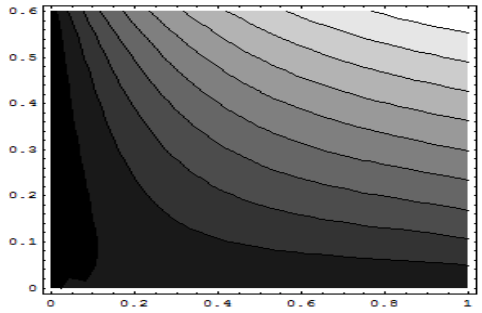

Fig. 2.5: Isothermal lines for q= 0.001.

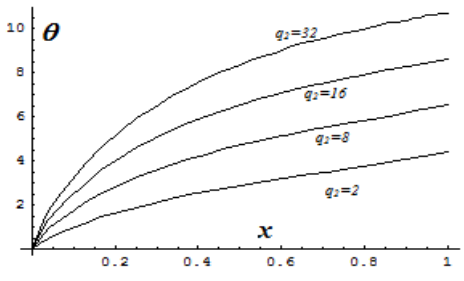

Fig. 2.6: Temperature at $y=y_0$.

In Fig. 2.6, temperature distribution at the top side of the plate is given. We notice that, as q_2, the heat flux increases, the temperature also increases.

2.5 Conclusions

Form this chapter, we observed that finding analytical solution is not easy for this type of problems. So, we considered numerical method for obtaining solution to this kind of problems in subsequent chapters of the thesis.

Chapter 3

Fluid Flow and Heat Transfer by Heat Function and Entropy Generation in a Rectangular Channel with Suction

A viscous fluid flow is generated in a rectangular channel of uniform cross section by applying suction/ injection at the adjacent side walls. The other opposite side walls are maintained at constant temperatures and the walls with suction are maintained at constant heat flux. The flow is assumed as Stokes flow and non-linear convective terms are neglected. The stream lines due to the flow and isothermal lines and heat function contours are drawn. The regions of high friction are found by plotting entropy generation number and Bejan number. The regions of low and high pressures are also drawn. The 13 point formula is used to solve the biharmonic equation (convective term is neglected) for stream function and 5 point formula is used to solve for all other harmonic equations. For derivative boundary conditions, central difference formula with fictitious nodes is used. It is observed that corner points are regions of high energy dissipation points. Least dissipation of energy is near to the wall where non-dimensional temperature is 1.

3.1 Introduction

The flow due to suction at the adjacent walls of rectangular channel was studied by Varapaev and Yagodkin (1969) wherein the problem was solved by a semi numerical technique to obtain flow pattern only. Heat transfer in rectangular ducts is studied experimentally by Alfarawi et al. (2017). Karimi et al. (2014) investigated the flow of an incompressible Newtonian fluid through a rectangular channel. Fluid flow and heat transfer in a rectangular channel have been studied by Mahdi et al. (2010), Wang et al. (2012), Chen et al. (2014), Ambethkar and Kushawaha (2017) and Sahar et al. (2017). Warrier et al. (2002) studied heat transfer and pressure drop in narrow rectangular channels. Attia (2005) studied the effect of suction and injection of a dusty conducting fluid in rectangular channel.

The classical problem of viscous fluid flow in a rectangular cavity generated by uniform motion of the lid has been source of many researchers for getting a numerical solution. It is also treated as a benchmark problem for testing numerical scheme of a method. Kawaguti (1961) obtained numerical solution for different aspect ratios of the channel. Moffatt (1964) obtained a similarity solution to get flow near the corners of the channel. Weiss & Florsheim (1965) have obtained a solution by variational method. Since these methods are not accurate enough, the problem was therefore treated numerically by means of the relaxation procedure by Burggraf (1966). The analytical solutions of the problem have been obtained by Joseph and Sturges (1978) by using biorthogonal functions and found a solution which is fast converging and accurate. Kundu et al. (2011) are established the analytical techniques to determine the velocity distribution for laminar fluid flow through rectangular channels. Chorin (1968) developed a numerical scheme for unsteady motion of viscous fluid. Kaushik (2019) studied 2D incompressible flow in a rectangular domain using Chorin's projection method numerically at high Reynolds number.

In the past for many years, heat transfer by convection was studied by examining temperature field and first law of thermodynamics. Nowadays emphasis on design of a model is developed as a science. Hence a deeper study of the subject is necessary. The study of flow lines, temperature and heat flow lines together with second law of thermodynamics are important, since by this one can know the regions of available energy or useful energy and regions of dissipation of energy.

But for the study of flow due to suction on adjacent walls is paid very less attention. Hence in this chapter our aim is to study the heat transfer in a rectangular channel with suction on adjacent walls. The entropy analysis is also taken to see the region of available energy. Bejan number plot is drawn to see the regions where friction is dominating.

3.2 Mathematical Formulation

The two dimensional laminar viscous flow through a rectangular channel of uniform cross section due to suction/injection at the neighboring walls is considered. The physical representation of the problem is given in Fig. 3.1. The Cartesian coordinate system with origin at the bottom left corner and X and Y axes along the walls is taken.

The channel is of length a along X direction and height b along Y direction. Injection with velocity V_1 at the wall $Y=b$ and suction with velocity V_2 at the wall $X=a$ are imposed. The flow is developed because of the suction.

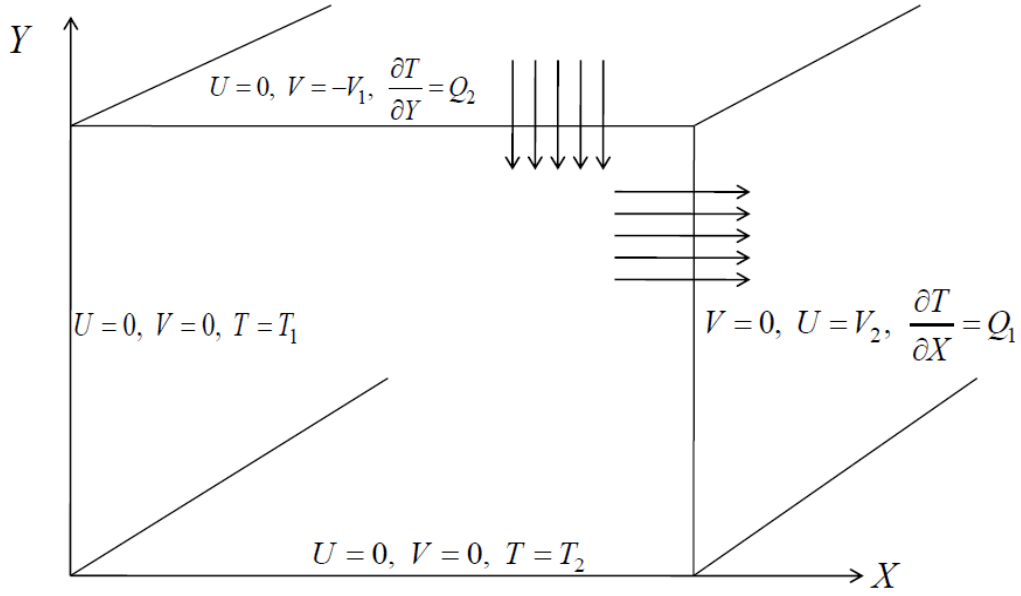

Fig. 3.1. Stokes flow configuration in a rectangular channel with adjacent wall suction.

Governing Equations

The equations of motion for the flow are given below:

$$\nabla.\mathbf{Q}=0 \tag{3.1}$$

$$\rho\frac{d\mathbf{Q}}{dt}=-\nabla P+\mu\nabla^2\mathbf{Q} \tag{3.2}$$

$$\rho c_p\frac{dT}{dt}=k\nabla^2T \tag{3.3}$$

where $\mathbf{Q}$ is the velocity of fluid particle, P is pressure, T is the temperature, ρ is fluid density, μ is the coefficient of viscosity, k is the thermal conductivity of the fluid and c_p heat capacity at constant pressure.

The flow is two dimensional and hence $\mathbf{Q}=(U, V)$.

Boundary conditions for the problem

Velocity of fluid satisfies impermeability condition and no slip condition on walls $X=0$, $Y=0$ and suction and no slip condition at the permeable walls $X=a$ and $Y=b$. The temperature field satisfies constant heat flux at the permeable walls $X=a$ and $Y=b$ and constant temperature is maintained on the impermeable walls $X=0$, $Y=0$. Due to no slip condition on the walls $X=0$ and $Y=0$, the tangential velocities are zero.

i.e., on X=0, V=0 $\Rightarrow \frac{\partial \psi}{\partial X} = 0$ and on Y=0, U=0 $\Rightarrow \frac{\partial \psi}{\partial Y} = 0$.

Due to impermeability condition on the walls X=0 and Y=0, the normal velocities are also zero.

i.e., on X=0, U=0 $\Rightarrow \frac{\partial \psi}{\partial Y} = 0$ and on Y=0, V=0 $\Rightarrow \frac{\partial \psi}{\partial X} = 0$.

Due to no slip condition on the walls $X=a$ and $Y=b$, the tangential velocities are zero.

i.e., on $X=a$, V=0 $\Rightarrow \frac{\partial \psi}{\partial X} = 0$ and on $Y=b$, U=0 $\Rightarrow \frac{\partial \psi}{\partial Y} = 0$.

On permeable walls, the suction velocity on $X=a$ is V_2 and the injection velocity on $Y=b$ is V_1.

i.e., on $X=a$, $U=V_2 \Rightarrow \frac{\partial \psi}{\partial Y} = V_2$ and on $Y=b$, $V=-V_1 \Rightarrow \frac{\partial \psi}{\partial X} = V_1$.

The walls X=0 and Y=0 are maintained at constant temperatures. i.e., $T=T_1$ on X=0 and $T=T_2$ on Y=0.

On the walls $X=a$ and $Y=b$ constant heat fluxes are imparted.

i.e., $\frac{\partial T}{\partial X} = Q_1$ on $X = a$ and $\frac{\partial T}{\partial Y} = Q_2$ on $Y = b$.

Non-dimensionalization

We introduce the following non–dimensional scheme and non–dimensional parameters V_0=suction parameter, y_0=geometric parameter, Pe=Peclet number, Re=Reynolds number.

$$X = ax,\ Y = ay,\ U = V_1 u,\ V = V_1 v,\ P = \rho V_1^2 p,\ T - T_1 = \theta(T_2 - T_1) \qquad (3.4)$$

$$\mathrm{Re} = \frac{\rho V_1 a}{\mu},\ \ Pe = \frac{\rho c_p V_1 a}{k} = \mathrm{Re}^* \mathrm{Pr},\ \ y_0 = \frac{b}{a},\ \ V_0 = \frac{V_2}{V_1} \qquad (3.5)$$

For the flow the Reynolds number is so small that the convective terms in equation (3.2) are neglected. The flow is steady and hence independent of time t.

3.3 Solution of the problem

3.3.1 Stream function

We introduce stream function ψ as below such that equation (3.1) is satisfied.

$$u = \frac{\partial \psi}{\partial y} \quad \text{and} \quad v = -\frac{\partial \psi}{\partial x} \tag{3.6}$$

Taking curl to equation (3.2) and substituting (3.6), we get the equation for the non-dimensional stream function ψ as

$$\nabla^4 \psi = 0 \tag{3.7}$$

with boundary conditions:

$$\frac{\partial \psi}{\partial x} = 0 \text{ on } x = 0 \text{ and on } x = 1$$

$$\frac{\partial \psi}{\partial y} = 0 \text{ on } x = 0 \text{ and } \frac{\partial \psi}{\partial y} = V_0 \text{ on } x = 1$$

$$\frac{\partial \psi}{\partial x} = 0 \text{ on } y = 0 \text{ and } \frac{\partial \psi}{\partial x} = 1 \text{ on } y = y_0$$

$$\frac{\partial \psi}{\partial y} = 0 \text{ on } y = 0 \text{ and on } y = y_0$$

These conditions, by integrating, are converted in to the conditions on ψ as follows:

$$\left.\begin{aligned} &\frac{\partial \psi}{\partial x} = 0 \text{ on } x = 0 \text{ and } x = 1 \\ &\psi = 0 \text{ on } x = 0 \text{ and } y = 0 \\ &\psi = x \text{ on } y = y_0 \\ &\psi = V_0 y \text{ on } x = 1 \\ &\frac{\partial \psi}{\partial y} = 0 \text{ on } y = 0 \text{ and } y = y_0 \end{aligned}\right\} \tag{3.8}$$

We solve the equation (3.7) with conditions (3.8) by Finite Difference Method. The cavity is covered with a mesh of step size h with (M–1) intervals on X direction and (N–1) intervals on Y direction. For each grid point (i, j) within the cavity, the biharmonic equation is approximated by 4th order 13 point scheme as given in Titus Petrila and Damian Trif (2005) and Pozrikidis (1998). Then equation (3.7) can be written as:

$$\begin{aligned} \nabla^4 \psi_{i,j} = \frac{1}{h^4} [&20\psi_{i,j} - 8(\psi_{i+1,j} + \psi_{i-1,j} + \psi_{i,j+1} + \psi_{i,j-1}) \\ &+ 2(\psi_{i+1,j+1} + \psi_{i-1,j+1} + \psi_{i+1,j-1} + \psi_{i-1,j-1}) + (\psi_{i,j+2} + \psi_{i,j-2} + \psi_{i+2,j} + \psi_{i-2,j})] = 0 \\ &\text{for } i = 2, 3, \ldots, M-1 \;\&\; j = 2, 3, \ldots, N-1 \end{aligned} \tag{3.9}$$

For the boundary conditions containing derivatives, we used central difference scheme. The nodes numbering is as follows:

Along X direction	Along Y direction
x_1 node on the boundary $x = 0$.	y_1 node on the boundary $y = 0$.
x_2 , x_3, … , x_{M-1} inside the computational	y_2 , y_3, … , y_{N-1} inside the computational
x_M node on the boundary x=1	y_N node on the boundary y=y_0

Thus at x=0, we have, $\psi(0, y) = 0$ and $\frac{\partial \psi}{\partial x} = 0$.

i.e., $\psi_{1,j} = 0$ and $\frac{\psi_{2,j} - \psi_{0,j}}{2h} = 0$ or $\psi_{2,j} = \psi_{0,j}$ for j=1,2,...,N (3.10)

at x=1, we will have, $\psi(1, y) = V_0 y$ and $\frac{\partial \psi}{\partial x} = 0$.

i.e., $\psi_{M,j} = V_0 (j-1)h$ and $\frac{\psi_{M+1,j} - \psi_{M-1,j}}{2h} = 0$ or $\psi_{M+1,j} = \psi_{M-1,j}$ for j=1,2,...,N (3.11)

Similarly at y=0 we have,

$\psi_{i,1} = 0$ and $\psi_{i,2} = \psi_{i,0}$ for i=2,3,...,$M-1$ (3.12)

Finally at y=y_0 we have,

$\psi_{i,N} = (i-1)h$ and $\psi_{i,N+1} = \psi_{i,N-1}$ for i=2,3,...,$M-1$ (3.13)

Equation (3.9) involves (M–2)(N–2) internal points +(2M+2N–4) boundary points +(2M+2N) external or fictitious points and hence in total MN +2M +2N–8 number of unknowns. Now equation (3.9) gives (M–2)(N–2) number of equations, (3.10) gives 2N equations, (3.11) gives 2N equations, (3.12) gives 2(M–2) equations and (3.13) gives 2(M–2) equations and hence in total MN+2M+2N–8 equations. Thus the scheme in (3.9) can be solved uniquely by introducing fictitious nodes externally through central difference formula for the derivative conditions on the boundary.

Now by eliminating known boundary values, the equation (3.9) can be written in the form:

$$\left.\begin{array}{ll}
\text{for } i=2, & A_1\psi_2 + A_2\psi_3 + \psi_4 = a_2 \\
\text{for } i=3, & A_2\psi_2 + A_3\psi_3 + A_2\psi_4 + \psi_5 = a_3 \\
\text{for } 3<i<M-2, & I\psi_{i-2} + A_2\psi_{i-1} + A_3\psi_i + A_2\psi_{i+1} + \psi_{i+2} = a_i \\
\text{for } i=M-2, & I\psi_{M-4} + A_2\psi_{M-3} + A_1\psi_{M-2} + A_2\psi_{M-1} = a_{M-2} \\
\text{for } i=M-1, & I\psi_{M-3} + A_2\psi_{M-2} + A_1\psi_{M-1} = a_{M-1}
\end{array}\right\} \quad (3.14)$$

where $A_1 = \begin{bmatrix} 22 & -8 & 1 & 0 & \ldots\ldots\ldots & 0 \\ -8 & 21 & -8 & 1 & 0 & \ldots\ldots\ldots & 0 \\ \ldots\ldots\ldots\ldots\ldots\ldots\ldots\ldots\ldots\ldots\ldots\ldots \\ \ldots\ldots\ldots\ldots\ldots\ldots\ldots\ldots\ldots\ldots\ldots\ldots \\ 0 & \ldots\ldots\ldots & 1 & -8 & 21 & -8 & 1 \\ 0 & \ldots\ldots\ldots & 0 & 1 & -8 & 21 & -8 \\ 0 & \ldots\ldots\ldots\ldots & 0 & 1 & -8 & 22 \end{bmatrix}$, $A_2 = \begin{bmatrix} -8 & 2 & 0 & \ldots\ldots & 0 \\ 2 & -8 & 2 & \ldots\ldots & 0 \\ \ldots\ldots\ldots\ldots\ldots\ldots\ldots \\ \ldots\ldots\ldots\ldots\ldots\ldots\ldots \\ 0 & \ldots\ldots & 2 & -8 & 2 \\ 0 & \ldots\ldots & 0 & 2 & -8 \end{bmatrix}$,

$A_3 = \begin{bmatrix} 21 & -8 & 1 & 0 & \ldots\ldots\ldots & 0 \\ -8 & 20 & -8 & 1 & 0 & \ldots\ldots & 0 \\ \ldots\ldots\ldots\ldots\ldots\ldots\ldots\ldots\ldots\ldots\ldots\ldots \\ \ldots\ldots\ldots\ldots\ldots\ldots\ldots\ldots\ldots\ldots\ldots\ldots \\ 0 & \ldots\ldots\ldots & 1 & -8 & 20 & -8 & 1 \\ 0 & \ldots\ldots\ldots & 0 & 1 & -8 & 20 & -8 \\ 0 & \ldots\ldots\ldots\ldots & 0 & 1 & -8 & 21 \end{bmatrix}$, $\psi_i = \begin{bmatrix} \psi_{i,2} \\ \psi_{i,3} \\ . \\ . \\ \psi_{i,N-2} \\ \psi_{i,N-1} \end{bmatrix}$, $a_i = h \begin{bmatrix} 0 \\ . \\ . \\ 1-i \\ 4(i-1) \end{bmatrix}$ for $2 \le i \le M-3$,

$$a_{M-2} = h \begin{bmatrix} -a \\ -2a \\ . \\ . \\ -a(N-3)-(M-3) \\ -a(N-2)-2(M-4)+8(M-3)-2(M-2) \end{bmatrix},$$

$$a_{M-1} = h \begin{bmatrix} 4a \\ 8a \\ . \\ . \\ -(M-2)-2a(N-4)+8a(N-3)-2a(N-2) \\ -2(M-3)+8(M-2)-2a(N-3)+8a(N-2)-2a(N-1) \end{bmatrix}.$$

These equations in (3.14) are solved by Gauss-Seidel iteration method. All ψ_i, i>2 are set to zero and equation for i=2 is solved for ψ_2, then equation for i=3 is solved for ψ_3. So on to find all ψ_i. For the next iteration, all these are taken as known and the procedure is repeated until, the difference between two iterations for ψ is less than ε (=10^{-4}).

3.3.2 Temperature

The energy equation, given by (3.3), by using (3.4), (3.5) can be reduced to the non-dimensional form as:

$$\nabla^2\theta = Pe\left(u\frac{\partial\theta}{\partial x}+v\frac{\partial\theta}{\partial y}\right) \tag{3.15}$$

with boundary conditions:

$$\left.\begin{aligned}&\frac{\partial\theta}{\partial x}=q_1 \quad \text{on} \quad x=1;\ \ \theta=0 \quad\ \ \text{on} \quad x=0\\ &\theta=1 \quad\ \ \text{on} \quad y=0;\ \ \frac{\partial\theta}{\partial y}=q_2 \quad \text{on} \quad y=y_0\end{aligned}\right\} \tag{3.16}$$

The equation (3.15) by second order finite differences can be written as

$$\begin{aligned}&\left[1+\frac{Pe}{4}\left(\psi_{i,j+1}-\psi_{i,j-1}\right)\right]\theta_{i-1,j}+\left[1-\frac{Pe}{4}\left(\psi_{i+1,j}-\psi_{i-1,j}\right)\right]\theta_{i,j-1}-4\theta_{i,j}\\ &\quad+\left[1+\frac{Pe}{4}\left(\psi_{i+1,j}-\psi_{i-1,j}\right)\right]\theta_{i,j+1}+\left[1-\frac{Pe}{4}\left(\psi_{i,j+1}-\psi_{i,j-1}\right)\right]\theta_{i+1,j}=0 \qquad (3.17)\\ &\qquad\qquad\qquad\qquad \text{for } i=2,3,\ \ldots,M \text{ and } j=2,3,\ \ldots,N\end{aligned}$$

The boundary conditions in (3.16) are now expressed as:

$$\text{at } x=0,\ \theta=0 \text{ which implies that } \theta_{1,j}=0 \text{ for } j=2,3,...,N \tag{3.18}$$

$$\text{at } y=0,\ \theta=1 \text{ which implies that } \theta_{i,1}=1 \text{ for } i=2,3,...,M \tag{3.19}$$

$$\text{at } x=1,\ \frac{\partial\theta}{\partial x}=q_1 \text{ which implies that } \theta_{M+1,j}=\theta_{M-1,j}+2hq_1 \text{ for } j=2,3,...,N \tag{3.20}$$

$$\text{at } y=y_0,\ \frac{\partial\theta}{\partial y}=q_2 \text{ which implies that } \theta_{i,N+1}=\theta_{i,N-1}+2hq_2 \text{ for } i=2,3,...,M \tag{3.21}$$

Equation (3.17) involves (M–2)(N–2) internal points +2(M+N–2)–1 boundary points +(M+N–2) external points and a total of MN+M+N–3 unknowns. Now equation (3.17) yields (M–1)(N–1) equations, (3.18) yields N–1 equations, (3.19) yields M–1 equations, (3.20) yields N–1 equations and (3.21) yields M–1 equations and hence a total of MN+M+N–3 equations. Hence the equations in (3.17) can be solved uniquely. Equation (3.17) does not contain the corner points (1, 1), (1, N+1), (M, 1) & (M, N+1). The equation (3.17) can be put in matrix form as below:

$$\left.\begin{aligned}&\text{for } i=2: && B_{22}\theta_2+B_{32}\theta_3=b_2\\ &\text{for } 2<i<M-2: && B_{1i}\theta_{i-1}+B_{2i}\theta_i+B_{3i}\theta_{i+1}=b_i\\ &\text{for } i=M: && 2I\theta_{M-1}+B_{2M}\theta_M=b_M\end{aligned}\right\} \tag{3.22}$$

where $B_{1i} = \begin{bmatrix} 1+u_{i2} & 0 & 0 & \ldots\ldots\ldots & 0 & 0 & 0 \\ 0 & 1+u_{i3} & 0 & \ldots\ldots\ldots & 0 & 0 & 0 \\ \ldots & \ldots & \ldots & \ldots & \ldots & \ldots & \ldots \\ 0 & \ldots\ldots\ldots & 0 & 1+u_{iN-1} & 0 & & \\ 0 & \ldots\ldots\ldots & 0 & 0 & 1 & & \end{bmatrix}$,

$B_{2i} = \begin{bmatrix} -4 & 1+v_{i2} & 0 & \ldots\ldots\ldots & 0 & 0 \\ 1-v_{i3} & -4 & 1+v_{i3} & \ldots\ldots\ldots & 0 & 0 \\ \ldots & \ldots & \ldots & \ldots & \ldots & \ldots \\ 0 & 0 & \ldots\ldots\ldots & 1-v_{iN-1} & -4 & 1+v_{iN-1} \\ 0 & 0 & \ldots\ldots\ldots & 0 & 2 & -4 \end{bmatrix}$,

$B_{3i} = \begin{bmatrix} 1-u_{i2} & 0 & 0 & \ldots\ldots\ldots & 0 & 0 & 0 \\ 0 & 1-u_{i3} & 0 & \ldots\ldots\ldots & 0 & 0 & 0 \\ \ldots & \ldots & \ldots & \ldots & \ldots & \ldots & \ldots \\ 0 & \ldots\ldots\ldots & 0 & 1-u_{iN-1} & 0 & & \\ 0 & \ldots\ldots\ldots & 0 & 0 & 1 & & \end{bmatrix}$, $\theta_i = \begin{bmatrix} \theta_{i2} \\ \theta_{i3} \\ \ldots\ldots \\ \ldots\ldots \\ \theta_{iN} \end{bmatrix}$,

$b_i = \begin{bmatrix} 1-v_{i2} \\ 0 \\ \ldots\ldots\ldots \\ 0 \\ 2h(1+v_{iN}) \end{bmatrix}$ for $2 \le i \le M-1$, $b_M = -\begin{bmatrix} 1+2hq_1(1-u_{M,2}) \\ 2hq_1(1-u_{M,3}) \\ \ldots\ldots\ldots \\ 2hq_1(1-u_{M,N-1}) \\ 2h(q_1+q_2) \end{bmatrix}$,

where $u_{ij} = \frac{Pe}{4}(\psi_{i,j+1} - \psi_{i,j-1})$, $v_{ij} = \frac{Pe}{4}(\psi_{i+1,j} - \psi_{i-1,j})$.

The equations in (3.22) for temperature are solved by Gauss-Seidel iteration method as in (3.14) for stream function.

3.3.3 Entropy Generation and Bejan Number

The dimensional local entropy generation $\bar{S}_{gen}$, (Woods (1975) and by Mikhail et al. (2016)) is expressed as

$$\bar{S}_{gen} = \frac{k}{T_0^2}\left[\left(\frac{\partial T}{\partial X}\right)^2 + \left(\frac{\partial T}{\partial Y}\right)^2\right] + \frac{\mu}{T_0}\left[2\left(\frac{\partial U}{\partial X}\right)^2 + 2\left(\frac{\partial V}{\partial Y}\right)^2 + \left(\frac{\partial U}{\partial Y} + \frac{\partial V}{\partial X}\right)^2\right] \quad (3.23)$$

where reference temperature T_0 is taken as $T_0 = 0.5(T_1+T_2)$.

Equation (3.23) consists two terms: the first is the local entropy generation due to heat transfer by conduction $\bar{S}_{gen,\,ht}$ and the second is the dimensional local entropy generation due to fluid friction $\bar{S}_{gen,\,fr}$.

The corresponding non-dimensional entropy generation number N_s is defined as

$$N_s = \bar{S}_{gen}\frac{T_0^2 a^2}{k(T_2 - T_1)^2}$$

$$= \left[\left(\frac{\partial\theta}{\partial x}\right)^2 + \left(\frac{\partial\theta}{\partial y}\right)^2\right] + Br\left[2\left(\frac{\partial u}{\partial x}\right)^2 + 2\left(\frac{\partial v}{\partial y}\right)^2 + \left(\frac{\partial u}{\partial y} + \frac{\partial v}{\partial x}\right)^2\right]$$

$$N_s = N_h + N_f \tag{3.24}$$

where $Br = \dfrac{\mu V_1^2 T_0}{2k(T_2 - T_1)^2}$ is Brinkman Number.

N_s can be evaluated by writing the derivatives of u, v and θ in centred first order finite differences at inside and boundary nodes x=1, y=y_0 and on x=0, y=0 we use 3–point backward difference formula.

Further, the Bejan number *Be* is a parameter that shows the importance of heat transfer in the domain and is defines as

$$Be = \frac{N_h}{N_h + N_f} \tag{3.25}$$

3.3.4 Heat lines

Net energy flow in X and Y directions are given by (Bejan (2013)):

$$\frac{\partial H^*}{\partial Y} = \rho C_p U(T - T_0) - k\frac{\partial T}{\partial X} \tag{3.26}$$

$$-\frac{\partial H^*}{\partial X} = \rho C_p V(T - T_0) - k\frac{\partial T}{\partial Y} \tag{3.27}$$

Physically, H^*=constant represents a curve across which, the net flow of energy (thermal diffusion and enthalpy flow) is zero. H^* is called heat-function. Oztop et al. (2012) obtained heat lines for inclined channel for a nano-fluid flow. Kimura and Bejan (1983) worked an example problem for heat function in a natural convection in an enclosure heated from the side. Introducing the non–dimensional quantities,

$\theta = \dfrac{T - T_1}{\Delta T}$ and $H^* = Hk\Delta T$ where $\Delta T = T_2 - T_1$

The equation (3.26) and (3.27) reduces to

$$\frac{\partial H}{\partial y} = uPe(\theta - 0.5) - \frac{\partial \theta}{\partial x} \qquad \text{and} \qquad \frac{\partial H}{\partial x} = -vPe(\theta - 0.5) + \frac{\partial \theta}{\partial y} \tag{3.28}$$

The above equations in (3.28) can be combined to give

$$\nabla^2 H = Pe\left\{(\theta - 0.5)\left(\frac{\partial u}{\partial y} - \frac{\partial v}{\partial x}\right) + \left(u\frac{\partial \theta}{\partial y} - v\frac{\partial \theta}{\partial x}\right)\right\} = Th_{i,j} \tag{3.29}$$

so that the equations in (3.28) will serve as the boundary conditions for *H*. On x=0 and on x= 1, v=0 hence on x=0, $H_x = \theta_y = 0$ and on x=1, $H_x = \theta_y$.

Similarly other conditions are derived

$$\left.\begin{aligned} &\text{on } x = 0,\ \frac{\partial H}{\partial x} = \frac{\partial \theta}{\partial y} = 0 \text{ on } x = 1,\ \frac{\partial H}{\partial x} = \frac{\partial \theta}{\partial y} \\ &\text{on } y = 0,\ \frac{\partial H}{\partial y} = -\frac{\partial \theta}{\partial x} = 0 \text{ on } y = y_0,\ \frac{\partial H}{\partial y} = -\frac{\partial \theta}{\partial x} \end{aligned}\right\} \tag{3.30}$$

For discretization, we use 5 point formula and equation (3.29) can be written as

$$H_{i-1,j} + H_{i,j-1} - 4H_{i,j} + H_{i,j+1} + H_{i+1,j} = Th_{i,j} \quad \text{for } i = 2,3,...,M-1 \text{ and } j = 2,3,...,N-1 \tag{3.31}$$

on the boundary x=0, $\dfrac{\partial H}{\partial x} = 0$ which by using 3–point formula, reduces to

$$-3H_{1,j} + 4H_{2,j} - H_{3,j} = 0 \quad \text{for } j = 1,2,....,N \tag{3.32}$$

Similarly on y=0, we have $\dfrac{\partial H}{\partial y} = 0$ which gives to

$$-3H_{i,1} + 4H_{i,2} - H_{i,3} = 0 \quad \text{for } i = 2,3,....,M-1 \tag{3.33}$$

on $y=y_0$, $\dfrac{\partial H}{\partial y} = -\dfrac{\partial \theta}{\partial x}$ which by using 3–point formula for *H* and central difference formula for θ gives to

$$-3H_{i,N} + 4H_{i,N-1} - H_{i,N-2} = \theta_{i-1,N} - \theta_{i+1,N} \quad \text{for } i = 2,3,....,M-1 \tag{3.34}$$

Similarly x=1, $\dfrac{\partial H}{\partial x} = \dfrac{\partial \theta}{\partial y}$ yields to:

$$-3H_{M,j} + 4H_{M-1,j} - H_{M-2,j} = \theta_{M,j+1} - \theta_{M,j-1} \quad \text{for } j = 1,2,....,N \tag{3.35}$$

solving the system of *MN* equations in *MN* unknowns (3.31)–(3.35) using Gauss–Seidel iteration method for 500 iterations we get the values of *H*.

3.3.5 Pressure

The equations for pressure are

$$\frac{\partial P}{\partial X} = \mu\left(\frac{\partial^2 U}{\partial X^2} + \frac{\partial^2 U}{\partial Y^2}\right) \quad \text{and} \quad \frac{\partial P}{\partial Y} = \mu\left(\frac{\partial^2 V}{\partial X^2} + \frac{\partial^2 V}{\partial Y^2}\right) \tag{3.36}$$

using the non–dimensional quantities, these equations are reduced to

$$\frac{\partial p}{\partial x} = \frac{1}{\mathrm{Re}}\nabla^2 u \quad \text{and} \quad \frac{\partial p}{\partial y} = \frac{1}{\mathrm{Re}}\nabla^2 v \tag{3.37}$$

Taking curl to (3.37), we have

$$\nabla^2 p = 0 \tag{3.38}$$

subjected to the boundary conditions:

$$\left.\begin{aligned} &\text{on } x = 0 \text{ and } x = 1, \ \frac{\partial p}{\partial x} = \frac{1}{\mathrm{Re}}\nabla^2 u \\ &\text{on } y = 0 \text{ and } y = y_0, \ \frac{\partial p}{\partial y} = \frac{1}{\mathrm{Re}}\nabla^2 v \end{aligned}\right\} \tag{3.39}$$

Discretizing (3.38) by central differences, we get

$$\begin{aligned} &p_{i-1,j} + p_{i,j-1} - 4p_{i,j} + p_{i,j+1} + p_{i+1,j} = 0 \\ &\qquad \text{for } i = 2,3,...,M-1 \text{ and } j = 2,3,...,N-1 \end{aligned} \tag{3.40}$$

on the boundary x=0, we use central differences to get RHS as:

$$\left[\nabla^2 u\right]_{1,j} = \frac{1}{2h^3}\left[\psi_{0,j+1} - \psi_{0,j-1} - 2\psi_{1,j+1} + 2\psi_{1,j-1} + \psi_{2,j+1} - \psi_{2,j-1}\right] = U_{1,j}$$

By using 3–point formula for LHS, we have finally

$$-3p_{1,j} + 4p_{2,j} - p_{3,j} = 2hU_{1,j} \quad \text{for } j = 1,2,....,N \tag{3.41}$$

We use similarly central differences on RHS at x=1 and get:

$$\left[\nabla^2 u\right]_{M,j} = \frac{1}{2h^3}\left[\psi_{M-1,j+1} - \psi_{M-1,j-1} - 2\psi_{M,j+1} + 2\psi_{M,j-1} + \psi_{M+1,j+1} - \psi_{M+1,j-1}\right] = U_{M,j}$$

and hence the equation at x=1 is given by

$$-3p_{M,j} + 4p_{M-1,j} - p_{M-2,j} = 2hU_{M,j} \quad \text{for } j = 1,2,....,N \tag{3.42}$$

on y=0, we use central differences to get RHS as:

$$\left[\nabla^2 v\right]_{i,1} = \frac{1}{2h^3}\left[-\psi_{i+1,0} + \psi_{i-1,0} + 2\psi_{i+1,1} - 2\psi_{i-1,1} - \psi_{i+1,2} + \psi_{i-1,2}\right] = U_{i,1}$$

By using 3–point formula for LHS, we have finally

$$-3p_{i,1} + 4p_{i,2} - p_{i,3} = 2hU_{i,1} \quad \text{for } i = 2,3,....,M-1 \tag{3.43}$$

we use similarly central differences on RHS at $y=y_0$ and get:

$$\left[\nabla^2 v\right]_{i,N} = \frac{1}{2h^3}\left[-\psi_{i+1,N-1} + \psi_{i-1,N-1} + 2\psi_{i+1,N} - 2\psi_{i-1,N} - \psi_{i+1,N+1} + \psi_{i-1,N+1}\right] = U_{i,N}$$

and hence the equation at $y=y_0$ is given by

$$-3p_{i,N} + 4p_{i,N-1} - p_{i,N-2} = 2hU_{i,N} \quad \text{for } i = 2,3,....,M-1 \qquad (3.44)$$

Solving system of *MN* equations in *MN* unknowns in (3.40)–(3.44) by using Gauss–Seidel iteration for 500 iterations we get the values of *p*.

3.4 Results and Discussion

Our problem is similar in situation that in a big room, walls on two sides are at constant temperature and other two side walls are suction and injection of cool breeze by air coolers and then wind circulation is studied. Or it is similar to, in an industry materials are dried in wind by hot air blown in through side walls and we want study the percentage of wetness in the wind. For the fluid in the chamber, bi-harmonic equation for stream function is solved (for which suction rate or Reynolds number is moderately small). Using the stream function, temperature distribution in the chamber is solved. Using temperature field, the regions of available energy and regions of high friction are found by entropy generation number and Began number. Then the heat flow lines are drawn. Pressure field within the chamber is also found.

3.4.1 Streamlines

The stream lines generated due to injection at the top wall and suction at the right side wall are shown. The effect of Reynolds number will not present on these lines, since convective terms are neglected. At four different suction parameter values, the stream lines are shown in Fig. 3.2 to Fig. 3.5. We can observe that as the value of the suction parameter V_0 increases, stream function values on right side wall increases, since $\psi = V_0 y$ on x=1. The left bottom corner remains as stagnant region for all values of V_0.

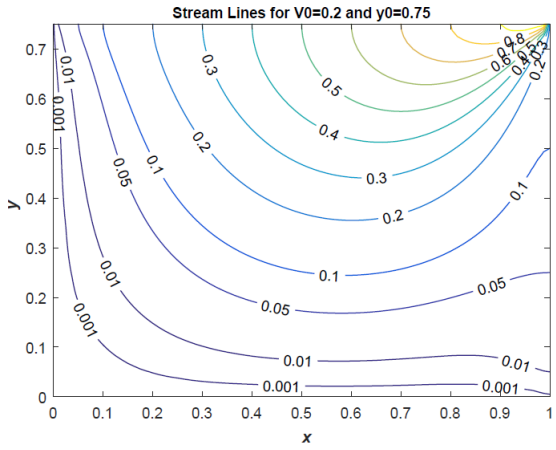

Fig. 3.2

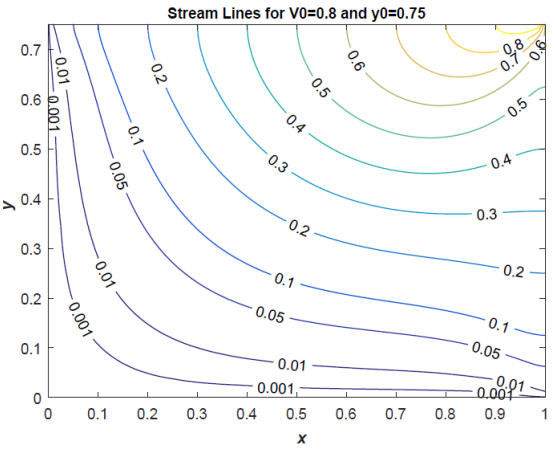

Fig. 3.3

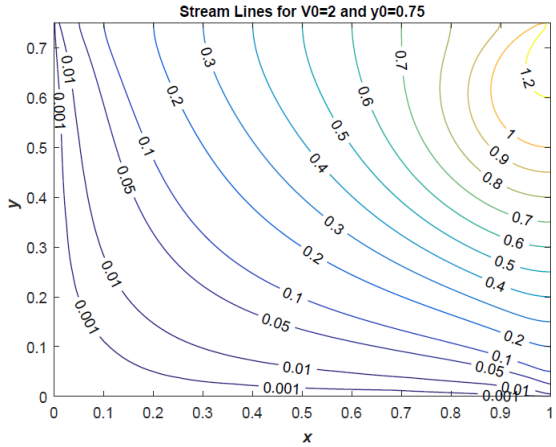

Fig. 3.4

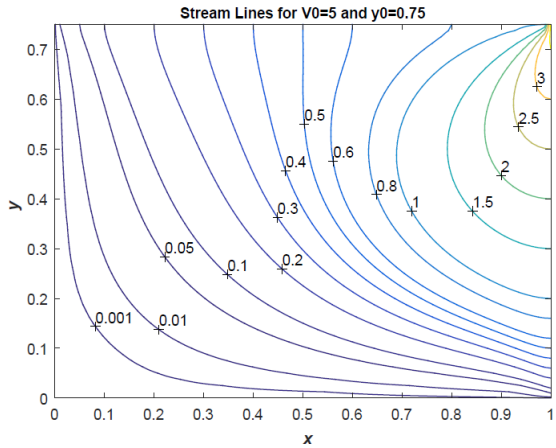

Fig. 3.5

3.4.2 Temperature field

The Fig. 3.6 to Fig. 3.9 display the nature of temperature contours. As the values of Reynolds number *Re* is increasing in Fig. 3.6, Fig. 3.7 and suction parameter increasing in Fig. 3.8, Fig. 3.9, we observe that more temperature lines enter into the flow i.e., density of heat transfer increases. That means as convective forces increase (as *Re* increases) the temperature within the chamber is taken away by convective flow and hence more and more temperature isotherms enter into the chamber. As *Re* increases, the temperature contours take bending near to the left down corner. But near to the bottom wall, isotherms remain almost unchanged for variations of *Re*.

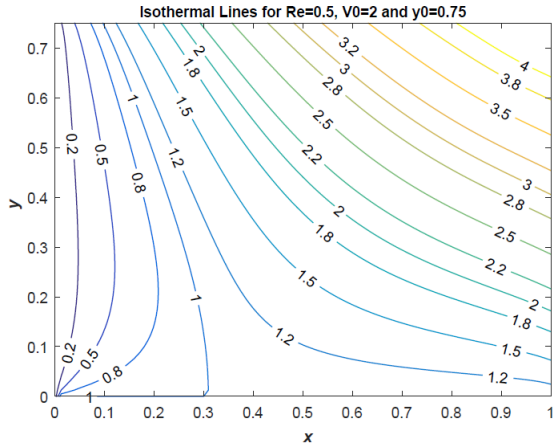

Fig. 3.6

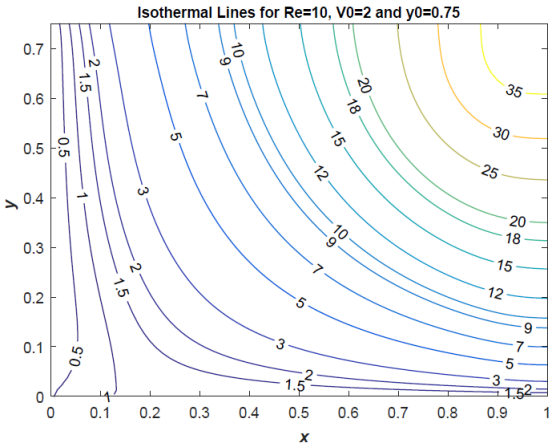

Fig. 3.7

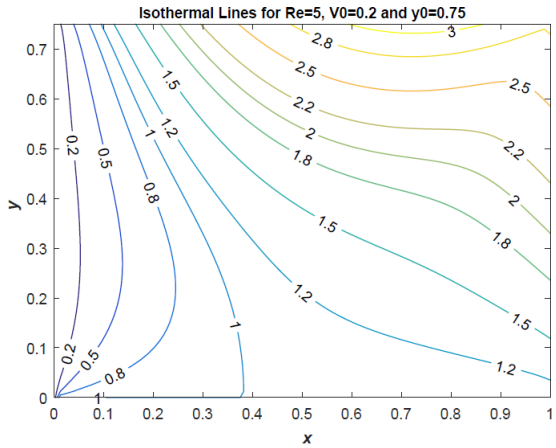

Fig. 3.8

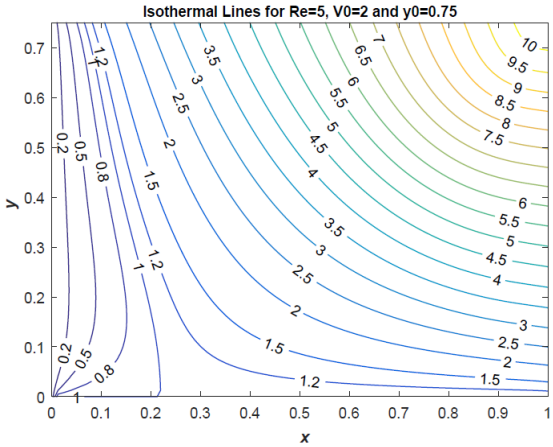

Fig. 3.9

3.4.3 Entropy generation Number *Ns*

From the Fig. 3.10–Fig. 3.13 we observe that maximum entropy occurs at the four corners. But the top left corner is not encircled properly by the constant entropy lines. Below the top left, the maximum entropy occurs. We may expect that minimum entropy may be present at bottom left corner, since temperature is zero and no flow by suction is imposed. But by graphs we observe a maximum entropy there at the bottom left corner also. But instead minimum entropy lays at a point near to the bottom left corner. As *Re* or *Br* increases, more and more entropy lines enter into the chamber without violating positions of maximum and minimum entropy points. By increasing *Br*, increases entropy with a light shift in the region. But much increase in the values of entropy lines is not observed. But increase in *Re*, increases values of entropy very much at the corners and within the chamber. *As Re increases, the irreversible region (region of high values of entropy) increases at right bottom and occupies half of the channel.*

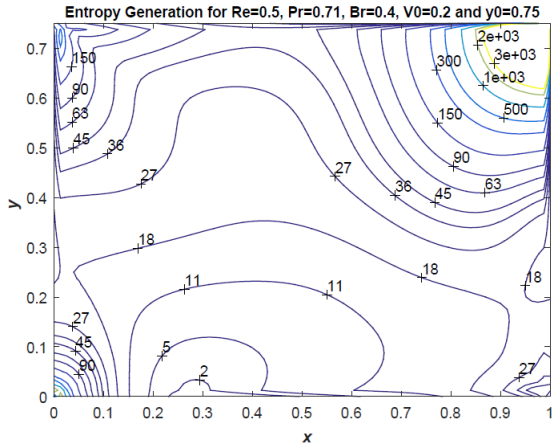

Fig. 3.10

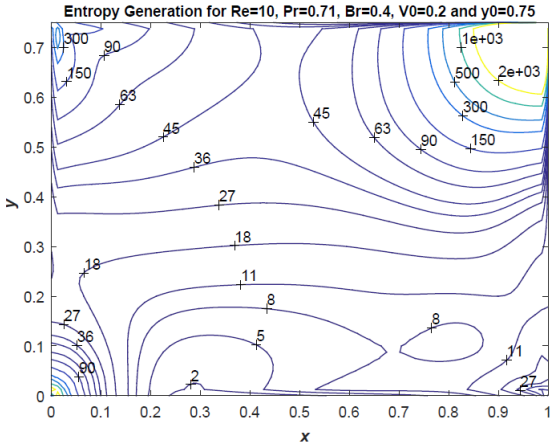

Fig. 3.11

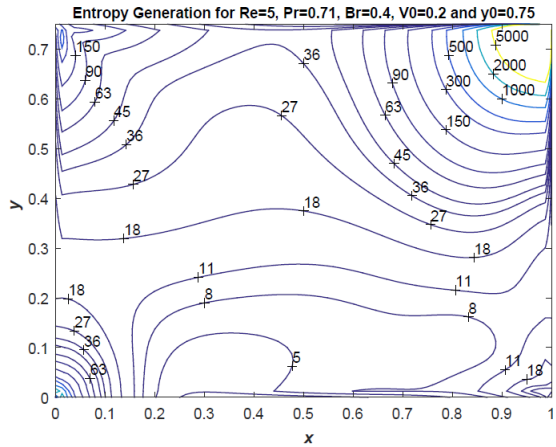

Fig. 3.12

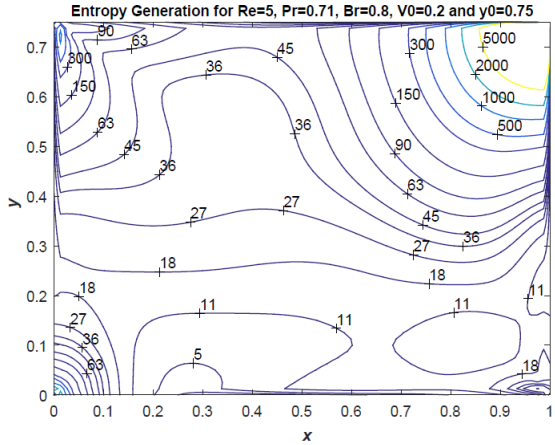

Fig. 3.13

3.4.4 Bejan Number *Be*

Bejan number shows the regions where heat transfer by conduction is more. It is to note that 0<*Be*< 1. If *Be* is near to zero indicate region of high friction and *Be* near to 1 indicates region of high conduction and less friction. The regions where *Be* is near to 1 are regions of available energy i.e., reversible heat transfer regions. In Fig. 3.14–Fig. 3.17, the contours of Bejan number are shown. We observe that as *Br*, the Brinkman number, increases, the region of friction spreads more and more. As *Re*, the Reynolds number increases, more and more Bejan contour lines increase. i.e., the heat transfer becomes faster or more dense. In any case at the corner points we observe *Be* is near to zero (0.1 or less) as in the case of Entropy generation number indicate the effect of friction and more generation of heat. Comparing both Entropy generation number *Ns* and Bejan number *Be*, we can observe that near bottom left corner both *Ns* and *Be* are having small values. *Which means though convection dominates, available energy is plenty at the bottom left corner.*

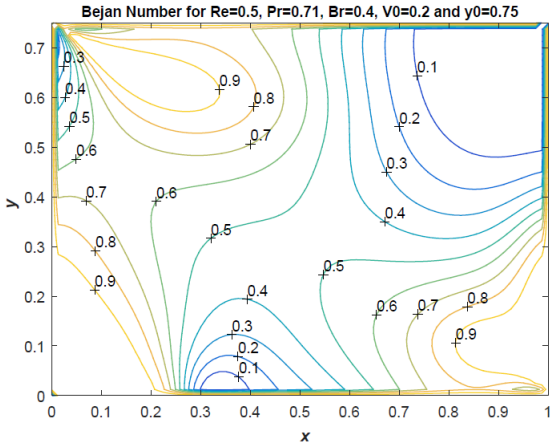

Fig. 3.14

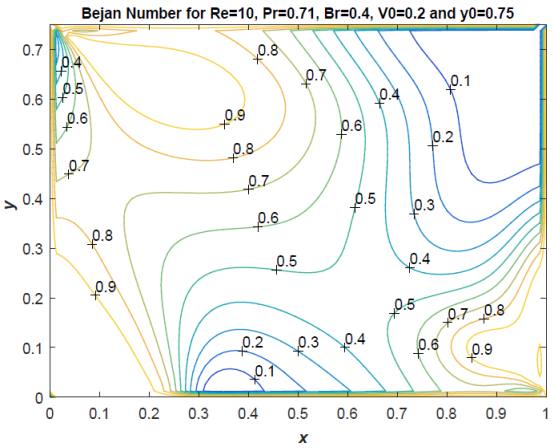

Fig. 3.15

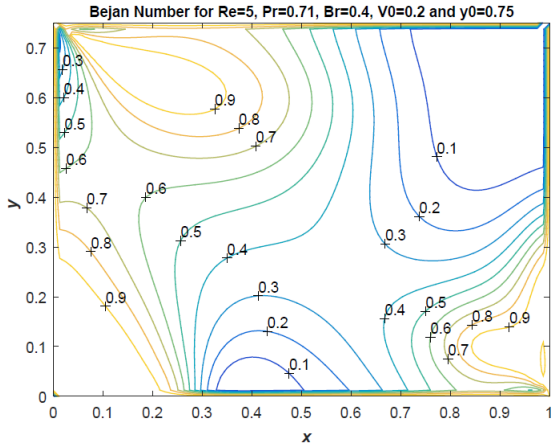

Fig. 3.16

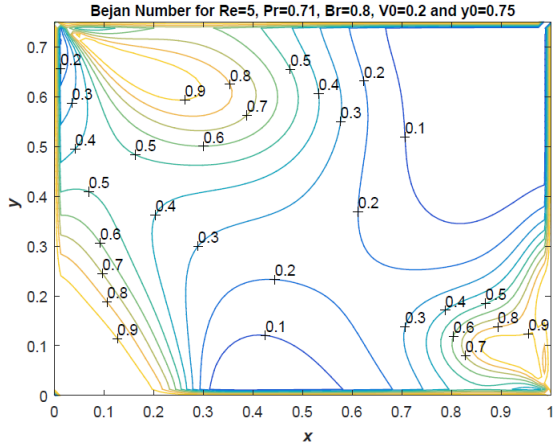

Fig. 3.17

3.4.5 Heat Lines

The energy equation in (3.15) can be split into two fist order equations by introducing Heat function H as in (3.28). Heat lines are shown within the chamber in the Fig. 3.18–Fig. 3.21. Heat lines are having positive values at the left top corner and negative values at the right bottom corner. These heat lines are changing their sign from right wall to the left wall. Negative values of heat lines indicate that the region in which they are present is the region where temperature is below the reference temprerature. As Reynolds number increases, these heat lines increases very much in value and attain maximum value when they reach the bottom right corner. If convection is neglected, isothermal lines and heat lines will be orthogonal to each other. Again we observe that for $V_0 = 2$, the 0–0 heat line which is vertical for Re=0.5 now becomes horizantal at Re=10 and moves up. Again we observe that as suction parameter V_0 increases, heat lines also increase for fixed Re value. *The 0–0 heat line moves up as* V_0 *the suction parameter increases*.

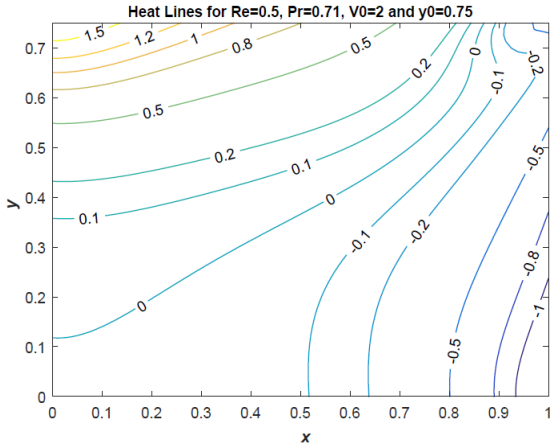

Fig. 3.18

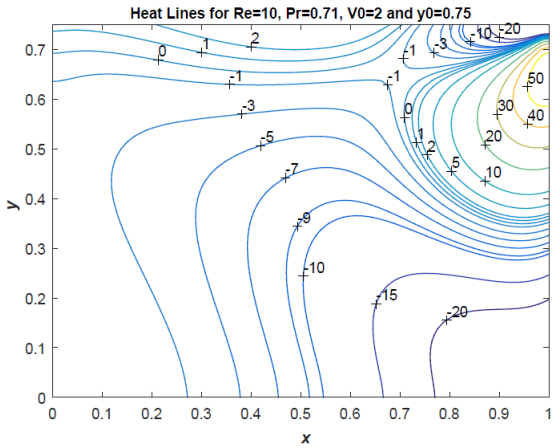

Fig. 3. 19

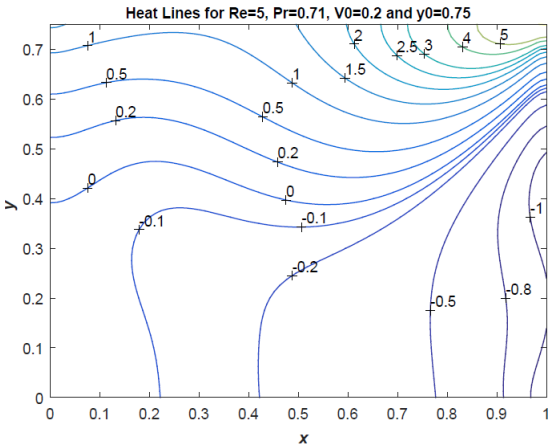

Fig. 3.20

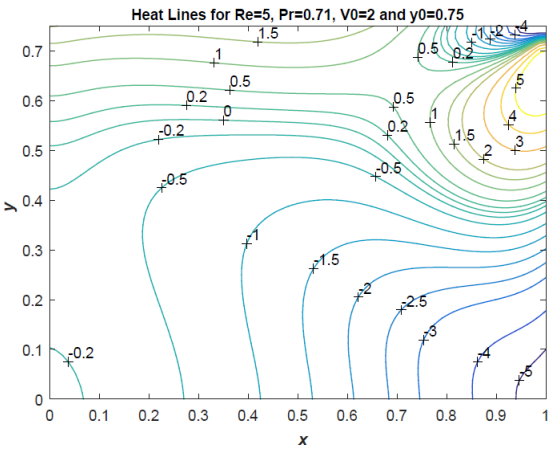

Fig. 3.21

3.4.6 Pressure Contours

The linear momentum equation in (3.2) can be split into two components along X and Y directions as in (3.36). Pressure is obtained from the numerical scheme as in (3.39) and contours are drawn within the chamber in the Fig. 3.22–Fig. 3.25. It is observed that as Reynolds number increases, values of pressure contours decrease very much. This is due to the fact that pressure gradient is inversely proportional to Reynolds number in (3.36). It is to be noted that though Reynolds number does not effect the stream lines, pressure is effected very much. Again as suction parameter V_0 increase, pressure also increases. The pressure is maximum at the top right corner.

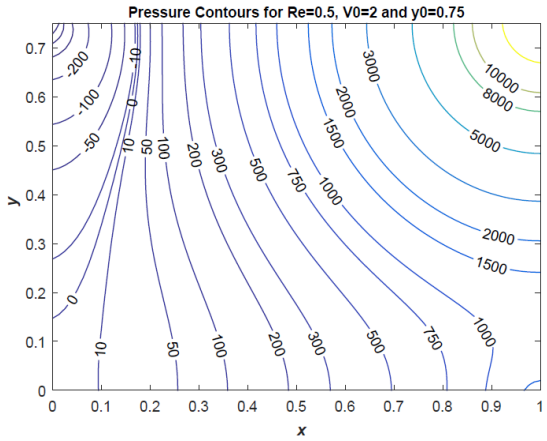

Fig. 3.22

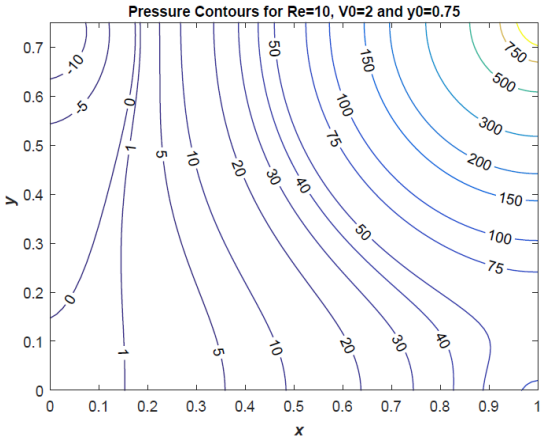

Fig. 3.23

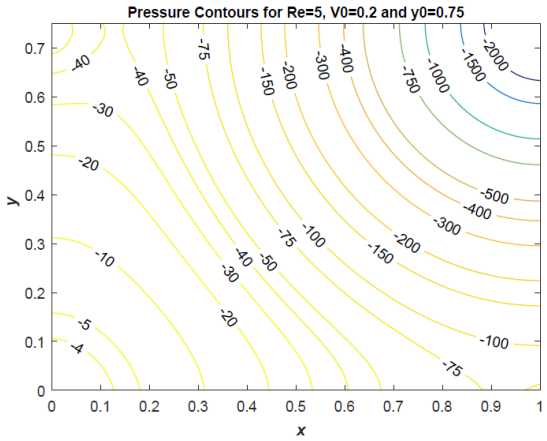

Fig. 3.24

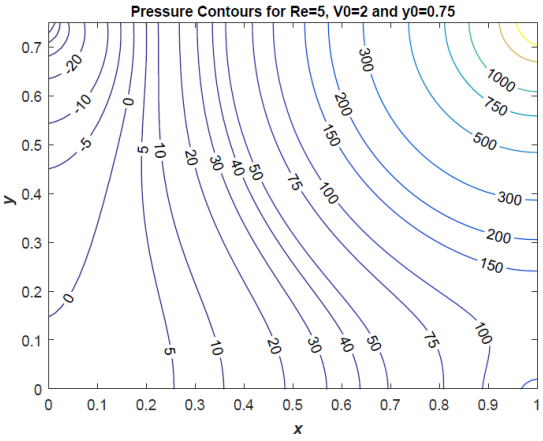

Fig. 3.25

3.5 Conclusions

From the figures drawn, we analyzed and observe that

- As V_0 increases, the stream function values are increases.
- As Reynolds number and suction parameter increases, due to convection more and more temperature lines enter into the flow region.
- Either by entropy generation number or by Bejan number contours, we observe that dissipation energy is very high at the corners.
- Energy dissipation is minimum near to the left bottom corner or where non-dimensional temperature is 1. (since *Ns* is minimum)
- Available energy or exergy is more in the centre of the channel. (since *Be* is near to 1)

- Heat lines have highest value at the top right corner. Heat lines show the actual path of the energy absorbed by the walls. Hence the lines are perpendicular to the walls.
- As Reynolds number increases, values of pressure contours decrease very much. This is due to the fact that pressure gradient is inversely proportional to Reynolds number.

Chapter 4

Entropy Analysis for Heat Transfer in a Rectangular Channel with Suction

In this chapter we considered the nonlinear convective term which we have neglected in chapter 3. The stream lines thus obtained due to the flow and isothermal lines and heat function are analyzed. The regions of high and low frictions are found by drawing contours of entropy generation number and Bejan number. Expressions for the heat transfer coefficient, Nusselt number are also derived. The 4^{th} order Partial Differential equation for stream function is numerically solved by FDM using 13 point formula and 5 point formula is used to solve for all other harmonic equations for temperature, heat function and pressure. This chapter analyses the heat transfer in the rectangular channel through heat function and Entropy generation number.

4.1 Introduction

For many years in the past, convection with heat transfer was studied by first law of thermo-dynamics to find temperature field. Heat transfer and fluid flow results for combined free and forced laminar convection with an upward flow in rectangular channel was studied by Ou et al. (1976). In recent times emphasis on design of a model is developed as a science. Therefore deeper study of the subject is essential. The study of heat flow, temperature and flow collectively with second law of thermo-dynamics is essential, due to the fact that one can understand the regions of dissipation of energy and regions of available energy. Heat transfer problems in boundary layer flow past a plate, the pipe flow, flow in the entrance region of a rectangular duct using entropy generation minimization was studied by Bejan (1979). Fakher Oueslati and Brahim Ben–Beya (2017) have studied the entropy analysis within a parallelepiped cavity. Rathish Kumar et al. (2013) have studied the heat transfer due to suction/injection with sinusoidal varying temperature in a cavity. Flow due to Lid driven and natural convection in a square cavity using lattice Boltzmann method was studied by Djamel et al. (2010). Wang et al. (2010) have analyzed the contributions of velocity and velocity gradient to the convective transport of heat flux in a square cavity.

But the study of flow generated due to suction on neighboring walls is paid very less consideration. Hence in this chapter our objective is to examine the two dimensional flow and the heat transfer due to laminar flow convection in a rectangular tube with suction on neighboring walls.

4.2 Mathematical Formulation

The two dimensional laminar viscous flow through a rectangular channel of uniform cross section due to suction/injection at the neighboring walls is considered. The physical representation of the problem is given Fig. 4.1. The Cartesian coordinate system with origin at the bottom left corner and X and Y axes along the walls is taken. The channel is of length a along X direction and height b along Y direction. Injection with velocity V_1 at the wall $Y=b$ and suction with velocity V_2 at the wall $X=a$ are imposed. The flow is developed because of the suction.

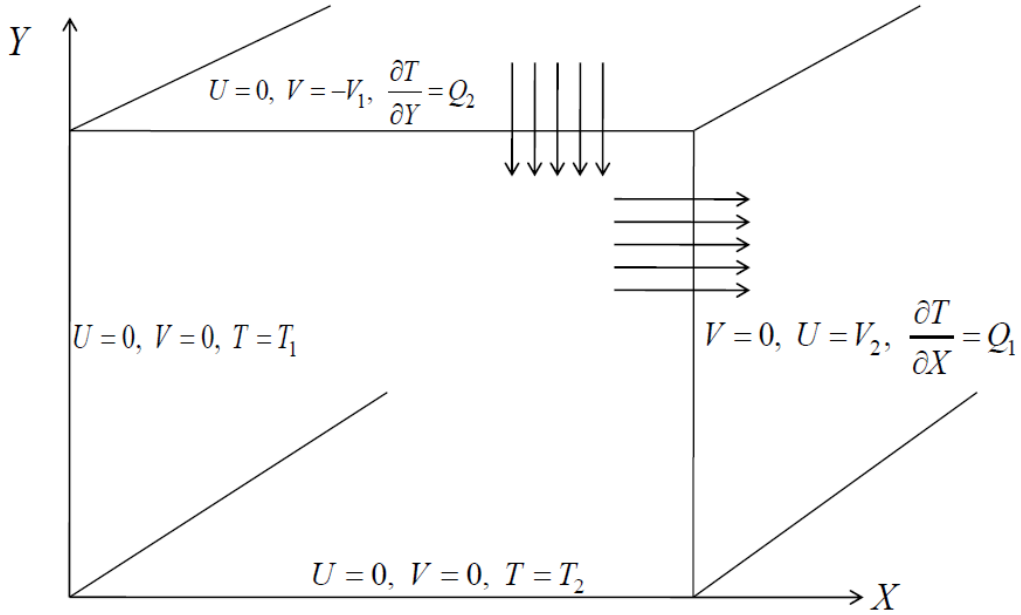

Fig. 4.1: Convective flow configuration in a rectangular channel with adjacent wall suction

Governing Equations

The equations of motion for the flow are given below:

$$\nabla.\mathbf{Q}=0 \tag{4.1}$$

$$\rho\frac{d\mathbf{Q}}{dt}=-\nabla P+\mu\nabla^2\mathbf{Q} \tag{4.2}$$

$$\rho c_p\frac{dT}{dt}=k\nabla^2T \tag{4.3}$$

where **Q** is the velocity of fluid particle, P is pressure, T is the temperature, ρ is fluid density, μ is the coefficient of viscosity, k is the thermal conductivity of the fluid and c_p heat capacity at constant pressure.

The flow is two dimensional and hence **Q**= (U, V).

Boundary conditions for the problem

Velocity of fluid satisfies impermeability condition and no slip condition on walls X=0, Y=0 and suction and no slip condition at the permeable walls X=a and Y=b. The temperature field satisfies constant heat flux at the permeable walls X=a and Y=b and constant temperature is maintained on the impermeable walls X=0, Y=0.

Due to no slip condition on the walls X=0 and Y=0, the tangential velocities are zero.

i.e., on X=0, V=0 $\Rightarrow \frac{\partial \psi}{\partial X} = 0$ and on Y=0, U=0 $\Rightarrow \frac{\partial \psi}{\partial Y} = 0$.

Due to impermeability condition on the walls X=0 and Y=0, the normal velocities are also zero.

i.e., on X=0, U=0 $\Rightarrow \frac{\partial \psi}{\partial Y} = 0$ and on Y=0, V=0 $\Rightarrow \frac{\partial \psi}{\partial X} = 0$.

Due to no slip condition on the walls X=a and Y=b, the tangential velocities are zero.

i.e., on X=a, V=0 $\Rightarrow \frac{\partial \psi}{\partial X} = 0$ and on Y=b, U=0 $\Rightarrow \frac{\partial \psi}{\partial Y} = 0$.

On permeable walls, the suction velocity on X=a is V_2 and the injection velocity on Y=b is V_1.

i.e., on X=a, U=V_2 $\Rightarrow \frac{\partial \psi}{\partial Y} = V_2$ and on Y=b, V=–V_1 $\Rightarrow \frac{\partial \psi}{\partial X} = V_1$.

The walls X=0 and Y=0 are maintained at constant temperatures. i.e., T=T_1 on X=0 and T=T_2 on Y=0.

On the walls X=a and Y=b constant heat fluxes are imparted.

i.e., $\frac{\partial T}{\partial X} = Q_1$ on $X = a$ and $\frac{\partial T}{\partial Y} = Q_2$ on $Y = b$.

Non-dimensionalization

We introduce the following non–dimensional scheme and non–dimensional parameters V_0=suction parameter, y_0=geometric parameter, Pe=Peclet number, Re=Reynolds number.

$$X = ax,\ Y = ay,\ U = V_1 u,\ V = V_1 v,\ P = \rho V_1^2 p,\ T - T_1 = \theta(T_2 - T_1) \tag{4.4}$$

$$\mathrm{Re} = \frac{\rho V_1 a}{\mu},\ \ Pe = \frac{\rho c_p V_1 a}{k} = \mathrm{Re}^* \mathrm{Pr},\ \ y_0 = \frac{b}{a},\ \ V_0 = \frac{V_2}{V_1} \tag{4.5}$$

The flow is steady and hence independent of time *t*.

4.3 Solution of the problem

4.3.1 Stream function

We introduce stream function ψ as below such that equation (4.1) is satisfied.

$$u = \frac{\partial \psi}{\partial y} \quad \text{and} \quad v = -\frac{\partial \psi}{\partial x} \tag{4.6}$$

Taking curl to equation (4.2) and substituting (4.6), we get the equation for the non-dimensional stream function ψ as

$$\nabla^4 \psi + \mathrm{Re}\left(\frac{\partial \psi}{\partial x} \frac{\partial}{\partial y}(\nabla^2 \psi) - \frac{\partial \psi}{\partial y} \frac{\partial}{\partial x}(\nabla^2 \psi) \right) = 0 \tag{4.7}$$

with boundary conditions:

$$\frac{\partial \psi}{\partial x} = 0 \ \text{ on } \ x = 0 \ \text{ and } \quad \text{on } \ x = 1$$

$$\frac{\partial \psi}{\partial y} = 0 \ \text{ on } \ x = 0 \ \text{ and } \ \frac{\partial \psi}{\partial y} = V_0 \ \text{ on } \ x = 1$$

$$\frac{\partial \psi}{\partial x} = 0 \ \text{ on } \ y = 0 \ \text{ and } \ \frac{\partial \psi}{\partial x} = 1 \ \text{ on } \ y = y_0$$

$$\frac{\partial \psi}{\partial y} = 0 \ \text{ on } \ y = 0 \ \text{ and } \quad \text{on } \ y = y_0$$

These conditions, by integrating, are converted in to the conditions on ψ as follows:

$$\left.\begin{aligned} &\frac{\partial \psi}{\partial x} = 0 \text{ on } x = 0 \text{ and } x = 1 \\ &\psi = 0 \text{ on } x = 0 \text{ and } y = 0 \\ &\psi = x \text{ on } y = y_0;\ \ \psi = V_0 y \text{ on } x = 1 \\ &\frac{\partial \psi}{\partial y} = 0 \text{ on } y = 0 \text{ and } y = y_0 \end{aligned}\right\} \tag{4.8}$$

We solve the equation (4.7) with conditions (4.8) by Finite Difference Method. The cavity is covered with a mesh of step size *h* with (*M*–1) intervals on *X* direction and (*N*–1) intervals on *Y* direction. For each grid point (*i*, *j*) within the cavity, the 4th order

term is approximated by 13 point scheme as given in Titus Petrila and Damian Trif (2005) and Pozrikidis (1998). Then equation (4.7) can be written as:

$$20\psi_{i,j}^{(n)} - 8(\psi_{i+1,j}^{(n)} + \psi_{i-1,j}^{(n)} + \psi_{i,j+1}^{(n)} + \psi_{i,j-1}^{(n)}) + 2(\psi_{i+1,j+1}^{(n)} + \psi_{i-1,j+1}^{(n)} + \psi_{i+1,j-1}^{(n)} + \psi_{i-1,j-1}^{(n)})$$
$$+(\psi_{i,j+2}^{(n)} + \psi_{i,j-2}^{(n)} + \psi_{i+2,j}^{(n)} + \psi_{i-2,j}^{(n)}) + \frac{\mathrm{Re}}{4}[(\psi_{i+1,j}^{(n-1)} - \psi_{i-1,j}^{(n-1)})(\psi_{i+1,j+1}^{(n)} - \psi_{i+1,j-1}^{(n)} + \psi_{i-1,j+1}^{(n)} - \psi_{i-1,j-1}^{(n)}$$
$$-4\psi_{i,j+1}^{(n)} + 4\psi_{i,j-1}^{(n)} + \psi_{i,j+2}^{(n)} - \psi_{i,j-2}^{(n)}) - (\psi_{i,j+1}^{(n-1)} - \psi_{i,j-1}^{(n-1)})(\psi_{i+2,j}^{(n)} - \psi_{i-2,j}^{(n)} - 4\psi_{i+1,j}^{(n)} + 4\psi_{i-1,j}^{(n)}$$
$$+\psi_{i+1,j+1}^{(n)} - \psi_{i-1,j+1}^{(n)} + \psi_{i+1,j-1}^{(n)} - \psi_{i-1,j-1}^{(n)})] = 0 \qquad \text{for } i = 2, 3, \ldots, M-1 \ \& \ j = 2, 3, \ldots, N-1 \tag{4.9}$$

For the boundary conditions containing derivatives, we used central difference scheme. The nodes numbering is as follows:

Along X direction	Along Y direction
x_1 node on the boundary $x = 0$.	y_1 node on the boundary $y = 0$.
$x_2, x_3, \ldots, x_{M-1}$ inside the computational	$y_2, y_3, \ldots, y_{N-1}$ inside the computational
x_M node on the boundary $x=1$	y_N node on the boundary $y=y_0$

Thus at $x=0$, we have, $\psi(0, y) = 0$ and $\dfrac{\partial \psi}{\partial x} = 0$.

i.e., $\psi_{1,j} = 0$ and $\dfrac{\psi_{2,j} - \psi_{0,j}}{2h} = 0$ or $\psi_{2,j} = \psi_{0,j}$ for j=1,2,...,N (4.10)

at x=1, we will have, $\psi(1, y) = V_0 y$ and $\dfrac{\partial \psi}{\partial x} = 0$.

i.e., $\psi_{M,j} = V_0(j-1)h$ and $\dfrac{\psi_{M+1,j} - \psi_{M-1,j}}{2h} = 0$ or $\psi_{M+1,j} = \psi_{M-1,j}$ for j=1,2,...,N (4.11)

Similarly at y=0 we have,

$\psi_{i,1} = 0$ and $\psi_{i,2} = \psi_{i,0}$ for i=2,3,...,$M-1$ (4.12)

Finally at $y=y_0$ we have,

$\psi_{i,N} = (i-1)h$ and $\psi_{i,N+1} = \psi_{i,N-1}$ for i=2,3,...,$M-1$ (4.13)

Equation (4.9) involves (M–2)(N–2) internal points +(2M+2N–4) boundary points +(2M+2N) external or fictitious points and hence in total MN +2M +2N–8 number of unknowns. Now equation (4.9) gives (M–2)(N–2) number of equations, (4.10) gives 2N equations, (4.11) gives 2N equations, (4.12) gives 2(M–2) equations and (4.13) gives 2(M–2) equations and hence in total MN+2M+2N–8 equations. Thus the scheme in (4.9) can be solved uniquely by introducing fictitious nodes externally through central difference formula for the derivative conditions on the boundary.

Now by eliminating known boundary values, the equation (4.9) can be written in the form:

$$\left.\begin{array}{lll} \text{for } i=2, & A_1\psi_2 + A_2\psi_3 + A_3\psi_4 = a_2 \\ \text{for } i=3, & A_4\psi_2 + A_5\psi_3 + A_2\psi_4 + A_3\psi_5 = a_3 \\ \text{for } 3 < i < M-2, & A_6\psi_{i-2} + A_4\psi_{i-1} + A_5\psi_i + A_2\psi_{i+1} + A_3\psi_{i+2} = a_i \\ \text{for } i=M-2, & A_6\psi_{M-4} + A_4\psi_{M-3} + A_5\psi_{M-2} + A_2\psi_{M-1} = a_{M-2} \\ \text{for } i=M-1, & A_6\psi_{M-3} + A_4\psi_{M-2} + A_7\psi_{M-1} = a_{M-1} \end{array}\right\} \quad (4.14)$$

where

$$A_1 = \begin{bmatrix} 22-\frac{\text{Re}}{4}(f_{i,2}-g_{i,2}) & -8-\text{Re}.f_{i,2} & 1+\frac{\text{Re}}{4}f_{i,2} & 0 & 0 & \cdots & 0 & \cdots & 0 \\ -8+\text{Re}.f_{i,3} & 21+\frac{\text{Re}}{4}g_{i,3} & -8-\text{Re}.f_{i,3} & 1+\frac{\text{Re}}{4}f_{i,3} & 0 & \cdots & 0 & \cdots & 0 \\ 1-\frac{\text{Re}}{4}f_{i,4} & -8+\text{Re}.f_{i,4} & 21+\frac{\text{Re}}{4}g_{i,4} & -8-\text{Re}.f_{i,4} & 1+\frac{\text{Re}}{4}f_{i,4} & 0 & \cdots & 0 & \cdots \; 0 \\ \cdots & & & & & & & & \\ \cdots & & & & & & & & \\ 0 & \cdots & 0 & \cdots & 0 & 1-\frac{\text{Re}}{4}f_{i,N-2} & -8+\text{Re}.f_{i,N-2} & 21+\frac{\text{Re}}{4}g_{i,N-2} & -8-\text{Re}.f_{i,N-2} \\ 0 & \cdots & 0 & \cdots & 0 & 0 & 1-\frac{\text{Re}}{4}f_{i,N-1} & -8+\text{Re}.f_{i,N-1} & 22+\frac{\text{Re}}{4}(f_{i,N-1}+g_{i,N-1}) \end{bmatrix},$$

for $i = 2, M-2$

$$A_2 = \begin{bmatrix} -8+\text{Re}.g_{i,2} & 2+\frac{\text{Re}}{4}(f_{i,2}-g_{i,2}) & 0 & 0 & \cdots & 0 \\ 2-\frac{\text{Re}}{4}(f_{i,3}+g_{i,3}) & -8+\text{Re}.g_{i,3} & 2+\frac{\text{Re}}{4}(f_{i,3}-g_{i,3}) & 0 & \cdots & 0 \\ \cdots & & & & & \\ \cdots & & & & & \\ 0 & \cdots & 0 & 2-\frac{\text{Re}}{4}(f_{i,N-2}+g_{i,N-2}) & -8+\text{Re}.g_{i,N-2} & 2+\frac{\text{Re}}{4}(f_{i,N-2}-g_{i,N-2}) \\ 0 & \cdots & 0 & 0 & 2-\frac{\text{Re}}{4}(f_{i,N-1}+g_{i,N-1}) & -8+\text{Re}.g_{i,N-1} \end{bmatrix},$$

for $i = 2,3,\ldots,M-2$

$$A_3 = \begin{bmatrix} 1-\frac{\text{Re}}{4}g_{i,2} & 0 & \cdots & 0 \\ 0 & 1-\frac{\text{Re}}{4}g_{i,3} & 0 & \cdots \; 0 \\ \cdots & & & \\ \cdots & & & \\ 0 & \cdots & 0 & 1-\frac{\text{Re}}{4}g_{i,N-2} \quad 0 \\ 0 & \cdots & 0 & 0 \quad 1-\frac{\text{Re}}{4}g_{i,N-1} \end{bmatrix}, \text{ for } i = 2,3,\ldots,M-3$$

$$A_4 = \begin{bmatrix} -8-\mathrm{Re}.g_{i,2} & 2+\frac{\mathrm{Re}}{4}(f_{i,2}+g_{i,2}) & 0 & 0 & \ldots & 0 \\ 2-\frac{\mathrm{Re}}{4}(f_{i,3}-g_{i,3}) & -8-\mathrm{Re}.g_{i,3} & 2+\frac{\mathrm{Re}}{4}(f_{i,3}+g_{i,3}) & 0 & \ldots & 0 \\ \ldots & \ldots & \ldots & \ldots & \ldots & \ldots \\ \ldots & \ldots & \ldots & \ldots & \ldots & \ldots \\ 0 & \ldots & 0 & 2-\frac{\mathrm{Re}}{4}(f_{i,N-2}-g_{i,N-2}) & -8-\mathrm{Re}.g_{i,N-2} & 2+\frac{\mathrm{Re}}{4}(f_{i,3}+g_{i,N-2}) \\ 0 & \ldots & 0 & 0 & 2-\frac{\mathrm{Re}}{4}(f_{i,N-1}-g_{i,N-1}) & -8-\mathrm{Re}.g_{i,N-1} \end{bmatrix},$$

for $i = 3,4,\ldots,M-1$

$$A_5 = \begin{bmatrix} 21-\frac{\mathrm{Re}}{4}f_{i,2} & -8-\mathrm{Re}.f_{i,2} & 1+\frac{\mathrm{Re}}{4}f_{i,2} & 0 & 0 & \ldots & 0 & \ldots & 0 \\ -8+\mathrm{Re}.f_{i,3} & 20 & -8-\mathrm{Re}.f_{i,3} & 1+\frac{\mathrm{Re}}{4}f_{i,3} & 0 & \ldots & 0 & \ldots & 0 \\ 1-\frac{\mathrm{Re}}{4}f_{i,4} & -8+\mathrm{Re}.f_{i,4} & 20 & -8-\mathrm{Re}.f_{i,4} & 1+\frac{\mathrm{Re}}{4}f_{i,4} & 0 & \ldots & 0 & \ldots & 0 \\ \ldots & \ldots & \ldots & \ldots & \ldots & \ldots & \ldots & \ldots & \ldots & \ldots \\ \ldots & \ldots & \ldots & \ldots & \ldots & \ldots & \ldots & \ldots & \ldots & \ldots \\ 0 & \ldots & 0 & \ldots & 0 & 1-\frac{\mathrm{Re}}{4}f_{i,N-2} & -8+\mathrm{Re}.f_{i,N-2} & 20 & -8-\mathrm{Re}.f_{i,N-2} \\ 0 & \ldots & 0 & \ldots & 0 & 0 & 1-\frac{\mathrm{Re}}{4}f_{i,N-1} & -8+\mathrm{Re}.f_{i,N-1} & 21+\frac{\mathrm{Re}}{4}f_{i,N-1} \end{bmatrix},$$

for $i = 3,4,\ldots,M-2$

$$A_6 = \begin{bmatrix} 1+\frac{\mathrm{Re}}{4}g_{i,2} & 0 & \ldots & 0 \\ 0 & 1+\frac{\mathrm{Re}}{4}g_{i,3} & 0 & \ldots & 0 \\ \ldots & \ldots & \ldots & \ldots & \ldots \\ \ldots & \ldots & \ldots & \ldots & \ldots \\ 0 & \ldots & 0 & 1+\frac{\mathrm{Re}}{4}g_{i,N-2} & 0 \\ 0 & \ldots & 0 & 0 & 1+\frac{\mathrm{Re}}{4}g_{i,N-1} \end{bmatrix}, \text{ for } i = 4,5,\ldots,M-1$$

$$A_7 = \begin{bmatrix} 22-\frac{\mathrm{Re}}{4}(f_{i,2}+g_{i,2}) & -8-\mathrm{Re}.f_{i,2} & 1+\frac{\mathrm{Re}}{4}f_{i,2} & 0 & 0 & \ldots & 0 & \ldots & 0 \\ -8+\mathrm{Re}.f_{i,3} & 21-\frac{\mathrm{Re}}{4}g_{i,3} & -8-\mathrm{Re}.f_{i,3} & 1+\frac{\mathrm{Re}}{4}f_{i,3} & 0 & \ldots & 0 & \ldots & 0 \\ 1-\frac{\mathrm{Re}}{4}f_{i,4} & -8+\mathrm{Re}.f_{i,4} & 21-\frac{\mathrm{Re}}{4}g_{i,4} & -8-\mathrm{Re}.f_{i,4} & 1+\frac{\mathrm{Re}}{4}f_{i,4} & 0 & \ldots & 0 & \ldots & 0 \\ \ldots & \ldots & \ldots & \ldots & \ldots & \ldots & \ldots & \ldots & \ldots & \ldots \\ \ldots & \ldots & \ldots & \ldots & \ldots & \ldots & \ldots & \ldots & \ldots & \ldots \\ 0 & \ldots & 0 & \ldots & 0 & 1-\frac{\mathrm{Re}}{4}f_{i,N-2} & -8+\mathrm{Re}.f_{i,N-2} & 21-\frac{\mathrm{Re}}{4}g_{i,N-2} & -8-\mathrm{Re}.f_{i,N-2} \\ 0 & \ldots & 0 & \ldots & 0 & 0 & 1-\frac{\mathrm{Re}}{4}f_{i,N-1} & -8+\mathrm{Re}.f_{i,N-1} & 22+\frac{\mathrm{Re}}{4}(f_{i,N-1}-g_{i,N-1}) \end{bmatrix},$$

for $i = M-1$

$$\psi_i = \begin{bmatrix} \psi_{i,2} \\ \psi_{i,3} \\ . \\ . \\ \psi_{i,N-2} \\ \psi_{i,N-1} \end{bmatrix}, \text{ for } i = 2,3,...,M-1$$

$$a_i = h\begin{bmatrix} 0 \\ 0 \\ . \\ . \\ -\left(1+\frac{\mathrm{Re}}{4} f_{i,N-2}\right)(i-1) \\ -\left(2+\frac{\mathrm{Re}}{4}(f_{i,N-1}+g_{i,N-1})\right)(i-2)+(8+\mathrm{Re}.f_{i,N-1})(i-1)-\left(2+\frac{\mathrm{Re}}{4}(f_{i,N-1}-g_{i,N-1})\right)i \end{bmatrix},$$

for $i = 2,3,...,M-3$

$$a_{M-2} = h\begin{bmatrix} -\left(1-\frac{\mathrm{Re}}{4} g_{M-2,2}\right)V_0 \\ -\left(1-\frac{\mathrm{Re}}{4} g_{M-2,3}\right)2V_0 \\ . \\ . \\ -\left(1-\frac{\mathrm{Re}}{4} g_{M-2,N-2}\right)V_0(N-3)-\left(1+\frac{\mathrm{Re}}{4} f_{M-2,N-2}\right)(M-3) \\ -\left(1-\frac{\mathrm{Re}}{4} g_{M-2,N-1}\right)V_0(N-2)-\left(2+\frac{\mathrm{Re}}{4}(f_{M-2,N-1}+g_{M-2,N-1})\right)(M-4)+(8+\mathrm{Re}.f_{M-2,N-1})(M-3)-... \\ \left(2+\frac{\mathrm{Re}}{4}(f_{M-2,N-1}-g_{M-2,N-1})\right)(M-2) \end{bmatrix}$$

$$a_{M-1} = h\begin{bmatrix} -(-8+\mathrm{Re}.g_{M-1,2})V_0-\left(2+\frac{\mathrm{Re}}{4}(f_{M-1,2}-g_{M-1,2})\right)2V_0 \\ -\left(2-\frac{\mathrm{Re}}{4}(f_{M-1,3}+g_{M-1,3})\right)V_0-(-8+\mathrm{Re}.g_{M-1,3})2V_0-\left(2+\frac{\mathrm{Re}}{4}(f_{M-1,3}-g_{M-1,3})\right)3V_0 \\ . \\ . \\ -\left(2-\frac{\mathrm{Re}}{4}(f_{M-1,N-2}+g_{M-1,N-2})\right)(N-4)V_0-(-8+\mathrm{Re}.g_{M-1,N-2})(N-3)V_0-... \\ \left(2+\frac{\mathrm{Re}}{4}(f_{M-1,N-2}-g_{M-1,N-2})\right)(N-2)V_0-\left(1+\frac{\mathrm{Re}}{4} f_{M-1,N-2}\right)(M-2) \\ -\left(2-\frac{\mathrm{Re}}{4}(f_{M-1,N-1}+g_{M-1,N-1})\right)(N-3)V_0-(-8+\mathrm{Re}.g_{M-1,N-1})(N-2)V_0-... \\ \left(2+\frac{\mathrm{Re}}{4}(f_{M-1,N-1}-g_{M-1,N-1})\right)(N-1)V_0-\left(2+\frac{\mathrm{Re}}{4}(f_{M-1,N-1}+g_{M-1,N-1})\right)(M-3)+... \\ (8+\mathrm{Re}.f_{M-1,N-1}+)(M-2) \end{bmatrix}$$

where $f_{i,j} = \psi_{i+1,j}^{n-1} - \psi_{i-1,j}^{n-1}$

and $g_{i,j} = \psi_{i,j+1}^{n-1} - \psi_{i,j-1}^{n-1}$

These equations in (4.14) are solved by Gauss–Seidel iteration method. All ψ_i, i>2 are set to zero and equation for i=2 is solved for ψ_2, then equation for i=3 is solved for ψ_3. So on to find all ψ_i. For the next iteration, all these are taken as known and the procedure is repeated until, the difference between two iterations for ψ is less than ε (=10^{-4}).

4.3.2 Temperature

The energy equation, given by (4.3), by using (4.4), (4.5) can be reduced to the non–dimensional form as:

$$\nabla^2\theta = Pe\left(u\frac{\partial\theta}{\partial x}+v\frac{\partial\theta}{\partial y}\right) \tag{4.15}$$

with boundary conditions:

$$\left.\begin{aligned} &\frac{\partial\theta}{\partial x}=q_1 \quad \text{on} \quad x=1;\ \ \theta=0 \quad\ \ \text{on} \quad x=0 \\ &\theta=1 \quad\ \ \text{on} \quad y=0;\ \ \frac{\partial\theta}{\partial y}=q_2 \quad \text{on} \quad y=y_0 \end{aligned}\right\} \tag{4.16}$$

The equation (4.15) by second order finite differences can be written as

$$\begin{aligned} &\left[1+\frac{Pe}{4}\left(\psi_{i,j+1}-\psi_{i,j-1}\right)\right]\theta_{i-1,j}+\left[1-\frac{Pe}{4}\left(\psi_{i+1,j}-\psi_{i-1,j}\right)\right]\theta_{i,j-1}-4\theta_{i,j} \\ &\quad+\left[1+\frac{Pe}{4}\left(\psi_{i+1,j}-\psi_{i-1,j}\right)\right]\theta_{i,j+1}+\left[1-\frac{Pe}{4}\left(\psi_{i,j+1}-\psi_{i,j-1}\right)\right]\theta_{i+1,j}=0 \\ &\qquad\qquad \text{for } i=2,3,\ \ldots,M \text{ and } j=2,3,\ \ldots,N \end{aligned} \tag{4.17}$$

The boundary conditions in (4.16) are now expressed as:

$$\text{at } x=0,\ \theta=0 \text{ which implies that } \theta_{1,j}=0 \text{ for } j=2,3,...,N \tag{4.18}$$

$$\text{at } y=0,\ \theta=1 \text{ which implies that } \theta_{i,1}=1 \text{ for } i=2,3,...,M \tag{4.19}$$

$$\text{at } x=1,\ \frac{\partial\theta}{\partial x}=q_1 \text{ which implies that } \theta_{M+1,j}=\theta_{M-1,j}+2hq_1 \text{ for } j=2,3,...,N \tag{4.20}$$

$$\text{at } y=y_0,\ \frac{\partial\theta}{\partial y}=q_2 \text{ which implies that } \theta_{i,N+1}=\theta_{i,N-1}+2hq_2 \text{ for } i=2,3,...,M \tag{4.21}$$

Equation (4.17) involves (M–2)(N–2) internal points +2(M+N–2)–1 boundary points +(M+N–2) external points and a total of MN+M+N–3 unknowns. Now equation (4.17) yields (M–1)(N–1) equations, (4.18) yields N–1 equations, (4.19) yields M–1 equations, (4.20) yields N–1 equations and (4.21) yields M–1 equations and hence a total of MN+M+N–3 equations. Hence the equations in (4.17) can be solved uniquely.

Equation (4.17) does not contain the corner points (1, 1), (1, N+1), (M, 1) & (M, N+1). The equation (4.17) can be put in matrix form as below:

$$\left.\begin{array}{ll} \text{for } i=2: & B_{22}\theta_2 + B_{32}\theta_3 = b_2 \\ \text{for } 2 < i < M-2: & B_{1i}\theta_{i-1} + B_{2i}\theta_i + B_{3i}\theta_{i+1} = b_i \\ \text{for } i=M: & 2I\theta_{M-1} + B_{2M}\theta_M = b_M \end{array}\right\} \quad (22)$$

where $B_{1i} = \begin{bmatrix} 1+u_{i2} & 0 & 0 & \ldots\ldots & 0 & 0 & 0 \\ 0 & 1+u_{i3} & 0 & \ldots\ldots & 0 & 0 & 0 \\ \ldots\ldots & & & & & & \\ 0 & \ldots\ldots & & 0 & 1+u_{iN-1} & 0 & \\ 0 & \ldots\ldots & & 0 & 0 & 1 & \end{bmatrix}$,

$$B_{2i} = \begin{bmatrix} -4 & 1+v_{i2} & 0 & \ldots\ldots & 0 & 0 \\ 1-v_{i3} & -4 & 1+v_{i3} & \ldots\ldots & 0 & 0 \\ \ldots\ldots & & & & & \\ 0 & 0 & \ldots\ldots & 1-v_{iN-1} & -4 & 1+v_{iN-1} \\ 0 & 0 & \ldots\ldots & 0 & 2 & -4 \end{bmatrix},$$

$$B_{3i} = \begin{bmatrix} 1-u_{i2} & 0 & 0 & \ldots\ldots & 0 & 0 & 0 \\ 0 & 1-u_{i3} & 0 & \ldots\ldots & 0 & 0 & 0 \\ \ldots\ldots & & & & & & \\ 0 & \ldots\ldots & & 0 & 1-u_{iN-1} & 0 & \\ 0 & \ldots\ldots & & 0 & 0 & 1 & \end{bmatrix},\ \theta_i = \begin{bmatrix} \theta_{i2} \\ \theta_{i3} \\ \ldots. \\ \ldots. \\ \theta_{iN} \end{bmatrix},$$

$$b_i = \begin{bmatrix} 1-v_{i2} \\ 0 \\ \ldots\ldots \\ 0 \\ 2h(1+v_{iN}) \end{bmatrix} \text{ for } 2 \le i \le M-1,\ b_M = -\begin{bmatrix} 1+2hq_1(1-u_{M,2}) \\ 2hq_1(1-u_{M,3}) \\ \ldots\ldots \\ 2hq_1(1-u_{M,N-1}) \\ 2h(q_1+q_2) \end{bmatrix}$$

where $u_{ij} = \frac{Pe}{4}(\psi_{i,j+1} - \psi_{i,j-1}),\ \ v_{ij} = \frac{Pe}{4}(\psi_{i+1,j} - \psi_{i-1,j})$

The equations in (4.22) for temperature are solved by Gauss-Seidel iteration method as in (4.14) for stream function.

4.3.3 Nusselt Number

Heat transfer coefficient at the walls is given by Fourier's law $\bar{\mathbf{h}} = -k\nabla T$. In non–dimensional form this represents Nusselt number $Nu = -\frac{\partial\theta}{\partial x}\Big]_{x=0,1}$ and $-\frac{\partial\theta}{\partial y}\Big]_{y=0,y_0}$.

The Nusselt number *Nu* is the ratio of convective to conductive heat transfer across the walls. This is studied only at the walls of the channel.

Nusselt number at the wall $x = 0$ is

$$Nu = \left(-\frac{\partial \theta}{\partial x} \right)_{1,j} = \frac{-3\theta_{1,j} + 4\theta_{2,j} - \theta_{3,j}}{2h} \text{ for } j = 1, 2, ..., N$$

Nusselt number at the wall $x = 1$ is

$$Nu = \left(-\frac{\partial \theta}{\partial x} \right)_{M,j} = \frac{-3\theta_{M,j} + 4\theta_{M-1,j} - \theta_{M-2,j}}{2h} \text{ for } j = 1, 2, ..., N$$

Nusselt number at the wall $y = 0$ is

$$Nu = \left(-\frac{\partial \theta}{\partial y} \right)_{i,1} = \frac{-3\theta_{i,1} + 4\theta_{i,2} - \theta_{i,3}}{2h} \text{ for } i = 1, 2, ..., M$$

Nusselt number at the wall $y = y_0$ is

$$Nu = \left(-\frac{\partial \theta}{\partial y} \right)_{i,N} = \frac{-3\theta_{i,N} + 4\theta_{i,N-1} - \theta_{i,N-2}}{2h} \text{ for } i = 1, 2, ..., M$$

Average Nusselt number at the wall x=0 is $\frac{1}{y_0} \int_0^{y_0} Nu \, dy$ evaluated by Trapezoidal rule.

Average Nusselt number at the wall x=1 is $\frac{1}{y_0} \int_0^{y_0} Nu \, dy$ evaluated by Trapezoidal rule.

Average Nusselt number at the wall y=0 is $\int_0^1 Nu \, dx$ evaluated using Trapezoidal rule.

Average Nusselt number at the wall y=y_0 is $\int_0^1 Nu \, dx$ evaluated using Trapezoidal rule.

4.3.4 Entropy Generation and Bejan Number

The dimensional local entropy generation $\bar{S}_{gen}$, (Woods (1975) and by Mikhail et al. (2016)) is expressed as

$$\bar{S}_{gen} = \frac{k}{T_0^2} \left[\left(\frac{\partial T}{\partial X} \right)^2 + \left(\frac{\partial T}{\partial Y} \right)^2 \right] + \frac{\mu}{T_0} \left[2\left(\frac{\partial U}{\partial X} \right)^2 + 2\left(\frac{\partial V}{\partial Y} \right)^2 + \left(\frac{\partial U}{\partial Y} + \frac{\partial V}{\partial X} \right)^2 \right] \quad (4.23)$$

where reference temperature T_0 is taken as $T_0 = 0.5(T_1 + T_2)$.

Equation (4.23) consists two terms: the first is the local entropy generation due to heat transfer by conduction $\bar{S}_{gen,\,ht}$ and the second is the dimensional local entropy generation due to fluid friction $\bar{S}_{gen,\,fr}$.

The corresponding non-dimensional entropy generation number N_s is defined as

$$N_s = \bar{S}_{gen}\frac{T_0^2 a^2}{k(T_2 - T_1)^2}$$

$$= \left[\left(\frac{\partial\theta}{\partial x}\right)^2 + \left(\frac{\partial\theta}{\partial y}\right)^2\right] + Br\left[2\left(\frac{\partial u}{\partial x}\right)^2 + 2\left(\frac{\partial v}{\partial y}\right)^2 + \left(\frac{\partial u}{\partial y} + \frac{\partial v}{\partial x}\right)^2\right]$$

$$N_s = N_h + N_f \tag{4.24}$$

where $Br = \dfrac{\mu V_1^2 T_0}{2k(T_2 - T_1)^2}$ is Brinkman Number.

N_s can be evaluated by writing the derivatives of u, v and θ in centred first order finite differences at inside and boundary nodes x=1, y=y_0 and on x=0, y=0 we use 3–point backward difference formula.

Further, the Bejan number *Be* is a parameter that shows the importance of heat transfer in the domain and is defines as

$$Be = \frac{N_h}{N_h + N_f} \tag{4.25}$$

4.3.5 Heat lines

Net energy flow in X and Y directions are given by (Bejan (2013)):

$$\frac{\partial H^*}{\partial Y} = \rho C_p U(T - T_0) - k\frac{\partial T}{\partial X} \tag{4.26}$$

$$-\frac{\partial H^*}{\partial X} = \rho C_p V(T - T_0) - k\frac{\partial T}{\partial Y} \tag{4.27}$$

Physically, H^*=constant represents a curve across which, the net flow of energy (thermal diffusion and enthalpy flow) is zero. H^* is called heat-function. Oztop et al. (2012) obtained heat lines for inclined channel for a nano-fluid flow. Kimura and Bejan (1983) worked an example problem for heat function in a natural convection in an enclosure heated from the side. Introducing the non–dimensional quantities,

$\theta = \dfrac{T - T_1}{\Delta T}$ and $H^* = Hk\Delta T$ where $\Delta T = T_2 - T_1$

The equation (4.26) and (4.27) reduces to

$$\frac{\partial H}{\partial y} = uPe(\theta - 0.5) - \frac{\partial \theta}{\partial x}, \qquad \frac{\partial H}{\partial x} = -vPe(\theta - 0.5) + \frac{\partial \theta}{\partial y} \tag{4.28}$$

The above equations in (4.28) can be combined to give

$$\nabla^2 H = Pe\left\{(\theta - 0.5)\left(\frac{\partial u}{\partial y} - \frac{\partial v}{\partial x}\right) + \left(u\frac{\partial \theta}{\partial y} - v\frac{\partial \theta}{\partial x}\right)\right\} = Th_{i,j} \tag{4.29}$$

so that the equations in (4.28) will serve as the boundary conditions for *H*. On *x*=0 and on *x*=1, *v*=0 hence on *x*=0, $H_x = \theta_y = 0$ and on *x*=1, $H_x = \theta_y$.

Similarly other conditions are derived

$$\left.\begin{array}{l} \text{on } x = 0,\ \dfrac{\partial H}{\partial x} = \dfrac{\partial \theta}{\partial y} = 0 \text{ on } x = 1,\ \dfrac{\partial H}{\partial x} = \dfrac{\partial \theta}{\partial y} \\ \text{on } y = 0,\ \dfrac{\partial H}{\partial y} = -\dfrac{\partial \theta}{\partial x} = 0 \text{ on } y = y_0,\ \dfrac{\partial H}{\partial y} = -\dfrac{\partial \theta}{\partial x} \end{array}\right\} \tag{4.30}$$

For discretization, we use 5 point formula and equation (4.29) can be written as

$$H_{i-1,j} + H_{i,j-1} - 4H_{i,j} + H_{i,j+1} + H_{i+1,j} = Th_{i,j} \quad \text{for } i = 2,3,...,M-1 \text{ and } j = 2,3,...,N-1 \tag{4.31}$$

on the boundary *x*=0, $\dfrac{\partial H}{\partial x} = 0$ which by using 3–point formula, reduces to

$$-3H_{1,j} + 4H_{2,j} - H_{3,j} = 0 \quad \text{for } j = 1,2,....,N \tag{4.32}$$

Similarly on *y*=0, we have $\dfrac{\partial H}{\partial y} = 0$ which gives to

$$-3H_{i,1} + 4H_{i,2} - H_{i,3} = 0 \quad \text{for } i = 2,3,....,M-1 \tag{4.33}$$

on $y = y_0$, $\dfrac{\partial H}{\partial y} = -\dfrac{\partial \theta}{\partial x}$ which by using 3–point formula for *H* and central difference formula for θ gives to

$$-3H_{i,N} + 4H_{i,N-1} - H_{i,N-2} = \theta_{i-1,N} - \theta_{i+1,N} \quad \text{for } i = 2,3,....,M-1 \tag{4.34}$$

Similarly *x*=1, $\dfrac{\partial H}{\partial x} = \dfrac{\partial \theta}{\partial y}$ yields to:

$$-3H_{M,j} + 4H_{M-1,j} - H_{M-2,j} = \theta_{M,j+1} - \theta_{M,j-1} \quad \text{for } j = 1,2,....,N \tag{4.35}$$

solving the system of *MN* equations in *MN* unknowns (4.31)–(4.35) using Gauss–Seidel iteration method for 500 iterations we get the values of *H*.

4.3.6 Pressure

The equations for pressure, by using the non–dimensional quantities, are reduced to

$$u\frac{\partial u}{\partial x}+v\frac{\partial u}{\partial y}=-\frac{\partial p}{\partial x}+\frac{1}{\mathrm{Re}}\nabla^2 u \tag{4.36}$$

and $$u\frac{\partial v}{\partial x}+v\frac{\partial v}{\partial y}=-\frac{\partial p}{\partial y}+\frac{1}{\mathrm{Re}}\nabla^2 v \tag{4.37}$$

Using continuity condition, from (4.36) and (4.37), we get

$$\nabla^2 p=2\left(\frac{\partial u}{\partial x}\frac{\partial v}{\partial y}-\frac{\partial u}{\partial y}\frac{\partial v}{\partial x}\right)=2\frac{\partial(u,v)}{\partial(x,y)} \tag{4.38}$$

subjected to the boundary conditions:

$$\left.\begin{aligned}&\text{on } x=0 \text{ and } x=1,\ \frac{\partial p}{\partial x}=\frac{1}{\mathrm{Re}}\nabla^2 u\\&\text{on } y=0 \text{ and } y=y_0,\ \frac{\partial p}{\partial y}=\frac{1}{\mathrm{Re}}\nabla^2 v\end{aligned}\right\} \tag{4.39}$$

(Roache (1972) gave different methods to solve for pressure.) Discretizing (4.38) by central differences, we get

$$p_{i-1,j}+p_{i,j-1}-4p_{i,j}+p_{i,j+1}+p_{i+1,j}=\frac{2}{h^2}\left(\psi_{i+1,j}-2\psi_{i,j}+\psi_{i-1,j}\right)\left(\psi_{i,j+1}-2\psi_{i,j}+\psi_{i,j-1}\right)$$
$$-\frac{1}{8h^2}\left(\psi_{i+1,j+1}-\psi_{i-1,j+1}-\psi_{i+1,j-1}+\psi_{i-1,j-1}\right)^2 \quad \text{for } i=2,3,\ldots M-1 \text{ and } j=2,3,\ldots N-1 \tag{4.40}$$

on the boundary x=0, we use central differences to get RHS as:

$$\left[\nabla^2 u\right]_{1,j}=\frac{1}{2h^3}\left[\psi_{0,j+1}-\psi_{0,j-1}-2\psi_{1,j+1}+2\psi_{1,j-1}+\psi_{2,j+1}-\psi_{2,j-1}\right]=U_{1,j}$$

By using 3–point formula for LHS, we have finally

$$-3p_{1,j}+4p_{2,j}-p_{3,j}=2hU_{1,j} \quad \text{for } j=1,2,\ldots,N \tag{4.41}$$

We use similarly central differences on RHS at x=1 and get:

$$\left[\nabla^2 u\right]_{M,j}=\frac{1}{2h^3}\left[\psi_{M-1,j+1}-\psi_{M-1,j-1}-2\psi_{M,j+1}+2\psi_{M,j-1}+\psi_{M+1,j+1}-\psi_{M+1,j-1}\right]=U_{M,j}$$

and hence the equation at x=1 is given by

$$-3p_{M,j}+4p_{M-1,j}-p_{M-2,j}=2hU_{M,j} \quad \text{for } j=1,2,\ldots,N \tag{4.42}$$

on y=0, we use central differences to get RHS as:

$$\left[\nabla^2 v\right]_{i,1}=\frac{1}{2h^3}\left[-\psi_{i+1,0}+\psi_{i-1,0}+2\psi_{i+1,1}-2\psi_{i-1,1}-\psi_{i+1,2}+\psi_{i-1,2}\right]=U_{i,1}$$

By using 3–point formula for LHS, we have finally

$$-3p_{i,1} + 4p_{i,2} - p_{i,3} = 2hU_{i,1} \quad \text{for } i = 2,3,....,M-1 \tag{4.43}$$

we use similarly central differences on RHS at $y=y_0$ and get:

$$\left[\nabla^2 v\right]_{i,N} = \frac{1}{2h^3}\left[-\psi_{i+1,N-1} + \psi_{i-1,N-1} + 2\psi_{i+1,N} - 2\psi_{i-1,N} - \psi_{i+1,N+1} + \psi_{i-1,N+1}\right] = U_{i,N}$$

and hence the equation at $y=y_0$ is given by

$$-3p_{i,N} + 4p_{i,N-1} - p_{i,N-2} = 2hU_{i,N} \quad \text{for } i = 2,3,....,M-1 \tag{4.44}$$

Solving system of *MN* equations in *MN* unknowns in (4.40)–(4.44) by using Gauss–Seidel iteration for 500 iterations we get the values of *p*.

4.4 Results and Discussion

For the fluid flow in the chamber, bi-harmonic equation for stream function is solved. Using the stream function, temperature distribution is obtained. Using temperature field, the regions of available energy and regions of high friction are found by entropy generation number and Began number. Then the heat flow lines are drawn and Pressure field is also found.

4.4.1 Streamlines

The stream lines generated due to injection at the top wall and suction at the right wall are shown in Fig. 4.2 to Fig. 4.4. The figures are drawn at two geometric parameter values y_0=0.75 and 10. We can observe that as the value of the suction parameter V_0 increases, stream function values on right wall increases, because $\psi = V_0 y$ on x=1. Again for small values of V_0, stream lines reenter the side x=1 at the top corner. As the geometric parameter y_0 increases, we get narrow parallel wall geometry. In this case of nearly parallel plate geometry, *we observe that near to top right corner high flow and little circulation for small values of V_0 and for high values of Re.*

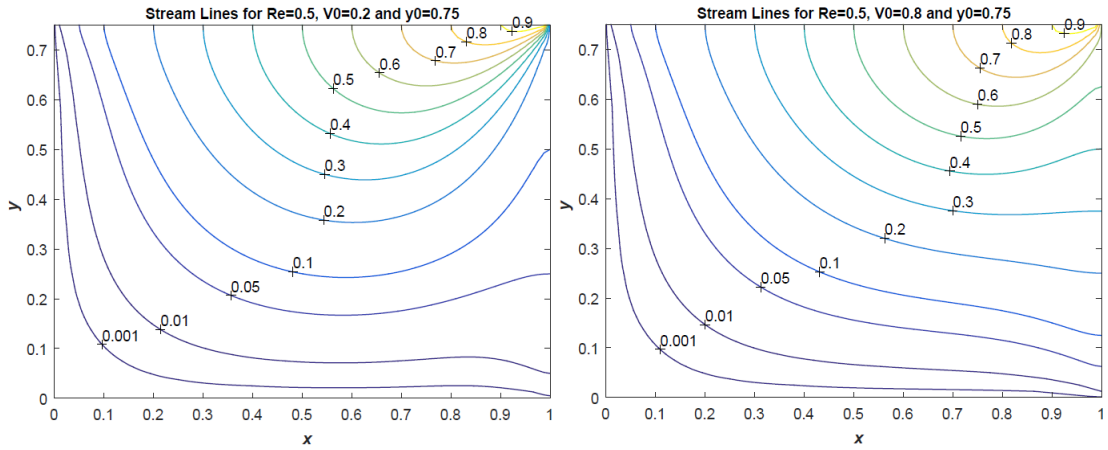

Fig. 4.2: Stream Lines for different values of V_0 at Re = 0.5 and y_0 = 0.75.

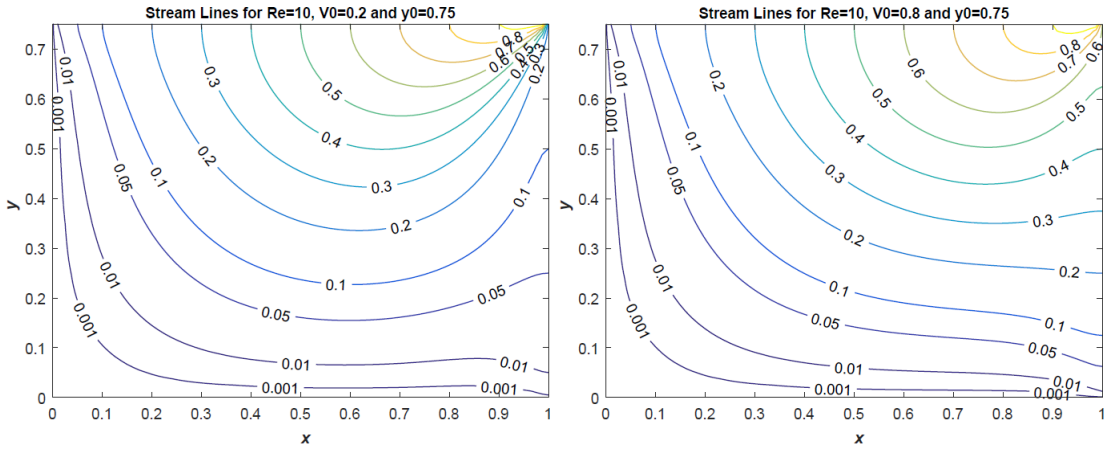

Fig. 4.3: Stream Lines for different values of V_0 at Re = 10 and y_0 = 0.75.

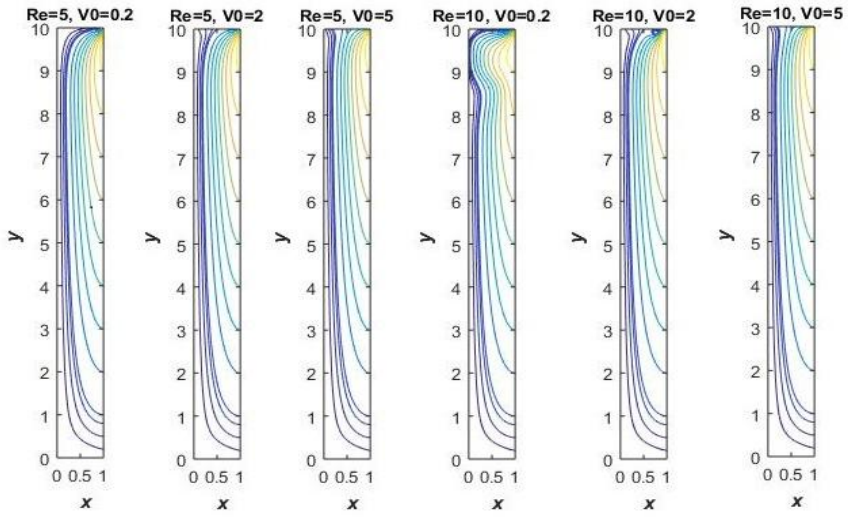

Fig. 4.4: Stream Lines for y_0 = 10 at different values of Re and V_0.

4.4.2 Temperature field

The Fig. 4.5 and Fig. 4.6 display the nature of temperature contours. As the values of Reynolds number Re is increasing, more temperature lines enter into the flow i.e.,

density of heat transfer increases and in this case *when V_0 is small temperature lines re–enter near to the top corner*. As *Re* increases, the temperature contours take bending near to the left down corner.

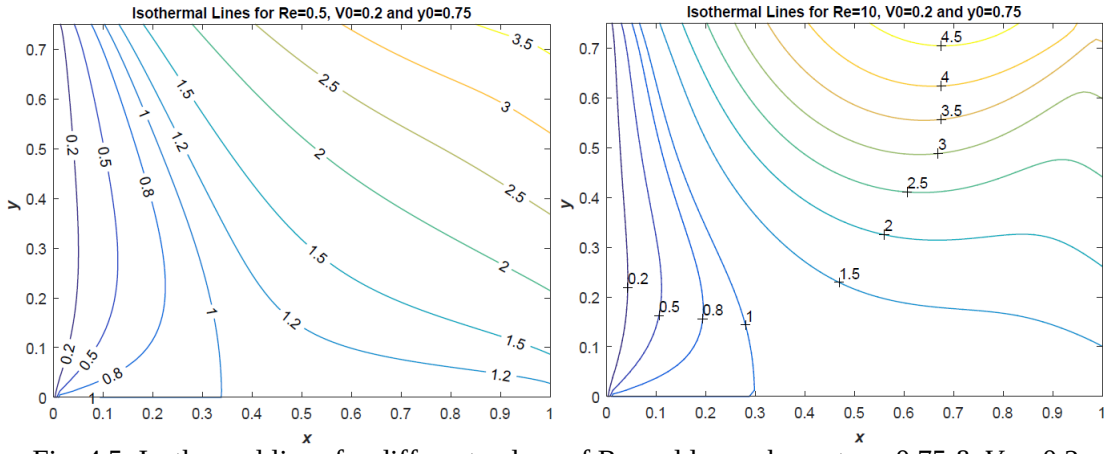

Fig. 4.5: Isothermal lines for different values of Reynolds numbers at y_0=0.75 & V_0 = 0.2.

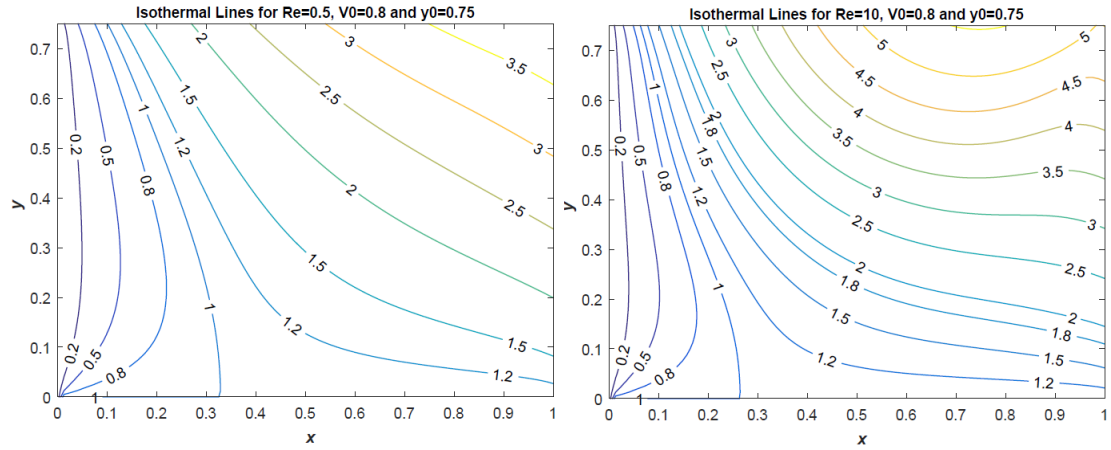

Fig. 4.6: Isothermal lines for different values of Reynolds numbers at y_0=0.75 & V_0 = 0.8.

4.4.3 Mesh Sensitivity Analysis (Davis Test)

In Table. 4.1 to Table. 4.3, the value of the stream function at the mid-point $|\psi_{mid}|$ and maximum value of the stream function $|\psi_{max}|$ and its location (and similarly for temperature) for different mesh sizes are shown. We find that as *h* is decreasing the values are converging with error less than 1 percent if V_0<1. Hence suction parameter V_0 is important factor which effects the numerical solution. Here we get convergent solution for V_0<1. In the case of Davis (1983), Davis and Jones (1983), Mallinson and Davis (1977), Nusselt number is nearly in the range of Rayleigh number. In the present case since we did not consider natural convection the Nusselt number is also very small (<10).

Table. 4.1: The original Solution for *Re*=0.5 and V_0=0.8

Mesh Size *h*	$\lvert\psi_{mid}\rvert$	$\lvert\psi_{max}\rvert$ (x, y)	$\lvert\theta_{mid}\rvert$	$\lvert\theta_{max}\rvert$ (x, y)
0.05	0.2306	0.95 (0.95, 0.75)	1.69075	4.0029 (1, 0.75)
0.025	0.2306	0.9750 (0.975, 0.75)	1.6858	3.9709 (1, 0.75)
0.0125	0.2306	0.9875 (0.9875, 0.75)	1.6838	3.95 (1, 0.75)

Table. 4.2: The original Solution for *Re*=5 and V_0=0.8

Mesh Size *h*	$\lvert\psi_{mid}\rvert$	$\lvert\psi_{max}\rvert$ (x, y)	$\lvert\theta_{mid}\rvert$	$\lvert\theta_{max}\rvert$ (x, y)
0.05	0.24215	0.95 (0.95, 0.75)	1.8298	3.8177 (0.75, 0.75)
0.025	0.2420	0.9750 (0.975, 0.75)	1.8227	3.8224 (0.775, 0.75)
0.0125	0.2420	0.9875 (0.9875, 0.75)	1.8210	3.8245 (0.7625, 0.75)

Table 4.3. The original Solution for *Re*=10 and V_0=0.8

Mesh Size *h*	$\lvert\psi_{mid}\rvert$	$\lvert\psi_{max}\rvert$ (x, y)	$\lvert\theta_{mid}\rvert$	$\lvert\theta_{max}\rvert$ (x, y)
0.05	0.2511	0.95 (0.95, 0.75)	2.62785	5.4931 (0.75, 0.75)
0.025	0.2508	0.9750 (0.975, 0.75)	2.6048	5.5260 (0.75, 0.75)
0.0125	0.2507	0.9875 (0.9875, 0.75)	2.5968	5.5321 (0.75, 0.75)

4.4.4 Nusselt Number Nu

Average Nusselt number at the walls for different suction parameters and for fixed *Re* = 0.5 is calculated and shown in Table. 4.4.

Table. 4.4

Average Nusselt Number for *Re* = 0.5	*At x*=0	*At x*=1	*At y*=0	*At y*=y_0
V_0 = 0.2	–8.342662	1.996419	0.484387	3.967440
V_0 = 0.8	–8.438753	1.983457	0.324371	3.964564
V_0 = 2	–8.696321	1.952621	– 1.122284	3.956074

From Table. 4.4, we can say that the wall x = 0 is absorbing the heat and the wall y = y_0 is releasing the heat. In all cases, Nusselt number decreases as V_0 is increases.

From Fig. 4.7 we observe that the Nusselt number is almost same for all V_0 at any wall, but it is decreasing at the wall y=0 for all V_0. The Nusselt number is increasing at the beginning values of y and x at the walls x=1 and y=y_0 respectively and constant for the remaining values of y and x for all V_0. This is due to the boundary conditions $\frac{\partial \theta}{\partial x} = q_1$ and $\frac{\partial \theta}{\partial y} = q_2$.

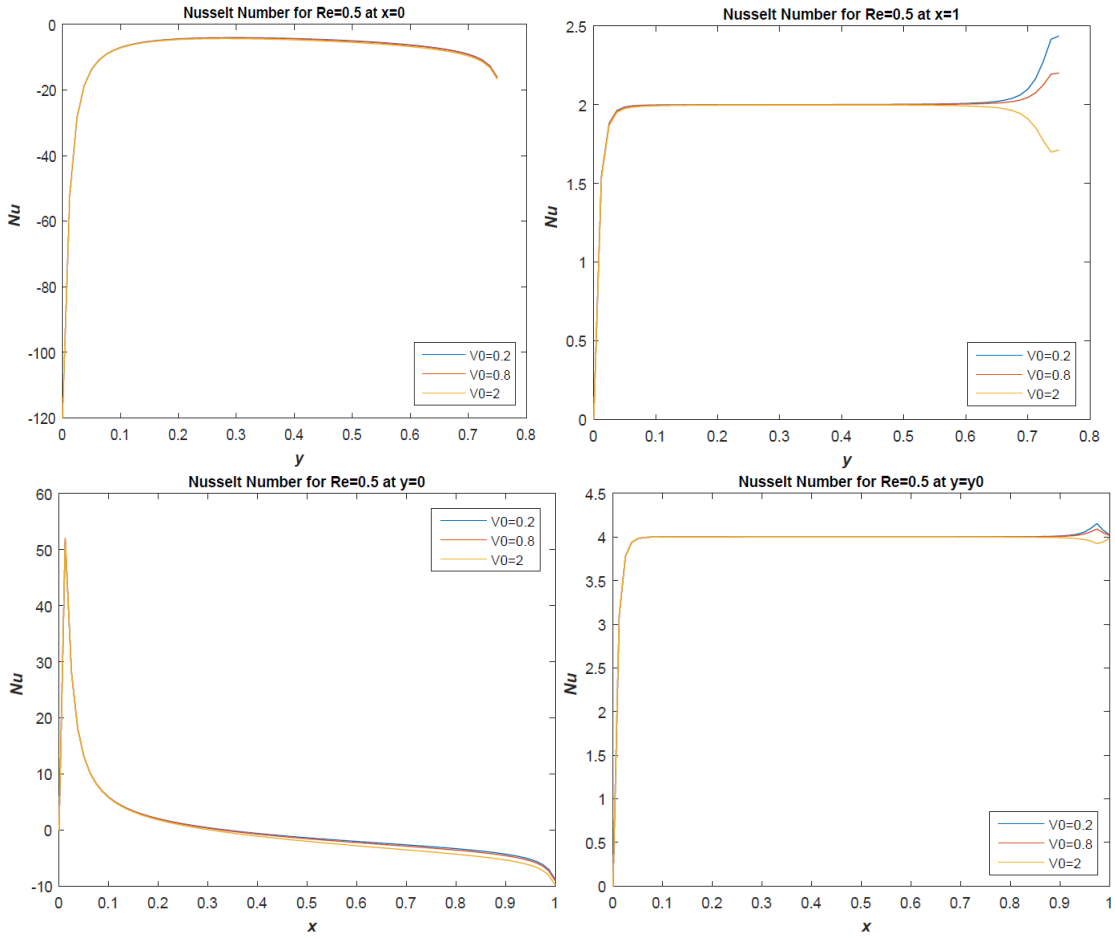

Fig. 4.7: Nusselt number for different values of suction parameter at *Re* = 0.5.

4.4.5 Entropy generation Number Ns

From the Fig. 4.8 and Fig. 4.9 we observe that maximum entropy occurs at the four corners. Again by graphs we observe a minimum entropy near to the bottom left corner. As V_0 increases, more and more entropy lines enter into the chamber without violating positions of maximum and minimum entropy points. By increasing V_0, entropy increases with a light shift in the region. But increase in *Re*, increases values of entropy very much at the corners and within the chamber. *As Re increases, the irreversible region (region of high values of entropy) increases at right bottom. In a small region at the top right corner entropy is maximum.*

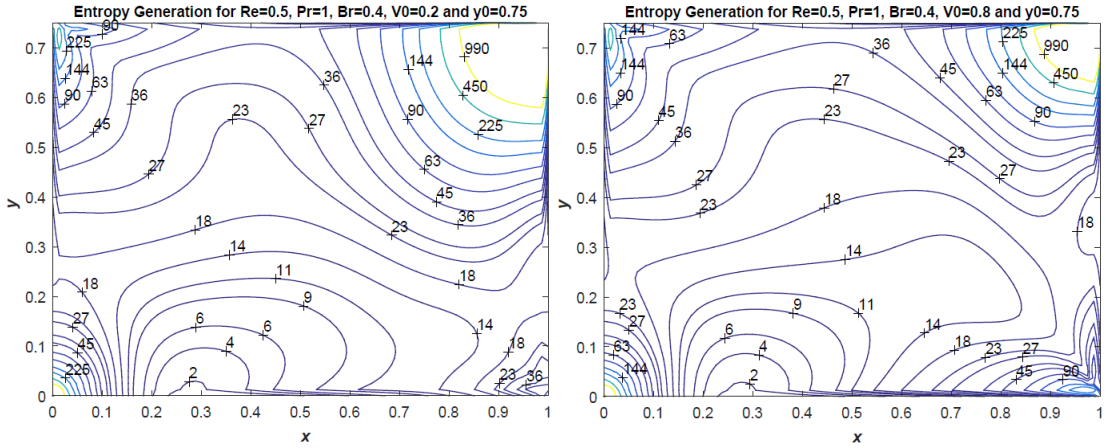

Fig. 4.8: Entropy generation number at different values of V_0 at Re = 0.5, Pr = 1, Br = 0.4 and y_0=0.75.

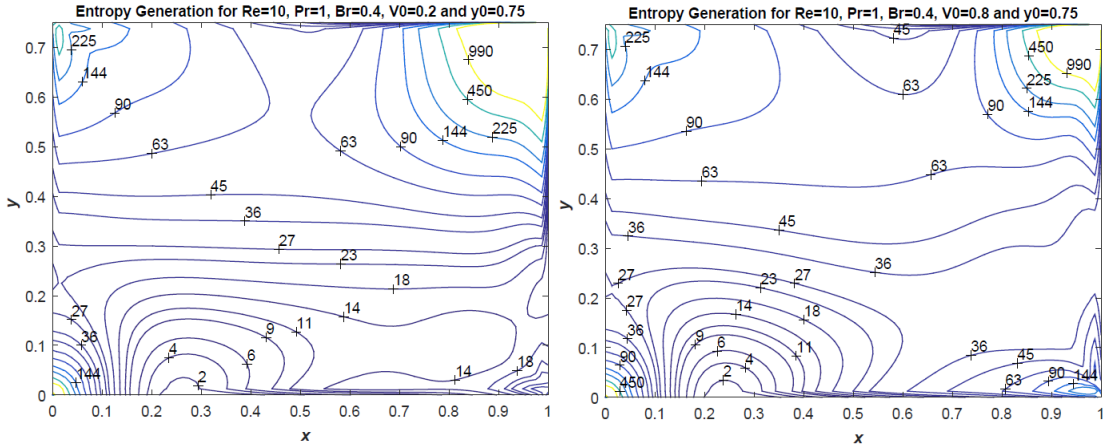

Fig. 4.9: Entropy generation number at different values of V_0 at Re = 10, Pr = 1, Br = 0.4 and y_0=0.75.

4.4.6 Bejan Number Be

Bejan number shows the regions where heat transfer by conduction is more. It is to note that 0<*Be*< 1. If *Be* is near to zero, it indicates region of high friction and *Be* near to 1 indicates region of high conduction and less friction. The regions where *Be* is near to 1 are regions of available energy (exergy) i.e., reversible heat transfer regions. In Fig. 4.10 and Fig. 4.11, the contours of Bejan number are shown. We observe that as V_0, the suction parameter, increases, the region of friction spreads more and more. As *Re*, the Reynolds number increases, more and more Bejan contour lines increase. In any case at the corner points, *Be* is near to zero (0.1 or less) as in the case of Entropy generation number indicate the effect of friction and more generation of heat. Comparing both Entropy generation number *Ns* and Bejan number *Be*, we conclude that near bottom left corner both *Ns* and *Be* are having high values (near to 0.9). *Which means though convection dominates, available energy is plenty at the bottom left corner.*

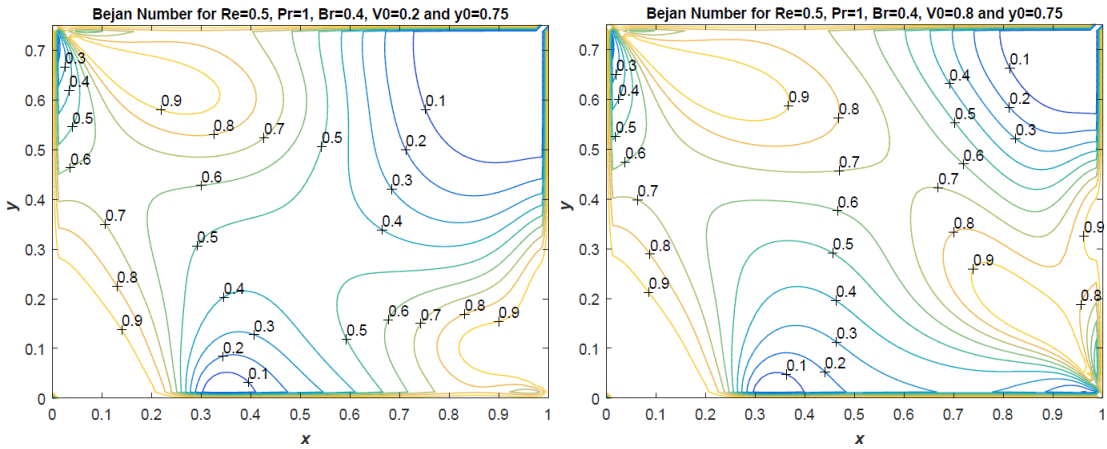

Fig. 4.10: Bejan number at different values of V_0 at Re = 0.5, Pr = 1, Br = 0.4 and y_0=0.75.

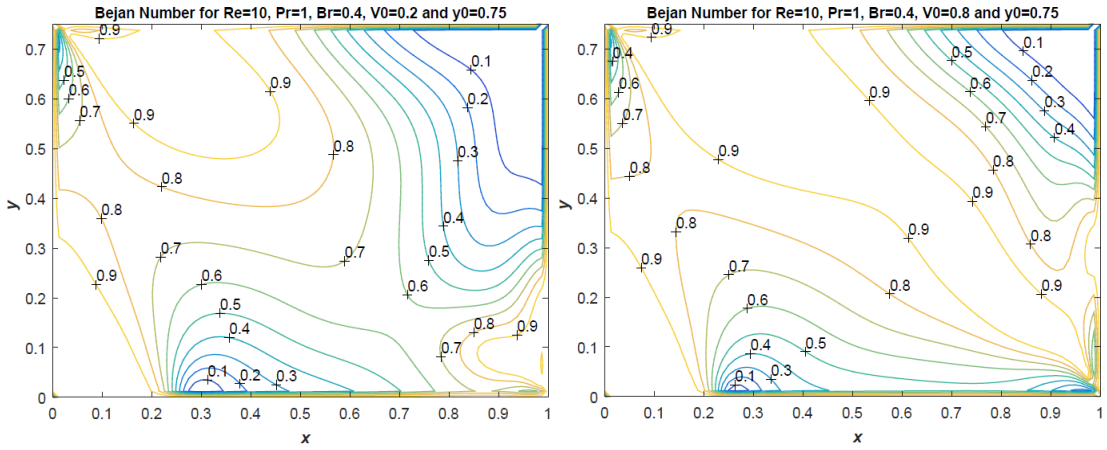

Fig. 4.11: Bejan number at different values of V_0 at Re = 10, Pr = 1, Br = 0.4 and y_0=0.75.

4.4.7 Heat Lines

The energy equation in (4.15) can be split into two first order equations by introducing Heat function H as in (4.28). Heat lines are shown within the chamber in the Fig. 4.12 and Fig. 4.13. Heat lines are having positive values at the left top corner and negative values at the right bottom corner. Negative values of heat lines indicates the region where temperature is below the reference temperature. As Prandtl number increases, these heat lines increases very much in value and attain maximum value when they reach the top right corner. If convection is neglected, isothermal lines and heat lines will be orthogonal to each other. *The 0–0 heat line moves up as V_0 the suction parameter increases. As Pr increases (i.e for thick fluids), heat lines re-enter at bottom surface.* This is the true path of energy flow.

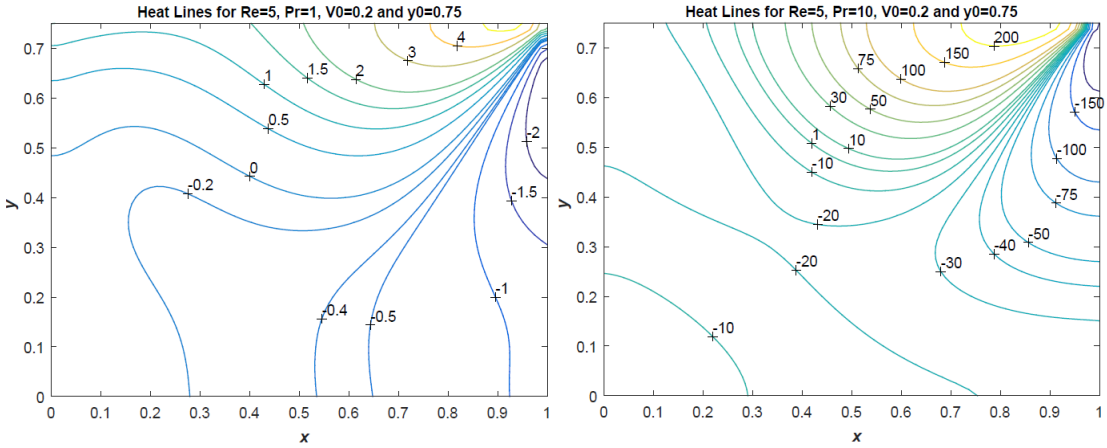

Fig. 4.12: Heat lines at Re = 5, V_0= 0.2, y_0= 0.75 and different values of Prandtl number Pr.

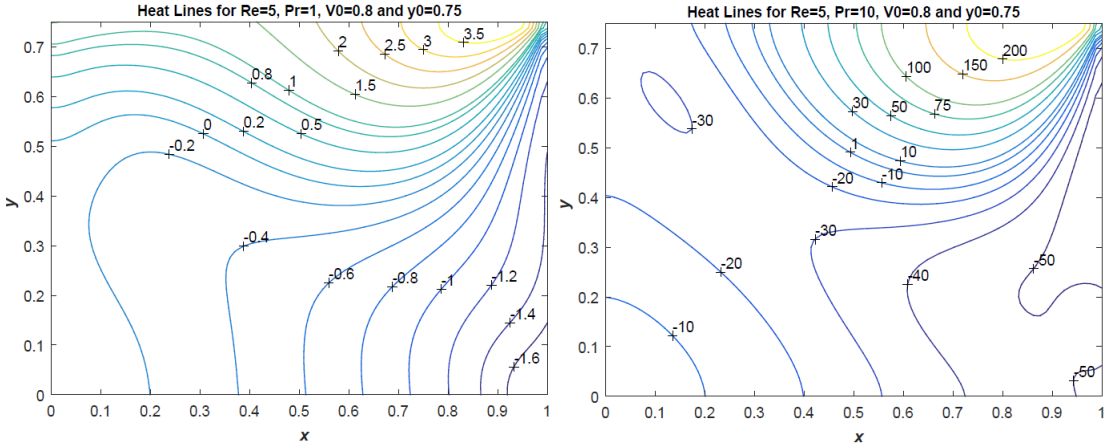

Fig. 4.13: Heat lines at Re = 5, V_0= 0.8, y_0= 0.75 and different values of Prandtl number Pr.

4.4.8 Pressure Contours

Pressure is obtained from the numerical scheme as in (4.40) and contours are drawn within the chamber in the Fig. 4.14–Fig. 4.16. It is observed that values of pressure contours increase very much as V_0 increases and decrease very much as Re increases. This is due to the fact that pressure gradient is inversely proportional to Reynolds number (as in eq. (4.36) & (4.37)). The pressure is numerically maximum at the top right corner in all cases. We observe, pressure changes its sign at the right bottom region. Hence in this region flow reversal takes place.

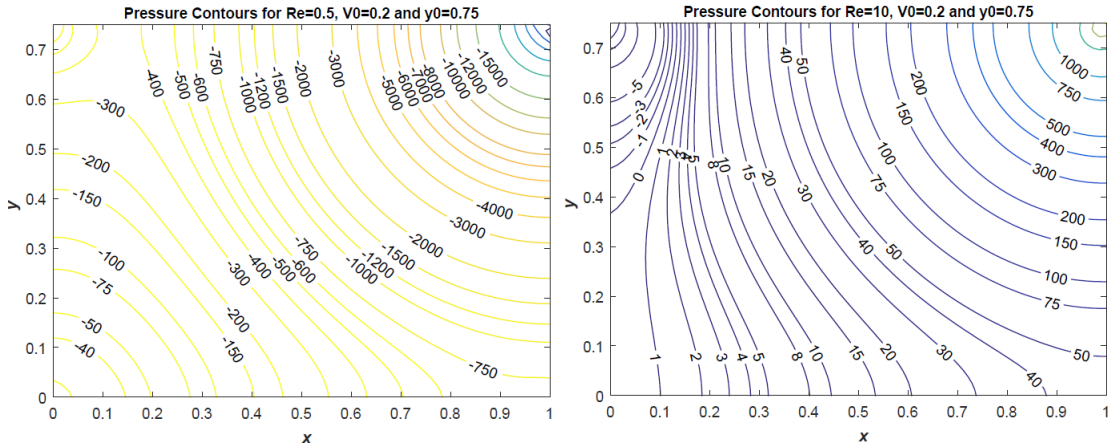

Fig. 4.14: Pressure contours at V_0 = 0.2, y_0=0.75 and for different values of Reynolds number *Re*.

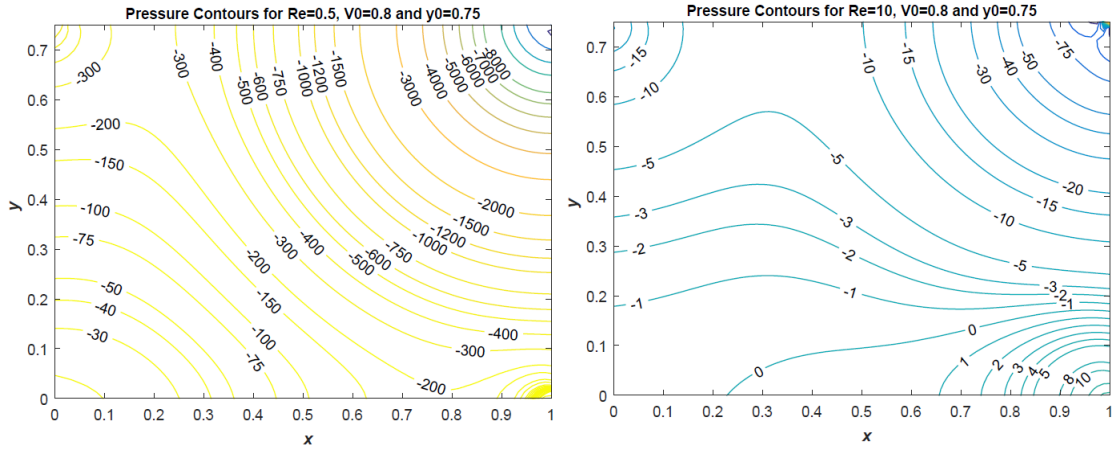

Fig. 4.15: Pressure contours at V_0 = 0.8, y_0=0.75 and for different values of Reynolds number *Re*.

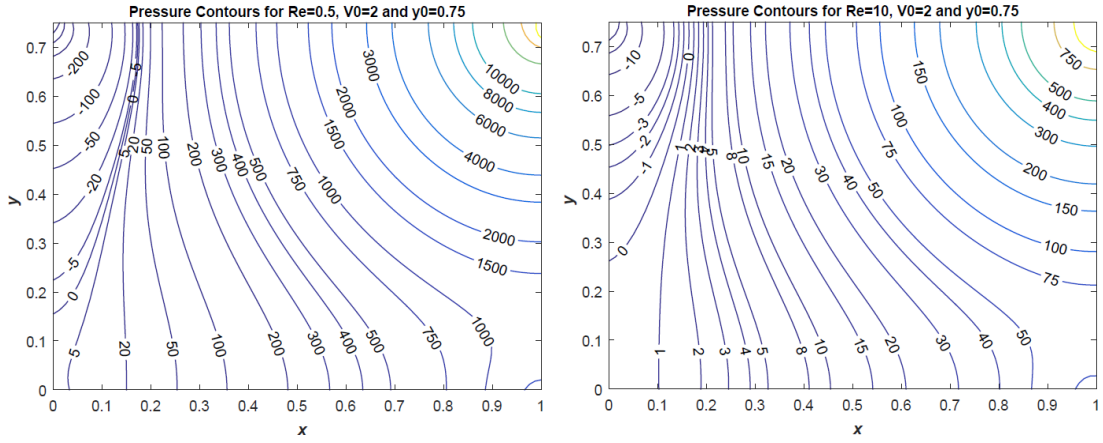

Fig. 4.16: Pressure contours at V_0 = 2, y_0=0.75 and for different values of Reynolds number *Re*.

4.5 Conclusions

From figures drawn, we analyze and observe that

- For large y_0 values, i.e., for slit like geometry, if suction number V_0 is small for high Reynolds numbers, the flow circulation is generated near top right corner.
- As Reynolds number increases, due to convection more and more temperature lines enter into the flow region.
- The contour θ=1 divides the temperature field into two regions (θ<1 and θ>1). As *Re* increases, the temperature contour for θ=1 shifts to left edge.
- Average Nusselt number decreases as suction parameter V_0 increases. i.e., high suction/ injection enhances the heat transfer.
- Either by entropy generation number or by Bejan number contours, we observe that dissipation energy is very high at the corners.
- Energy dissipation is minimum near to the left bottom corner where non-dimensional temperature is 1. (since *Ns* is minimum).
- Available energy or exergy is more in the center of the channel and at bottom left corner (since *Be* is near to 1).
- Heat lines have highest value at the top right corner.
- Pressure increases within the chamber as Reynolds number decreases.

Part – III

COUPLE STRESS FLUID FLOWS

Chapter 5

Steady Flow of Couple Stress Fluid through a Rectangular Channel Under Transverse Magnetic Field

In this chapter, the steady flow of an incompressible conducting couple stress fluid in the presence of transverse magnetic field through a rectangular channel with uniform cross–section, is considered. The induced magnetic field is neglected. We consider the case that there is no externally applied electric field. Under these conditions, we get 4^{th} order PDE for velocity *w* along the axis of the rectangular tube. The usual no slip and hyper stick boundary conditions are used to obtain the solution for *w*. We obtained the velocity *w* in terms of Fourier series. Skin friction on the walls and volumetric flow rate are obtained in terms of physical parameters like couple stress parameter and Hartmann number. The effects of these parameters on skin friction and volumetric flow rate are studied through graphs.

5.1 Introduction

The steady flow of a conducting fluid through a straight channel under a uniform transverse magnetic field presents one of the elementary problems in magneto hydrodynamics. Tani (1962) has given an approximate method of solution for the steady laminar incompressible flow of an electrically conducting fluid through a straight avenue of arbitrary cross section with conducting or non-conducting walls in the presence of a uniform transverse magnetic field based on a minimum principle. Ahmed and Attia (1998) further studied the viscous and joule dissipation effects under an external uniform magnetic field in an eccentric annulus of an electrically conducting incompressible fluid. Abel et al. (2004) studied the momentum, mass and heat transfer past a stretching sheet using the Walters-B visco-elastic model in the presence of a transverse magnetic field. Ahmed and Attia (2000), Attia (2005), Aboul Hasan and Attia (2002), Srnivasacharya and Shiferaw (2008) studied the MHD flow and heat transfer of a viscous, dusty and micro polar fluids through a rectangular duct.

In the above studies of non-Newtonian fluids like couple stress fluids with MHD effect, have not been considered. Stokes (1966) introduced the theory of couple stresses and gave the simplest generalization of the classical viscous fluid theory that maintains the couple stresses and body couples. Couple stress fluids are not much complicated than micro-polar fluids (Bhargava et al. 2007). As the microstructure was not available at the kinematic level, hence kinematics of such fluids were explained using the velocity field. Stokes flow problems were studied by Devakar and Iyengar (2008) under the isothermal conditions for an incompressible couple stress fluid. The magnetic field effects in 3D flow subject to convective boundary condition were investigated by Hayat et al. (2015) for couple stress nano-fluid over a nonlinear stretched surface. Srinivasacharya and Kaladhar (2012) studied the mixed convection flow of couple stress fluid with Soret and Dufour effects in a non-Darcy porous medium. The effects of inclined magnetic field on couple stress material in a porous medium was recently inspected by Ramesh (2016) in peristaltic flow.

As far as the author knows, though the magneto hydrodynamic flow of couple stress fluid has many applications, the flow of couple stress fluids has not been treated analytically through a rectangular channel. Hence, in this chapter, we have studied the MHD flow of a couple stress fluid through a rectangular channel. We have used Cartesian co-ordinate system for formulating the mathematical equations and obtained the exact solution for velocity. Skin friction on the walls and volumetric flow rate are obtained in terms of physical parameters like couple stress parameter and Hartmann number. We have studied the effects of these parameters on volumetric flow rate, skin friction and illuminated the results through graphs.

5.2 Mathematical Formulation

An incompressible and couple stress fluid flow through a channel is considered with uniform rectangular cross section with side lengths a and b. Using a Cartesian co-ordinate system (X,Y,Z) with center of rectangular cross section as origin and the axis of the tube as Z axis along which the flow is assumed. H_0, a constant magnetic field in the perpendicular direction to the flow is applied. Along the rectangular tube a constant pressure gradient causes generation of the flow in it. Since magnetic parameter (Hartmann number M) is very small, the induced magnetic and electrical fields are neglected. The physical representation of the problem is given in Fig. 5.1.

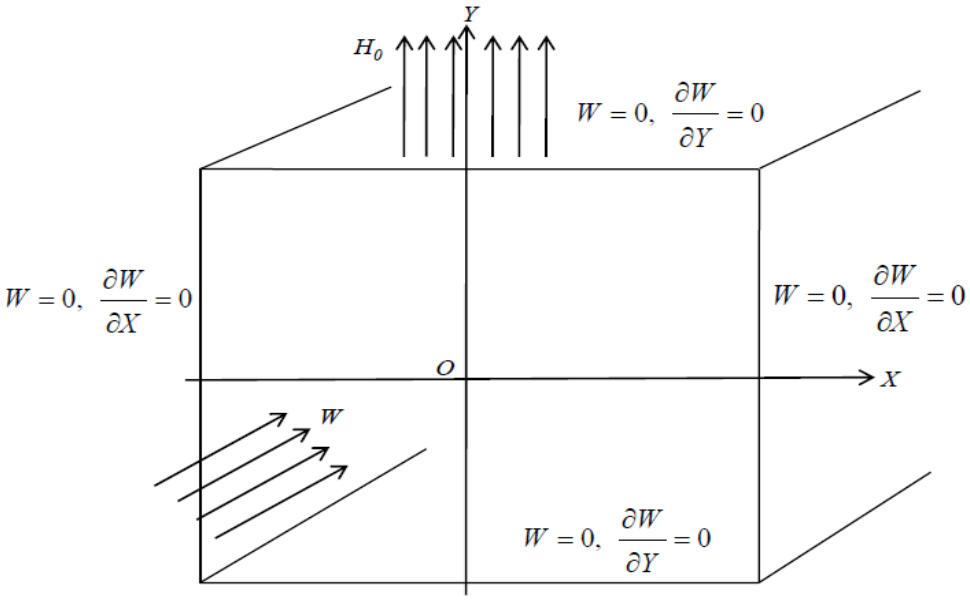

Fig. 5.1: Flow configuration in a rectangular channel without suction.

Governing Equations

The coupled equations for steady, incompressible and couple stress fluid flow with transverse magnetic field are given by

$$\nabla_0 . \mathbf{Q} = 0 \tag{5.1}$$

$$\rho \mathbf{Q} . \nabla_0 \mathbf{Q} = -\nabla_0 P + \mu \nabla_0^2 \mathbf{Q} - \eta \nabla_0^4 \mathbf{Q} + \mathbf{J} \times \mathbf{H} \tag{5.2}$$

where $\mathbf{Q}$ is the velocity, P is the pressure, ρ is the density, μ is the viscosity coefficient, η is the couple stress viscosity parameter.

We take by the geometry of the problem given in Fig. 5.1 and nature of the flow

$\mathbf{Q} = W\bar{k},\ \mathbf{H} = H_0\bar{j},\ \mathbf{J} = \frac{\sigma}{c}\mathbf{Q} \times \mathbf{H} = -\frac{\sigma}{c} H_0 W\bar{i}$ where $W=W(X, Y)$.

Hence $\mathbf{J} \times \mathbf{H} = -\frac{\sigma}{c} H_0^2 W\bar{k}$ and $\mathbf{Q} . \nabla_0 \mathbf{Q} = 0$.

Now equation (5.2) reduces to

$$\nabla_0 P = \mu \nabla_0^2 \mathbf{Q} - \eta \nabla_0^4 \mathbf{Q} - \frac{\sigma}{c} H_0^2 \mathbf{Q} \tag{5.3}$$

Non-dimensionalization

We introduce the following non–dimensional scheme:

$$X = ax,\ Y = ay,\ W = W_0 w,\ Z = az \text{ and } P = \rho W_0^2 p \tag{5.4}$$

where W_0 an average entrance velocity. Substituting (5.4) in equation (5.3) we obtain

$$\nabla^4 w - S\nabla^2 w + SM^2 w = -L_0 \tag{5.5}$$

The equation (5.5) is solved with no slip boundary conditions:

$$w = 0 \text{ on } x = \pm 1 \text{ and } y = \pm y_0 \text{ where } y_0 = \frac{b}{a} \tag{5.6}$$

and hyper stick boundary conditions:

$$\frac{1}{2}\nabla \times \mathbf{Q} = \frac{1}{2}\frac{\partial w}{\partial y}\bar{i} - \frac{1}{2}\frac{\partial w}{\partial x}\bar{j} = 0$$

$$\text{i.e., } \frac{\partial w}{\partial x} = 0 \text{ on } x = \pm 1 \text{ and } \frac{\partial w}{\partial y} = 0 \text{ on } y = \pm y_0 \tag{5.7}$$

where couple stress parameter $S = \dfrac{\mu a^2}{\eta}$, magnetic parameter $M = \sqrt{\dfrac{\sigma H_0^2 a^2}{c\mu}}$,

Reynolds Number $\mathrm{Re} = \dfrac{\rho W_0 a}{\mu}$ and $L_0 = S.L = \mathrm{Re}.S.\dfrac{dp}{dz} = \text{constant.}$

Equation (5.5) can be written as:

$$(\nabla^2 - \lambda_1^2)(\nabla^2 - \lambda_2^2)w = -L_0$$

where $\lambda_1^2 + \lambda_2^2 = S, \quad \lambda_1^2\lambda_2^2 = SM^2$.

5.3 Solution of the Problem

5.3.1 Velocity

Let us choose

$$w = -\frac{L}{M^2} + \sum_{n=1}^{\infty} f_n(y)\cos r_n x + \sum_{n=1}^{\infty} g_n(x)\cos t_n y \tag{5.8}$$

where $r_n = \dfrac{(2n-1)\pi}{2}$, $t_n = \dfrac{r_n}{y_0}$. Substituting (5.8) in (5.5) we get,

$$\sum_{n=1}^{\infty}\left(r_n^4 f_n - 2r_n^2 f_n^{ii} + f_n^{(iv)}\right)\cos r_n x + \sum_{n=1}^{\infty}\left(t_n^4 g_n - 2t_n^2 g_n^{ii} + g_n^{(iv)}\right)\cos t_n y$$
$$- S\left[\sum_{n=1}^{\infty}\left(-r_n^2 f_n + f_n^{ii}\right)\cos r_n x + \sum_{n=1}^{\infty}\left(-t_n^2 g_n + g_n^{ii}\right)\cos t_n y\right] + SM^2\sum_{n=1}^{\infty}\left(f_n \cos r_n x + g_n \cos t_n y\right) = 0$$

$$\Rightarrow f_n^{(iv)} - (2r_n^2 + S)f_n^{ii} + (r_n^4 + Sr_n^2 + SM^2)f_n = 0 \tag{5.9}$$

$$\text{and } g_n^{(iv)} - (2t_n^2 + S)g_n^{ii} + (t_n^4 + St_n^2 + SM^2)g_n = 0 \tag{5.10}$$

Equations (5.9) and (5.10) can be written as

$$\left(D^2 - u_n^2\right)\left(D^2 - v_n^2\right)f_n = 0 \text{ and } \left(D_1^2 - \alpha_n^2\right)\left(D_1^2 - \beta_n^2\right)g_n = 0 \tag{5.11}$$

where $D = \frac{d}{dy}$ and $D_1 = \frac{d}{dx}$

$$\therefore u_n^2 + v_n^2 = S + 2r_n^2 = \lambda_1^2 + \lambda_2^2 + 2r_n^2, \quad u_n^2 v_n^2 = r_n^4 + Sr_n^2 + SM^2 = r_n^4 + (\lambda_1^2 + \lambda_2^2) r_n^2 + \lambda_1^2 \lambda_2^2$$
$$\therefore \alpha_n^2 + \beta_n^2 = S + 2t_n^2 = \lambda_1^2 + \lambda_2^2 + 2t_n^2, \quad \alpha_n^2 \beta_n^2 = t_n^4 + St_n^2 + SM^2 = t_n^4 + (\lambda_1^2 + \lambda_2^2) t_n^2 + \lambda_1^2 \lambda_2^2$$

$$\therefore u_n^2 = \lambda_1^2 + r_n^2, \quad v_n^2 = \lambda_2^2 + r_n^2 \text{ and } \alpha_n^2 = \lambda_1^2 + t_n^2, \quad \beta_n^2 = \lambda_2^2 + t_n^2$$

Solving (5.11) we get

$$f_n(y) = A_n \frac{\cosh u_n y}{\cosh u_n y_0} + B_n \frac{\cosh v_n y}{\cosh v_n y_0} \text{ and } g_n(x) = C_n \frac{\cosh \alpha_n x}{\cosh \alpha_n} + D_n \frac{\cosh \beta_n x}{\cosh \beta_n}$$

$$\therefore w = -\frac{L}{M^2} + \sum_{n=1}^{\infty} \left(A_n \frac{\cosh u_n y}{\cosh u_n y_0} + B_n \frac{\cosh v_n y}{\cosh v_n y_0} \right) \cos r_n x + \sum_{n=1}^{\infty} \left(C_n \frac{\cosh \alpha_n x}{\cosh \alpha_n} + D_n \frac{\cosh \beta_n x}{\cosh \beta_n} \right) \cos t_n y \tag{5.12}$$

By no slip condition on $x = \pm 1, \ w = 0$ gives

$$\frac{L}{M^2} = \sum_{n=1}^{\infty} (C_n + D_n) \cos t_n y \tag{5.13}$$

Similarly by no slip condition on $y = \pm y_0, \ w = 0$ gives

$$\frac{L}{M^2} = \sum_{n=1}^{\infty} (A_n + B_n) \cos r_n x \tag{5.14}$$

By hyper-stick condition, on $y = \pm y_0, \ \frac{\partial w}{\partial y} = 0$ which gives

$$\sum_{n=1}^{\infty} (A_n u_n \tanh u_n y_0 + B_n v_n \tanh v_n y_0) \cos r_n x + \sum_{n=1}^{\infty} \left(C_n \frac{\cosh \alpha_n x}{\cosh \alpha_n} + D_n \frac{\cosh \beta_n x}{\cosh \beta_n} \right) t_n (-1)^n = 0 \tag{5.15}$$

Similarly by hyper-stick condition on $x = \pm 1, \ \frac{\partial w}{\partial x} = 0$ which gives

$$\sum_{n=1}^{\infty} \left(A_n \frac{\cosh u_n y}{\cosh u_n y_0} + B_n \frac{\cosh v_n y}{\cosh v_n y_0} \right) r_n (-1)^n + \sum_{n=1}^{\infty} (C_n \alpha_n \tanh \alpha_n + D_n \beta_n \tanh \beta_n) \cos t_n y = 0 \tag{5.16}$$

Using the orthogonality property, we have $\frac{1}{y_0} \int_{-y_o}^{y_0} \cos t_n y \ \cos t_m y \ dy = \delta_{\text{mn}}$

From (5.14) we obtain, $A_n + B_n = \frac{2L}{M^2 r_n} (-1)^{n+1}$

$$\Rightarrow \qquad B_n = \frac{2L}{M^2 r_n} (-1)^{n+1} - A_n \tag{5.17}$$

From (5.13) we obtain, $C_n + D_n = \dfrac{2L}{M^2 r_n}(-1)^{n+1}$

$$\Rightarrow \qquad D_n = \frac{2L}{M^2 r_n}(-1)^{n+1} - C_n \tag{5.18}$$

From (5.15) we obtain,

$$A_n u_n \tanh u_n y_0 + B_n v_n \tanh v_n y_0 = \sum_{m=1}^{\infty} (-1)^{m+1} t_m \left(C_m \frac{2r_n(-1)^{n+1}}{\alpha_m^2 + r_n^2} + D_m \frac{2r_n(-1)^{n+1}}{\beta_m^2 + r_n^2} \right) \tag{5.19}$$

From (5.16) we obtain,

$$C_n \alpha_n \tanh \alpha_n + D_n \beta_n \tanh \beta_n = \frac{1}{y_0} \sum_{m=1}^{\infty} (-1)^{m+1} r_m \left(A_m \frac{2t_n(-1)^{n+1}}{u_m^2 + t_n^2} + B_m \frac{2t_n(-1)^{n+1}}{v_m^2 + t_n^2} \right) \tag{5.20}$$

Substituting (5.17) and (5.18) in (5.19) and (5.20) we get

$$A_n \left(u_n \tanh u_n y_0 - v_n \tanh v_n y_0 \right) + \sum_{m=1}^{\infty} C_m \left(\frac{2r_m r_n (\alpha_m^2 - \beta_m^2)(-1)^{m+n}}{y_0 (\alpha_m^2 + r_n^2)(\beta_m^2 + r_n^2)} \right) = \sum_{m=1}^{\infty} \left(\frac{4Lr_n(-1)^{n+1}}{y_0 M^2 (\beta_m^2 + r_n^2)} \right) - \frac{2Lv_n(-1)^{n+1} \tanh v_n y_0}{M^2 r_n} \tag{5.21}$$

and

$$C_n \left(\alpha_n \tanh \alpha_n - \beta_n \tanh \beta_n \right) + \sum_{m=1}^{\infty} A_m \left(\frac{2r_m r_n (u_m^2 - v_m^2)(-1)^{m+n}}{y_0^2 (u_m^2 + t_n^2)(v_m^2 + t_n^2)} \right) = \sum_{m=1}^{\infty} \left(\frac{4Lr_n(-1)^{n+1}}{y_0^2 M^2 (v_m^2 + t_n^2)} \right) - \frac{2L\beta_n(-1)^{n+1} \tanh \beta_n}{M^2 r_n} \tag{5.22}$$

Equations (5.21) and (5.22) are in the form

$$a1_n A_n + \sum_{m=1}^{\infty} C_m e_{nm} = b1_n \tag{5.23}$$

$$c1_n C_n + \sum_{m=1}^{\infty} A_m f_{nm} = d1_n \tag{5.24}$$

where $a1_n = u_n \tanh u_n y_0 - v_n \tanh v_n y_0$, $c1_n = \alpha_n \tanh \alpha_n - \beta_n \tanh \beta_n$,

$$e_{nm} = \frac{2r_m r_n (\alpha_m^2 - \beta_m^2)(-1)^{m+n}}{y_0 (\alpha_m^2 + r_n^2)(\beta_m^2 + r_n^2)}, \quad f_{nm} = \frac{2r_m r_n (u_m^2 - v_m^2)(-1)^{m+n}}{y_0^2 (u_m^2 + t_n^2)(v_m^2 + t_n^2)},$$

$$b1_n = \sum_{m=1}^{\infty} \left(\frac{4Lr_n(-1)^{n+1}}{y_0 M^2 (\beta_m^2 + r_n^2)} \right) - \frac{2Lv_n(-1)^{n+1} \tanh v_n y_0}{M^2 r_n},$$

$$d1_n = \sum_{m=1}^{\infty} \left(\frac{4Lr_n(-1)^{n+1}}{y_0^2 M^2 (v_m^2 + t_n^2)} \right) - \frac{2L\beta_n(-1)^{n+1} \tanh \beta_n}{M^2 r_n}$$

Eliminating C_n from equations (5.23) and (5.24) we get

$$\sum_{m=1}^{\infty} a_{nm} A_{\ m} = b_n \tag{5.25}$$

where $a_{nm} = \begin{cases} a1_n - \sum_{k=1}^{\infty} e_{nk} \frac{f_{kn}}{c1_k} & \text{if } n = m \\ -\sum_{k=1}^{\infty} e_{nk} \frac{f_{km}}{c1_k} & \text{if } n \neq m \end{cases}$ and $b_n = b1_n - \sum_{m=1}^{\infty} e_{nm} \frac{d1_m}{c1_m}$

The equation (5.25) is an infinite system of equations in A_n. We truncate the system to n=10 and solve for A_n. Then from (5.23) C_n, from (5.17) B_n, and from (5.18) D_n can be found. Hence all the coefficients in (5.12) for the velocity w are now known.

5.3.2 Volumetric Flow Rate

Volumetric flow rate V (non-dimensional) is given by

$$V = \int_{-1}^{1} \int_{-y_0}^{y_0} w \, dydx$$

$$= -\frac{4Ly_0}{M^2} + 4\sum_{n=1}^{\infty} \frac{(-1)^{n+1}}{r_n} \left[A_n \frac{\tanh u_n y_0}{u_n} + B_n \frac{\tanh v_n y_0}{v_n} + y_0 C_n \frac{\tanh \alpha_n}{\alpha_n} + y_0 D_n \frac{\tanh \beta_n}{\beta_n} \right] \quad (5.26)$$

5.3.3 Skin Friction

Skin friction is the force acting on the surface per unit area. It is obtained from constitutive equation of couple stress fluid.

$$\mathbf{T}^* = -\mathbf{I}p + 2\mu\mathbf{E} + \frac{1}{2}\mathbf{I} \times div\ \mathbf{M}$$

where $\mathbf{M} = m\mathbf{I} + 4\eta\nabla W + 4\eta'(\nabla W)^T$ with $W = \frac{1}{2}\nabla \times \mathbf{Q}$.

For our problem, $\mathbf{M} = \begin{bmatrix} m + 4(\eta + \eta')W_{1,1} & 4\eta W_{1,2} + 4\eta' W_{2,1} & 0 \\ 4\eta W_{2,1} + 4\eta' W_{1,2} & m + 4W_{2,2} & 0 \\ 0 & 0 & m \end{bmatrix}$

Hence $div\ \mathbf{M} = 2\eta' \left\{ \frac{\partial \nabla^2 W}{\partial Y} \bar{i} - \frac{\partial \nabla^2 W}{\partial X} \bar{j} \right\}$

and $\mathbf{I} \times div\ \mathbf{M} = 2\eta' \begin{bmatrix} 0 & 0 & -\frac{\partial \nabla^2 W}{\partial X} \\ 0 & 0 & -\frac{\partial \nabla^2 W}{\partial Y} \\ \frac{\partial \nabla^2 W}{\partial X} & \frac{\partial \nabla^2 W}{\partial Y} & 0 \end{bmatrix}$.

These equations give non-dimensional stress $\mathbf{T} = \frac{\mathbf{T}^* a}{\mu W_0}$

i.e., $T_{13} = \frac{\partial}{\partial x}\left(w - \frac{e}{S}\nabla^2 w \right)$ and $T_{23} = \frac{\partial}{\partial y}\left(w - \frac{e}{S}\nabla^2 w \right)$.

Hence the skin friction on faces $x = \pm 1$ is $C_f = T_{13}$ and on faces $y = \pm y_0$ is $C_f = T_{23}$.

On $x = \pm 1$,

$$C_f = \frac{e}{S}\sum_{n=1}^{\infty}\left\{ r_n\left[A_n\lambda_1^2 \frac{\cosh u_n y}{\cosh u_n} + B_n\lambda_2^2 \frac{\cosh v_n y}{\cosh v_n} \right](-1)^{n+1} - \left[C_n\lambda_1^2\alpha_n \tanh\alpha_n + D_n\lambda_2^2\beta_n \tanh\beta_n \right]\cos t_n y \right\} \qquad (5.27)$$

This skin friction is function of y locally. Hence we find average skin friction $= \frac{1}{2y_0}\int_{-y_0}^{y_0} C_f \, dy$.

5.4 Results and Discussion

For particular value of physical parameters S and M, the values of λ_1 and λ_2 are calculated using the quadratic equation

$\lambda^2 - S\lambda + SM^2 = 0$.

Then u_n, v_n, α_n and β_n are found. Now velocity w is computed using (5.12). The effects of physical parameters S and M on velocity, Volumetric flow rate and skin friction are found. We can observe that for a fixed S value, to get real values of λ, $S \geq 4M^2$.

5.4.1 Velocity *w*

In Fig. 5.2, velocity contours at different values of M for a fixed value of S=50 are shown.

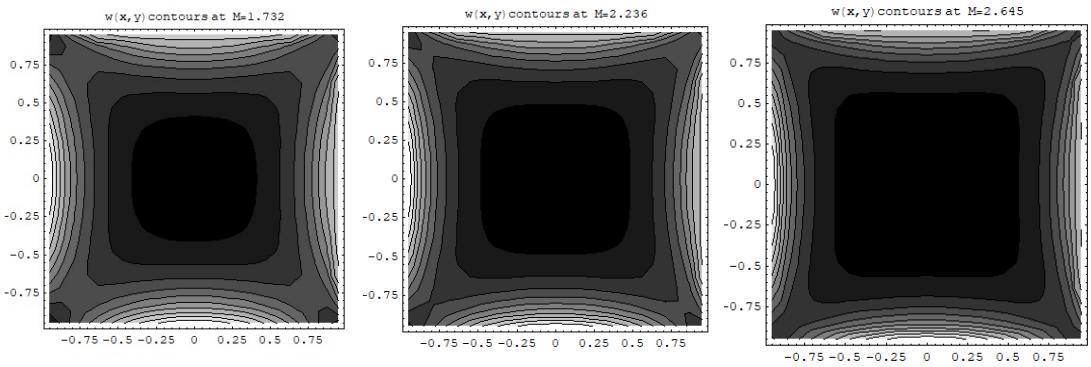

Fig. 5.2: For S = 50, Velocity $w(x, y)$ at M=1.732, M= 2.236, M= 2.645.

We notice that as M increases, fluid is having high velocity near the walls and more and more fluid is drifted towards walls of the channel and the centre of the channel being maintained flat. In the figure, black region shows low values and bright region

indicates high values of w. To show this clearly w is plotted in Fig. 5.3 at fixed values of cross-sections for y=0.25, y=0.5, y=0.75 and y=0.9.

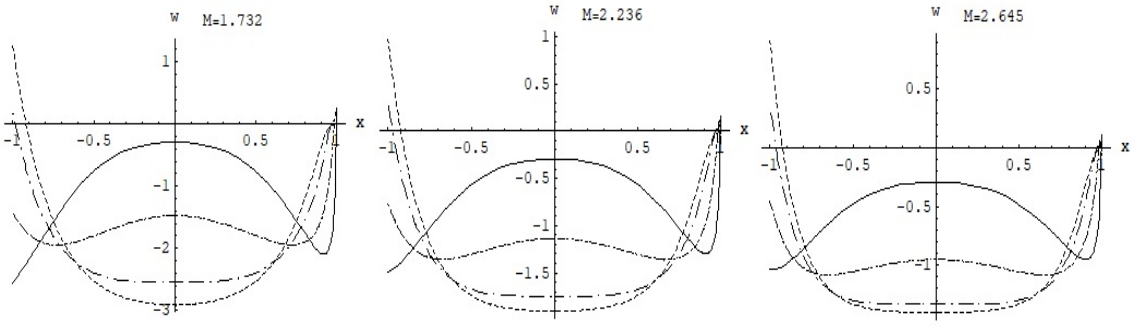

Fig. 5.3: At S=50 and M=1.732, M=2.236, M=2.645, $w(x, y)$ at cross-sections y=0.25, y=0.5, y=0.75 and y=0.9.

5.4.2 Volumetric Flow rate

In Fig. 5.4, volumetric flow rate V is shown at different values of magnetic parameter M. It is observed that as M increases, volumetric flow rate decreases drastically. But when M is fixed, as S increases, volumetric flow rate is almost constant.

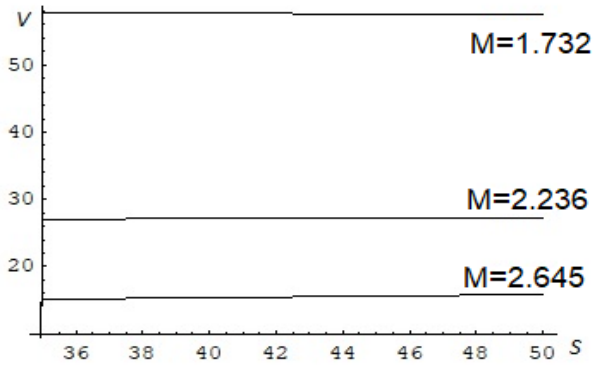

Fig. 5.4: Volumetric flow rate vs Couple stress parameter at different values of magnetic parameter M.

5.4.3 Skin Friction

At S=50, e=0.5, and for different values of M^2 the average skin friction is found and tabulated in Table. 5.1.

Table. 5.1: Average skin friction values for different values of M^2 at S = 50, e = 0.5.

M^2	3	5	7
Average c_f	171.483	104.032	75.0971

From this we observe that as Hartmann number M increases, skin friction decreases.

5.5 Conclusions

From figures drawn, we analyze and observe that

- By applying Magnetic field, for couple stress fluids the volumetric flow rate and skin friction on the walls are controlled i.e., decrease.
- For a fixed value of *M*, the effect of Couple stress parameter on volumetric flow rate is almost nil.
- Skin friction is decreases as couple stress parameter increases.

Chapter 6

Steady Flow of Couple Stress Fluid through a Rectangular Channel Under Transverse Magnetic Field with Suction

In this chapter, we have considered the steady flow of an incompressible conducting couple stress fluid through a rectangular channel with suction/ injection at the opposite side walls in the presence of transverse magnetic field. We obtained the velocity w and temperature θ in terms of Fourier series. The volumetric flow rate and skin friction are obtained and the effects of physical parameters like magnetic parameter, Reynolds number and couple stress parameter on this are studied through graphs.

6.1 Introduction

The steady flow of micro-polar fluid with suction and injection under transverse magnetic field through a rectangular channel and a circular pipe was studied by Ramana Murthy et al. (2011, 2009). Song and Sundmacher (2010), Sai and Nageswar Rao (2000) studied the viscous flow in a rectangular duct with suction and injection imposed on opposite walls. But as far as the author knows the magneto hydrodynamic flow of couple stress fluid through a rectangular channel with suction has not been treated analytically.

Hence, in this chapter, our objective is to study the flow of the magneto hydrodynamic couple stress fluid through a rectangular channel with suction/ injection. The exact solutions for velocity and temperature are obtained. Skin friction on the walls and volumetric flow rate are obtained in terms of physical parameters like couple stress parameter and magnetic parameter.

6.2 Mathematical Formulation

An incompressible and couple stress fluid flow through a channel is considered with uniform rectangular cross section with side lengths a and b. Using a Cartesian co-

ordinate system (X, Y, Z) with center of rectangular cross section as origin and the axis of the tube as Z axis along which the flow is assumed. H_0, a constant magnetic field in the perpendicular direction to the flow is applied. Along the rectangular tube a constant pressure gradient causes generation of the flow in it. U_0 is the suction velocity in the direction of X axis. Due to small values of Hartmann number, the induced magnetic and electrical fields are negligible. The physical representation of the problem is given in Fig. 6.1.

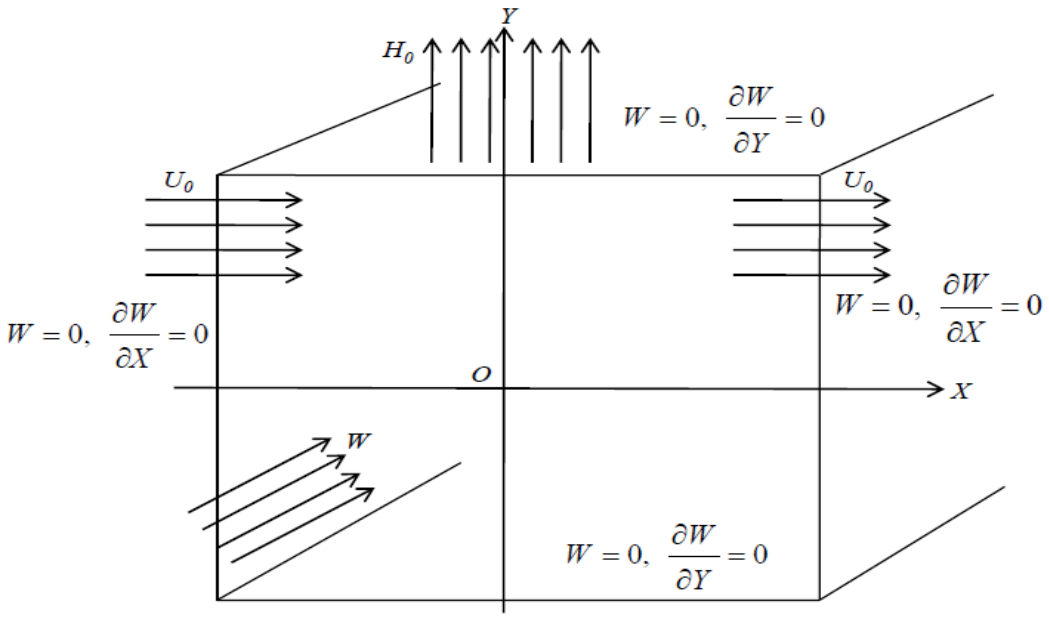

Fig. 6.1: Flow configuration in a rectangular channel with opposite wall suction.

Governing Equations

The coupled equations for steady, incompressible and couple stress fluid flow with transverse magnetic field are given by

$$\nabla_0.\mathbf{Q}=0 \tag{6.1}$$

$$\rho\mathbf{Q}.\nabla_0\mathbf{Q}=-\nabla_0 P+\mu\nabla_0^2\mathbf{Q}-\eta\nabla_0^4\mathbf{Q}+\mathbf{J}\times\mathbf{H} \tag{6.2}$$

$$\rho c_p U_0\frac{dT}{dX}=k\nabla_0^2 T \tag{6.3}$$

where $\mathbf{Q}$ is the velocity, P is the pressure, ρ is the density, μ is the viscosity coefficient, η is the couple stress viscosity parameter, T is the temperature, k is the thermal conductivity of the fluid and c_p heat capacity at constant pressure.

We take by the geometry of the problem given in Fig. 6.1 and nature of the flow

$\mathbf{Q}=U_0\bar{i}+W\bar{k}$, $\mathbf{H}=H_0\bar{j}$, $\mathbf{J}=\frac{\sigma}{c}\mathbf{Q}\times\mathbf{H}=\frac{\sigma}{c}H_0\left(U_0\bar{k}-W\bar{i}\right)$, where W=W(X, Y).

Hence $\mathbf{J}\times\mathbf{H} = -\frac{\sigma}{c}H_0^2\left(U_0\bar{i} + W\bar{k}\right)$ and $\mathbf{Q}.\nabla_0\mathbf{Q} = U_0\frac{\partial W}{\partial X}\bar{k}$.

Now equation (6.2) reduces to

$$\rho U_0\frac{\partial W}{\partial X} = -\nabla_0 P + \mu\nabla_0^2\mathbf{Q} - \eta\nabla_0^4\mathbf{Q} - \frac{\sigma}{c}H_0^2\mathbf{Q} \tag{6.4}$$

Non-dimensionalization

We introduce the following non–dimensional scheme:

$$X = ax,\ Y = ay,\ Z = az,\ W = W_0 w,\ T = T_1 + \Delta T.\theta \text{ and } P = \rho W_0^2 p. \tag{6.5}$$

Using (6.5) in equation (6.4) we obtain

$$\nabla^4 w - S\nabla^2 w + SM^2 w + S.\mathrm{Re}.\frac{\partial w}{\partial x} = -L_0. \tag{6.6}$$

The equation (6.6) is solved with no slip boundary conditions:

$$w = 0 \text{ on } x = \pm 1 \text{ and } y = \pm y_0 \text{ where } y_0 = \frac{b}{a} \tag{6.7}$$

and hyper stick boundary conditions along tangential direction on the wall where suction imposed is given by

$$\frac{1}{2}\nabla\times\mathbf{Q}.\bar{j} = \frac{1}{2}\left(\frac{\partial w}{\partial y}\bar{i} - \frac{\partial w}{\partial x}\bar{j}\right).\bar{j} = 0$$

i.e., $\frac{\partial w}{\partial x} = 0$ on $x = \pm 1$ (6.8)

where couple stress parameter $S = \frac{\mu a^2}{\eta}$, magnetic parameter $M = \sqrt{\frac{\sigma H_0^2 a^2}{c\mu}}$,

Reynolds Number $\mathrm{Re} = \frac{\rho W_0 a}{\mu}$ and $L_0 = S.L = \mathrm{Re}.S.\frac{dp}{dz} = \text{constant}.$

Using (6.5) in equation (6.3), the energy equation reduces to

$$Pe\frac{d\theta}{dx} = \nabla^2\theta \tag{6.9}$$

where $Pe = \frac{\rho c_p U_0 a}{k}$, is Peclet number.

The boundary conditions for θ are:

$$\theta = 0 \text{ on } y = 0,\ \theta = 1 \text{ on } y = 1,\ \frac{\partial\theta}{\partial x} = q_1 \text{ on } x = 0,\ \frac{\partial\theta}{\partial x} = q_2 \text{ on } x = 1 \tag{6.10}$$

6.3 Solution of the Problem

6.3.1 Velocity

Let us choose *w* in the form:

$$w = \sum_{n=1}^{\infty} w_n(x)\cos t_n y \tag{6.11}$$

where $t_n = \dfrac{(2n-1)\pi}{2y_0}$.

Substituting (6.11) in (6.6) and using Fourier series for RHS of (6.6) we get

$$w_n^{iv} - \left(2t_n^2 + S\right)w_n^{ii} + S.\mathrm{Re}.w_n^{i} + \left(t_n^4 + St_n^2 + SM^2\right)w_n = \frac{2L_0}{y_0 t_n}(-1)^n \tag{6.12}$$

The equation (6.12) is an ordinary differential equation with constant coefficients and hence the solution can be taken as

$$w_n = a_{1n}e^{\alpha_1 x} + a_{2n}e^{\alpha_2 x} + a_{3n}e^{\alpha_3 x} + a_{4n}e^{\alpha_4 x} + L_1 \tag{6.13}$$

where $L_1 = \dfrac{2L_0(-1)^n}{y_0 t_n\left(t_n^4 + St_n^2 + SM^2\right)}$ and $\alpha_1, \alpha_2, \alpha_3, \alpha_4$ are the roots of the auxiliary equation $\alpha^4 - \left(2t_n^2 + S\right)\alpha^2 + S.\mathrm{Re}.\alpha + \left(t_n^4 + St_n^2 + SM^2\right) = 0.$

We have $w = 0$ on $x = \pm 1$. Applying this condition on equation (6.11), we get

$$a_{1n}e^{\alpha_1} + a_{2n}e^{\alpha_2} + a_{3n}e^{\alpha_3} + a_{4n}e^{\alpha_4} = -L_1 \tag{6.14}$$

and $a_{1n}e^{-\alpha_1} + a_{2n}e^{-\alpha_2} + a_{3n}e^{-\alpha_3} + a_{4n}e^{-\alpha_4} = -L_1$ (6.15)

also we have $\dfrac{\partial w}{\partial x} = 0$ on $x = \pm 1$. Applying this condition on equation (6.11), we get

$$a_{1n}\alpha_1 e^{\alpha_1} + a_{2n}\alpha_2 e^{\alpha_2} + a_{3n}\alpha_3 e^{\alpha_3} + a_{4n}\alpha_4 e^{\alpha_4} = 0 \tag{6.16}$$

and $a_{1n}\alpha_1 e^{-\alpha_1} + a_{2n}\alpha_2 e^{-\alpha_2} + a_{3n}\alpha_3 e^{-\alpha_3} + a_{4n}\alpha_4 e^{-\alpha_4} = 0$ (6.17)

The equations (6.14) to (6.17) are solved for a_{1n}, a_{2n}, a_{3n}, a_{4n} and hence the solution for *w* can be found.

6.3.2 Temperature

Let $\theta = \theta_0 + y$ (6.18)

using (6.18), the equation (6.9) reduces to

$$Pe\frac{d\theta_0}{dx} = \nabla^2\theta_0 \tag{6.19}$$

subject to the boundary conditions:

$$\theta_0 = 0 \text{ on } y = 0,\ \theta_0 = 0 \text{ on } y = 1,\ \frac{\partial \theta_0}{\partial x} = q_1 \text{ on } x = 0 \text{ and } \frac{\partial \theta_0}{\partial x} = q_2 \text{ on } x = 1 \qquad (6.20)$$

Let us choose

$$\theta_0 = \sum_{n=1}^{\infty} f_n(x) sinn\pi y \qquad (6.21)$$

substituting (6.21) in (6.19) and using Fourier series, we get

$$f_n^{ii} - Pe\, f_n^{i} - r_n^2 f_n = 0 \qquad (6.22)$$

where $r_n = n\pi$

The equation (6.22) is an ordinary differential equation with constant coefficients and hence the solution can be taken as

$$f_n = b_{1n} e^{\beta_1 x} + b_{2n} e^{\beta_2 x} \qquad (6.23)$$

where β_1, β_2 are the roots of the auxiliary equation

$$\beta^2 - Pe.\beta - r_n^2 = 0$$

we have $\frac{\partial \theta_0}{\partial x} = q_1$ on $x = 0$ and $\frac{\partial \theta_0}{\partial x} = q_2$ on $x = 1$.

Applying these conditions and using Fourier series on equation (6.21), we get

$$f_n^{i}(0) = b_{1n}\beta_1 + b_{2n}\beta_2 \qquad (6.24)$$

and $f_n^{i}(1) = b_{1n}\beta_1 e^{\beta_1} + b_{2n}\beta_2 e^{\beta_2}$ (6.25)

where $f_n^{i}(0) = \frac{4q_1}{(2n-1)\pi}$ and $f_n^{i}(1) = \frac{4q_2}{(2n-1)\pi}$.

The equations (6.24) and (6.25) can be solved for b_{1n}, b_{2n} and hence the solution for θ_0 can be found.

Finally θ can be obtained from equation (6.18).

6.3.3 Volumetric Flow rate

Volumetric flow rate V (non-dimensional) is given by

$$V = \int_{-1}^{1} \int_{-y_0}^{y_0} w\, dydx$$
$$= \sum_{n=1}^{\infty} \frac{4(-1)^{n+1}}{t_n} \left[\frac{a_{1n}}{\alpha_1} \sinh \alpha_1 + \frac{a_{2n}}{\alpha_2} \sinh \alpha_2 + \frac{a_{3n}}{\alpha_3} \sinh \alpha_3 + \frac{a_{4n}}{\alpha_4} \sinh \alpha_4 + L_1 \right] \qquad (6.26)$$

6.3.4 Skin friction

Skin friction is the force acting on the surface per unit area. It is obtained from constitutive equation of couple stress fluid.

$$\mathbf{T}^* = -\mathbf{I}p + 2\mu\mathbf{E} + \frac{1}{2}\mathbf{I}\times div\ \mathbf{M}$$

where $\mathbf{M} = m\mathbf{I} + 4\eta\nabla W + 4\eta'(\nabla W)^T$ with $W = \frac{1}{2}\nabla\times\mathbf{Q}$.

For our problem, $\mathbf{M} = \begin{bmatrix} m+4(\eta+\eta')W_{1,1} & 4\eta W_{1,2}+4\eta' W_{2,1} & 0 \\ 4\eta W_{2,1}+4\eta' W_{1,2} & m+4W_{2,2} & 0 \\ 0 & 0 & m \end{bmatrix}$

Hence $div\ \mathbf{M} = 2\eta'\left\{\frac{\partial\nabla^2 W}{\partial Y}\bar{i} - \frac{\partial\nabla^2 W}{\partial X}\bar{j}\right\}$

and $\mathbf{I}\times div\ \mathbf{M} = 2\eta'\begin{bmatrix} 0 & 0 & -\frac{\partial\nabla^2 W}{\partial X} \\ 0 & 0 & -\frac{\partial\nabla^2 W}{\partial Y} \\ \frac{\partial\nabla^2 W}{\partial X} & \frac{\partial\nabla^2 W}{\partial Y} & 0 \end{bmatrix}$.

These equations give non-dimensional stress $\mathbf{T} = \frac{\mathbf{T}^* a}{\mu W_0}$

i.e., $T_{13} = \frac{\partial}{\partial x}\left(w - \frac{e}{S}\nabla^2 w\right)$ and $T_{23} = \frac{\partial}{\partial y}\left(w - \frac{e}{S}\nabla^2 w\right)$.

Hence the skin friction on faces $x = \pm 1$ is $C_f = T_{13}$ and on faces $y = \pm y_0$ is $C_f = T_{23}$.

On $x = \pm 1$,

$$C_f = -\frac{e}{S}\sum_{n=1}^{\infty}\left[\begin{array}{l}\left(\alpha_1^3 - t_n^2\alpha_1\right)a_{1n}e^{\alpha_1 x} + \left(\alpha_2^3 - t_n^2\alpha_2\right)a_{2n}e^{\alpha_2 x} \\ \qquad + \left(\alpha_3^3 - t_n^2\alpha_3\right)a_{3n}e^{\alpha_3 x} + \left(\alpha_4^3 - t_n^2\alpha_4\right)a_{4n}e^{\alpha_4 x}\end{array}\right]\cos t_n y \qquad (6.27)$$

This skin friction is function of y locally. Hence we find average skin friction $= \frac{1}{2y_0}\int_{-y_0}^{y_0} C_f\ dy$.

6.4 Results and Discussion

6.4.1 Velocity *w*

Effect of Magnetic parameter

In Fig. 6.2, velocity contours at different values of *M* for a fixed value of *S*=50 and *Re*=0.5 are shown. We notice that fluid is having high velocity near the walls and as *M* increases the values of velocity decreases numerically. As *M* increases, the absolute maximum velocity decreases. The region of absolutely maximum velocity increases and appears flat. This is known as Hartmann effect. In the figure, red region shows low values (absolutely high values).

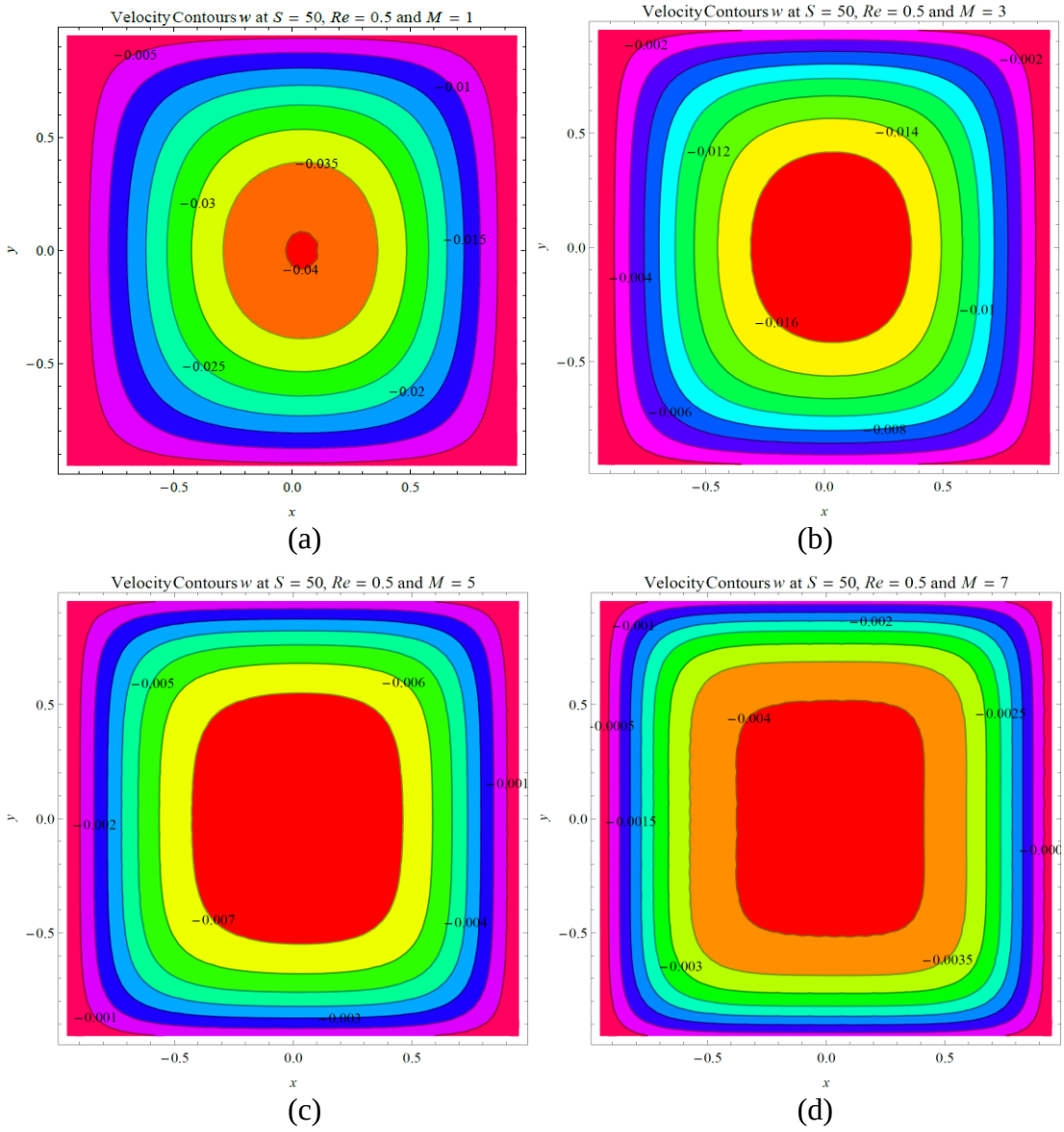

Fig. 6.2: For *S* = 50 and *Re*=0.5, Velocity *w*(*x*, *y*) at (a) *M*=1, (b) *M*=3, (c) *M*=5 and (d) *M*=7.

Effect of Reynolds number

In Fig. 6.3, velocity contours at different values of *Re* for a fixed value of *S*=50 and *M*=5 are shown. We notice that as *Re* increases, the region of minimum velocity of the fluid is drifted towards the wall in the direction of suction. In the figure, red region shows low values of *w*.

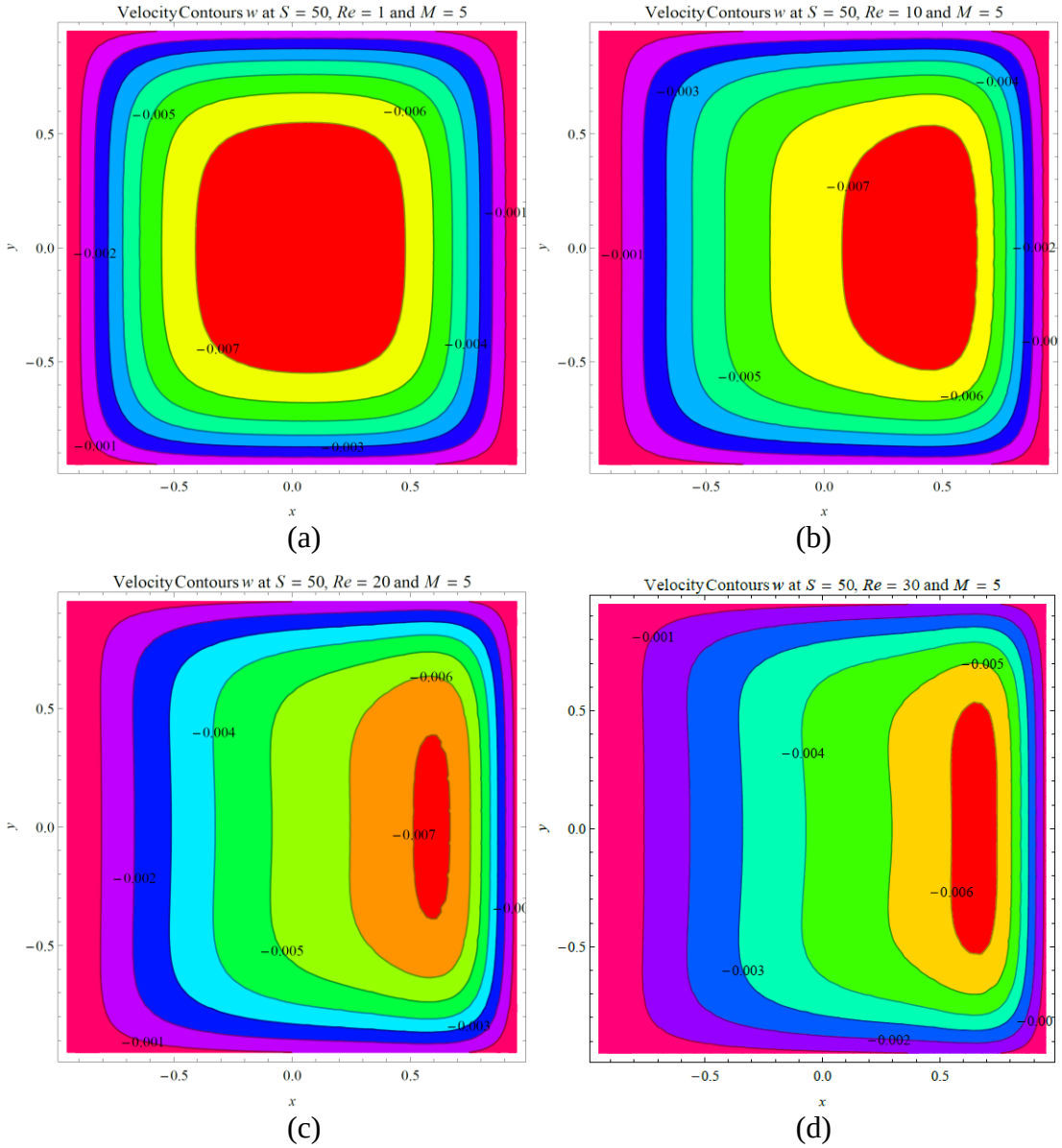

Fig. 6.3: For *S* = 50 and *M*=5, Velocity *w*(*x*, *y*) at (a) *Re*=1, (b) *Re*=10, (c) *Re*=20 and (d) *Re*=30.

Effect of Couple-stress parameter

In Fig. 6.4, velocity contours at different values of *S* for a fixed value of *Re*=0.5 and *M*=5 are shown. We notice that as *S* increases, the region of minimum velocity

increases (For example, in Fig. 6.4 (a) w_{min}= –0.18, in (b) w_{min}= –0.035, in (c) w_{min}= –0.0175 and in (d) w_{min}= –0.012, the region having these values is increasing). For a particular value of S, the region of minimum velocity spreads to a maximum area and for higher values of S, this region decreases.

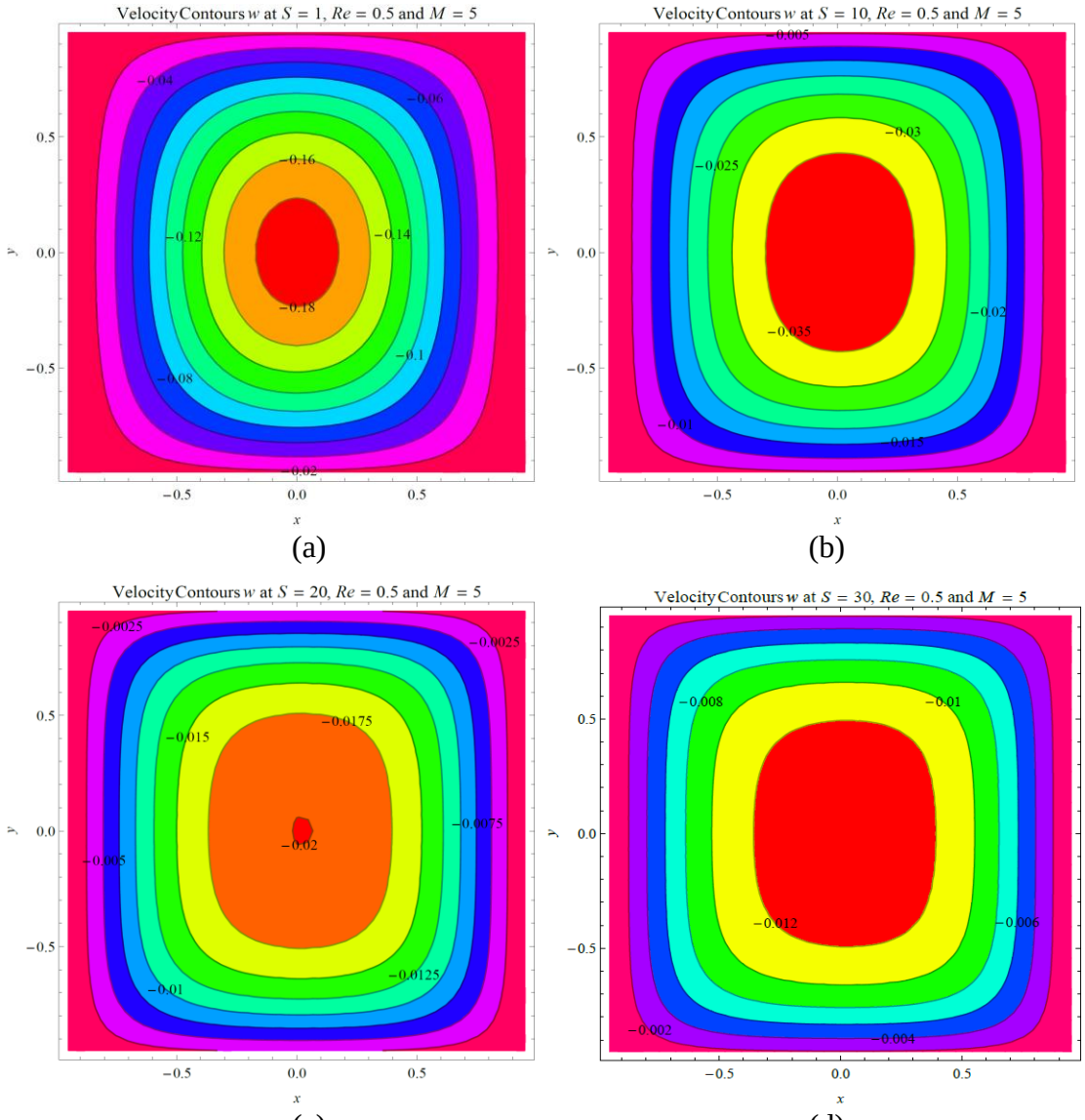

Fig. 6.4: For Re=0.5 and M=5, Velocity $w(x, y)$ at (a) S=1, (b) S=10, (c) S=20 and (d) S=30.

6.4.2 Temperature θ

In Fig. 6.5, temperature contours at different values of Re are shown. We notice that for high values of Re, the contours of temperature are symmetrically distributed about a horizontal line. For low values of Re, some temperature contours are positive and

some are negative. For $Re \leq 1$, temperature profiles are positive and negative for Re >20.

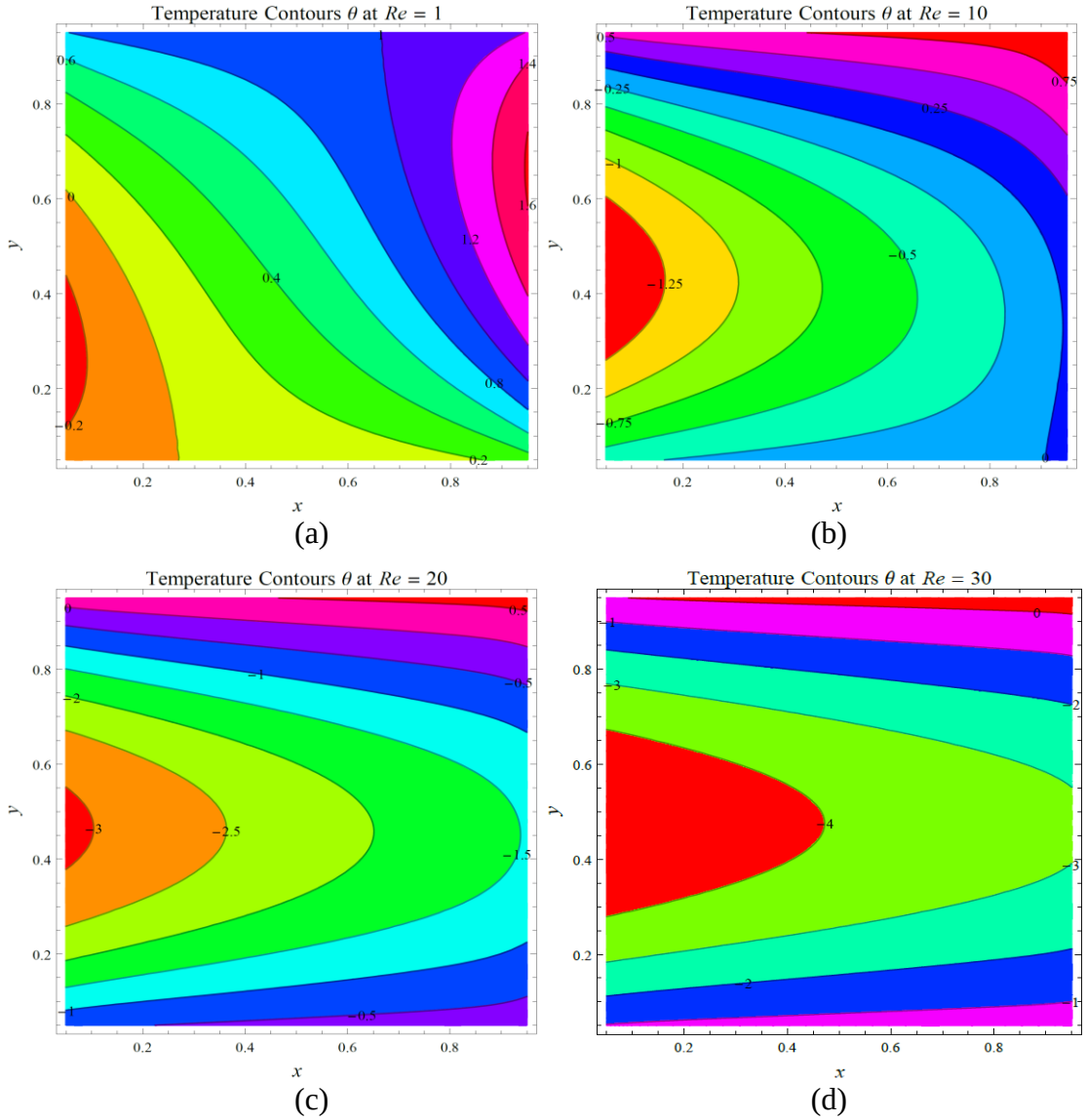

Fig. 6.5: Temperature $\theta(x, y)$ at (a) Re=1, (b) Re=10, (c) Re=20 and (d) Re=30.

6.4.3 Volumetric Flow Rate

Volumetric flow rate V is computed from equation (6.26) and is shown in Fig. 6.6 vs Couple stress parameter S at different values of Reynolds number Re and magnetic parameter M. It is observed that as Re or S or M increases, Volumetric flow rate decreases. After a critical value of S, volumetric flow rate becomes constant. This may be due to the fact that as suction increases, more fluid is taken out as suction. Velocity decreases as M or S increases, and hence volumetric flow rate decreases.

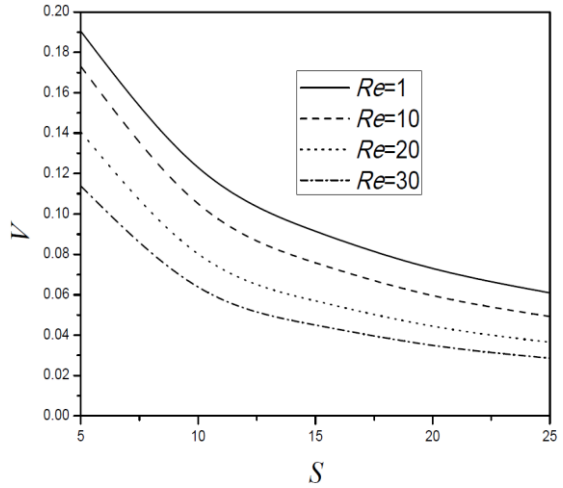

(a) at different values of Reynolds number *Re*

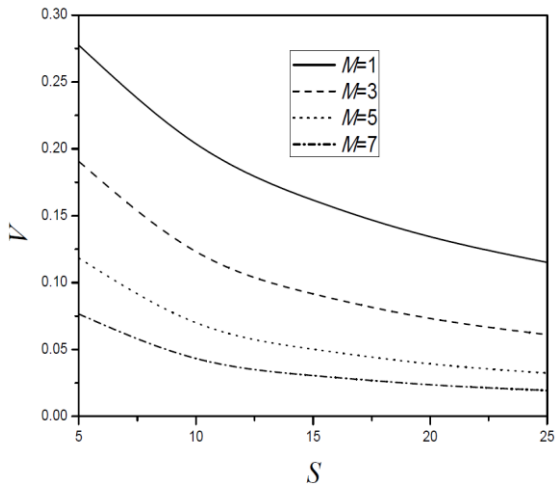

(b) at different values of Magnetic parameter *M*

Fig. 6.6: Volumetric flow rate vs Couple stress parameter.

6.4.4 Skin Friction

In Fig. 6.7 and Fig. 6.8, the skin friction at $x = \pm 1$ for different values of Couple stress parameter *S* at fixed *e*=0.5, *M*=3 and *M*=5 are shown respectively. We observe that at *x*=1, skin friction C_f is positive and negative at *x*= –1. This is a natural observation since opposite walls will have opposite shear stresses. As *S* increases, C_f also decreases. This may be due to the fact that couple stresses in the fluid contribute to shear stresses to decrease.

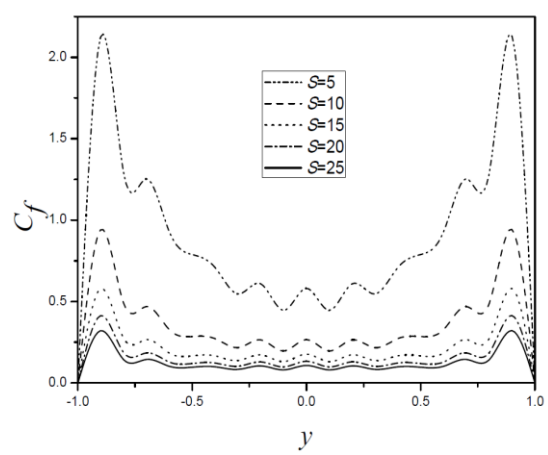

(a) *x*=1

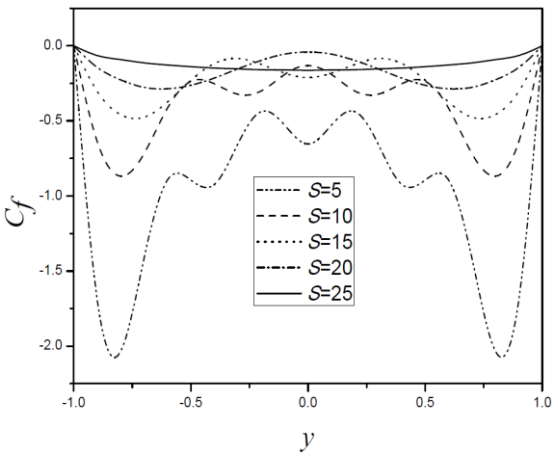

(b) *x*= –1

Fig. 6.7: Skin friction at *M*=3 for different values of Couple stress parameter *S*.

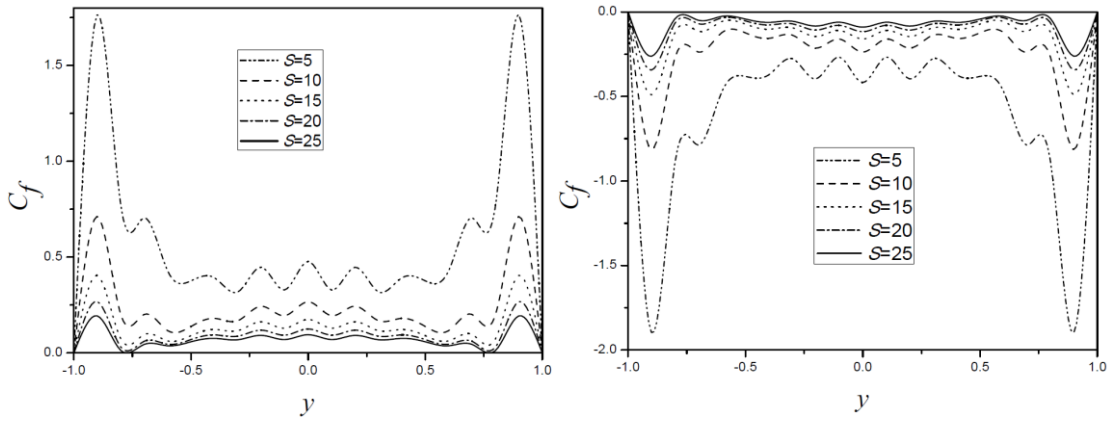

(a) x=1 (b) x= –1

Fig. 6.8: Skin friction at M=5 for different values of Couple stress parameter S.

At S=50, e=0.5 and for different values of M the average skin friction using equation (6.27) at x=1 is tabulated in Table. 6.1 and at x= –1 is tabulated in Table. 2.

Table. 1: Average skin friction values at x=1 for different values of M at S=50, e=0.5.

M	3	5	7
Average C_f	0.0517621	0.0307316	0.0257768

Table. 2: Average skin friction values at x=–1 for different values of M at S=50, e=0.5.

M	3	5	7
Average C_f	–0.036376	–0.0348286	–00255526

From this, we observe that as magnetic parameter M increases, skin friction decreases at x=1 and increases at x= –1.

6.5 Conclusions

From figures drawn, we analyze and observe that for couple stress fluids

- By applying magnetic field, the volumetric flow rate and skin friction on the walls are controlled i.e., decrease.
- After a critical value of Couple stress parameter, the volumetric flow rate is almost constant.
- For high suction, the temperature is distributed symmetrically about a horizontal line.
- As couple stress parameter increases, the area occupied by minimum value of the velocity increases.
- As magnetic parameter increases, the velocity at the center of the channel becomes horizontal (This is Hartman effect).

Part – IV

STOKES FLOW PAST A CYLINDER

Chapter 7

Stokes Flow and Heat Transfer Past a Circular Cylinder in a Square Cavity with Suction/Injection on Side Walls

A laminar viscous fluid flow past a circular cylinder placed in a square cavity of uniform cross section, generated by applying suction/ injection at the adjacent side walls, is studied. The other opposite side walls and the boundary of the cylinder are maintained at constant temperatures and the walls with suction are maintained at constant heat flux. The stream lines due to the flow and isothermal lines are drawn. The flow is assumed to be Stokesian and hence neglecting nonlinear convective terms, the equation for stream function satisfies biharmonic equation. This biharmonic equation for stream function is put in the vorticity form by writing it into two coupled equations and 5 point formula is used to solve the equations. For derivative boundary conditions of stream function, central difference formula with fictitious nodes and for derivative boundary conditions of temperature 3 point backward difference formula are used.

7.1 Introduction

The flow field effected by suction/injection across the walls is encountered in fuel cell manifolds, micro reactor channels, filtration units, and in membrane reactor ducts. Guoping et al. (1995) studied the viscous fluid flow and heat transfer due to a square obstacle placed asymmetrically between the parallel sliding walls. Moukalled et al. (1996) and Cesini et al. (1999) have performed numerical and experimental analysis on natural convection heat transfer from a horizontal cylinder enclosed in a rectangular cavity. Breuer et al. (2000) investigated the confined flow around a cylinder with square cross-section seated inside a channel. Salvatici et al. (2003) studied large-eddy simulations of the flow around a circular cylinder. Projahn et al. (1981) carried out numerical analysis to investigate the local and overall heat transfer between concentric and eccentric horizontal cylinder. Kim et al. (2008) analysed numerically the natural convection induced by a temperature difference due to a hot circular cylinder placed in a cold outer square enclosure. Akhilesh et al. (2009) made a numerical study of the

unsteady free stream flow of power law fluids past a long square cylinder. Salam et al. (2010) examined 2D steady natural convection numerically for a uniform heat source applied on the inner circular cylinder placed in a square enclosure filled with air. Berrone et al. (2011) investigated the flow past rectangular cylinders. Minguez et al. (2011) have conducted experimental/numerical study of turbulent flow past a square cylinder. Sandip et al. (2012) studied entropy generation number due to a mixed convection of water based nano-fluid past a square cylinder in vertically upward flow. Weiwei et al. (2013) applied an efficient immersed boundary method for thermal flow problems with heat flux boundary conditions. Lin et al. (2014) numerically investigated laminar flow past a circular cylinder with multiple small-diameter control rods. Prasenjit et al. (2015) investigated flow around an extended triangular solid (thorn) attached to a square cylinder numerically. Ali et al. (2017) studied the convection of heat from two rotating hot cylinders in a cold square cavity. Yang et al. (2017) made a numerical investigation of natural convection in a Cu–water nano-fluid filled eccentric annulus with constant heat flux wall. Kim et al. (2018) studied the effect of corner modifications on fluid flow and heat transfer characteristics across a square cylinder.

In the classical problems, most of the researchers analysed the flow past a circular cylinder only. But the study of flow past a circular cylinder in a cavity due to suction on walls is paid very less attention. Hence in the present chapter our aim is to study the flow past a circular cylinder in a square cavity with suction on adjacent walls.

7.2 Mathematical Formulation

The flow of viscous fluid past a cylinder in a square cavity of uniform cross section due to applied suction/injection at the side walls is considered. The physical representation of the problem is given Fig. 7.1. The Cartesian coordinate system with origin at the bottom left corner and X and Y axes along the bottom and left walls is taken. The cavity is of length a_0 along X direction, height b_0 along Y direction and a cylinder with radius r_0 is kept in the middle of the cavity. Injection with velocity V_1 at the top wall $Y=b_0$ and suction with velocity V_2 at the right wall $X=a_0$ are imposed. The flow is generated within the cavity due to the injection and suction applied at adjacent walls.

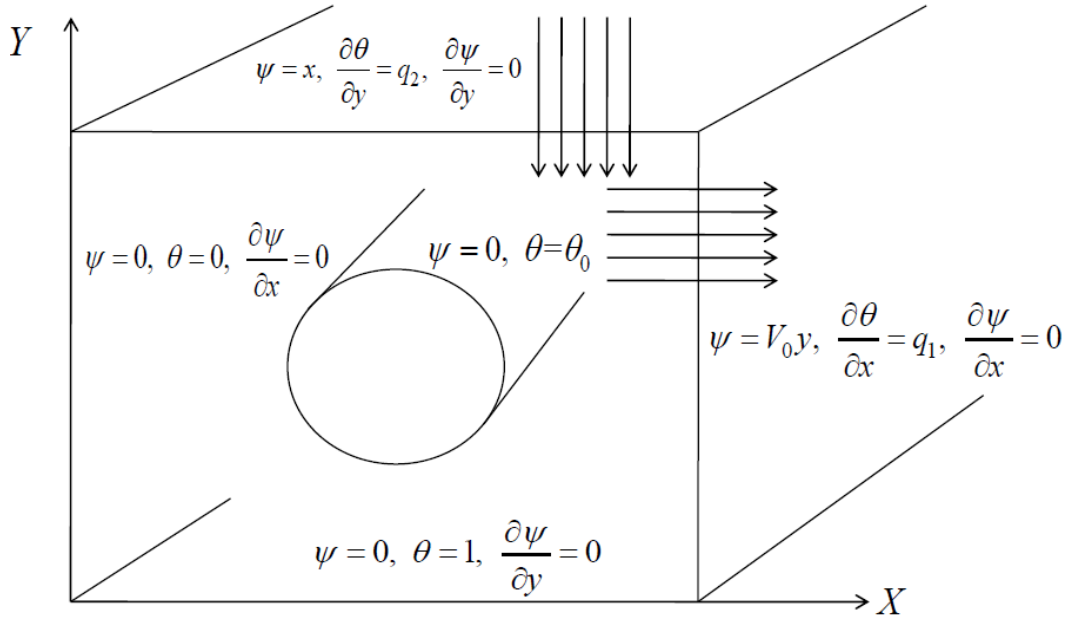

Fig. 7.1: Flow configuration in a square cavity with adjacent wall suction.

Governing Equations

The equations of motion for the flow are given below:

$$\nabla.\mathbf{Q} = 0 \tag{7.1}$$

$$\rho\frac{d\mathbf{Q}}{dt} = -\nabla P + \mu\nabla^2\mathbf{Q} \tag{7.2}$$

$$\rho c_p\frac{dT}{dt} = k\nabla^2 T \tag{7.3}$$

where **Q** is the velocity of fluid particle, P is pressure, T is the temperature, ρ is fluid density, μ is the coefficient of viscosity, k is the thermal conductivity of the fluid and c_p heat capacity at constant pressure.

The flow is two dimensional and hence **Q**= (U, V).

Boundary conditions for the problem

Velocity of fluid particles satisfies no slip condition on the walls with no suction or injection and no slip condition and impermeability condition on the cylinder. Again permeability conditions, suction on the right wall and injection on the top wall, are imposed. The temperature field satisfies constant temperature on the impermeable walls X=0, Y=0 and on the cylinder. Condition of constant heat flux at the permeable walls X=a_0 and Y=b_0 is taken.

Due to no slip condition on the walls X=0 and Y=0, the tangential velocities are zero.

i.e., on X=0, V=0 $\Rightarrow \frac{\partial \psi}{\partial X} = 0$ and on Y=0, U=0 $\Rightarrow \frac{\partial \psi}{\partial Y} = 0$.

Due to impermeability condition on the walls X=0 and Y=0, the normal velocities are also zero.

i.e., on X=0, U=0 $\Rightarrow \frac{\partial \psi}{\partial Y} = 0$ and on Y=0, V=0 $\Rightarrow \frac{\partial \psi}{\partial X} = 0$.

Due to no slip condition on the walls $X=a_0$ and $Y=b_0$, the tangential velocities are zero.

i.e., on $X=a_0$, V=0 $\Rightarrow \frac{\partial \psi}{\partial X} = 0$ and on $Y=b_0$, U=0 $\Rightarrow \frac{\partial \psi}{\partial Y} = 0$.

On permeable walls, the suction velocity on $X=a_0$ is V_2 and the injection velocity on $Y=b_0$ is V_1.

i.e., on $X=a_0$, $U=V_2$ $\Rightarrow \frac{\partial \psi}{\partial Y} = V_2$ and on $Y=b_0$, $V=-V_1$ $\Rightarrow \frac{\partial \psi}{\partial X} = V_1$.

The walls X=0 and Y=0 are maintained at constant temperatures. i.e., $T=T_1$ on X=0 and $T=T_2$ on Y=0.

On the walls $X=a_0$ and $Y=b_0$ constant heat fluxes are imparted.

i.e., $\frac{\partial T}{\partial X} = Q_1$ on $X = a_0$ and $\frac{\partial T}{\partial Y} = Q_2$ on $Y = b_0$.

Non-dimensionalization

We introduce the following non-dimensional scheme and non-dimensional parameters like Pe= Peclet number, y_0=geometric parameter, V_0=suction parameter as below.

$$X = a_0 x,\ Y = a_0 y,\ U = V_1 u,\ V = V_1 v,\ P = \rho V_1^2 p,\ T - T_1 = \theta(T_2 - T_1) \qquad (7.4)$$

$$Pe = \frac{\rho C_p V_1 a_0}{k},\ y_0 = \frac{b_0}{a_0},\ V_0 = \frac{V_2}{V_1} \qquad (7.5)$$

For the flow the Reynolds number is so small that the convective terms in equation (7.2) are neglected. The flow is steady and hence independent of time t.

7.3 Solution of the problem

7.3.1 Stream function

We introduce stream function ψ as below such that equation (7.1) is satisfied.

$$u = \frac{\partial \psi}{\partial y} \quad \text{and} \quad v = -\frac{\partial \psi}{\partial x} \qquad (7.6)$$

Taking curl to equation (7.2) and substituting (7.6), we get the equation for the non-dimensional stream function ψ as

$$\nabla^4 \psi = 0 \tag{7.7}$$

with boundary conditions:

$$\frac{\partial \psi}{\partial x} = 0 \text{ on } x = 0 \text{ and on } x = 1 \text{ and } \psi = 0 \text{ on } \Gamma$$

$$\frac{\partial \psi}{\partial y} = 0 \text{ on } x = 0 \text{ and } \frac{\partial \psi}{\partial y} = V_0 \text{ on } x = 1$$

$$\frac{\partial \psi}{\partial x} = 0 \text{ on } y = 0 \text{ and } \frac{\partial \psi}{\partial x} = 1 \text{ on } y = y_0$$

$$\frac{\partial \psi}{\partial y} = 0 \text{ on } y = 0 \text{ and on } y = y_0$$

These conditions, by integrating, are converted in to the conditions on ψ as follows:

$$\left.\begin{aligned} &\frac{\partial \psi}{\partial x} = 0 \text{ on } x = 0 \text{ and } x = 1 \\ &\psi = 0 \text{ on } x = 0 \text{ and } y = 0 \\ &\psi = x \text{ on } y = y_0 \\ &\psi = V_0 y \text{ on } x = 1 \\ &\frac{\partial \psi}{\partial y} = 0 \text{ on } y = 0 \text{ and } y = y_0 \\ &\psi = 0 \text{ on the cylinder } \Gamma \end{aligned}\right\} \tag{7.8}$$

We solve the equation (7.7) with conditions (7.8) by Finite Difference Method. The cavity is covered with a mesh of step size h with (M–1) intervals on X direction and (N–1) intervals on Y direction. For each grid point (i, j) within the cavity, the bi-harmonic equation (7.7) can be split into two coupled equations as given in Biringen and Chow (2011) as below:

$$\nabla^2 \psi = -\zeta \tag{7.9}$$

and $$\nabla^2 \zeta = 0 \tag{7.10}$$

For the boundary conditions containing derivatives, we used central difference scheme. The nodes numbering is as follows:

Along X direction	Along Y direction
x_1 node on the boundary $x = 0$.	y_1 node on the boundary $y = 0$.
x_2 , x_3, … , x_{M-1} inside the computational	y_2 , y_3, … , y_{N-1} inside the computational
x_M node on the boundary x=1	y_N node on the boundary y=y_0

Thus at x=0 (i.e., i=1) we have, $\psi(0, y) = 0$.

These conditions are taken as $\psi_{1,j} = 0$ for j=1,2,...,N (7.11)

at x=1 (i.e., i=M) we have, $\psi(1, y) = V_0 y$.

These conditions are taken as $\psi_{M,j} = V_0(j-1)h$ for j=1,2,...,N (7.12)

Similarly at y = 0 we have, $\psi(x, 0) = 0$.

These conditions are taken as $\psi_{i,1} = 0$ for i=2,3,...,$M-1$ (7.13)

Finally at y =y_0 we have, $\psi(x, y_0) = x$.

These conditions are taken as $\psi_{i,N} = (i-1)h$ for i=2,3,...,$M-1$ (7.14)

Now, we derive expressions for boundary values of ζ in terms of ψ, which are required for solving (7.10). We now assume for vorticity on x=0 (i.e., at (1, j)):

$$\zeta_{1,j} = -\left(\frac{\partial^2\psi}{\partial x^2} + \frac{\partial^2\psi}{\partial y^2}\right)_{1,j} = \alpha_1\psi_{2,j-1} + \alpha_2\psi_{2,j} + \alpha_3\psi_{2,j+1} + \alpha_4\psi_{3,j} + \alpha_5\left(\frac{\partial\psi}{\partial x}\right)_{1,j} \quad (7.15)$$

Substituting from the Taylor's series expansions,

$$\psi_{2,j\pm1} = \psi_{1,j} + h\left(\frac{\partial\psi}{\partial x}\right)_{1,j} \pm h\left(\frac{\partial\psi}{\partial y}\right)_{1,j} + \frac{h^2}{2}\left(\frac{\partial^2\psi}{\partial x^2}\right)_{1,j} + \frac{h^2}{2}\left(\frac{\partial^2\psi}{\partial y^2}\right)_{1,j} + O\left(h^3\right)$$

$$\psi_{2,j} = \psi_{1,j} + h\left(\frac{\partial\psi}{\partial x}\right)_{1,j} + \frac{h^2}{2}\left(\frac{\partial^2\psi}{\partial x^2}\right)_{1,j} + O\left(h^3\right)$$

$$\psi_{3,j} = \psi_{1,j} + 2h\left(\frac{\partial\psi}{\partial x}\right)_{1,j} + \frac{(2h)^2}{2}\left(\frac{\partial^2\psi}{\partial x^2}\right)_{1,j} + O\left(h^3\right)$$

and retaining only terms up to $O(h^2)$, equation (7.15) becomes

$$-\left(\frac{\partial^2\psi}{\partial x^2} + \frac{\partial^2\psi}{\partial y^2}\right)_{1,j} = (\alpha_1 + \alpha_2 + \alpha_3 + \alpha_4)\psi_{1,j} + \left[(\alpha_1 + \alpha_2 + \alpha_3 + 2\alpha_4)h + \alpha_5\right]\left(\frac{\partial\psi}{\partial x}\right)_{1,j} + (\alpha_3 - \alpha_1)h\left(\frac{\partial\psi}{\partial y}\right)_{1,j}$$
$$+ \left[(\alpha_1 + \alpha_2 + \alpha_3 + 4\alpha_4)\frac{h^2}{2}\right]\left(\frac{\partial^2\psi}{\partial x^2}\right)_{1,j} + (\alpha_1 + \alpha_3)\frac{h^2}{2}\left(\frac{\partial^2\psi}{\partial y^2}\right)_{1,j}$$

The constants α's are determined by equating the coefficients of like terms on the both sides of this equation. Substitution of these values in (7.15) gives

$$\zeta_{1,j} = \frac{1}{h^2}\left(-\psi_{2,j-1} + \frac{8}{3}\psi_{2,j} - \psi_{2,j+1} - \frac{2}{3}\psi_{3,j}\right) \text{ for } j = 2, 3, ...N \quad (7.16)$$

where $\left(\frac{\partial\psi}{\partial x}\right)_{1,j} = 0$ from the boundary condition (7.8).

Similarly, the expressions for vorticity at the remaining boundaries as:

On $x = 1$,

$$\zeta_{M,j} = \frac{1}{h^2}\left(-\psi_{M-1,j-1} + \frac{8}{3}\psi_{M-1,j} - \psi_{M-1,j+1} - \frac{2}{3}\psi_{M-2,j}\right) \text{ for } j = 2,3,....N \qquad (7.17)$$

on $y = 0$, $\zeta_{i,1} = \frac{1}{h^2}\left(-\psi_{i-1,2} + \frac{8}{3}\psi_{i,2} - \psi_{i+1,2} - \frac{2}{3}\psi_{i,3}\right)$ for $i = 2,3,....M$ (7.18)

on $y = y_0$,

$$\zeta_{i,N} = \frac{1}{h^2}\left(-\psi_{i-1,N-1} + \frac{8}{3}\psi_{i,N-1} - \psi_{i+1,N-1} - \frac{2}{3}\psi_{i,N-2}\right) \text{ for } i = 2,3,....M \qquad (7.19)$$

in which the derivative boundary conditions in (7.8) have been employed.

Along with these boundary conditions, we have ζ on the cylinder is given by Thom (1933).

$$\zeta_S = \frac{(\psi_G - \psi_S)}{D} \qquad (7.20)$$

where G is the point on the normal which cuts either vertical or horizontal grid line in the flow region, S is the point on the cylinder and D is the distance between the points G and S.

The equation (7.10) numerically will be solved using Liebmann's iterative formula:

$$\zeta_{i,j} = \frac{1}{4}\left(\zeta_{i-1,j} + \zeta_{i+1,j} + \zeta_{i,j-1} + \zeta_{i,j+1}\right) \qquad (7.21)$$

boundary points on the cylinder are defined as the intersections of the horizontal-vertical grid lines and the body surface. These points do not usually coincide with the grid points. Thus the formula (7.21) cannot be used at some grid points in the immediate neighbourhood of the cylinder.

Equation (7.21) is the Laplace equation (7.10) replaced by a finite difference approximation on the assumption that the point (i, j) is equally spaced from its other four neighbouring grid points. The difference equation (7.21) is generalized for an arbitrary situation as shown in Fig. 7.2, where the point (i, j) is at different distances a, b, c and d from four neighbouring points.

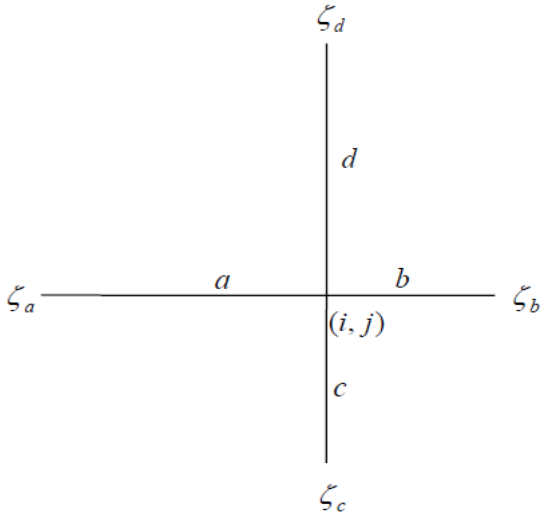

Fig. 7.2: Evaluation of $\zeta_{i,j}$.

We let the vorticity function evaluated at these neighbouring points be denoted by ζ_a, ζ_b, ζ_c, and ζ_d respectively, and then approximate the left hand side of (7.10) at (i, j) by the linear function:

$$\left(\frac{\partial^2\zeta}{\partial x^2}+\frac{\partial^2\zeta}{\partial y^2}\right)_{i,j} = \alpha_0\zeta_{i,j}+\alpha_a\zeta_a+\alpha_b\zeta_b+\alpha_c\zeta_c+\alpha_d\zeta_d \qquad (7.22)$$

where α's are coefficient to be determined. Expanding the four vorticity functions in Taylor's series about (i, j),

$$\zeta_{i-1,j}=\zeta_a=\zeta_{i,j}-a\left(\frac{\partial\zeta}{\partial x}\right)_{i,j}+\frac{a^2}{2}\left(\frac{\partial^2\zeta}{\partial x^2}\right)_{i,j}-O\left(a^3\right)$$

$$\zeta_{i,j+1}=\zeta_d=\zeta_{i,j}+d\left(\frac{\partial\zeta}{\partial y}\right)_{i,j}+\frac{d^2}{2}\left(\frac{\partial^2\zeta}{\partial y^2}\right)_{i,j}+O\left(d^3\right)$$

and so forth. Substitution of these equations in (7.22) after rearrangement and neglecting the cubic and higher order terms, we get

$$\left(\frac{\partial^2\zeta}{\partial x^2}+\frac{\partial^2\zeta}{\partial y^2}\right)_{i,j}=(\alpha_0+\alpha_a+\alpha_b+\alpha_c+\alpha_d)\zeta_{i,j}+(b\alpha_b-a\alpha_a)\left(\frac{\partial\zeta}{\partial x}\right)_{i,j}+(d\alpha_d-c\alpha_c)\left(\frac{\partial\zeta}{\partial y}\right)_{i,j}$$
$$+\frac{1}{2}(a^2\alpha_a+b^2\alpha_b)\left(\frac{\partial^2\zeta}{\partial x^2}\right)_{i,j}+\frac{1}{2}(c^2\alpha_c+d^2\alpha_d)\left(\frac{\partial^2\zeta}{\partial y^2}\right)_{i,j}$$

Equating corresponding coefficients on both the sides results in five simultaneous algebraic equations whose solution is

$$\alpha_0=-2\left(\frac{1}{ab}+\frac{1}{cd}\right),\ \alpha_a=\frac{2}{a(a+b)},\ \alpha_b=\frac{2}{b(a+b)},\ \alpha_c=\frac{2}{c(c+d)},\ \alpha_d=\frac{2}{d(c+d)}$$

vanishing of the right hand side of (7.22) gives the desired difference approximation of the Laplace equation:

$$\zeta_{i,j} = \left[\frac{\zeta_a}{a(a+b)} + \frac{\zeta_b}{b(a+b)} + \frac{\zeta_c}{c(c+d)} + \frac{\zeta_d}{d(c+d)} \right] / \left(\frac{1}{ab} + \frac{1}{cd} \right) \qquad (7.23)$$

for i=2,3, …, M–1 and j=2,3, …, N–1.

It can easily be shown that (7.23) is equivalent to (7.21) when $a=b=c=d=h$.

In the similar manner we solve equation (7.9) numerically using

$$\psi_{i,j} = \left[\frac{\psi_a}{a(a+b)} + \frac{\psi_b}{b(a+b)} + \frac{\psi_c}{c(c+d)} + \frac{\psi_d}{d(c+d)} + \frac{\zeta_{i,j}}{2} \right] / \left(\frac{1}{ab} + \frac{1}{cd} \right) \qquad (7.24)$$

for i=2,3, …, M–1 and j=2,3, …, N–1.

The vorticity boundary conditions derived (7.16)–(7.20) help us to solve (7.10) if ψ is known at some interior points. But, the evaluation of ψ from (7.9) depends on the distribution of vorticity within the bounded domain. Thus, ψ and ζ are inter-linked, and an iterative scheme will be build up to find the solution.

For initial guess, an equilibrium state is assumed first so that ψ =0 everywhere in the flow region. Based on this initial guess, the boundary values for ζ are found from (7.16)–(7.20) which shows that vorticity is initially generated at the boundary. This concentrated vorticity at the boundary starts to diffuse into the cavity, resulting in a temporary vorticity distribution which is the solution of (7.10) that satisfies the present boundary conditions. This computed vorticity distribution causes a modification to the assumed ψ after solving (7.9) subject to the restriction that we have in (7.8) on the boundary. In this way we have completed the first iteration. To start the next iteration, based on the modified stream function, the boundary values of vorticity are recomputed. To obtain a new solution for ψ and ζ, the same procedure is repeated. At every grid point, the difference between the newly computed ζ and the previous value is recorded as the local error during each iteration and the sum of absolute errors at all grid points is called ERZETA. Similarly we find ERPSI, the corresponding sum of absolute errors of ψ. Iteration is terminated when both ERPSI and ERZETA are smaller than a small positive value EPSLON (=10^{-4}). Since the desired accuracy is reached, at this stage the solution is then considered to be satisfactory.

7.3.2 Temperature

The energy equation, given in (7.3), by using (7.4), (7.5) can be reduced to the non-dimensional form as below:

$$\nabla^2\theta = Pe\left(u\frac{\partial\theta}{\partial x} + v\frac{\partial\theta}{\partial y}\right) \tag{7.25}$$

Temperature is subjected to the boundary conditions that i) the sides x=0, y=0 and on cylinder are maintained at constant temperatures and ii) the other sides are supplied with constant heat or constant heat flux. The conditions are given explicitly as

$$\left.\begin{array}{l} \theta = 0 \text{ on } x = 0,\ \theta = 1 \text{ on } y = 0,\ \theta = \theta_0 \text{ on cylinder} \\ \dfrac{\partial\theta}{\partial x} = q_1 \text{ on } x = 1,\ \dfrac{\partial\theta}{\partial y} = q_2 \text{ on } y = y_0 \end{array}\right\} \tag{7.26}$$

Let $u_{i,j} = \left(\dfrac{\partial\psi}{\partial y}\right)_{i,j} = \dfrac{\psi_{i,j+1} - \psi_{i,j-1}}{2h} = f_2$ and $v_{i,j} = -\left(\dfrac{\partial\psi}{\partial x}\right)_{i,j} = -\dfrac{\psi_{i+1,j} - \psi_{i-1,j}}{2h} = -f_1$

Proceeding as in the stream function and vorticity function equation (7.25) can be generalizes as:

$$\theta_{i,j} = \frac{1}{2\left(\dfrac{1}{ab} + \dfrac{1}{cd}\right)}\left[\begin{array}{r} \dfrac{(2 + af_2Pe)\theta_a}{a(a+b)} + \dfrac{(2 - bf_2Pe)\theta_b}{b(a+b)} + \dfrac{(2 - cf_1Pe)\theta_c}{c(c+d)} \\ + \dfrac{(2 + df_1Pe)\theta_d}{d(c+d)} \end{array}\right] \tag{7.27}$$

for i=2,3, …, M and j=2,3, …, N

The boundary conditions in (7.26) are now expressed as:

$$\left.\begin{array}{l} \text{at } x = 0,\ \theta = 0 \text{ which implies that } \theta_{1,j} = 0 \text{ for } j = 2,3,...,N \\ \text{at } y = 0,\ \theta = 1 \text{ which implies that } \theta_{i,1} = 1 \text{ for } i = 2,3,...,M \\ \text{at } x = 1,\ \dfrac{\partial\theta}{\partial x} = q_1 \quad \Rightarrow \theta_{M,j} = \dfrac{1}{3}\left[4\theta_{M-1,j} - \theta_{M-2,j} - 2hq_1\right] \text{ for } j = 2,3,\ldots,N \\ \text{at } y = y_0,\ \dfrac{\partial\theta}{\partial y} = q_2 \quad \Rightarrow \theta_{i,N} = \dfrac{1}{3}\left[4\theta_{i,N-1} - \theta_{i,N-2} - 2hq_2\right] \text{ for } i = 2,3,\ldots,M \end{array}\right\} \tag{7.28}$$

and on the cylinder $\theta_{i,j} = \theta_0 = 0.5$ where θ_0 is the reference temperature.

As in stream function and vorticity function in the equation (7.27) subjected to the boundary conditions (7.28) will be solved for the temperature in the cavity.

7.4 Results and Discussion

We have obtained the values of stream function and temperature for step length h=0.01. The accuracy near to 4 decimal places is obtained by taking 1000 iterations. Here the important steps involved in the computation are to calculate 1). *a, b, c, d* values adjacent to the cylinder and 2). *D* the distance between *G* and *S* in equation (7.20). Here *S* is a point on the cylinder and *G* is a point on the grid line obtained by intersection of normal with the grid. These are explained in the appendix.

7.4.1 Streamlines

The stream lines generated due to injection at the top wall and suction at the right wall are shown in Fig. 7.3 to Fig. 7.5. The figures are drawn for different suction parameter values V_0. We observe from Fig. 7.3 when the cylinder is middle of the cavity that as suction parameter V_0 increases, the region of high stream values increases at the right end of the cylinder and the stream lines with low values (example ψ = 0.001) which are separated and near to the left wall are merging in the circulation region of the cylinder. Again as V_0 increases, a second circulation region is formed at the top left corner. For small values of V_0, the stream lines are nearly parallel to the left wall.

Form Fig. 7.4, when the cylinder is bottom left corner, for small suction V_0=5, stream lines have small values and high values within small region near the left side of the cylinder. The presence of cylinder effects entire region dominating suction. As suction parameter increases, effect of suction spreads near to the cylinder and the values of stream lines away from the cylinder also increase. It is important to note that *even though cylinder is small placed at left bottom corner effects the entire flow dominating the suction.*

Form Fig. 7.5 when the cylinder is at the top right corner, for small values of suction, a circulation region below the cylinder spreads half of the cavity. But when suction increases, the circulation almost disappears and suction dominates the flow by increasing the values of stream lines.

It is important to note that *when the cylinder is at the top right corner, circulation below the cylinder spreads in the cavity* and this disappears when suction increases.

Though the circulation behind the cylinder is there in all cases of position of the cylinder in the cavity, it is best observed when it is in the top corner.

When there is no cylinder, the steam line pattern is shown in Fig. 7.13. For high suction when the small cylinder is on the top corner, the flow is similar to the flow without cylinder.

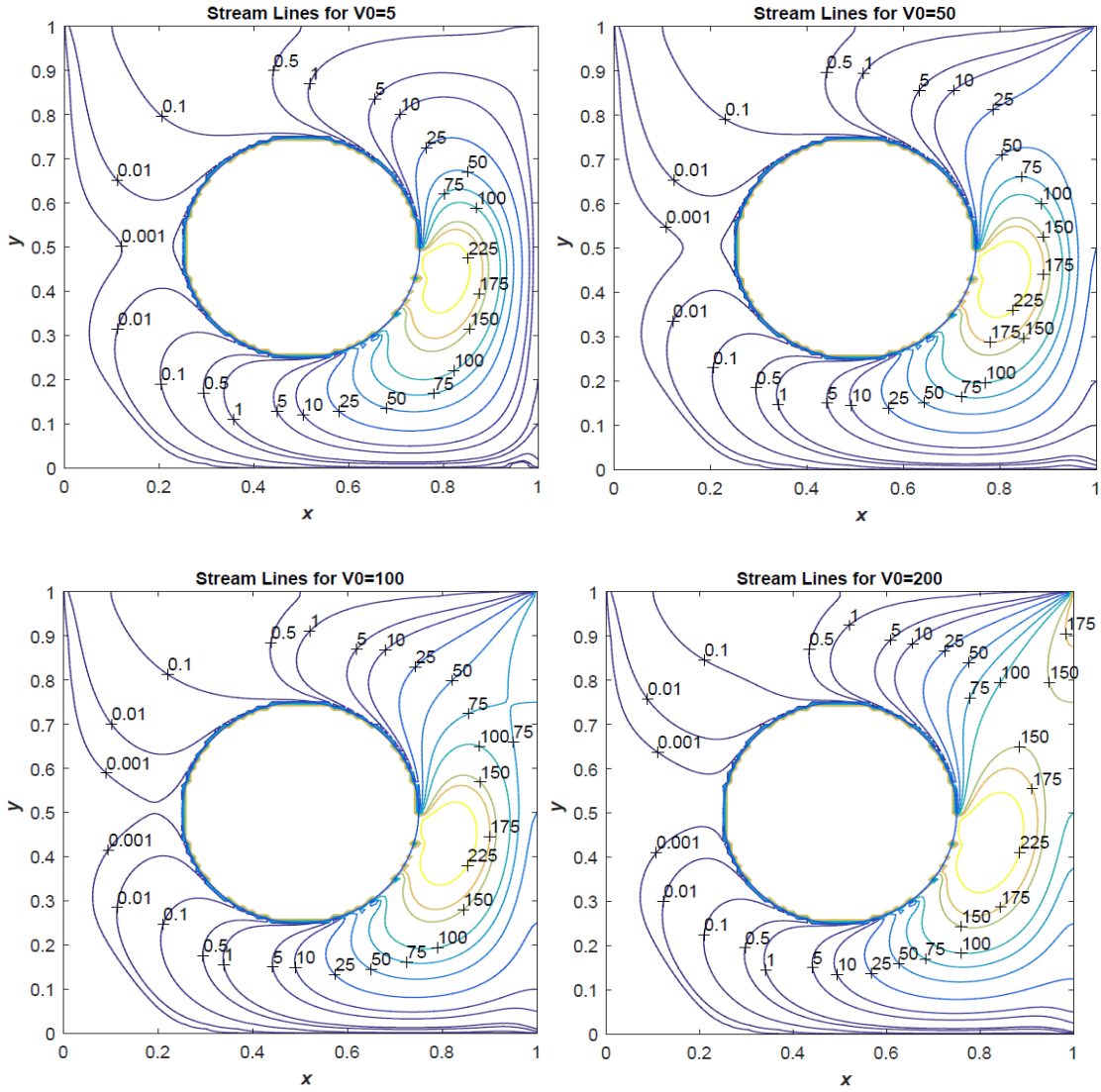

Fig. 7.3: Streamlines for different values of V_0.

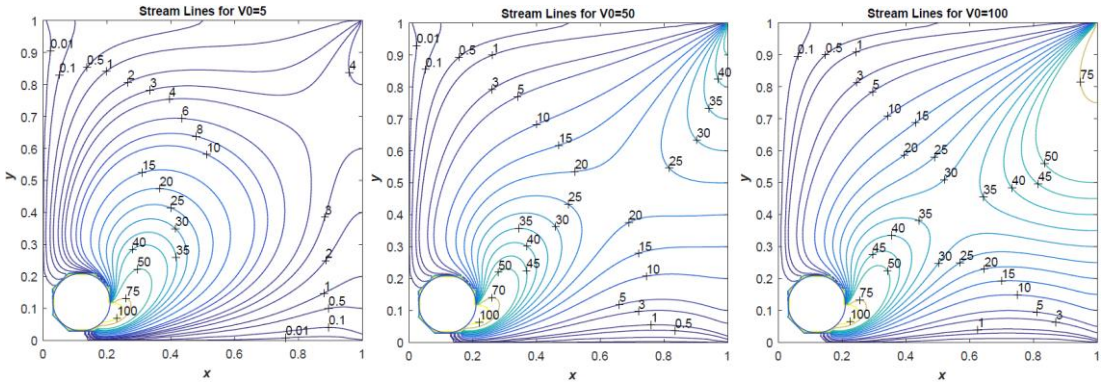

Fig. 7.4: Streamlines for different values of V_0(=5,50,100) when cylinder is at lower left corner of the cavity.

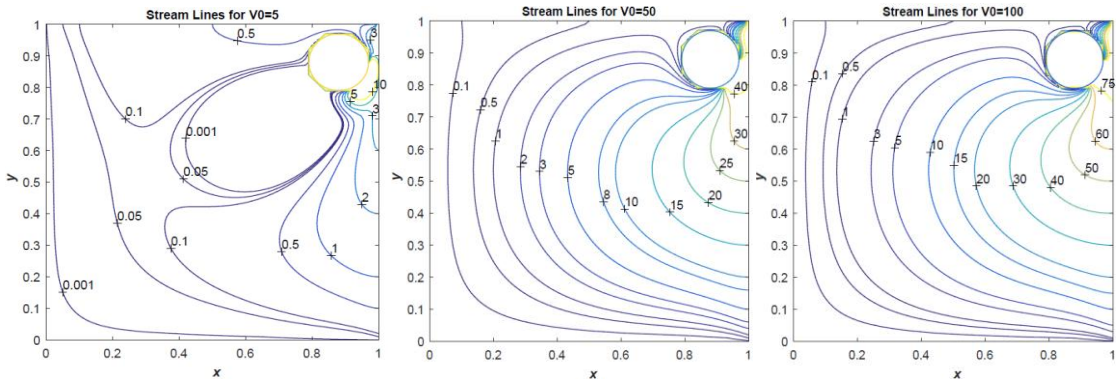

Fig. 7.5: Streamlines for different values of V_0(=5, 50, 100) when cylinder is at top right corner of the cavity.

7.4.2 Vorticity Contours

The vorticity contours generated due to injection at the top wall and suction at the right wall are shown in Fig. 7.6 to Fig. 7.8. The figures are drawn for different suction parameter values V_0. We observe that as V_0 increases, when the cylinder is middle of the cavity, the circulation of vortex lines on the right side of cylinder increases and opens to the right top corner. The values of vorticity are very high at the right wall and in the circulation region of vorticity. Outside of the circulation region, vorticity takes negative values except at top left region.

From Fig. 7.7, when a small cylinder is placed at the bottom left corner, for small values of suction, circulation region above the cylinder spreads to the top corner. High values of vorticity are found on the left wall which is opposite to the above case (when the cylinder is in the middle).

From Fig. 7.8, when a small cylinder is placed at the top right corner, for small suction parameter circulation region below the cylinder is in small region and this region spreads in the entire cavity when suction increases. Here we find high negative values of vorticity at the top and bottom walls.

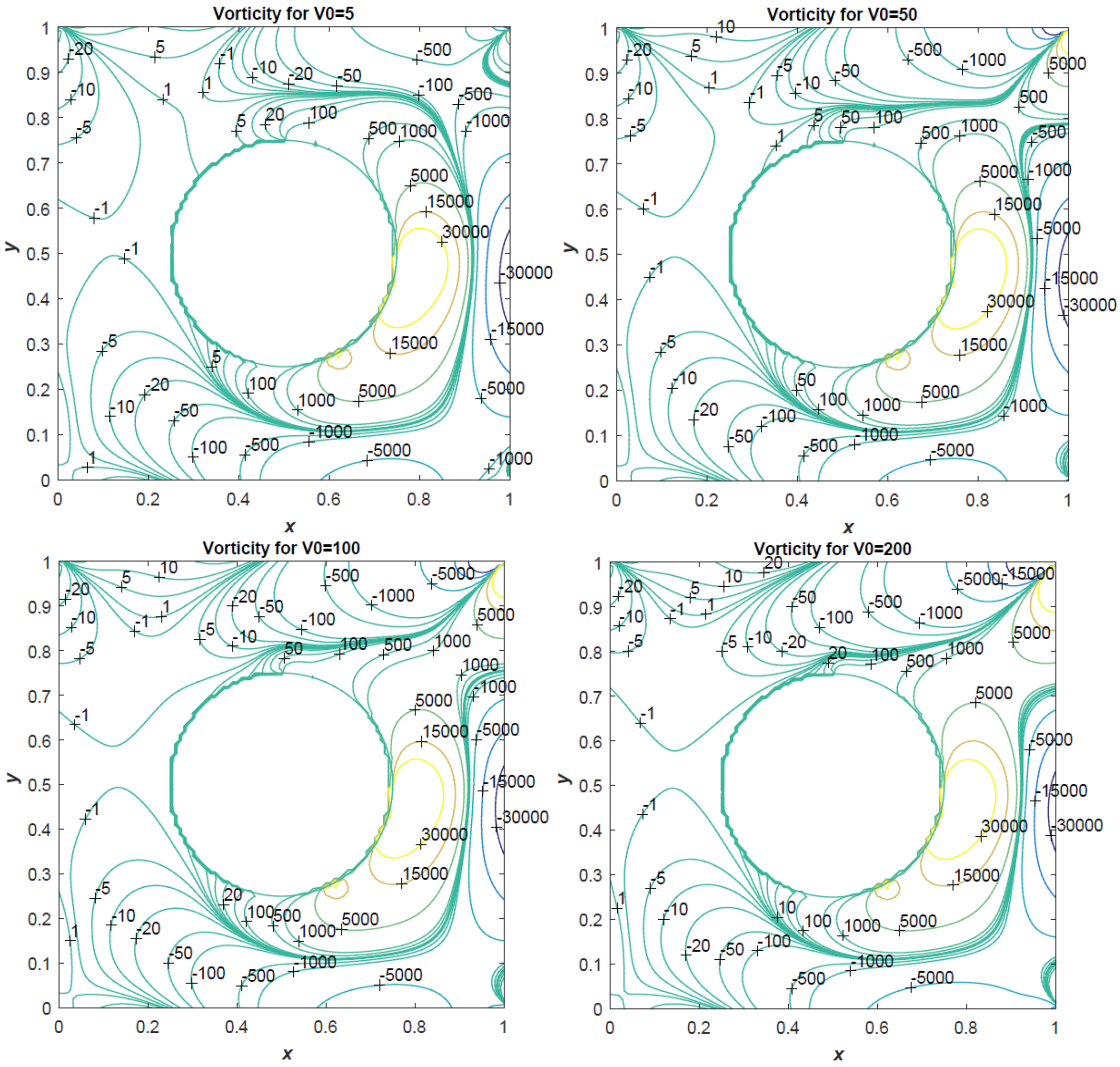

Fig. 7.6: Vorticity contours for different values of V_0.

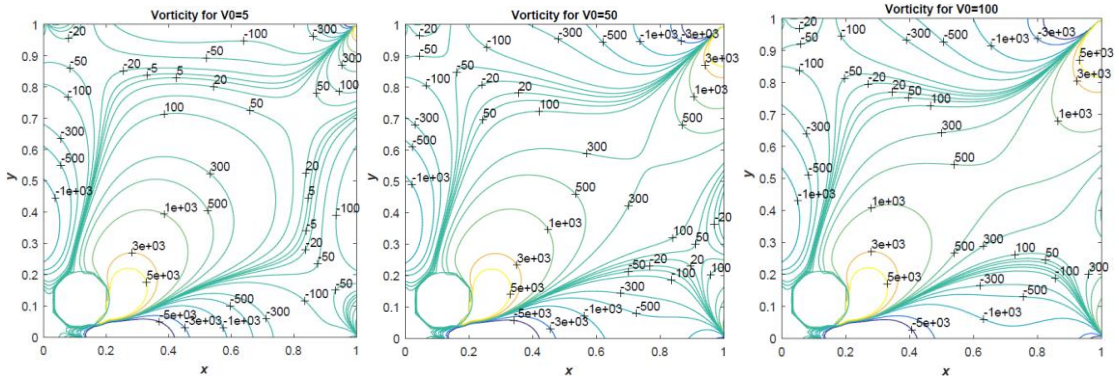

Fig. 7.7: Vorticity contours for different values of V_0(=5, 50, 100) when cylinder is at lower left corner of the cavity.

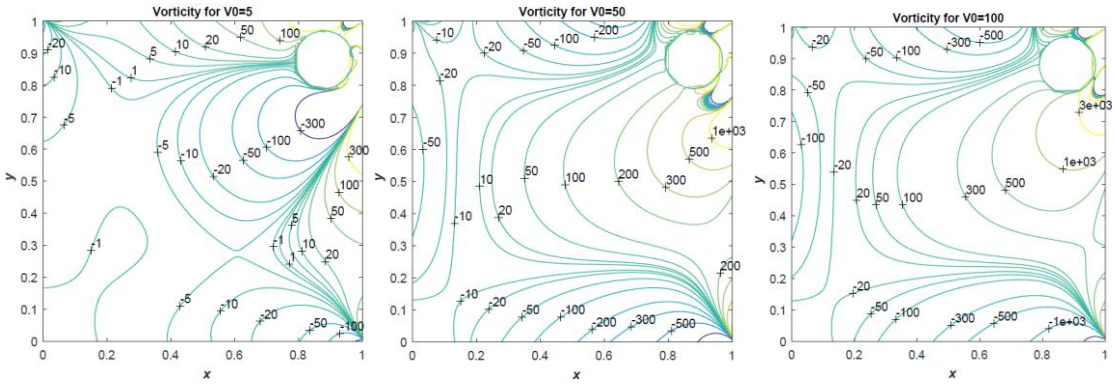

Fig. 7.8: Vorticity contours for different values of V_0(=5, 50, 100) when cylinder is at top right corner of the cavity.

7.4.3 Temperature field

The Fig. 7.9 to Fig. 7.12 display the nature of temperature contours. Fig. 7.9 shows the isothermal lines for different values of V_0 at Pe=0.02. We observe that the line θ=1 divides the entire region into two parts: the region in which θ is less than 1 and the region in which θ is more than 1. As V_0 increases, the region with θ<1 increases and spreads to the left wall. As Peclet number Pe increases, the temperature in the region θ>1 also increases.

Fig. 7.10 shows the isothermal lines for different values of V_0 at Pe=0.02 when a small cylinder is placed at the lower left corner. The region θ<1 is left to the cylinder in a small area for all suction values. Near the right side of the cylinder we find very high temperature.

Fig. 7.11 shows the isothermal lines for different values of Pe at V_0=10. We observe that Peclet number does not show much effect on the isothermal lines.

Fig. 7.12 shows the isothermal lines for different values of V_0 at Pe=0.02 when the cylinder is placed on the top right corner. We observe that θ<1 is spreading half of the cavity. All circulations in the temperature are in the region θ>1 and spreads only that region when suction value increases.

From Fig. 7.14 and Fig. 7.12, we observe that temperature lines are similar for the region θ<1. In this case when cylinder becomes smaller and smaller both profiles will be same.

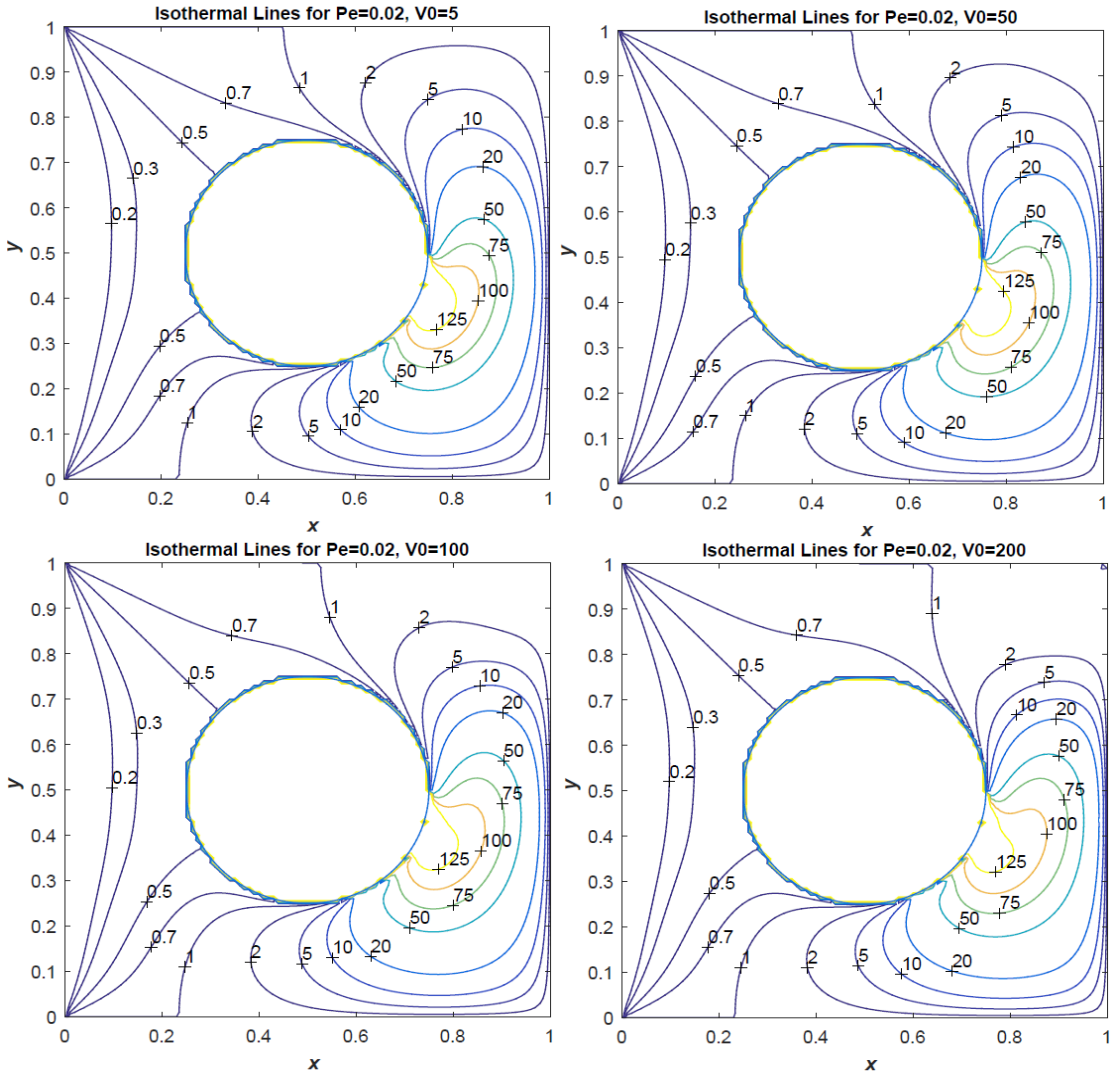

Fig. 7.9: Isothermal lines for different values of V_0 at Pe=0.02.

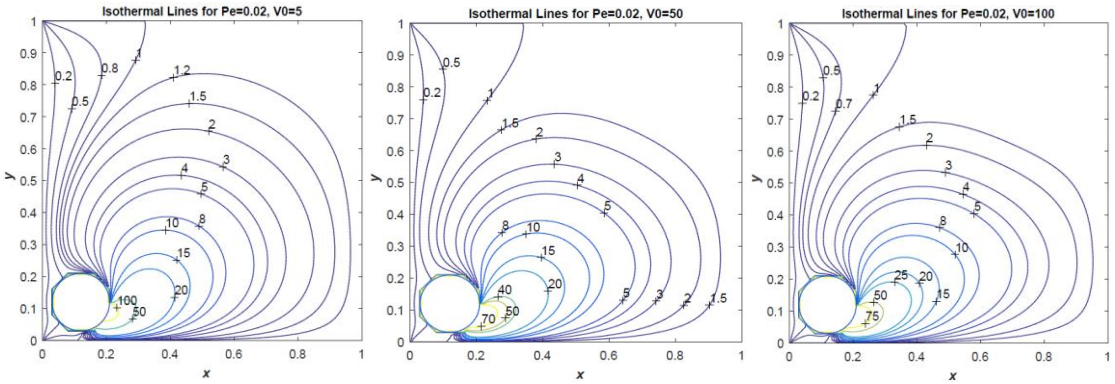

Fig. 7.10: Isothermal lines for different values of V_0(=5, 50, 100) at Pe=0.02 when cylinder is at lower left corner of the cavity.

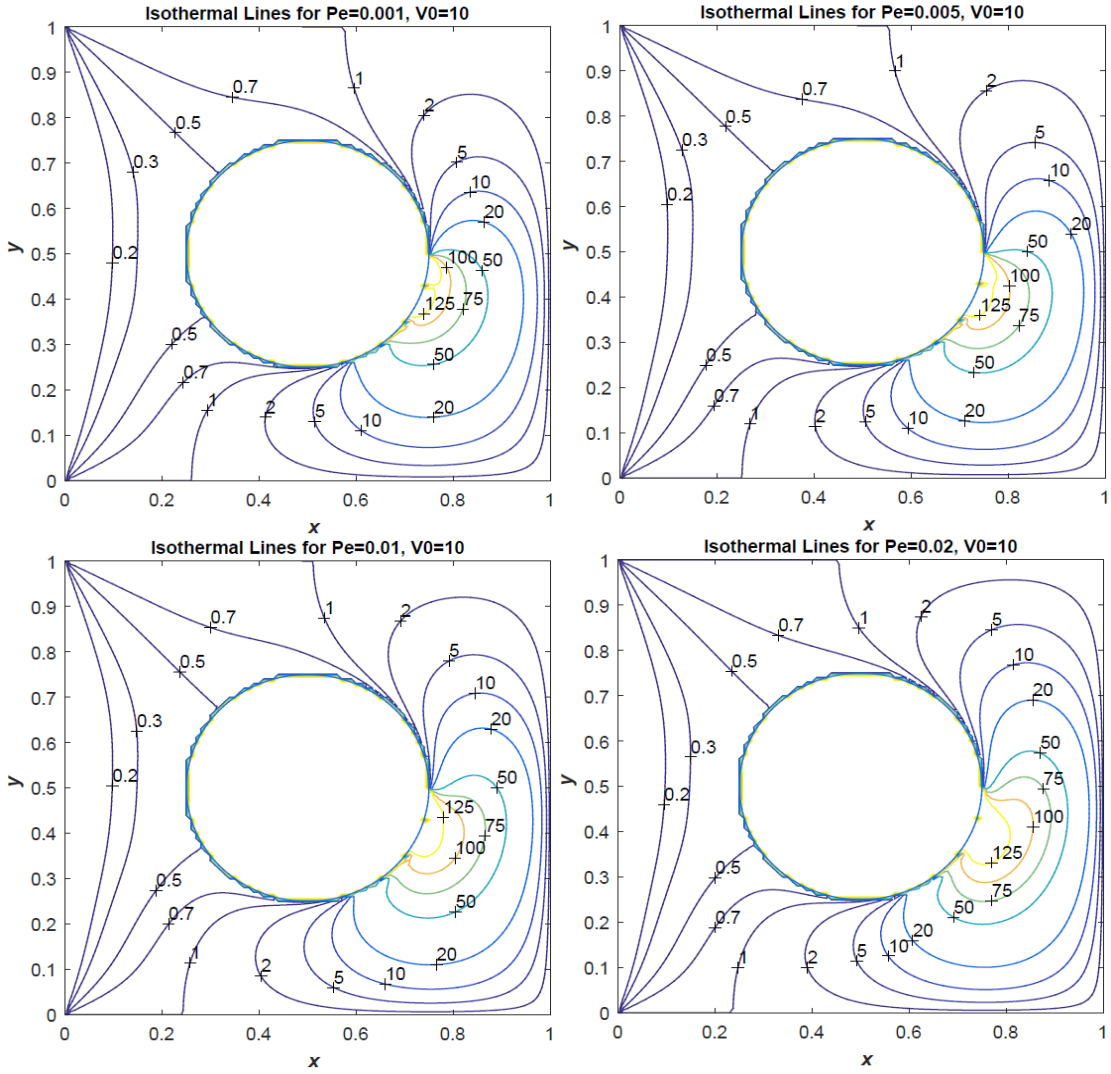

Fig. 7.11: Isothermal lines for different values of *Pe* at V_0=5.

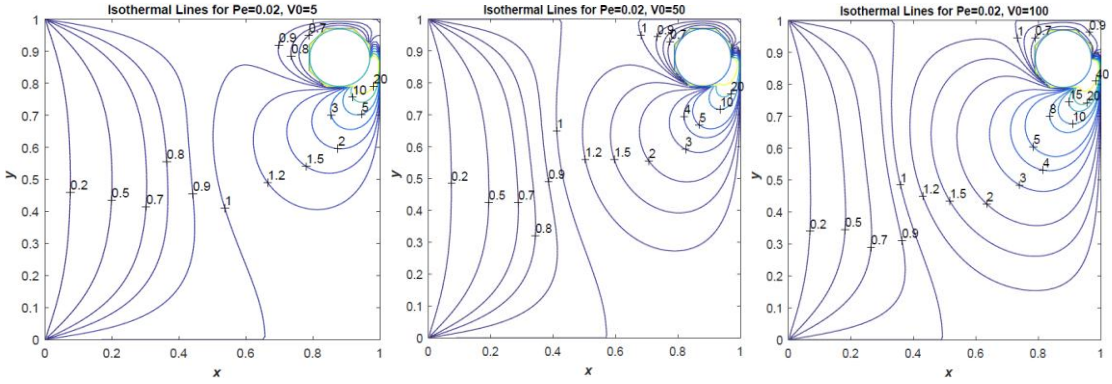

Fig. 7.12: Isothermal lines for different values of V_0(=5, 50, 100) at *Pe*=0.02 when cylinder is at top right corner of the cavity.

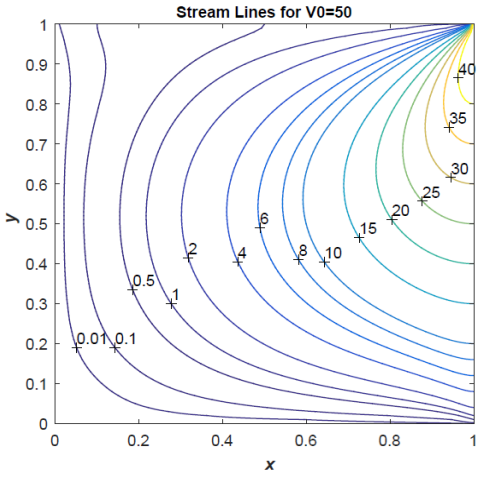

Fig. 7.13: Streamlines for V_0=50 when cylinder is absent in the cavity.

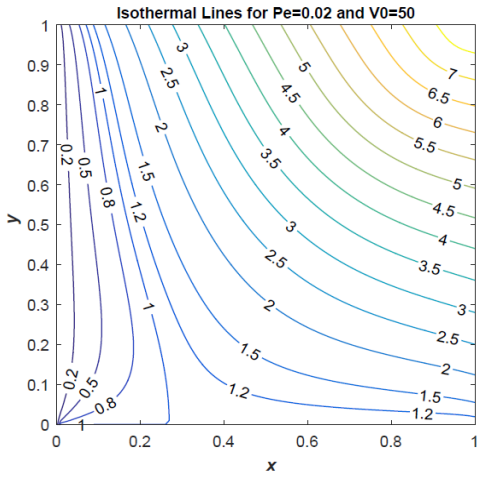

Fig. 7.14: Isothermal lines for Pe=0.05 and V_0=50 when cylinder is absent in the cavity.

7.5 Conclusions

From the above observations we conclude that

- As suction parameter V_0 increases, stream line pattern will not change much when the cylinder is in the middle of the cavity. But when it is at the top right corner suction effect is very much high.
- Entire temperature zone is divided into two regions $\theta<1$ and $\theta>1$.
- As suction parameter V_0 increases region $\theta<1$ spreads to suction wall when the cylinder is at the top right corner.

Chapter 8

Stokes Flow and Heat Transfer Past a Circular Cylinder in a Square Cavity with Suction/Injection on Opposite Side Walls

8.1 Introduction

In this chapter, flow past a cylinder in a cavity with suction/ injection at the opposite side walls is considered. The flow in a lid driven cavity was examined by many researchers using analytical and Numerical methods (Shankar (1993), Joseph and Sturges (1978), Ambethkar and Durgesh Kushawaha (2017), Kawaguti (1961)). The flow due to suction/injection applied at the walls was analysed by Varapaev and Yagodkin (1969). But the flow past a cylinder in a cavity was paid very less attention may be due to complexity of the problem. Hence, here we considered the flow past a cylinder in a cavity due to suction and injection on opposite walls.

8.2 Mathematical Formulation

The flow of viscous fluid past a cylinder in a square cavity of uniform cross section due to applied suction/injection at the opposite side walls is considered. The physical representation of the problem is given Fig. 8.1. The Cartesian coordinate system with origin at the bottom left corner and X and Y axes along the bottom and left walls is taken. The cavity is of length a_0 along X direction, height b_0 along Y direction and a cylinder with radius r_0 is kept in the middle of the cavity. Injection with velocity V_1 at the left wall X=0 and suction with velocity V_2 at the right wall X=a_0 are imposed. The flow is generated within the cavity due to the injection and suction applied at opposite side walls.

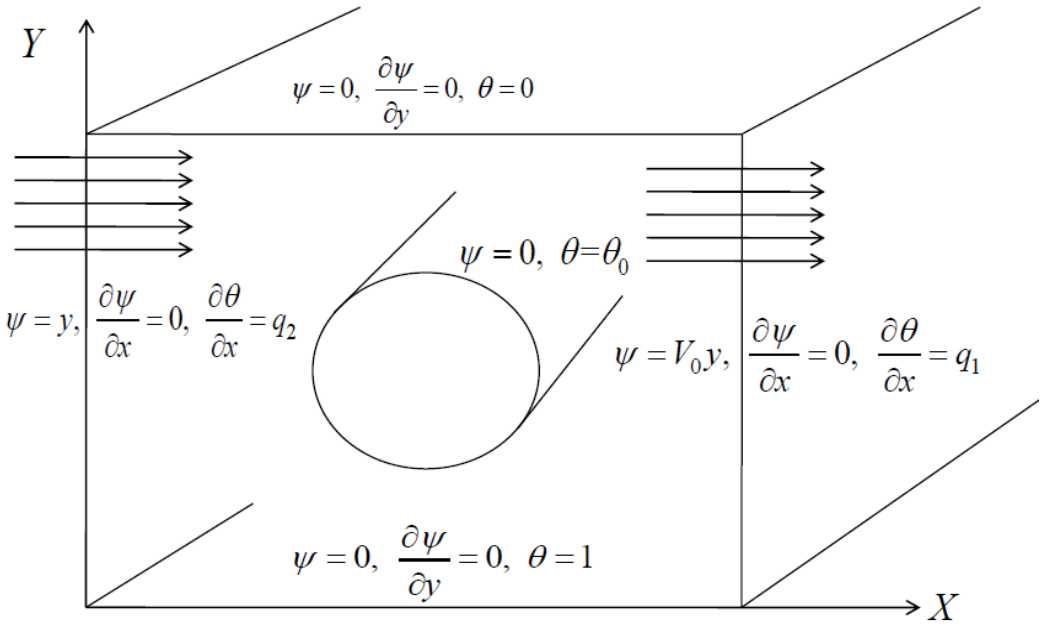

Fig. 8.1: Flow configuration in a square cavity with opposite wall suction.

Governing Equations

The equations of motion for the flow are given below:

$$\nabla.\mathbf{Q} = 0 \tag{8.1}$$

$$\rho \frac{d\mathbf{Q}}{dt} = -\nabla P + \mu \nabla^2 \mathbf{Q} \tag{8.2}$$

$$\rho c_p \frac{dT}{dt} = k \nabla^2 T \tag{8.3}$$

where **Q** is the velocity of fluid particle, P is pressure, T is the temperature, ρ is fluid density, μ is the coefficient of viscosity, k is the thermal conductivity of the fluid and c_p heat capacity at constant pressure.

The flow is two dimensional and hence **Q**= (U, V).

Boundary conditions for the problem

Velocity of fluid particles satisfies no slip condition on the walls with no suction or injection and no slip condition and impermeability condition on the cylinder. Again permeability conditions i.e., suction on the right wall and injection on the left wall are imposed. The temperature field is subjected to constant temperature on the impermeable walls Y=0, Y=b_0 and on the cylinder and condition of constant heat flux at the permeable walls X=0 and X=a_0.

Due to no slip condition on the walls Y=0 and Y=b_0, the tangential velocities are zero.

i.e., on Y=0, U=0 $\Rightarrow \frac{\partial \psi}{\partial Y} = 0$ and on $Y=b_0$, U=0 $\Rightarrow \frac{\partial \psi}{\partial Y} = 0$.

Due to impermeability condition on the walls Y=0 and $Y=b_0$, the normal velocities are also zero.

i.e., on Y=0, V=0 $\Rightarrow \frac{\partial \psi}{\partial X} = 0$ and on $Y=b_0$, V=0 $\Rightarrow \frac{\partial \psi}{\partial X} = 0$.

Due to no slip condition on the walls X=0 and $X=a_0$, the tangential velocities are zero.

i.e., on X=0, V=0 $\Rightarrow \frac{\partial \psi}{\partial X} = 0$ and on $X=a_0$, V=0 $\Rightarrow \frac{\partial \psi}{\partial X} = 0$.

On permeable walls, the suction velocity on $X=a_0$ is V_2 and the injection velocity on X=0 is V_1.

i.e., on $X=a_0$, $U=V_2$ $\Rightarrow \frac{\partial \psi}{\partial Y} = V_2$ and on X=0, $U=V_1$ $\Rightarrow \frac{\partial \psi}{\partial Y} = V_1$.

The walls Y=0 and $Y=b_0$ are maintained at constant temperatures. i.e., $T=T_1$ on $Y=b_0$ and $T=T_2$ on Y=0.

On the walls X=0 and $X=a_0$ constant heat fluxes are imparted.

i.e., $\frac{\partial T}{\partial X} = Q_1$ on $X = a_0$ and $\frac{\partial T}{\partial X} = Q_2$ on $X = 0$.

Non-dimensionalization

We introduce the following non-dimensional scheme and non-dimensional parameters like Pe= Peclet number, y_0=geometric parameter, V_0=suction parameter as below.

$$X = a_0 x,\ Y = a_0 y,\ U = V_1 u,\ V = V_1 v,\ P = \rho V_1^2 p,\ T - T_1 = \theta(T_2 - T_1) \qquad (8.4)$$

$$Pe = \frac{\rho C_p V_1 a_0}{k},\ y_0 = \frac{b_0}{a_0},\ V_0 = \frac{V_2}{V_1} \qquad (8.5)$$

For the flow the Reynolds number is so small that the convective terms in equation (7.2) are neglected. The flow is steady and hence independent of time t.

8.3 Solution of the problem

8.3.1 Stream function

We introduce stream function ψ as below such that equation (8.1) is satisfied.

$$u = \frac{\partial \psi}{\partial y} \quad \text{and} \quad v = -\frac{\partial \psi}{\partial x} \qquad (8.6)$$

Taking curl to equation (8.2) and substituting (8.6), we get the equation for the non-dimensional stream function ψ as

$$\nabla^4 \psi = 0 \tag{8.7}$$

with boundary conditions:

$$\frac{\partial \psi}{\partial x} = 0 \text{ on } x = 0 \text{ and on } x = 1 \text{ and } \psi = 0 \text{ on } \Gamma$$

$$\frac{\partial \psi}{\partial y} = 1 \text{ on } x = 0 \text{ and } \frac{\partial \psi}{\partial y} = V_0 \text{ on } x = 1$$

$$\frac{\partial \psi}{\partial x} = 0 \text{ on } y = 0 \text{ and on } y = y_0$$

$$\frac{\partial \psi}{\partial y} = 0 \text{ on } y = 0 \text{ and on } y = y_0$$

These conditions, by integrating, are converted in to the conditions on ψ as follows:

$$\left.\begin{aligned} &\frac{\partial \psi}{\partial x} = 0 \text{ on } x = 0 \text{ and } x = 1 \\ &\psi = 0 \text{ on } y = 0 \text{ and } y = y_0 \\ &\psi = y \text{ on } x = 0 \\ &\psi = V_0 y \text{ on } x = 1 \\ &\frac{\partial \psi}{\partial y} = 0 \text{ on } y = 0 \text{ and } y = y_0 \\ &\psi = 0 \text{ on the cylinder } \Gamma \end{aligned}\right\} \tag{8.8}$$

We solve the equation (8.7) with conditions (8.8) by Finite Difference Method. The cavity is covered with a mesh of step size h with (M–1) intervals on X direction and (N–1) intervals on Y direction. For each grid point (i, j) within the cavity, the biharmonic equation (7.7) can be split into two coupled equations as given in Biringen and Chow (2011) as below:

$$\nabla^2 \psi = -\zeta \tag{8.9}$$

and $$\nabla^2 \zeta = 0 \tag{8.10}$$

For the boundary conditions containing derivatives, we used central difference scheme. The nodes numbering is as follows:

Along X direction	Along Y direction
x_1 node on the boundary $x = 0$.	y_1 node on the boundary $y = 0$.
x_2 , x_3, … , x_{M-1} inside the computational	y_2 , y_3, … , y_{N-1} inside the computational
x_M node on the boundary x=1	y_N node on the boundary y=y_0

Thus at $x = 0$ (i.e., i=1) we have, $\psi(0, y) = y$.

These conditions are taken as $\psi_{1,j} = (j-1)h$ for j=1,2,...,N (8.11)

at $x = 1$ (i.e., i=M) we have, $\psi(1, y) = V_0 y$.

These conditions are taken as $\psi_{M,j} = V_0(j-1)h$ for j=1,2,...,N (8.12)

Similarly at $y = 0$ we have, $\psi(x, 0) = 0$.

These conditions are taken as $\psi_{i,1} = 0$ for i=2,3,...,$M-1$ (8.13)

Finally at $y = y_0$ we have, $\psi(x, y_0) = 0$.

These conditions are taken as $\psi_{i,N} = 0$ for i=2,3,...,$M-1$ (8.14)

Now, we derive expressions for boundary values of ζ in terms of ψ , which are required for solving (8.10). We now assume for vorticity on x=0 (i.e., at (1, j)):

$$\zeta_{1,j} = -\left(\frac{\partial^2\psi}{\partial x^2} + \frac{\partial^2\psi}{\partial y^2}\right)_{1,j} = \alpha_1\psi_{2,j-1} + \alpha_2\psi_{2,j} + \alpha_3\psi_{2,j+1} + \alpha_4\psi_{3,j} + \alpha_5\left(\frac{\partial\psi}{\partial x}\right)_{1,j} \quad (8.15)$$

Substituting from the Taylor's series expansions,

$$\psi_{2,j\pm1} = \psi_{1,j} + h\left(\frac{\partial\psi}{\partial x}\right)_{1,j} \pm h\left(\frac{\partial\psi}{\partial y}\right)_{1,j} + \frac{h^2}{2}\left(\frac{\partial^2\psi}{\partial x^2}\right)_{1,j} + \frac{h^2}{2}\left(\frac{\partial^2\psi}{\partial y^2}\right)_{1,j} + O\left(h^3\right)$$

$$\psi_{2,j} = \psi_{1,j} + h\left(\frac{\partial\psi}{\partial x}\right)_{1,j} + \frac{h^2}{2}\left(\frac{\partial^2\psi}{\partial x^2}\right)_{1,j} + O\left(h^3\right)$$

$$\psi_{3,j} = \psi_{1,j} + 2h\left(\frac{\partial\psi}{\partial x}\right)_{1,j} + \frac{(2h)^2}{2}\left(\frac{\partial^2\psi}{\partial x^2}\right)_{1,j} + O\left(h^3\right)$$

and retaining only terms up to $O(h^2)$, equation (15) becomes

$$-\left(\frac{\partial^2\psi}{\partial x^2} + \frac{\partial^2\psi}{\partial y^2}\right)_{1,j} = (\alpha_1+\alpha_2+\alpha_3+\alpha_4)\psi_{1,j} + \left[(\alpha_1+\alpha_2+\alpha_3+2\alpha_4)h + \alpha_5\right]\left(\frac{\partial\psi}{\partial x}\right)_{1,j} + (\alpha_3-\alpha_1)h\left(\frac{\partial\psi}{\partial y}\right)_{1,j}$$
$$+\left[(\alpha_1+\alpha_2+\alpha_3+4\alpha_4)\frac{h^2}{2}\right]\left(\frac{\partial^2\psi}{\partial x^2}\right)_{1,j} + (\alpha_1+\alpha_3)\frac{h^2}{2}\left(\frac{\partial^2\psi}{\partial y^2}\right)_{1,j}$$

The constants α's are determined by equating the coefficients of like terms on the both sides of this equation. Substitution of these values in (8.15) gives

$$\zeta_{1,j} = \frac{1}{h^2}\left(-\psi_{2,j-1} + \frac{8}{3}\psi_{2,j} - \psi_{2,j+1} - \frac{2}{3}\psi_{3,j}\right) \quad \text{for } j = 2,3,....N \quad (8.16)$$

where $\left(\frac{\partial\psi}{\partial x}\right)_{1,j} = 0$ from the boundary condition (8.8).

Similarly, the expressions for vorticity at the remaining boundaries as:

on $x = 1$,

$$\zeta_{M,j} = \frac{1}{h^2}\left(-\psi_{M-1,j-1} + \frac{8}{3}\psi_{M-1,j} - \psi_{M-1,j+1} - \frac{2}{3}\psi_{M-2,j}\right) \quad \text{for } j = 2,3,....N \qquad (8.17)$$

on $y = 0$, $\zeta_{i,1} = \frac{1}{h^2}\left(-\psi_{i-1,2} + \frac{8}{3}\psi_{i,2} - \psi_{i+1,2} - \frac{2}{3}\psi_{i,3}\right)$ for $i = 2,3,....M$ (8.18)

on $y = y_0$,

$$\zeta_{i,N} = \frac{1}{h^2}\left(-\psi_{i-1,N-1} + \frac{8}{3}\psi_{i,N-1} - \psi_{i+1,N-1} - \frac{2}{3}\psi_{i,N-2}\right) \quad \text{for } i = 2,3,....M \qquad (8.19)$$

in which the derivative boundary conditions in (8.8) have been employed.

Along with these boundary conditions, we have ζ on the cylinder is given by Thom (1933).

$$\zeta_S = \frac{(\psi_G - \psi_S)}{D} \qquad (8.20)$$

where G is the point on the normal which cuts either vertical or horizontal grid line in the flow region, S is the point on the cylinder and D is the distance between the points G and S.

The equation (8.10) numerically will be solved using Liebmann's iterative formula:

$$\zeta_{i,j} = \frac{1}{4}\left(\zeta_{i-1,j} + \zeta_{i+1,j} + \zeta_{i,j-1} + \zeta_{i,j+1}\right) \qquad (8.21)$$

boundary points on the cylinder are defined as the intersections of the horizontal-vertical grid lines and the body surface. These points do not usually coincide with the grid points. Thus the formula (8.21) cannot be used at some grid points in the immediate neighbourhood of the cylinder.

Equation (8.21) is the Laplace equation (8.10) replaced by a finite difference approximation on the assumption that the point (i, j) is equally spaced from its other four neighbouring grid points. The difference equation (8.21) is generalized for an arbitrary situation as shown in Fig. 8.2, where the point (i, j) is at different distances a, b, c and d from four neighbouring points

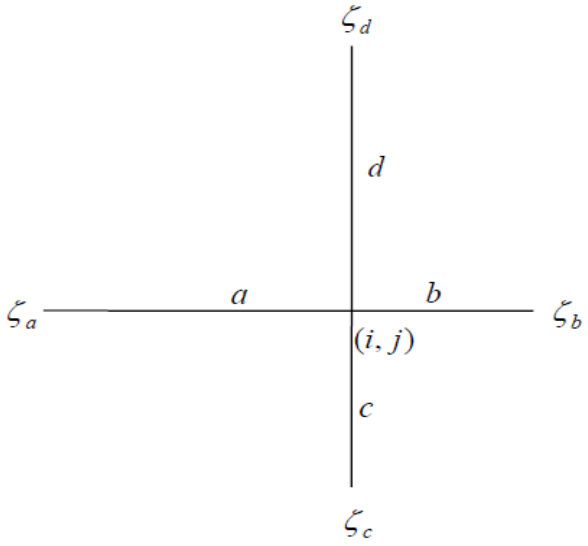

Fig. 8.2: Evaluation of $\zeta_{i,j}$.

We let the vorticity function evaluated at these neighbouring points be denoted by ζ_a, ζ_b, ζ_c, and ζ_d respectively, and then approximate the left hand side of (8.10) at (i, j) by the linear function:

$$\left(\frac{\partial^2\zeta}{\partial x^2}+\frac{\partial^2\zeta}{\partial y^2}\right)_{i,j} = \alpha_0\zeta_{i,j}+\alpha_a\zeta_a+\alpha_b\zeta_b+\alpha_c\zeta_c+\alpha_d\zeta_d \qquad (8.22)$$

where α's are coefficient to be determined. Expanding the four vorticity functions in Taylor's series about (i, j),

$$\zeta_{i-1,j}=\zeta_a=\zeta_{i,j}-a\left(\frac{\partial\zeta}{\partial x}\right)_{i,j}+\frac{a^2}{2}\left(\frac{\partial^2\zeta}{\partial x^2}\right)_{i,j}-O\left(a^3\right)$$

$$\zeta_{i,j+1}=\zeta_d=\zeta_{i,j}+d\left(\frac{\partial\zeta}{\partial y}\right)_{i,j}+\frac{d^2}{2}\left(\frac{\partial^2\zeta}{\partial y^2}\right)_{i,j}+O\left(d^3\right)$$

and so forth. Substitution of these equations in (8.22) after rearrangement and neglecting the cubic and higher order terms, we get

$$\left(\frac{\partial^2\zeta}{\partial x^2}+\frac{\partial^2\zeta}{\partial y^2}\right)_{i,j} = (\alpha_0+\alpha_a+\alpha_b+\alpha_c+\alpha_d)\zeta_{i,j}+(b\alpha_b-a\alpha_a)\left(\frac{\partial\zeta}{\partial x}\right)_{i,j}+(d\alpha_d-c\alpha_c)\left(\frac{\partial\zeta}{\partial y}\right)_{i,j}$$
$$+\frac{1}{2}(a^2\alpha_a+b^2\alpha_b)\left(\frac{\partial^2\zeta}{\partial x^2}\right)_{i,j}+\frac{1}{2}(c^2\alpha_c+d^2\alpha_d)\left(\frac{\partial^2\zeta}{\partial y^2}\right)_{i,j}$$

Equating corresponding coefficients on both the sides results in five simultaneous algebraic equations whose solution is

$$\alpha_0=-2\left(\frac{1}{ab}+\frac{1}{cd}\right),\ \alpha_a=\frac{2}{a(a+b)},\ \alpha_b=\frac{2}{b(a+b)},\ \alpha_c=\frac{2}{c(c+d)},\ \alpha_d=\frac{2}{d(c+d)}$$

vanishing of the right hand side of (8.22) gives the desired difference approximation of the Laplace equation:

$$\zeta_{i,j} = \left[\frac{\zeta_a}{a(a+b)} + \frac{\zeta_b}{b(a+b)} + \frac{\zeta_c}{c(c+d)} + \frac{\zeta_d}{d(c+d)} \right] / \left(\frac{1}{ab} + \frac{1}{cd} \right) \qquad (8.23)$$

for i=2,3, …, M–1 and j=2,3, …, N–1.

It can easily be shown that (8.23) is equivalent to (8.21) when $a=b=c=d=h$.

In the similar manner we solve equation (8.9) numerically using

$$\psi_{i,j} = \left[\frac{\psi_a}{a(a+b)} + \frac{\psi_b}{b(a+b)} + \frac{\psi_c}{c(c+d)} + \frac{\psi_d}{d(c+d)} + \frac{\zeta_{i,j}}{2} \right] / \left(\frac{1}{ab} + \frac{1}{cd} \right) \qquad (8.24)$$

for i=2,3, …, M–1 and j=2,3, …, N–1.

The vorticity boundary conditions derived (8.16)–(8.20) help us to solve (8.10) if ψ is known at some interior points. But, the evaluation of ψ from (8.9) depends on the distribution of vorticity within the bounded domain. Thus, ψ and ζ are inter-linked, and an iterative scheme will be build up to find the solution.

For initial guess, stationary state is first assumed so that ψ = 0 everywhere in the fluid region. Based on this initial assumption, the boundary values for ζ are computed from (8.16)–(8.20) which shows that vorticity is initially generated at the boundary. This concentrated vorticity at the boundary starts to diffuse into the cavity, resulting in a temporary vorticity distribution which is the solution of (8.10) that satisfies the present boundary conditions. This computed vorticity distribution causes a modification to the assumed ψ after solving (8.9) subject to the restriction that we have in (8.8) on the boundary. In this way we have completed the first iteration. To start the next iteration, based on the modified stream function, the boundary values of vorticity are recomputed. To obtain a new solution for ψ and ζ, the same procedure is repeated. At every grid point, the difference between the newly computed ζ and the previous value is recorded as the local error during each iteration and the sum of absolute errors at all grid points is called ERZETA. Similarly we find ERPSI, the corresponding sum of absolute errors of ψ. Iteration is terminated when both ERPSI and ERZETA are smaller than a small positive value EPSLON (=10^{-4}). Since the desired accuracy is reached, at this stage the solution is then considered to be satisfactory.

8.3.2 Temperature

The energy equation, given in (8.3), by using (8.4), (8.5) can be reduced to the non-dimensional form as below:

$$\nabla^2\theta = Pe\left(u\frac{\partial\theta}{\partial x} + v\frac{\partial\theta}{\partial y}\right) \tag{8.25}$$

Temperature is subjected to the boundary conditions that i) the sides y=0, y=y_0 and on cylinder are maintained at constant temperatures and ii) the other sides are supplied with constant heat or constant heat flux. The conditions are given explicitly as

$$\left.\begin{aligned} &\theta = 0 \text{ on } y = y_0,\ \theta = 1 \text{ on } y = 0,\ \theta = \theta_0 \text{ on cylinder} \\ &\frac{\partial\theta}{\partial x} = q_1 \text{ on } x = 1,\ \frac{\partial\theta}{\partial x} = q_2 \text{ on } x = 0 \end{aligned}\right\} \tag{8.26}$$

Let $u_{i,j} = \left(\frac{\partial\psi}{\partial y}\right)_{i,j} = \frac{\psi_{i,j+1} - \psi_{i,j-1}}{2h} = f_2$ and $v_{i,j} = -\left(\frac{\partial\psi}{\partial x}\right)_{i,j} = -\frac{\psi_{i+1,j} - \psi_{i-1,j}}{2h} = -f_1$

Proceeding as in the stream function and vorticity function equation (8.25) can be generalizes as:

$$\theta_{i,j} = \frac{1}{2\left(\frac{1}{ab} + \frac{1}{cd}\right)}\left[\frac{(2 + af_2Pe)\theta_a}{a(a+b)} + \frac{(2 - bf_2Pe)\theta_b}{b(a+b)} + \frac{(2 - cf_1Pe)\theta_c}{c(c+d)} + \frac{(2 + df_1Pe)\theta_d}{d(c+d)}\right] \tag{8.27}$$

for i=2,3, …, M and j=2,3, …, N

The boundary conditions in (8.26) are now expressed as:

$$\left.\begin{aligned} &\text{at } x\text{=}0,\ \frac{\partial\theta}{\partial x} = q_2 \quad \Rightarrow \theta_{1,j} = \frac{1}{3}\left[4\theta_{2,j} - \theta_{3,j} - 2hq_2\right] \text{ for } j\text{=}1,2,\ \ldots\ ,N \\ &\text{at } y\text{=}0,\ \theta = 1 \text{ which implies that } \theta_{i,1} = 1 \text{ for } i\text{=}2,3,...,M\text{–}1 \\ &\text{at } y\text{=}y_0,\ \theta = 0 \text{ which implies that } \theta_{i,N} = 0 \text{ for } i\text{=}2,3,...,M\text{–}1 \\ &\text{at } x\text{=}1,\ \frac{\partial\theta}{\partial x} = q_1 \quad \Rightarrow \theta_{M,j} = \frac{1}{3}\left[4\theta_{M-1,j} - \theta_{M-2,j} - 2hq_1\right] \text{ for } j\text{=}1,2,\ldots,N \end{aligned}\right\} \tag{8.28}$$

and on the cylinder $\theta_{i,j} = \theta_0 = 0.5$ where θ_0 is the reference temperature.

As in stream function and vorticity function in the equation (8.27) subjected to the boundary conditions (8.28) will be solved for the temperature in the cavity.

8.4 Results and Discussion

We have obtained the values of stream function and temperature for step length h=0.01. The accuracy near to 4 decimal places is obtained by taking 1000 iterations. Here the important steps involved in computation are to calculate 1). *a, b, c, d* values adjacent to the cylinder and 2). *D* the distance between *G* and *S* in equation (8.20). Here *S* is a point on the cylinder and *G* is a point on the grid line obtained by intersection of normal with the grid. These are explained in the appendix.

8.4.1 Streamlines

The stream lines generated due to injection at the left wall and suction at the right wall are shown in Fig. 8.3 to Fig. 8.5. The figures are drawn for different values of suction parameter V_0. We observe from Fig. 8.3 that when the cylinder is middle of the cavity, as suction parameter V_0 increases, the region of high stream values (ψ>1) forming loops increases at the right end of the cylinder and the stream lines with low values (ψ<1) are separated. Again as V_0 increases, a second circulation region is formed at the top left corner. For small values of V_0, the stream lines with high values (ψ>1) are nearly parallel to the right wall.

From Fig. 8.4, when a small cylinder is at the bottom left corner, for small suction V_0=5, stream lines having small values <1 are parallel to the top wall and having high values>1 are forming loops behind the cylinder and as V_0 increases, these loop lines open to the top side and bifurcate from the region of looping. The presence of cylinder effects entire region dominating suction. As suction parameter increases, effect of suction spreads near to the cylinder and the values of stream lines away from the cylinder also increase.

It is important to note that *even though cylinder is small placed at left corner effects the entire flow dominating the suction.*

Form Fig. 8.5 when a small cylinder is at the top right corner, we find that for any value of suction parameter, circulation loops are not found. It may be because there is no space behind the cylinder to form wakes. For small values of suction, the stream lines take small values and the flow is in four distinct regions. But when suction increases, all distinct regions merge to a single region. But for any value of V_0, we can

find flow regions with $\psi<1$ and $\psi>1$. As V_0 increases the region with $\psi>1$ occupies the most of the space.

It is important to note that *when the cylinder is at the top right corner, no circulation wakes are found*. The circulation wakes behind the cylinder are best observed when it is in the bottom left corner.

When there is no cylinder, the steam line pattern is shown in Fig. 8.13. For high suction when the small cylinder is on the top corner, the flow is similar to the flow without cylinder.

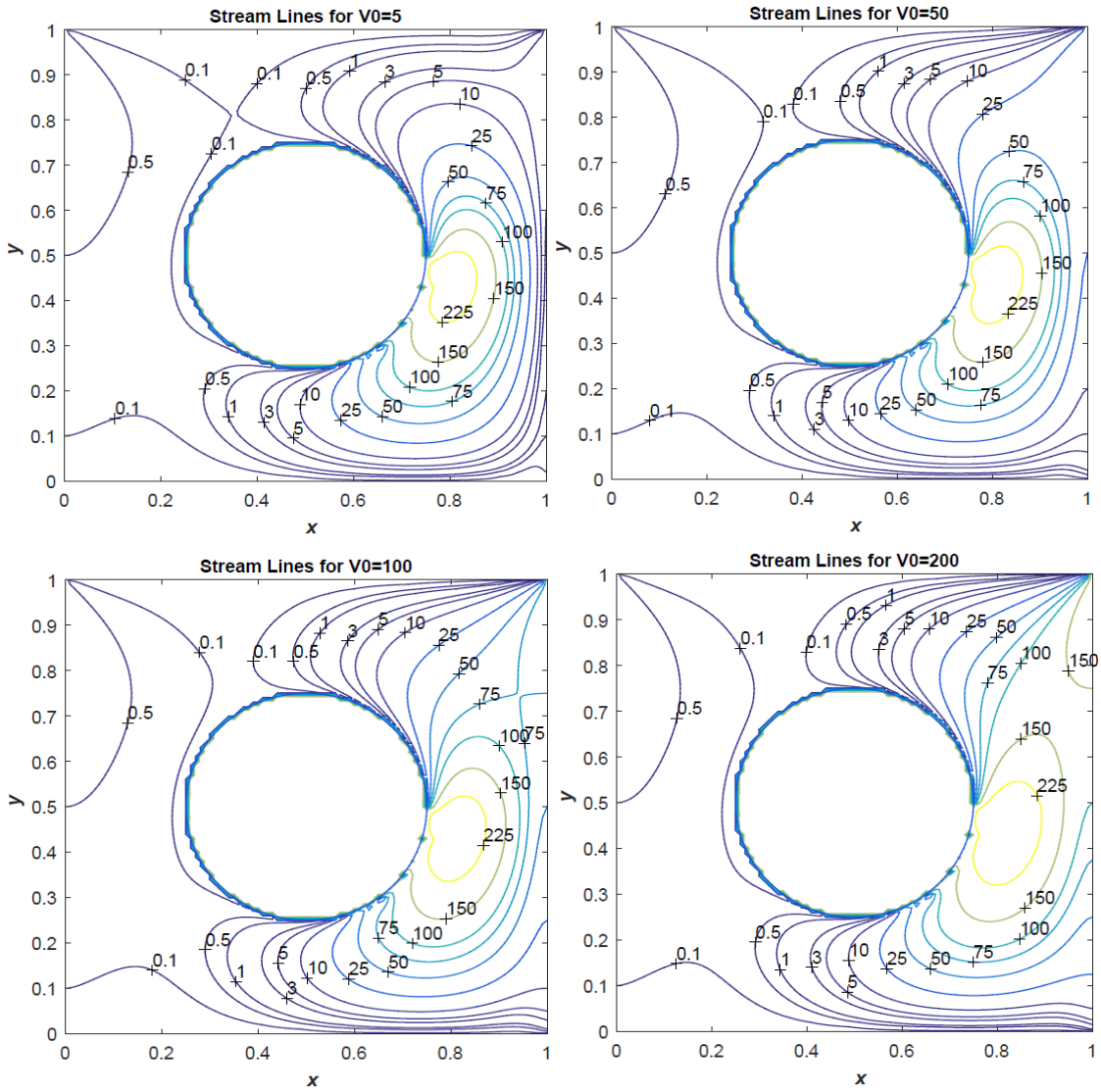

Fig. 8.3: Streamlines for different values of V_0.

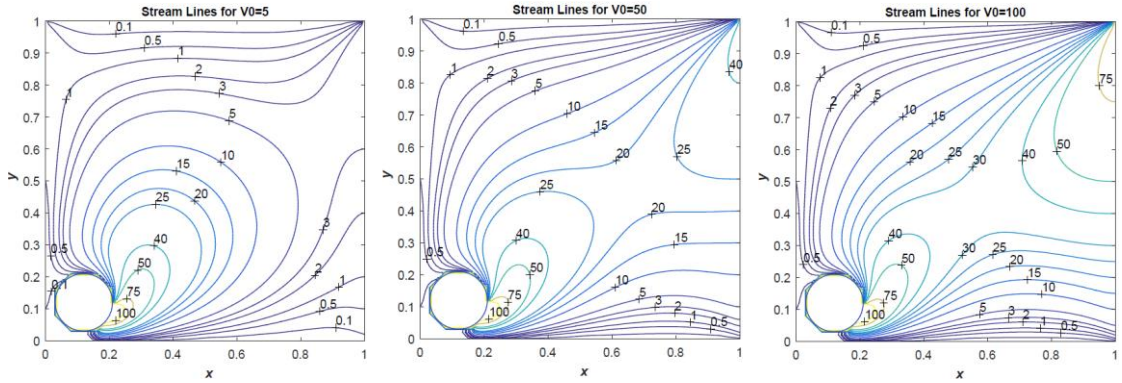

Fig. 8.4: Streamlines for different values of V_0(=5,50,100) when cylinder is at lower left corner of the cavity.

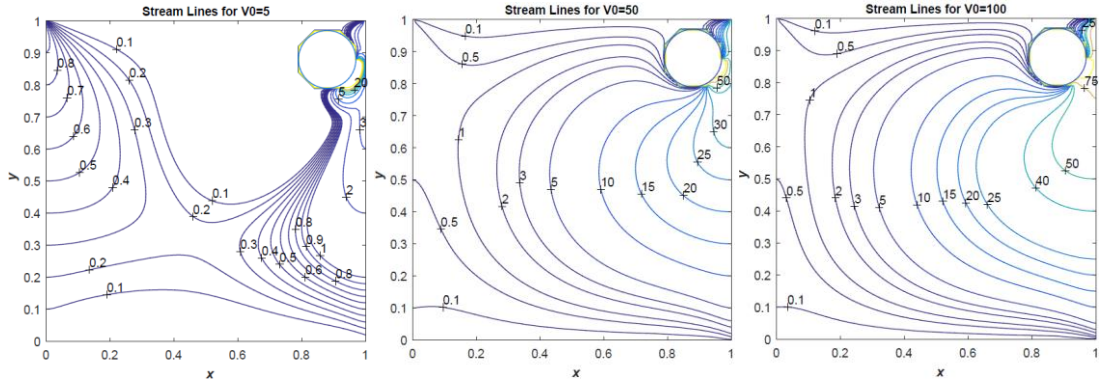

Fig. 5: Streamlines for different values of V_0(=5, 50, 100)when cylinder is at top right corner of the cavity.

8.4.2 Vorticity Contours

The vorticity contours generated due to injection at the left wall and suction at the right wall for different suction parameters V_0 are shown in Fig. 8.6 to Fig. 8.8. We observe that as V_0 increases, when the cylinder is middle of the cavity, the circulation of vortex lines on the right side of cylinder increases and opens to the right top corner. The values of vorticity are very high at the right wall and in the circulation region of vorticity. Outside of the circulation region, vorticity takes negative values except at top left region.

From Fig. 8.7, when a small cylinder is placed at the bottom left corner, for small values of suction, circulation region above the cylinder spreads to the top corner. As V_0 increases, High positive values of vorticity are found on the entire left wall which is opposite to the above case (when the cylinder is in the middle). As V_0 increases, circulation region confines to a small region near to the cylinder.

From Fig. 8.8, when a small cylinder is placed at the top right corner, for small suction parameter circulation region below the cylinder is small in area and this region spreads in the entire cavity when suction increases. Here we find high negative values of vorticity outside the circulation region at the top and bottom walls.

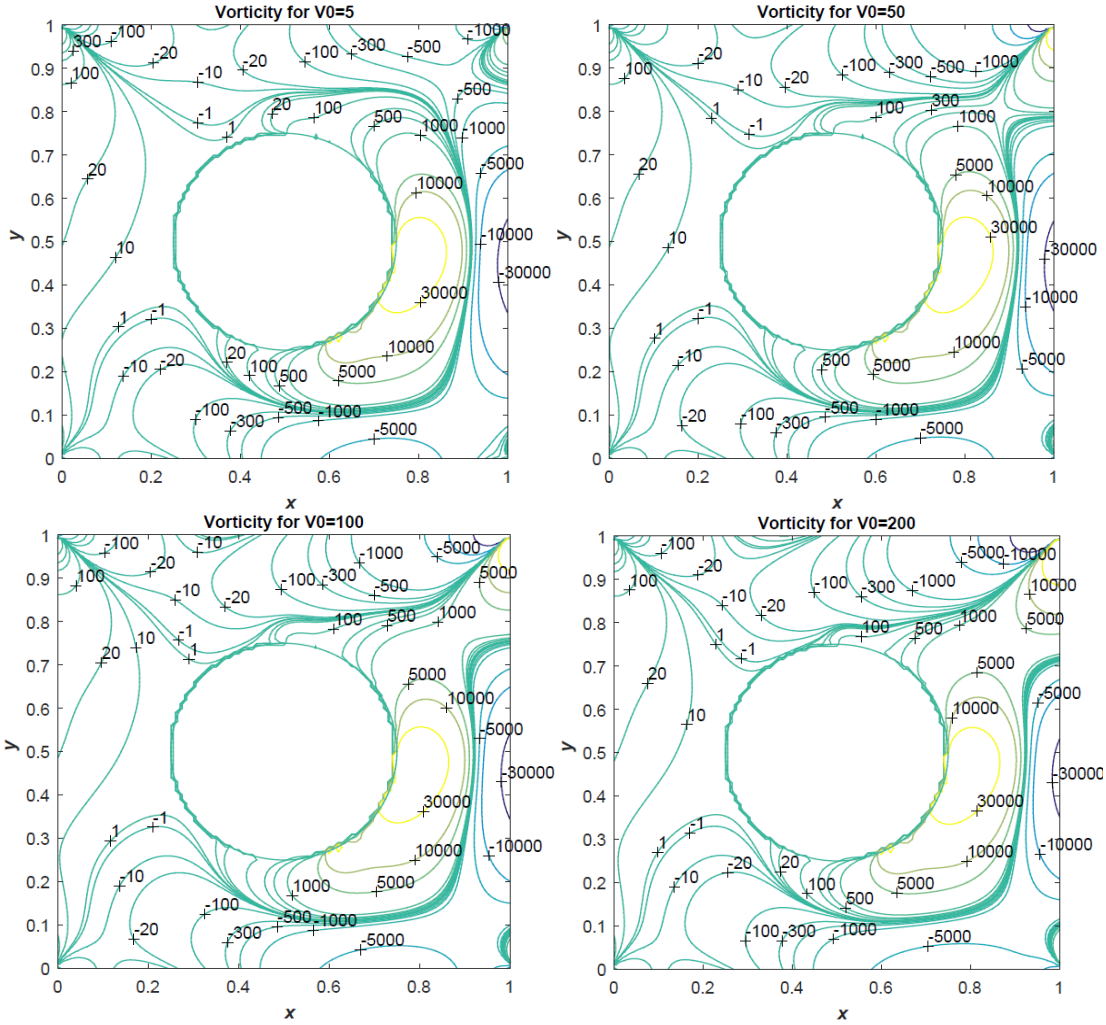

Fig. 8.6: Vorticity contours for different values of V_0.

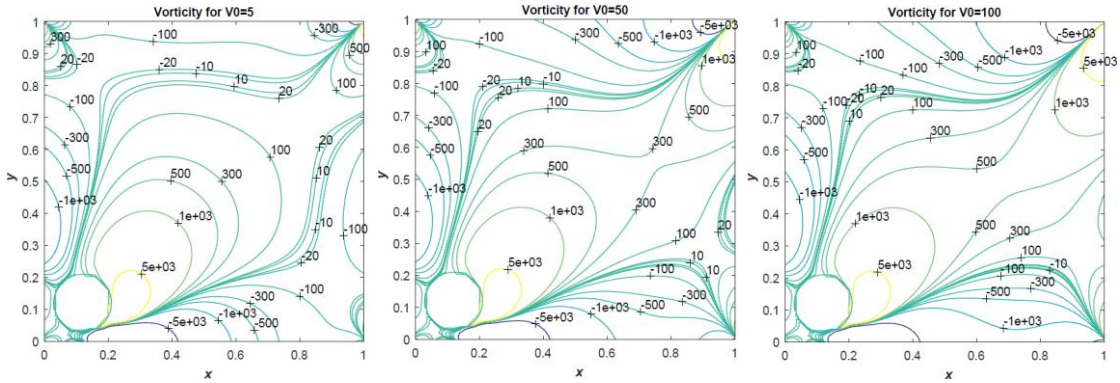

Fig. 8.7: Vorticity contours for different values of V_0(=5, 50, 100) when cylinder is at lower left corner of the cavity.

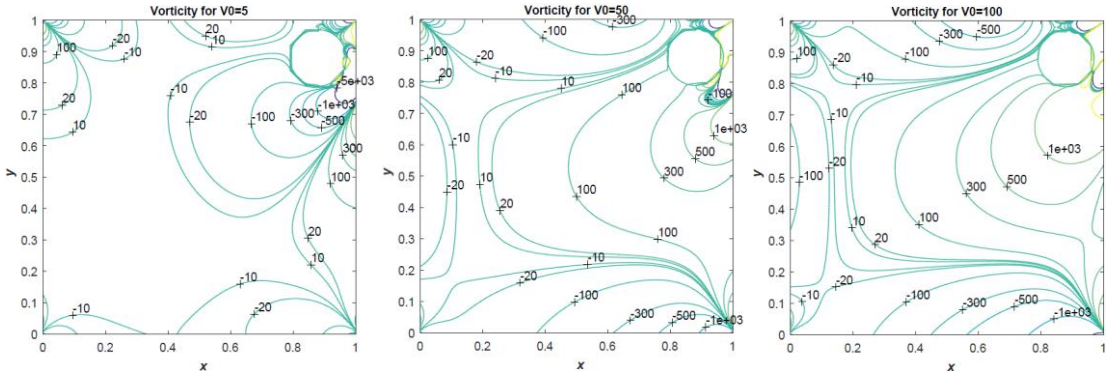

Fig. 8: Vorticity contours for different values of V_0(=5, 50, 100) when cylinder is at top right corner of the cavity.

8.4.3 Temperature field

The Fig. 8.9 to Fig. 8.12 display the nature of temperature contours. Fig. 8.9 shows the isothermal lines for different values of V_0 at Pe=0.02. We observe that the line θ=1 divides the entire region into two parts: the region in which θ is less than 1 and the region in which θ is more than 1. As V_0 increases, the region with θ<1 increases and spreads to the top wall. The region with θ>1 forms a circular loops. As V_0 increases, the temperature in the region θ>1 also increases slightly.

Fig. 8.10 shows the isothermal lines for different values of V_0 at Pe=0.02 when a small cylinder is placed at the lower left corner. The region θ<1 is at the top of the cylinder in a small area for all suction values. Near the right side of the cylinder we find very high temperature.

Fig. 8.11 shows the isothermal lines for different values of Pe at V_0=10. We observe that Peclet number does not show much effect on the isothermal lines.

Fig. 8.12 shows the isothermal lines for different values of V_0 at Pe=0.02 when the cylinder is placed on the top right corner. We observe that as V_0 increasing, the region θ<1 is decreasing. This is opposite to Fig. 8.10 where the area for θ<1 increases.

From Fig. 8.14 and Fig. 8.10, we observe that temperature lines are similar when cylinder becomes smaller and smaller. We observe that because of cylinder placed in the cavity the temperature increases drastically in all cases in comparison with without cylinder.

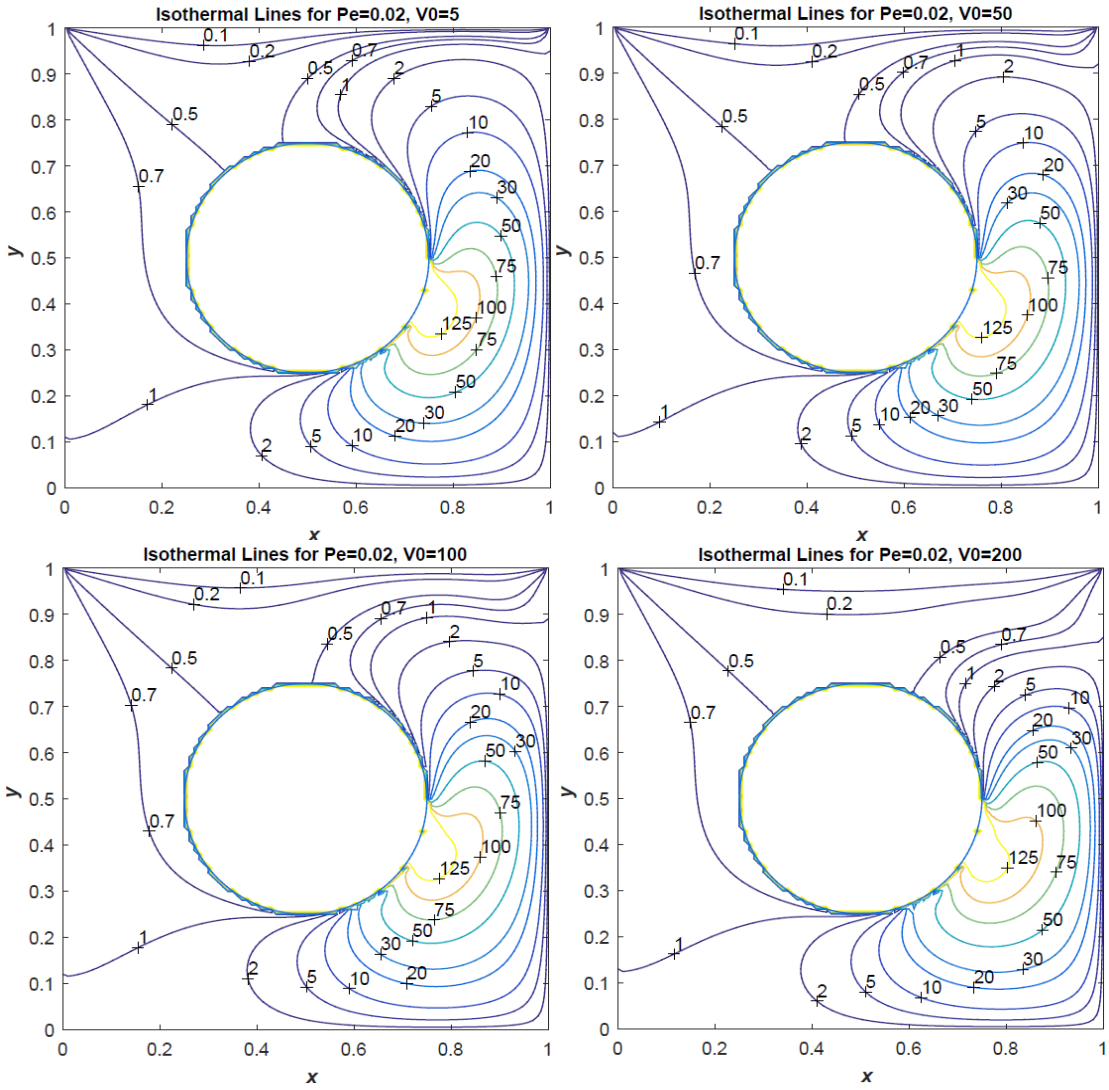

Fig. 8.9: Isothermal lines for different values of V_0 at Pe=0.02.

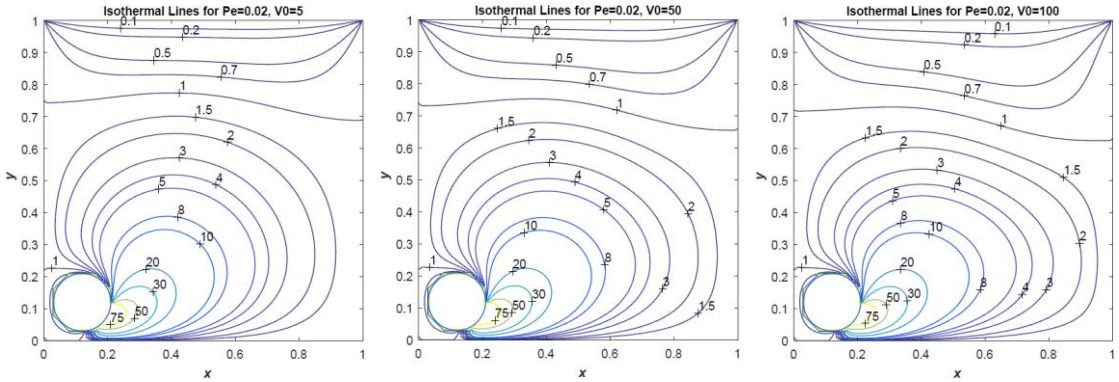

Fig. 8.10: Isothermal lines for different values of V_0(=5, 50, 100) at Pe=0.02 when cylinder is at lower left corner of the cavity.

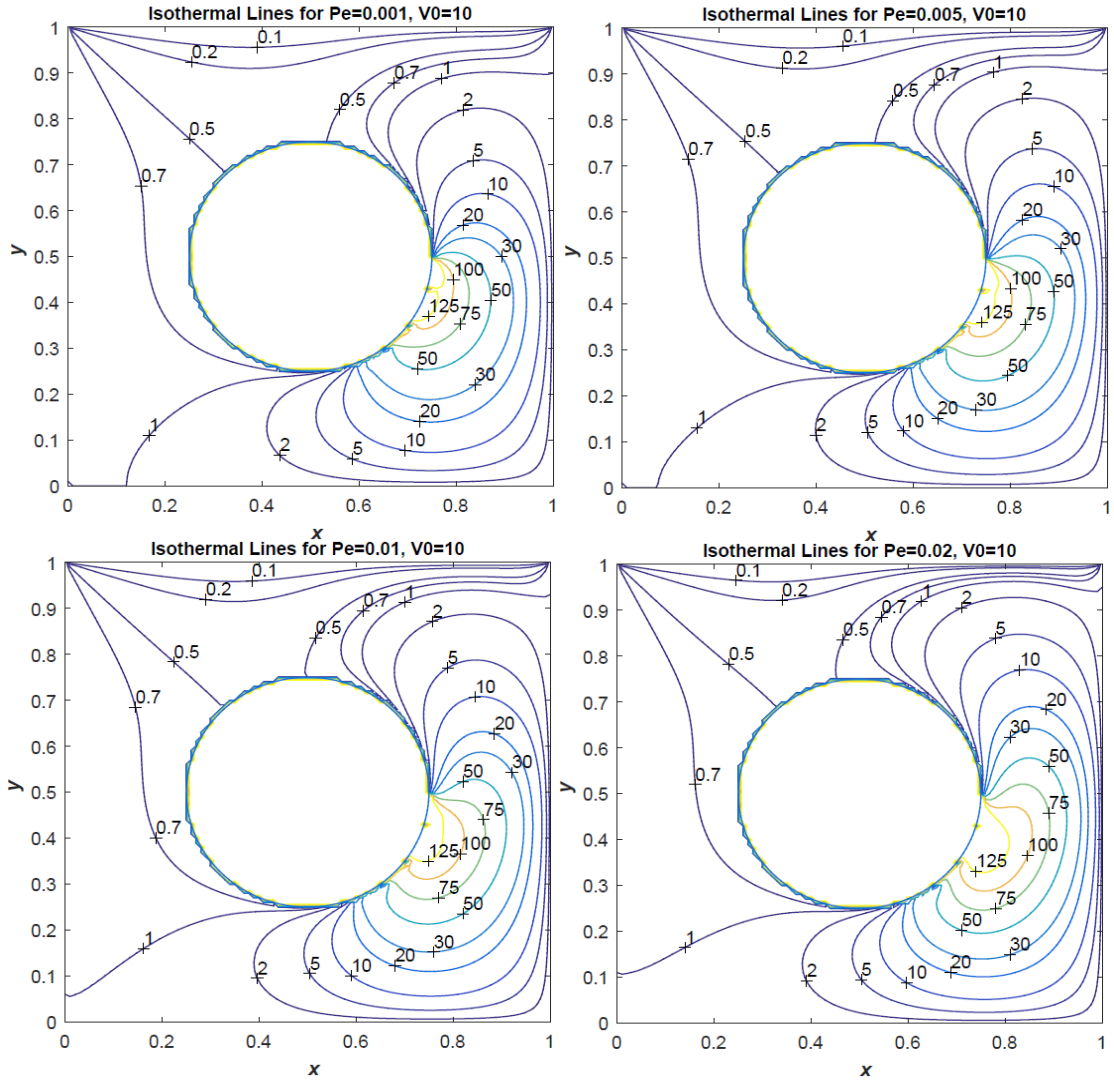

Fig. 8.11: Isothermal lines for different values of *Pe* at V_0=5.

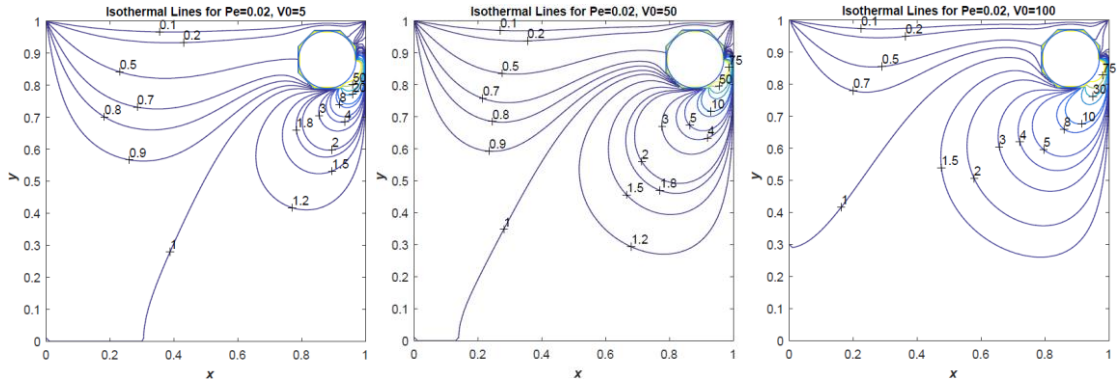

Fig. 8.12: Isothermal lines for different values of V_0(=5, 50, 100) at *Pe*=0.02 when cylinder is at top right corner of the cavity.

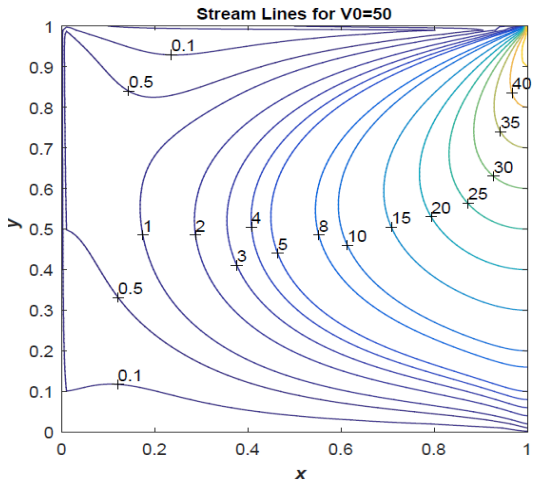

Fig. 8.13: Streamlines for V_0=50 when cylinder is absent in the cavity.

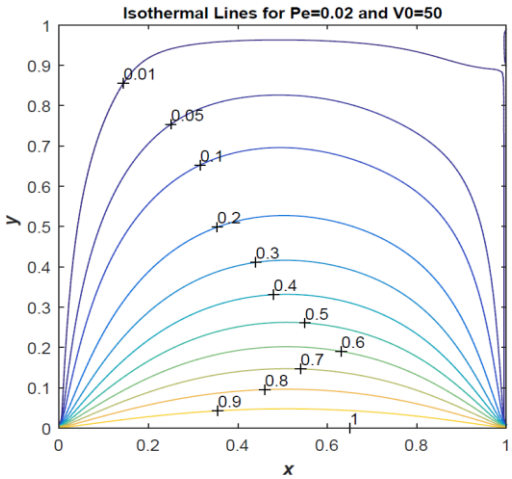

Fig. 8.14: Isothermal lines for Pe=0.05 and V_0=50 when cylinder is absent in the cavity.

8.5 Conclusions

From the above observations we conclude that

- As suction parameter V_0 increases, stream line pattern will not change much when the cylinder is in the middle of the cavity. But when it is at the top right corner suction effect is very much high.
- Entire temperature zone is divided into two regions θ<1 and θ>1.
- As suction parameter V_0 increases region θ<1 increases when cylinder is in left bottom corner and decreases when the cylinder is at top right corner.
- The temperature increases drastically when a cylinder is kept in cavity. i.e., to make quick heat transfer, we have to introduce some objects in the flow region of the cavity.

Part – V

CONCLUSIONS

Chapter 9

Summary and Conclusions

In this thesis, the flow of viscous fluids and couple stress fluids in a rectangular cavity is considered. The flow in a cavity is studied by many researchers by analytical methods and Numerical methods. In Analytical methods only streamlines are examined. In Numerical methods both flow and heat transfer are studied.

In the problems of present thesis, mainly the flow is generated due to the application of suction and injection at the walls of the cavity. We considered two cases i) suction/injection is applied on adjacent walls and ii) suction/ injection is applied on opposite walls. In both cases, heat transfer within the cavity is studied by considering entropy generation number and Bejan number.

Case: *Suction/injection is applied on adjacent walls for viscous fluid flow.*

For the flow of viscous fluids, the case of suction applied on opposite walls was studied by many researchers. Hence we considered this case. Here we considered the flow to be Stokesian and non-stokesian. When the flow is Stokesian, convective terms are neglected on the assumption that Reynolds number is very small. In this case stream lines are independent of Reynolds number and stream function satisfies Biharmonic equation.

We observe that when V_0 suction parameter is less than 1, stream lines reenter at the top right corner and when $V_0>1$, they re-enter at top left corner. The maximum value of stream lines in the cavity is the value of $V_0 y$ if $V_0>1$ and 1 if $V_0<1$.

Isothermal lines are divided into two regions $\theta>1$ and $\theta<1$. As suction parameter increases, θ values within the cavity also increases. By considering the Bejan number, it is observed that minimum fluid friction and maximum exergy is available at the bottom left corner. Flow of heat lines increases when Reynolds number increase.

When the flow is non-stokesian:

The above observations for stokesian flow for stream lines and isothermal lines are still valid. But now, for V_0<1 and *Re* is high, we can find a secondary flow at the top for a slit flow.

Case: *Couple stress fluid flow along the channel axis.*

In this case we observe that skin friction and volumetric flow rate decreases if magnetic parameter increases. But couple stress parameter has no effect on volumetric flow rate. The velocity profile takes more and more flat shape in the middle of the channel if magnetic parameter increases. This is in fact Hartmann effect.

When equal suction and injection is applied, the axial velocity is studied. As *Re* increases, the minimum value of contours of flow will be drifted towards left end where suction is imposed. But when couple stress parameter increases, the region of minimum contour value increases. After a critical value of Couple stress parameter, the volumetric flow rate is almost constant. Skin friction decreases numerically when magnetic parameter increases.

Case: *A circular cylinder is introduced in the flow*.

The vortex lines with value more than 1 form loops. The vortex lines outside this region have negative values. The position of the cylinder effects the stream line pattern very much. When the cylinder is near the bottom left corner, wakes behind the cylinder are predominant. When the cylinder is at top corner, wakes behind the cylinder are at minimum appearance. The temperature increases within the cavity when a cylinder is inserted in the cavity.

Future scope of the problems

In all the problems of couple-stress fluid flows and flow past cylinder in a cavity, the study of fluid friction by entropy analysis is interesting to examine. The couple-stress fluid flow in the cavity when suction/injection is imposed (both cases on opposite walls and adjacent walls) is also a challenging problem. The second law analysis can also be studied for couple stress fluid flow regions.

REFERENCES

1. Abel, S., Veena, P.H., Rajgopal, K. and Pravin, V.K. (2004), Non-Newtonian magneto-hydrodynamic flow over a stretching surface with heat and mass transfer, *International Journal of Non-Linear Mechanics*, 39, pp. 1067-1078.

2. Aboul-Hassan, A.L. and Attia, H.A. (2002), Hydromagnetic flow of a dusty fluid in a rectangular channel with Hall current and heat transfer, *Canadian Journal of Physics*, 80, pp. 579-589.

3. Ahmed Bahlaoui, Abdelghani Raji, Mohammed Hasnaoui and Mohamed Naimi (2014), Mixed Convection in A Nanofluid–Filled Vented Rectangular Cavity: Suction and Injection Heat Performance, *Computational Thermal Sciences*, 6(2), pp. 129–142.

4. Ahmed, M.E.S. and Attia, H.A. (1998), Magneto-hydrodynamic flow and heat transfer of a non-Newtonian fluid in an eccentric annulus, *Canadian Journal of Physics*, 76(5), pp. 391-401.

5. Ahmed, M.E.S. and Attia, H.A. (2000), MHD Flow and Heat Transfer in a Rectangular Duct with Temperature Dependent Viscosity and Hall Effect, *International Communications in Heat and Mass Transfer*, 27(8), pp. 1177-1187.

6. Aidun, C.K., Triantafillopoulos, N.G. and Benson, J.D. (1991), A numerical study of viscous flow in a cavity, *Phys. Fluids (A)*, 3, pp. 2081–2091.

7. Akhilesh K. Sahu, Chhabra R.P. and Eswaran, V. (2009), Two dimensional unsteady laminar flow of a power law fluid across a square cylinder, *Journal of Non–Newtonian Fluid Mechanics*, 160, pp. 157–167.

8. Alfarawi, S., Abdel Moneim, S.A. and Bodalal, A., (2017), Experimental investigations of heat transfer enhancement from rectangular duct roughened by hybrid ribs, *International Journal of Thermal Sciences*, 118, pp. 123–138.

9. Ali Ashrafizadeh and Ali Akbar Hosseinjani (2017), A phenomenological study on the convection heat transfer around two enclosed rotating cylinders via an immersed boundary method, *International Journal of Heat and Mass Transfer*, 107, pp. 667–685.

10. Ambethkar, V. and Kushawaha, D. (2017), Numerical simulations of fluid flow and heat transfer in a four-sided lid-driven rectangular domain, *International Journal of Heat and Technology*, 35(2), pp. 273–278.

11. Attia, H.A. (2005), Magnetic Flow and Heat Transfer in a Rectangular Channel with Variable Viscosity, *The Arabian Journal for Science and Engineering*, 30(2A), pp. 1-12.

12. Attia, H.A. (2005), The Effect of Suction and Injection on Unsteady Flow of a Dusty Conducting Fluid in Rectangular Channel, *Journal of Mechanical Science and Technology (KSME Int. J.)*, 19(5), pp. 1148–1157.

13. Baranyi L. and Lewis R.I. (2006), Comparison of a grid-based CFD method and vortex dynamics predictions of low Reynolds number cylinder flows, *The Aeronautical Journal*, 110(1103), pp. 63–71, 2006.

14. Bejan, A. (1979), A study of entropy generation in fundamental convective heat transfer, *Journal of Heat Transfer*, 101, pp. 718–725.

15. Bejan, A. (2013), *Convection Heat Transfer*, 4th Edition, Wiley, New Jersey, Page No 21.

16. Berman, A.S. (1953), Laminar flow in channels with porous walls, *Journal of Applied Physics*, 24(9), pp. 1232–1235.

17. Berrone, S., Garbero, V. and Marro, M. (2011), Numerical simulation of low Reynolds number flows past rectangular cylinders based on adaptive finite element and finite volume methods, *Computers & Fluids*, 40, pp. 92–112.

18. Bhargava, R., Sharma, S., Takhar, H. S., Be´g, O. A. and Bhargava, P. (2007), Numerical solutions for micropolar transport phenomena over a non linear stretching sheet, *Nonlinear Analysis: Modelling and Control*, 12(1), pp. 45-63.

19. Biringen S. and Chow, C.Y. (2011), *An Introduction to Computational Fluid Mechanics by Example*, John Wiley & Sons, Hoboken, New Jersey.

20. Breuer, M., Bernsdorf, J., Zeiser, T. and Durst, F. (2000), Accurate computations of the laminar flow past a square cylinder based on two different methods: lattice-Boltzmann and finite-volume, *International Journal of Heat and Fluid Flow*, 21, pp. 186–196.

21. Burggraf, O.R., (1966), Analytical and numerical studies of the structure of steady separated flows, *Journal of Fluid Mechanics*, 24, pp. 113-151.

22. Canedo, E.L. and Denson, C.D. (1989), Flow in driven cavities with a free surface, *American Institute of Chemical Engineers Journal*, 35(1), pp.129–138.

23. Cesini, G., Paromcini M., Cortella G. and Manzan M. (1999), Natural convection from a horizontal cylinder in a rectangular cavity, *International Journal of Heat and Mass Transfer*, 42, pp. 1801–1811.

24. Chabani, O., Stéphane Abide, Lamrous, N. and Zeghmati, B. (2017) Numerical Study Of Non–Boussinesq Convection In A Ventilated Cavity, *Computational Thermal Sciences*, 9(2), pp. 135–149.

25. Chen Chen, Teng Jyh-Tong, Cheng Ching-Hung, Shiping Jin, Huang Suyi, Chao Liu, Lee Ming-Tsang, Pan Hsin-Hung and Greif Ralph, (2014), A study on fluid flow and heat transfer in rectangular microchannels with various longitudinal vortex generators, *International Journal of Heat and Mass Transfer*, 69, pp. 203–214.

26. Cheng, Y.C., Hwang, G.J. and Ng, M.L. (1994), Developing laminar flow and heat transfer in a rectangular duct with one–walled injection and suction, *International Journal of Heat and Mass Transfer*, 37(17), pp. 2601–2613.

27. Chorin, A.J. (1968), Numerical solution of the Navier-Stokes equations, *Mathematics of Computation*, 22(104), pp. 745–762.

28. Crank. J. (1975), *Mathematics of Diffusion theory*; Clarenden Press, Oxford University.

29. Davis, G. De Vahl (1983), Natural Convection Of Air In A Square Cavity A Bench Mark Numerical Solution, *International Journal for Numerical Methods in Fluids*, 3, pp. 249–264.

30. Davis, G. De Vahl and Jones, I.P. (1983), Natural Convection In A Square Cavity: A Comparison Exercise, *International Journal for Numerical Methods in Fluids*, 3, pp. 227–248.

31. Dawson, P.A. (2001), *An Introduction to magneto-hydrodynamics*, Cambridge Texts in Applied Mathematics, ISBN-10: 0-521-79487-0.

32. Devakar, M. and Iyengar, T.K.V. (2008), Stokes problems for an incompressible couple stress fluid. *Nonlinear Analysis: Modelling and Control*, 1(2), pp. 181-190.

33. Devakar, M. and Iyengar, T.K.V. (2010). Run up flow of a couple stress fluid between parallel plates, *Nonlinear Analysis: Modelling and Control*, 15(1), pp. 29-37.

34. Dinesh P. ., Nalinaksh N. and Sandeep, N. (2015), Double diffusive mixed convection in a couple stress fluids with variable fluid properties, *Advances in Physics Theories and Applications*, 14, pp. 30-42.

35. Djamel Eddine Ameziani, Guo, Y., Rachid Bennacer, Mohammed El Ganaoui and Bouzidi, M. (2010), Competition between Lid-Driven and Natural Convection in Square Cavities Investigated with a Lattice Boltzmann Method, *Computational Thermal Sciences*, 2(3), pp. 269–282.

36. Fakher Oueslati and Brahim Ben–Beya (2017), Numerical Prediction of 3d Thermosolutal Natural Convection and Entropy Generation Pheomena within a Tilted Parallelepipedic Cavity with Various Aspet Rations, *Computational Thermal Sciences*, 9(4), pp. 363–382.

37. Fox, R.W., McDonald, A.T. and Pritchard, P.J. (2004), *Introduction to Fluid Mechanics*, 6th edition, John Wisely and Sons, Inc, United States of America.

38. Guoping, Li and Joseph A.C. Humphrey (1995), Numerical modelling of confined flow past a cylinder of square cross-section at various orientations, *International Journal for Numerical Methods in Fluids*, 20, pp. 1215–1236.

39. Hartmann, J. (1937), Hg-Dynamics I. Theory of the Laminar Flow of an Electrically Conductive Liquid in a Homogeneous Magnetic Field, *Kgl. Danske Videnskabernes Selskab*, bd. 15, nr. 6, Mathematisk-fysiske Meddelelser, Copenhagen.

40. Hartmann, J. and Lazarus, F. (1937), Hg-Dynamics II. Experimental Investigations on the Flow of Mercury in a Homogeneous Magnetic Field, *Kgl. Danske Videnskabernes Selskab*, bd. 15, nr. 7, Mathematisk-fysiske Meddelelser, Copenhagen.

41. Hayat, T., Aziz, A., Muhammad, T. and Ahmad, B. (2015), Influence of magnetic field in three dimensional flow of couple stress nano-fluid over a nonlinearly stretching surface with convective condition. *Plos One*, 10(12), pp. 1-18.

42. Hellebrand, H. (1996), *Tape casting, In Processing of Ceramics*, Part 1 (Ed. R. J. Brook), VCH Publishers.

43. Henderson, R.D. (1995), Details of the drag curve near the onset of vortex shedding, *Physics of Fluids*, 7(9), pp. 2102–2104.

44. Henderson, R.D. (1997), Nonlinear dynamics and pattern formation in Turbulent wake transition, *Journal of Fluid Mechanics*, 352, pp. 65–112.

45. Higgins, B.G. (1982), Dynamics of coating, adhesion and wetting, *Status Report Project 3328*, The Institute of Paper Chemistry.

46. Hwang, G.J., Cheng, Y.C. and Ng, M.L. (1993), Developing laminar flow and heat transfer in a square duct with one–walled injection and suction, *International Journal of Heat and Mass Transfer*, 36(9), pp. 2429–2440.

47. Joseph, D.D. and Sturges, L. (1978), The convergence of biorthogonal series for biharmonic and Stokes flow edge problems: Part II, *SIAM Journal on Applied Mathematics*, 34, pp. 7–26.

48. Karimi, M., Theuri, D. and Kinyanjui (2014), Modelling Fluid Flow in an Open Rectangular Channel with Lateral Inflow Channel, *International Journal of Sciences: Basic and Applied Research*, 17(1), pp. 186–193.

49. Kaushik, A. (2019), Numerical Study of 2D Incompressible Flow in a Rectangular Domain using Chorin's Method at High Reynolds Number, *International Journal of Mathematical, Engineering and Management Sciences*, 4(1), pp. 157–169.

50. Kawaguti, M. (1961), Numerical solution of the Navier-Stokes equations for the flow in a two-dimensional cavity, *Journal of the Physical Society of Japan*, 16, pp. 2307-2315.

51. Khan, W.A. and Yovanovich, M.M. (2008), Analytical Modelling of Fluid Flow and Heat Transfer in Microchannel/Nano-channel Heat Sinks, *Journal Of Thermophysics and Heat Transfer*, 22(3), pp. 352-358.

52. Kim, B.S., Lee, D.S., Ha, M.Y. and Yoon, H.S. (2008), A numerical study of natural convection in a square enclosure with a circular cylinder at different vertical locations, *International Journal of Heat and Mass Transfer*, 51, pp. 1888–1906.

53. Kimura, S. and Bejan, A. (1983), The heat-line visualisation of convective heat transfer, *Journal of Heat Transfer*, 105, pp. 916 – 919.

54. Kumar, K., Singh, V. and Sharma, S. (2015), On the onset of convection in a dusty couple stress fluid with variable gravity through a porous medium in hydro-magnetics, *Journal of Applied Fluid Mechanics*, 8(1), pp. 55-63.

55. Kundu, B., Simlandi, S. and Das, P.K. (2011), Analytical techniques for analysis of fully developed laminar flow through rectangular channels, *Heat Mass Transfer*, 47, pp. 1289–1299.

56. Lahmar, M. and Bou-Sad, B. (2008), Couple stress effects on the dynamic behaviour of connecting rod bearings in both gasoline and diesel engines, *Tribology Transactions*, 51, pp. 44-56.

57. Langlois William E. and Deville Michel O. (2014), *Slow viscous flows*; Springer international publishing, second edition, ISBN 978-3-319-03834-6.

58. Laplace. P.S. (1787), *Mémoire sur la théorie de l'anneau de Saturne*; Hist. Acad. Sci. Paris.

59. Laplace. P.S. (1832), *Méchanique Céleste, 4 vols*, (Translated by N. Bowditch), Boston.

60. Lee, P.S., Garimella, S.V. and Liu, D. (2005), Investigation of Convective Heat Transfer in Rectangular Microchannels, *CTRC Research Publications Paper 7*, 48(9), pp. 1688-1704.

61. Lin Lu, Ming-ming Liu, Bin Teng, Zhen-dong Cui, Guo-qiang Tang, Ming Zhao and Liang Cheng (2014), Numerical investigation of fluid flow past circular cylinder with multiple control rods at low Reynolds number, *Journal of Fluids and Structures*, 48, pp. 235–259.

62. Lin, J. . and Hung, C. . (2007), Combined effects of non-Newtonian couple stresses and fluid inertia on the squeeze film characteristics between a long cylinder and an infinite plate, *Fluid Dynamics Research*, 39(8), pp. 616-631.

63. Mahdi, A., Abdulwaheed, F. and Ammar (2010), Laminar flow forced convection in rectangular cross-sectional duct, *KUFA Journal of Engineering*, 1, pp. 1–22.

64. Mallinson, G.D. and Davis, G. De Vahl (1977), Three-Dimensional Natural Convection In A Box :A Numerical Study, *Journal of Fluid Mechanics*, 83(1), pp.1–31.

65. Mikhail A Sheremet, Hakan F Oztop, Ioan Pop and Nidal Abu-Hamdeh (2016), Analysis of Entropy Generation in Natural Convection of Nano-fluid inside a Square Cavity Having Hot Solid Block: Tiwari and Das' Model, *Entropy*, 18(9), pp. 1-15.

66. Minguez, M., Brun, C., Pasquetti, R. & Serre, E. (2011), Experimental and high order LES analysis of the flow in near-wall region of a square cylinder, *International Journal of Heat and Fluid Flow*, 32, pp. 558–566.

67. Mirmanto, Kenning, D.B.R., Lewis, J.S. and Karayiannis, T.G. (2012), Pressure drop and heat transfer characteristics for single phase developing flow of water in rectangular microchannels, *Journal of Physics: Conference Series* 395.

68. Moffatt, H.K. (1964), Viscous and resistive eddies near a sharp corner, *Journal of Fluid Mechanics*, 18, pp. 1–18.

69. Moukalled, F. and Acharya, S. (1996), Natural Convection in the Annulus Between Concentric Horizontal Circular and Square Cylinders, *Journal of Thermophysics and Heat Transfer*, 10(3), pp. 524–531.

70. Naduvinamani, N.B. and Patil, S.B. (2009), Numerical solution of finite modified Reynolds equation for couple stress squeeze film lubrication of porous journal bearings, *Computers and Structures*, 87(21-22), pp. 1287-1295.

71. Nakayama, Y. and Boucher, R.F. (1999), *Introduction to fluid mechanics*, John Wiley and Sons Inc., New York. ISBN 0 340 67649 3.

72. Norberg C. (2003), Fluctuating lift on a circular cylinder: review and new measurements, *Journal of Fluids and Structures*, 17(1), pp. 57–96.

73. Ou Jenn–Wuu, Cheng, K.C. and Ran–Chau Lin (1976), Combined Free and Forced Laminar Convection in Inclined Rectangular Channels, *International Journal of Heat and Mass Transfer*, 19, pp. 277–283.

74. Oztop, H.F., Moghtada Mobedi, Eiyad Abu-Nada and Ioan Pop (2012), A heat line analysis of natural convection in a square inclined enclosure filled with a CuO nano-fluid under non-uniform wall heating condition, *International Journal of Heat and Mass Transfer*, 55, pp. 5076–5086.

75. Pan, F. and Acrivos, A. (1967), Steady flows in rectangular cavities. *Journal of Fluid Mechanics*, 28(4), pp. 643-655.

76. Pozrikidis C. (1998), *Numerical Computation in Science and Engineering*, Oxford University Press, Oxford.

77. Prasenjit Dey and Ajoy Kr. Das (2015), Numerical analysis of drag and lift reduction of square cylinder, *Engineering Science and Technology*: *an International Journal*, 18, pp. 758–768.

78. Projahn, U., Rieger, H. and Beer, H. (1981), Numerical Analysis of Laminar Natural Convection Between Concentric & Eccentric Cylinders, *Numerical Heat Transfer*, 4, pp. 131–146.

79. Rajput, R.K. (2004), *A textbook of fluid mechanics and hydraulic machines*, S. Chand and Company L.T.D., RAM NAGAR, New Delhi-110055, ISBN: 9789385401374.

80. Ramana Murthy, J.V. and Bahali, N. K. (2009), Steady flow of micropolar fluid through a circular pipe under a transverse magnetic field with constant suction/injection, *International Journal of Applied Mathematics and Mechanics*, 5(3), pp. 1-10.

81. Ramana Murthy, J.V., Sai, K.S. and Bahali, N. K. (2011), Steady flow of Micropolar Fluid in a Rectangular Channel Under Transverse Magnetic Field With Suction, *AIP Advances*, 1, 032123 1-10.

82. Ramesh, K. (2016), Influence of heat and mass transfer on peristaltic flow of a couple stress fluid through porous medium in the presence of inclined magnetic field in an inclined asymmetric channel, *Journal of Molecular Liquids*, 219, pp. 256-271.

83. Rani, H.P., Reddy, G.J. and Kim, C.N. (2011), Numerical analysis of couple stress fluid past an infinite vertical cylinder, *Engineering Applications of Computational Fluid Mechanics*, 5(2), pp. 159-169.

84. Rathish Kumar, B.V. and Krishna Murthy, S.V.S.S.N.V.G. (2013), Darcy Mixed Convection in a Porous Square Enclosure Under Suction/Injection Effects with Sinusoidally Varying Temperature on the Left Vertical Wall, *Computational Thermal Sciences*, 5(6), pp. 473–487.

85. Roache, P.J. (1972), *Computational Fluid Dynamics*, Hermosa Publishers, Albuquerque, New Mexico.

86. Rudraiah, N. and Chandrashekara, G. (2010), Effects of couple stress on the growth rate of Rayleigh-Taylor instability at the interface in a finite thickness couple stress fluid, *Journal of Applied Fluid Mechanics*, 3(1), pp. 83-89.

87. Sahar, A.M., Wissink, J., Mahmoud, M.M., Karayiannis, T.G. and Ashrul Ishak, M.S. (2017), Effect of hydraulic diameter and aspect ratio on single phase flow and heat transfer in a rectangular micro-channel, *Applied Thermal Engineering*, 115, pp. 793–814.

88. Sai, K.S. and Nageswara Rao, B. (2000), Magnetohydrodynamic flow in a rectangular duct with suction and injection, *Acta Mechanica*, 140.

89. Salam Hadi Hussain and Ahmed Kadhim Hussein (2010), Numerical investigation of natural convection phenomena in a uniformly heated circular cylinder immersed in square enclosure filled with air at different vertical locations, *International Communications in Heat and Mass Transfer*, 37, pp. 1115–1126.

90. Salvatici, E. and Salvetti, M.V. (2003), Large eddy simulations of the flow around a circular cylinder: Effects of grid resolution and sub-grid scale modelling, *Wind and Structures*, 6(6), pp. 1–18.

91. Sandip Sarkar, Suvankar Ganguly and Amaresh Dalal (2012), Analysis of Entropy Generation During Mixed Convective Heat Transfer of Nanofluids Past a Square Cylinder in Vertically Upward Flow, *Journal of Heat Transfer*, 134, pp. 122501 1–8.

92. Schmitt, J.D. and Kandlikar, S.G. (2005), Effects of Repeating Microstructures on Pressure Drop in Rectangular Mini-channels, *Proceedings of ICMM2005*, Toronto, Ontario, Canada, 2005.

93. Schnack, D.D. (2009), Lectures in magneto-hydrodynamics: With an appendix on extended MHD, *Lecture Notes in Physics*. 780 (Springer, Berlin Heidelberg) DOI 10.1007/ 978-3-642-00688-3.

94. Shankar, P.N. (1993), The eddy structure in Stokes flow in a cavity, *Journal of Fluid Mechanics*, 250, pp. 371–383.

95. Shankar, P.N. (1997), Three-dimensional eddy structure in a cylindrical container, *Journal of Fluid Mechanics*, 32, pp. 97–118.

96. Shankar, P.N. (1998), Three-dimensional Stokes flow in a cylindrical container, *AIP: Physics of Fluids*, 10(3), pp. 540–549.

97. Shankar, P.N. and Deshpande, M.D. (2000), Fluid Mechanics in the Driven Cavity container, *Annu. Rev. Fluid Mech.*, 32, pp. 93–136.

98. Shehawey, E.L.E.F. and Mekheimer, K.S. (1994), Couple-stresses in peristaltic transport of fluids, *J. Phys D: Appl Phys*, 27(6), pp. 1163-1170.

99. Sheremet, M.A., Pop, I. and Nazar, R. (2015), Natural convection in a square cavity filled with a porous medium saturated with a nano-fluid using the thermal non-equilibrium model with a Tiwari and Das nano-fluid model, *International Journal of Mechanical Sciences*, 100, pp. 312-321.

100. Shokouhmand. H. and Jomeh. S. (2007), Slip Flow Convection Heat Transfer in a Rectangular Microchannel with Exponential Wall Heat Flux, *Proceedings of the World Congress on Engineering*, Vol II.

101. Sivasankaran, S., Sivakumar, V. and Prakash, P. (2010), Numerical study on mixed convection in a lid-driven cavity with non-uniform heating on both sidewalls, *International Journal of Heat and Mass Transfer*, 53, pp.4304-4315.

102. Song, Y. and Sundmacher, K. (2010), Approximation of Laminar Flow Field in Rectangular Channels with Suction/Injection along One Wall, *Chemical Engineering Communications*, 197(4), pp. 551–571.

103. Srinivasacharya, D. and Kaladhar, K. (2012), Analytical solution of mixed convection flow of couple stress fluid between two circular cylinders with Hall and ion-slip effects, *Turkish Journal of Engineering and Environmental Sciences*, 36, pp. 226-235.

104. Srinivasacharya, D. and Kaladhar, K. (2012), Mixed convection flow of couple stress fluid in a non-darcy porous medium with Soret and Dufour effects. *Journal of Applied Science and Engineering*, 15(4), pp. 415-422.

105. Srinivasacharya, D. and Mekonnen Shiferaw (2008), MHD Flow of Micropolar Fluid in a Rectangular Duct with Hall and Ion Slip Effects. *Journal of the Brazilian Society of Mechanical Sciences & Engineering*, 4, pp. 313-318.

106. Srivastava, L.M. (1985), Flow of couple stress fluid through stenotic blood vessels, *Journal of Biomechanics*, 18(7), pp. 479-485.

107. Stokes, V.K. (1966), Couple stresses in fluids. *The Physics of Fluids*, 9, pp. 1709-1715.

108. Sunil, Sharma, R.C. and Chandel, R.S. (2002), On superposed couple-stress fluids in porous medium in hydro-magnetics, *Zeitschrift fur Naturforschung*, 57a, pp. 955-960.

109. Symon R. Keith (1971), *Mechanics* (Third ed.). Addison-Wesley. ISBN 0-201-07392-7.

110. Tani, I. (1962), Steady Flow of Conducting Fluids in Channels Under Transverse Magnetic Fields With Consideration of Hall Effect. *Journal of the Aerospace Sciences*, 29, pp.297-305.

111. Taylor, G. (1956), Fluid Flow in Regions bounded by Porous surfaces, *Proceedings of The Royal Society A*, 234(1199), pp. 456–475.

112. Tehmina Ambreen and Man-Hoe Kim (2018), Flow and heat transfer characteristics over a square cylinder with corner modifications, *International Journal of Heat and Mass Transfer*, 117, pp. 50–57.

113. Thom A. (1933), The flow past circular Cylinders at low speeds, *Proc. R. Soc. Lond. A*, 141, pp. 651–669.

114. Titus Petrila and Damian Trif (2005), *Basics of Fluid Mechanics and Introduction to Computational Fluid Dynamics*, Springer Science + Business Media, Boston, Page No. 314.

115. Van Male. P, de Croon, M.H.J.M, Tiggelaar, R.M., Van den Berg, A. and Schouten. J.C. (2004), Heat and mass transfer in a square microchannel with asymmetric heating, *International Journal of Heat and Mass Transfer*, 47, pp. 87–99.

116. Varapaev, V.N. and Yagodkin V.I. (1969), Flow stability in a channel with porous walls, *Fluid Dynamics*, 4(5), pp. 60–62.

117. Walicki, E. and Walicka, A. (1999), Inertial effect in the squeeze film of couple-stress fluids in biological bearings, *International Journal of Applied Mechanics and Engineering*, 4, pp. 363-373.

118. Wang, F., Zhang, J. and Wang, S. (2012), Investigation on flow and heat transfer characteristics in rectangular channel with drop-shaped pin fins, *Propulsion and Power Research*, 1(1), pp. 64–70.

119. Wang, L.Bi., Zhi–Min Lin, Ke–Wei Song, Xiang Wu and Kun Hong (2010), Splitting the Contributions of Velocity and Velocity Gradient to Transport of Heat Flux in Laminar Convection through a Square Duct with Uniform Wall Temperature, *Computational Thermal Sciences*, 2(5), pp. 439–454.

120. Warrier, G.R., Dhir, V.K. and Momoda, L.A. (2002), Heat transfer and pressure drop in narrow rectangular channels, *Experimental Thermal and Fluid Science*, 26, pp. 53–64.

121. Weiss, R.F. and Florsheim, B.H. (1965), Flow in a Cavity at Low Reynolds Number, *Physics of Fluids* (1958-1988), 8, pp. 1631–1635.

122. Weiwei Ren, Chang Shu & Wenming Yang (2013), An efficient immersed boundary method for thermal flow problems with heat flux boundary conditions, *International Journal of Heat and Mass Transfer*, 64, pp. 694–705.

123. Williamson C.H.K. (1989), Oblique and parallel modes of vortex shedding in the wake of a circular cylinder at low Reynolds numbers, *Journal of Fluid Mechanics*, 206, pp. 579–627.

124. Woods, L.C. (1975), *Thermodynamics of Fluid Systems*, Oxford University Press, Oxford.

125. Yang Hu, Decai Li, Shi Shu and Xiaodong Niu (2017), Natural convection in a Nano-fluid filled eccentric annulus with constant heat flux wall: A lattice Boltzmann study with immersed boundary method, *International Communications in Heat and Mass Transfer*, 86, pp. 262–273.

126. Zakaria, M., (2002), Hydro-magnetic fluctuating flow of a couple stress fluid through a porous medium, *The Korean Journal of Computational and Applied Mathematics Archive*, 10(1-2), pp. 175-191.

Appendix

Let the grid along x and y directions cut the circle at Q_1 and Q_2 respectively. The normals on the circle at Q_1 and Q_2 cut the grid at G_1 and G_2 along y and x directions. Refer the figure 15.

Let S be the circle. The interval [0, 1] along x direction is divided into M–1 intervals. The interval [0, y_0] along y direction is divided into N–1 intervals. The grid points along x, y directions are indicated by i and j. we take M and such that $h = \frac{1}{M-1} = \frac{y_0}{N-1}$ or $y_0 = \frac{N-1}{M-1}$. i=j=1 and i=M, j=N are on the walls of the cavity. Any point P has coordinates (x^*, y^*) and has the corresponding grid numbers (x, y) such that x^*=(x–1)h, y^*=(y–1)h. [we define grid number as (distance x)/(grid length h)]. We take centre of the circle C at the grid numbers $\left(\frac{M+1}{2},\ \frac{N+1}{2}\right)$. The corresponding coordinates for $C = \left(\frac{M-1}{2}h,\ \frac{N-1}{2}h\right)$. Let r be the radius of the circle and $r = r_0 h$. (r_0 = number of intervals or grid numbers contained in cylinder)

The equation of the circle S: $\left(x^* - \frac{M-1}{2}h\right)^2 + \left(y^* - \frac{N-1}{2}h\right)^2 = r^2$

$\Rightarrow \left(x - M_1\right)^2 + \left(y - N_1\right)^2 = r_0^2$ where $M_1 = \frac{M+1}{2}$, $N_1 = \frac{N+1}{2}$.

Let the distance $PG = \begin{cases} a_1 h, & \text{if } G \text{ is left to } P \\ b_1 h, & \text{if } G \text{ is right to } P \\ c_1 h, & \text{if } G \text{ is below } P \\ d_1 h, & \text{if } G \text{ is above } P \end{cases}$ and

$Q_1 = \begin{cases} \left(x_0^*,\ (j-1)h\right) & - \text{ coordinates} \\ \left(x_0, j\right) & - \text{ grid number} \end{cases}$

$Q_2 = \begin{cases} \left((i-1)h,\ y_0^*\right) & - \text{ coordinates} \\ \left(i, y_0\right) & - \text{ grid number} \end{cases}$

Let P_1(i, j+1), P_2(i, j–1), P_3(i+1, j) and P_4(i–1, j) be the grid points adjacent to P=(i,j) in the cavity. Grid numbers for the adjacent points of P are PP_4=a, PP_3=b, PP_2=c and PP_1=d

Calculating ζ on the cylinder when grid point (*i, j*) is adjacent to cylinder:

3rd Quarter of the circle: If $CP_3 < r_0$, then $x_0 = M_1 - \sqrt{r_0^2 - (j - N_1)^2}$

$PQ_1 = b = (x_0 - i) =$ grid numbers and hence $c_1 = \dfrac{b(N_1 - j)}{\sqrt{r_0^2 - (j - N_1)^2}}$

$\therefore \psi_{G_1} = c_1\psi_{i,j-1} + (1 - c_1)\psi_{i,j}$ by interpolating and $\zeta_{Q_1} = \dfrac{\psi_{G_1}}{h\sqrt{b^2 + c_1^2}}$

If $CP_1 < r_0$, then $y_0 = N_1 - \sqrt{r_0^2 - (i - M_1)^2}$.

$PQ_2 = d = (y_0 - j) =$ grid numbers and hence $a_1 = \dfrac{d(M_1 - i)}{\sqrt{r_0^2 - (i - M_1)^2}}$

$\psi_{G_2} = a_1\psi_{i-1,j} + (1 - a_1)\psi_{i,j}$ by interpolation and $\zeta_{Q_2} = \dfrac{\psi_{G_2}}{h\sqrt{d^2 + a_1^2}}$

Similar derivations are used when a grid point P is adjacent to the circle in 2nd, 1st and 4th quarters of the circle.

Calculating ζ on the cylinder when grid point (*i, j*) is on the cylinder ($CP = r_0$):

Let $\delta = \left|\dfrac{i - M_1}{j - N_1}\right|$

Where P=*S* is the grid point on the cylinder: If $\delta < 1$, normal at *S* cuts grid parallel to *x*–axis and If $\delta > 1$, normal at *S* cuts grid parallel to *y*–axis.

$D = GS = \begin{cases} h\sqrt{1 + \delta^2}, & \text{if } \delta < 1 \\ h\sqrt{1 + \dfrac{1}{\delta^2}}, & \text{if } \delta > 1 \end{cases}$ and $\zeta_S = \dfrac{\psi_G - \psi_S}{D} = \dfrac{\psi_G}{D}$, since $\psi_S = 0$ on the cylinder.

If P=S is on the 3rd Quarter of the circle:

if $\delta < 1$, $\psi_G = \delta\psi_{i-1,j-1} + (1 - \delta)\psi_{i,j-1}$ and $\zeta_S = \dfrac{\psi_G}{h\sqrt{1 + \delta^2}}$

if $\delta > 1$, $\psi_G = \frac{1}{\delta}\psi_{i-1,j-1} + (1-\frac{1}{\delta})\psi_{i-1,j}$ and $\zeta_S = \frac{\psi_G}{h\sqrt{1+\frac{1}{\delta^2}}}$

Similar calculations follow for 2nd , 1st and 4th quarters of the circle.

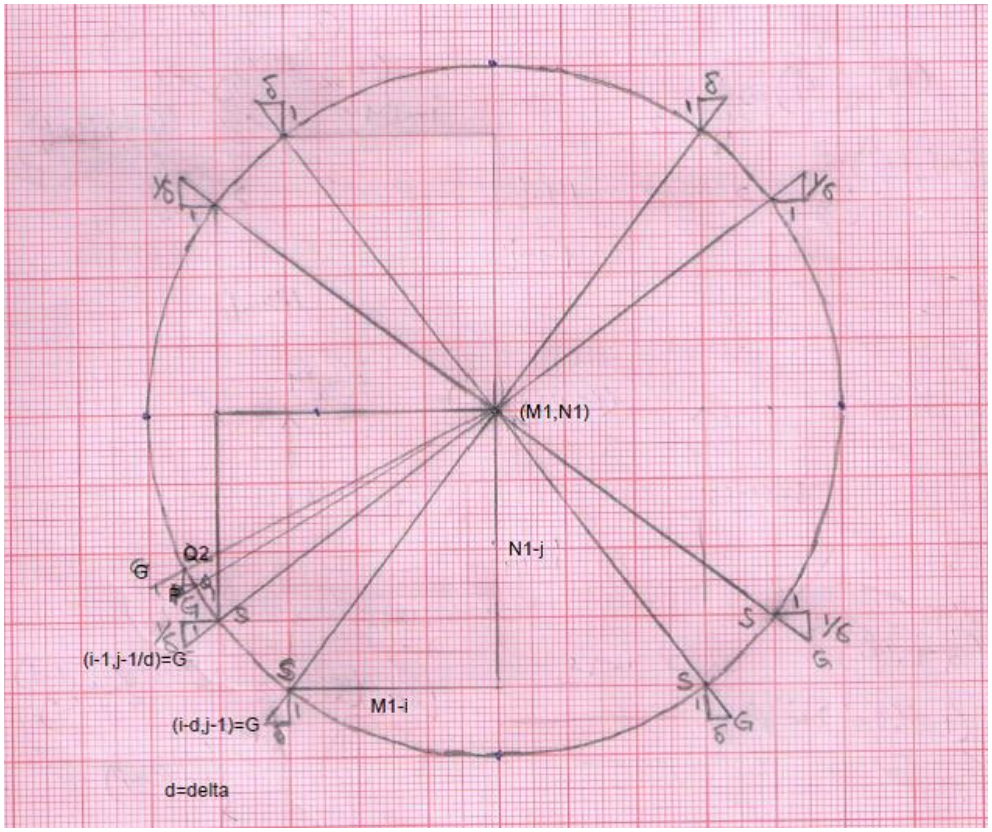

Point *P* adjacent to and on cylinder. Point *G* where normal on cylinder cuts the grid.

List of Published Papers

1. M. Pavankumar Reddy and J. V. Ramana Murthy, "**Heat Flow in a Rectangular Plate**", **Published in Lecture Notes in mechanical Engineering**, **NHTFF** Book, pp. 223-231, 2018.

2. M. Pavankumar Reddy and J. V. Ramana Murthy, "**Entropy Analysis for Heat Transfer In a Rectangular Channel with Suction**", *Published in Heat Transfer – Asian Research* **48**:2773-2798 (2019). DOI: 10.1002/htj.21513.

3. M. Pavankumar Reddy and J. V. Ramana Murthy, "**Steady Flow of Couple Stress Fluid through a Rectangular Channel Under Transverse Magnetic Field**", *International Journal of Advanced Trends in Computer Application*, Special Issue 1(1), pp. 174–181, 2019.

4. J. V. Ramana Murthy and M. Pavankumar Reddy, "**Hall effect on steady MHD flow and heat transfer of a viscous fluid in a rectangular channel with suction and injection**". *E3S Web of Conferences* **128,** 07008, 2019.

List of Communicated Papers

5. J. V. Ramana Murthy and M. Pavankumar Reddy, "**Fluid Flow and Heat Transfer by Heat Function and Entropy Generation in a Rectangular Channel with Suction**", *International Journal of Heat and Technology*.

6. M. Pavankumar Reddy and J. V. Ramana Murthy, "**Steady Flow of Couple Stress Fluid through a Rectangular Channel Under Transverse Magnetic Field with Suction**", *Nonlinear Engineering Modeling and Application*.

7. J. V. Ramana Murthy and M. Pavankumar Reddy, "**Stokes Flow and Heat Transfer Past A Circular Cylinder In A Square Cavity With Suction/Injection On Side Walls**", *Heat Transfer – Asian Research*.

8. J. V. Ramana Murthy and M. Pavankumar Reddy, "**Stokes Flow and Heat Transfer Past A Circular Cylinder In A Square Cavity With Suction/Injection On Opposite Walls**", *SN Applied Sciences*.